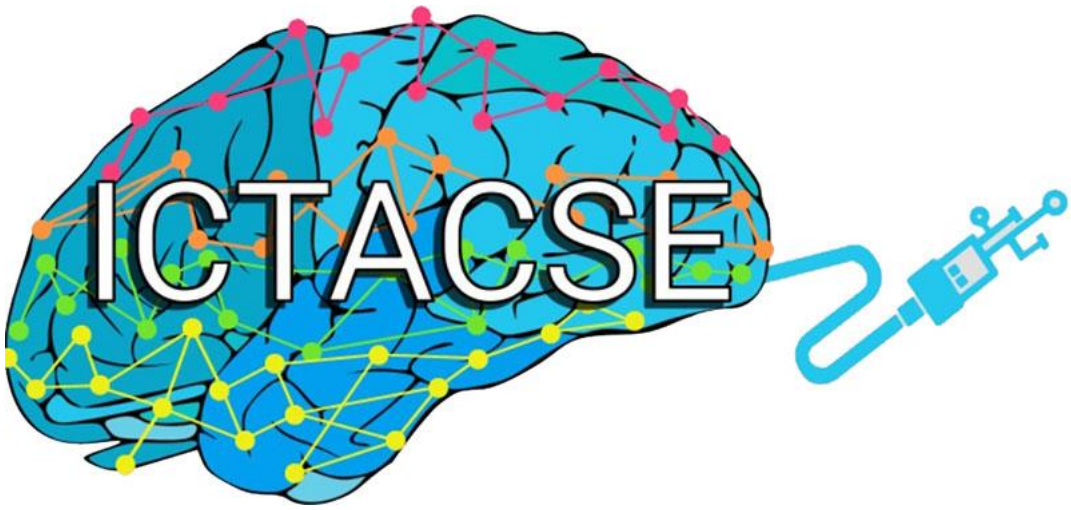

PROCEEDINGS OF BOOK

II. International Conference on Theoretical and Applied Computer Science and Engineering 2018-Summer

ICTACSE 2018

ISBN:978-605-9546-12-6

JUNE 29 – 30, 2018
ISTANBUL, TURKEY

FOREWORD

II. International Conference on Theoretical and Applied Computer Science and Engineering (ICTACSE) will take place on June 29, 2019 in İstanbul, the glamorous city at the heart of two large continents with significant historical heritage from both Byzantine ages and the Ottoman era.

Our conference aims at bringing together researchers and academics for the presentation and discussion of novel theories and applications of computer science and engineering. The conference covers a broad spectrum of topics in the field. Last conference was a great success and we hope that this second event will continue to constitute a base for a long lasting conference series to provide an environment that will strive for academic excellence in research.

ICTACSE provides an ideal academic platform for researchers and scientists to present the latest research findings in computer science and engineering. The conference aims to bring together leading academic scientists, researchers and research scholars to exchange and share their experiences and research results about computer science and engineering studies.

We would like to thank to Promech for their invaluable supports in organizing this event. We would also like to thank to all contributors to conference, especially to plenary speakers who share their significant scientific knowledge with us, to organizing and scientific committee for their great effort on evaluating the manuscripts and participants for sharing their research experience and findings with us. We do believe and hope that each contributor will benefit from the conference.

We hope to see you in our third conference ICTACSE 2018-Winter, which will be announced in our conference website shortly after the conference.

Yours Sincerely,

Asst. Prof. Dr. Gazi Erkan BOSTANCI
Chair of ICTACSE

SCIENTIFIC COMMITTEE

Dr. Ahmad Alzahrani, Umm Alqura University, SA

Dr. Ahmed Mohamed, British Telecom, UK

Dr. Anasol Pena-Rios, University of Essex, British Telecom, UK

Dr. Ayhan Aydın, Ankara University, TR

Dr. Aysenur Bilgin, University of Amsterdam, NL

Dr. Bülent Tuğrul, Ankara University, TR

Dr. Çiğdem Acı, Mersin University, TR

Dr. Erinç Karataş, Ankara University, TR

Dr. Fatih V. Çelebi, Yıldırım Beyazıt, University, TR

Dr. Felix Ngobigha, University of Essex, UK

Dr. Femi Adeyemi-Ejeye, University of Surrey, UK

Dr. Gazi Erkan Bostancı, Ankara University, TR

Dr. Hacer Yalım Keleş, Ankara University, TR

Dr. İman Askerbeyli, Ankara University, TR

Dr. Kurtuluş Küllü, Ankara University, TR

Dr. Mamoona Asghar, Islamia University, PK

Dr. Mehmet Acı, Mersin University, TR

Dr. Mehmet Dikmen, Başkent University, TR

Dr. Mehmet Serdar Güzel, Ankara University, TR

Dr. Murat Osmanoğlu, Ankara University, TR

Dr. Nadia Kanwal, Lahore College for Woman University, PK

Dr. Panitnat Yimyam, Burapha University, TH

ORAL PRESANTATIONS

A Visual Demonstration based on Social Media Analysis of Refugees in Turkey

Abdullah Bulbul
Ankara Yildirim Beyazit University
Ankara - Turkey
Email: abulbul@ybu.edu.tr

Salah Haj Ismail
Ankara Yildirim Beyazit University
Ankara-Turkey
Email:sismail@ybu.edu.tr

***Abstract*—Since 2014 to date, the population of refugees in Turkey exceeded three millions which creates a necessity to study their needs and conditions as well as their opinions. We propose a method to analyze the dataset collected from social media accounts of refugees in Turkey in a textual and visual manner. Firstly, we acquire social media activities of refugees, then we make textual analysis for which the results are presented using wordclouds. Finally, for the most significant words obtained from the textual analysis, we perform a visual analysis to find out the most representative image or a group of images shared in social networks. This association between textual and visual results enhance their perceptibility and help decreasing the ambiguity of inferences over analysis results.**

I. Introduction

Turkey accommodates more than 3 millions of Syrian refugees who were forced to leave their country [1], due to seven years war in Syria. Social media is considered in many studies as one of the accelerators of the Arab spring and its usage have accompanied majority of the events [19]. Having a dataset of refugees in Turkey has the potential to facilitate a number of future studies.

"A picture is worth ten thousand words", as the historical Arab philosopher Alnafri said. In contrary, analysis of the social networks are usually based on textual information, for which it is not easy to understand the underlying meaning of the textual results out of their context. Thus, it should be accompanied with additional cognitive elements such as auditory or visual items.

Moreover, in the case of Arabic, the difficulty of correctly stemming words and absence of accents and movements in the digital text [6] leads to less comprehensible results, i.e, same textual representation may have totally different meanings. Since this paper deals with analysis of refugee's activity on Social Media and the big majority of refugees in Turkey communicate in Arabic [1], a visual demonstration of the analysis is essential to decrease the aforementioned ambiguity.

In addition, to enhance the perception of analysis results, in this paper, we propose a method to summarize the refugees perspective in Turkey by choosing an image or group of images out of the shared multimedia in specific time margin related to a specific word or topic. The images are automatically selected so that the most representative ones are gathered and shown while also avoiding unnecessary repetition among the set of selected images.

This graphical presentation could enable a better understanding of refugees' needs for better planning in future intervention to solve social, economical and maybe political refugee issues and aspects in Turkey; the country hosting highest number of refugees in the world today[21].

II. Related Works

People share enormous amounts of data on social media which led to numerous studies in the last decade. These studies cover, on the first hand, a wide range of aspects according to availability of various kinds of data, e.g, textual [12], [13], locational [2], and visual [18], etc; on the other hand, it deals with a rich variety of applications and topics.

One of the most popular topics is arguably elections. During this time, social media produces numerous comments and news concerning candidates' statements. Quite a few studies take place on literature in order to predict the elections in terms of forecasting the results [15], [5], [11]and understand how posts reflect the political sentiment in society [20] . On the other hand, this popularity of social media data being analyzed to predict elections or similar concepts and the easiness of proposed methods in relevant articles to announce the winner beforehand led some researches to question the reliability of such research. For instance, in [8] it is claimed that predicted results obtained via Twitter data has been exaggerated.

Immigration and refugee was an important issue to be studied and analyzed, thus many papers performed these studies in order to understand the motivations, challenges and hopes of refugees. As an example of refugees related work, the study in [9] explores the ideas of users towards refugees by means of collected tweets including #refugeesnotwelcome hashtag. The work in [14] also exploits tweets including same hashtag to understand the portrayal of male Syrian refugees on social media.

Most of the aforementioned studies rely on textual analysis. In addition to textual data, multimedia content existing in social media is also valuable for performing analysis and there are also studies in that category [16]. Snavely et al. [18] proposed a method for exploring large amounts of photographs which can be possibly acquired from social media. Another study tries to calculate 3D visual popularity from social media

images by estimating the visual space covered by the images [3]. Sharma et al. [17] performs image summarization using SIFT features and topic modeling. This study is mainly aimed to summarize hundreds of photos taken by a single user.

III. Used Method

In order to analyze and choose the most representative images reflecting the events and issues of refugees in Turkey, we looked for the mostly shared visual elements linked to the trending topics determined from text analysis. The process to reach that objective includes following steps:

- Collecting relevant data
- Textual analysis to determine the trending events and issues.
- Visual analysis to define the representative image.

A. Collecting relevant data

To retrieve information from refugee related social media accounts, we analyzed public Twitter activity using Twitter API[1]. applying the method used in [4] consists of the following sub steps: Firstly, we tried to figure out a method to define the accounts of Syrian refugees in Turkey. Secondly, we traced back those chosen users' accounts, collecting the tweets. Finally we filtered out the irrelevant and unreliable data.

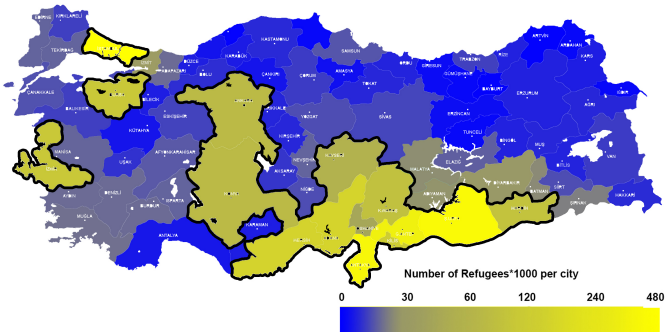

Fig. 1. Distribution of Syrian refugees in Turkish cities generated according to the statistics in [7].

Determining the accounts. To determine the refugee owned accounts we check the accounts associated with Arabic language, since refugees (95% [21]) have Arabic as their mother tongue and refugees are forming 90% of the registered foreigners in Turkey, Thus we assume that Twitter accounts in Turkey which uses Arabic as the main language are probably refugees'.

Then, we checked number of Syrian refugees registered in each Turkish city. Figure 1 shows the distribution of Syrian refugees in Turkey. The image is generated according to the statistics in [7] Using a logarithmic color code. The bold border shows the regions chosen in our study, which host the majority of Syrian refugees. The cities in these regions accommodate 90% of them while they only have 48% of the total Turkish population. Table I shows the number of refugees in chosen cities and the ratio of refugees to the city populations.

[1]https://developer.twitter.com/en/docs

TABLE I
Main Cities Hosting Refugees

City	N.Refugs	Ratio	City	N.Refugs	Ratio
Adana	150790	6.85%	Ankara	73198	1.37%
Bursa	106000	3.68%	G.Antep	329670	16.70%
Hatay	384024	24.69%	Istanbul	479555	3.24%
Izmir	108306	2.58%	K.Maras	90100	8.11%
Kayseri	59938	4.34%	Kilis	124000	95.15%
Konyai	73445	3.40%	Mardin	94340	11.85%
Mersin	146931	8.28%	Osmaniye	43773	8.38%
S.Urfa	420532	21.67%	Total	2685669	6.28%

Twitter API allows searching for recent (seven days) tweets according to keywords, location, and used language. To avoid a biased collection of data, we don't provide any keywords. We search for Arabic tweets in specific locations wherein refugees are accommodated intensely.

For practical purposes we limited the search to 1000 tweets per region. Later, we extracted the individual user IDs posting these tweets. As one account can post multiple tweets, we have less amount of user accounts then the number of tweets. As a result we collected a total of 5707 twitter users who were active recently. Table II shows the number of discovered users in each region.

TABLE II
Data collected: users- Tweets per city

City	N.Users	N.Tweets	City	N.Users	N.Tweet
Adana	160	127031	Ankara	1050	2297028
Bursa	2023	4543793	G.Antep	535	1139878
Hatay	12	13874	Istanbul	1183	2910948
Izmir	78	107263	K.Maras	35	13538
Kayseri	62	55275	Kilis	3	558
Konyai	137	158845	Mardin	30	24130
Mersin	269	461598	Osmaniye	22	11811
S.Urfa	108	156736	Total	5707	12022306

Collecting tweets data. Twitter API lets accessing up to last 3200 of a user's tweets including retweets. Therefore, we gathered tweets of each user we extracted in the previous step until the limit is reached or there is no more tweet from that user. In one query, it is possible to access only 200 tweets, thus, we run multiple queries to collect the maximum possible number of tweets. Table II includes the number of tweets collected from each city.

Data filtering. Firstly we have excluded the tweets from 2018, only tweets up to the end of 2017 were analyzed, since in 2018, millions of tweets (3,678,739) were retrieved in less than 20 days which are unreliable, due to the fact that tweeting 3200 tweets in those days means more than 160 tweets per day, implying that these tweets are neither coming from a real user, nor expressing an individual user opinion. And among the traced accounts, there are ones which do not belong to individual users but to press or companies for instance. These accounts mostly post with a very high frequency including a big ratio of retweets. This information helps differentiating the

users we are interested in to analyze in this study. Moreover, we have excluded the Twitter accounts created or have all the activities after 2014 since these accounts are incapable to reflect the continuous change of refugees' conditions and needs.To analyze the development of refugee related issues and events, we focus more on the users for whom we have data that covers the years when refugees arrived to Turkey (See Figure 2).

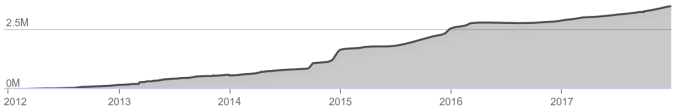

Fig. 2. Number of Refugees in Turkey per year [1].

Table III shows the number of accounts with the date of their oldest tweets collected.

With the aforementioned approach, out of 5707 accounts and 12 million tweets, we have refined the accounts into 633 and the tweets to almost 800 thousands, and classified these tweets into: tweets (435,378) and RT(336,753).

TABLE III
NUMBER OF USERS WITH THEIR OLDEST KNOWN ACTIVITY

Year	2018	2017	2016	2015	2014 & before
N.Users	876	2997	815	397	633

B. Textual analysis

In this study, we are concerned on the direct opinions of refugees. Thus, we didn't include retweets in our analysis. We find out the frequency of occurrence of each word in the combined text from all tweets. Since most of the conjunction and pronouns etc in Arabic have less than three letters, we discarded any word which has less than three letters to select useful and meaningful words.

Conducting an analysis based on the direct count of words, misleadingly favors the commonly used words of daily life rather than the representative words that reflect a specific event or topic. To avoid highlighting such common words we use the following simple approach: subtracting the frequency of occurrence of a word in the whole period from the frequency of occurrence of the word in a specific year.
This approach highlights the representative words in a domain of interest and suppresses the misleadingly high frequency of common words e.g., pronouns, conjunction, suffixes. Using the results, we have created the word clouds seen in Figure 3. The analysis shown is an example which was conducted for the total tweets in Turkey in the whole period, and another example of a yearly based analysis of 2016.

C. Visual analysis

As a result the textual analysis step, we figured out the keywords reflecting the important events in a specific domain of interest. These keywords are still ambiguous out of their

Fig. 3. Generated wordclouds for years 2012 to 2017. Same wordclouds for 2016 presented: Original Arabic words (right), translation to English (left).

context. High complexity of written Arabic language also increases the ambiguity level. Thus, to find out what is really meant by these keywords, associated media can be helpful. Therefore, we download images from tweets including a keyword in its specific time domain. Subsequently, for each keyword, we have media sets containing more than hundreds of images. To determine the most representative images among each set we applied the following method (See Figure 4).

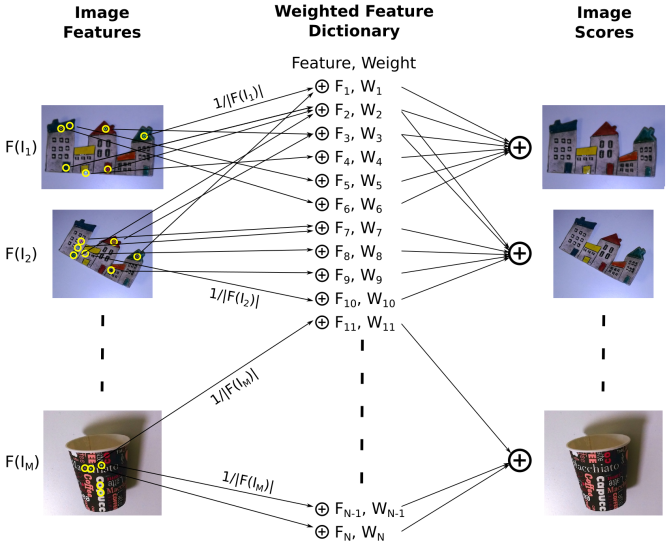

Fig. 4. Calculating image scores.

1st round	1.85	1.9	3.53	3.95	3.86	**4.08**	1.2	1.3	1.69	1.57
2nd round	1.85	**1.9**	0.48	0.49	0.63	0	1.1	1.2	1.69	1.39
3rd round	0.34	0	0.48	0.49	0.63	0	1.1	1.2	**1.45**	1.39

Fig. 5. Multiple image selection process.

Firstly, we extract SIFT features [10] of all images. To increase the performance, we limit the number of SIFT features extracted from each image to 50. Each feature is assigned a value of $1/|F(I_i)|$ where $|F(I_i)|$ depicts the number of features in image i.

By accumulating all images, a dictionary of features is generated where each feature has a score according to the number of its occurrences among different images, i.e., if an image feature exist in many images it will have a higher score.

After determining the scores of each feature, these scores are used to calculate the score of images such that an image will obtain a score that is the sum of all its features' scores. This approach prioritizes visual elements that are shared frequently. Note that, in this approach, the shared images do not have to be identical to get prioritized but they need to include similar visual features, e.g., two images of the same scene from different angles will both contribute to this scene's score.

At the end of this procedure, the image with the highest score can be selected as the representative image for that keyword. Nevertheless, it is possible for a keyword to have multiple representative images. In such a case, we need to avoid selecting images with little difference. To achieve that we used a mechanism as follows. When the highest score image is selected, scores of all similar images will be lowered according to their similarity level. Specifically, when an image is selected, scores of all its visual features in the dictionary becomes zero and image scores are updated. This procedure is shown in Figure 5.

IV. Results and Discussion

The approach applied in this study shows two kinds of analysis results. Firstly the text analysis, which is presented in word clouds seen in Figure 3 which are created to show the

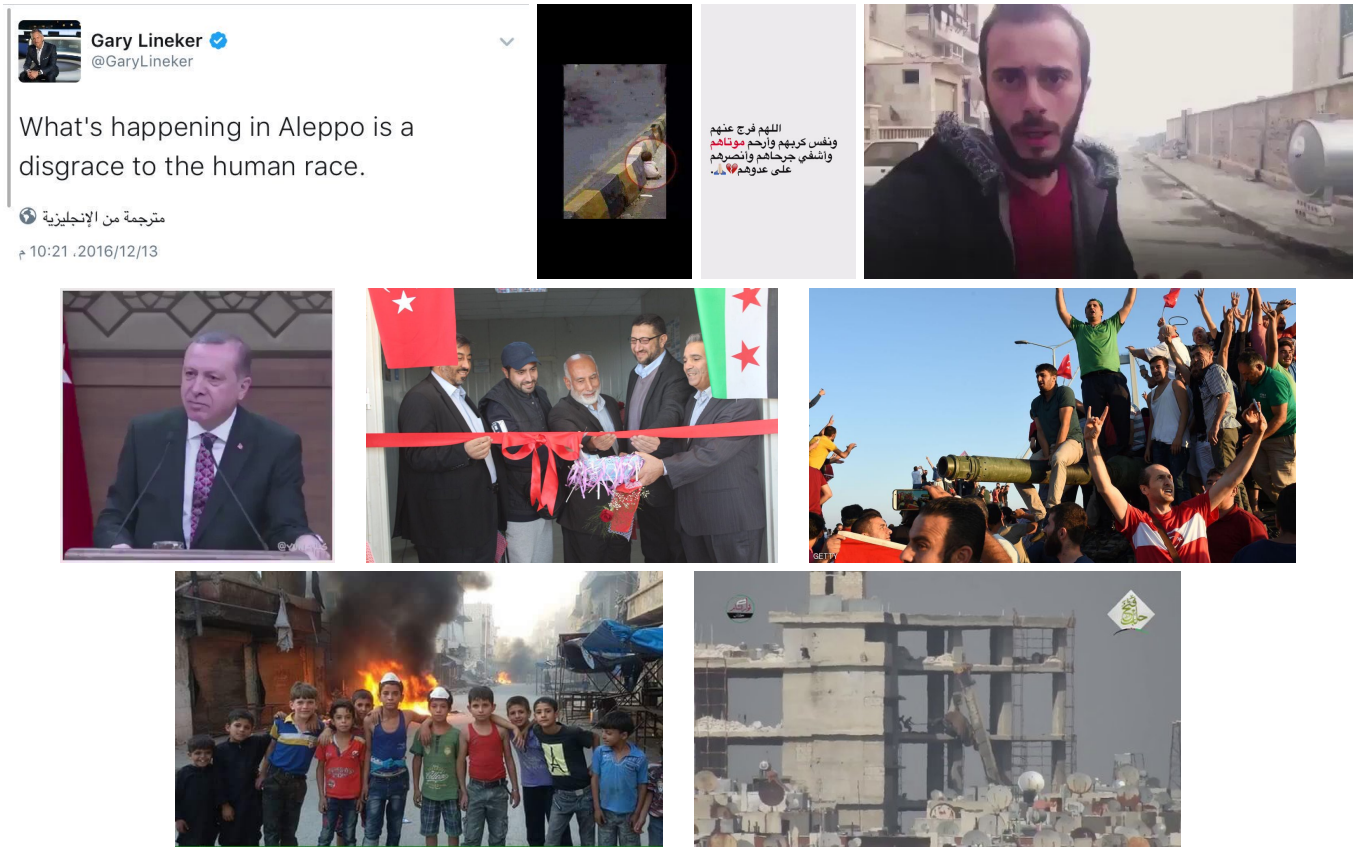

Fig. 6. Demonstration of visual analysis results for year 2016. Top row: images for Aleppo, middle: Turkiye, bottom: epic ('melhame' in Arabic). Number of chosen images for each word also represents the word's weight.

trends and most frequent words in the collected data set. These results remains ambiguous, partially because the language used is Arabic, in which without writing the correct movements and accents,a word can have multiple meanings, which varies widely between unrelated meanings. Thus, second analysis of linked media is performed, to explain and define the correct meaning by associating these words to related images.

Choosing the most representative images is performed using a novel process, and the results of this analysis are shown in Figure 6. This analysis is performed over the significant words of 2016. The first row shows four automatically chosen images for word 'Aleppo' out of 302 images in the dataset. Second row shows three images for word 'Turkiye' out of 136 images and third row contains 2 words for word 'melhame' out of 10 images.

The approach applied helps to clarify the meaning of the keywords in a specific domain. In our case the most shared words by refugees in Turkey are presented, and the most related images are chosen, this combination eases the understanding of the most important issues the refugees cared about or considered to discuss through their social media accounts. For instance, reading the text 'Halep' could mean milking or Aleppo (the Syrian city) and 'melhame' could mean epic or butcher; by associating these words with images, the ambiguity is removed and the meanings are revealed so we can tell that the topics are Aleppo city and epic respectively. This does not only help the presentation objectives but also enhance the possibilities of future planning and development of solutions for their problems and obstacles in Turkey.

V. Conclusion

An approach to retrieve and analyze refugees' issues in Turkey, is presented in this paper, using Twitter as a data source to define refugees accounts and trace their activities back in time is explained too. The data set gathered contains horizontal and vertical dimensions for a multilevel analysis, such as time, location, inference, opinion, sentiment, and politically oriented accounts. This provides wide potentials for deeper future analysis to better understanding the conditions of refugees, and to enhance the public plans for their integration.

To understand the issues and topics shared and discussed by refugees who are forced to leave and refuge in other countries, visual means are used to communicate and present these topics. A potential future work is the creation of image clouds associated with wordclouds about specific domain of interest. Social and cultural identity could be studied in order to be presented by using this approach to choose the most representative images the refugees in Turkey has shared during their refuge years.

Acknowledgments

One of the authors, Abdullah Bülbül, is supported by TUBİTAK BİDEB 2232 program (Project number: 117C010).

References

[1] 3rp:syria regional refugee response inter-agency information sharing portal. http://data.unhcr.org/syrianrefugees/country.php?id=224 (2018), accessed: 2018-01-19

[2] Bulbul, A., Dahyot, R.: Populating virtual cities using social media. Computer Animation and Virtual Worlds 28(5) (2017)

[3] Bulbul, A., Dahyot, R.: Social media based 3d visual popularity. Comput. Graph. 63(C), 28–36 (Apr 2017), https://doi.org/10.1016/j.cag.2017.01.005

[4] Bulbul, A., Kaplan, C., Ismail, S.H.: Social media based analysis of refugees in turkey. In: BroDyn18: Workshop on Analysis of Broad Dynamic Topics over Social Media. pp. 35–40 (2018)

[5] Burnap, P., Gibson, R., Sloan, L., Southern, R., Williams, M.: 140 characters to victory?: Using twitter to predict the uk 2015 general election. Electoral Studies 41, 230–233 (2016)

[6] Dahab, M.Y., Ibrahim, A., Al-Mutawa, R.: A comparative study on arabic stemmers. International Journal of Computer Applications 125(8) (2015)

[7] Esnek, F.: Basin ilan kurumu, hangi ilde ne kadar suriyeli var? iste il il liste. http://www.bik.gov.tr/hangi-ilde-ne-kadar-suriyeli-var-iste-il-il-liste/ (2017), accessed: 2018-01-19

[8] Gayo-Avello, D.: " i wanted to predict elections with twitter and all i got was this lousy paper"–a balanced survey on election prediction using twitter data. arXiv preprint arXiv:1204.6441 (2012)

[9] Kreis, R.: # refugeesnotwelcome: Anti-refugee discourse on twitter. Discourse & Communication 11(5), 498–514 (2017)

[10] Lowe, D.G.: Distinctive image features from scale-invariant keypoints. International journal of computer vision 60(2), 91–110 (2004)

[11] Mascaro, C., Agosto, D., Goggins, S.P.: The method to the madness: The 2012 united states presidential election twitter corpus. In: Proceedings of the 7th 2016 International Conference on Social Media & Society. p. 15. ACM (2016)

[12] Paltoglou, G., Thelwall, M.: Twitter, myspace, digg: Unsupervised sentiment analysis in social media. ACM Transactions on Intelligent Systems and Technology (TIST) 3(4), 66 (2012)

[13] Pang, B., Lee, L., et al.: Opinion mining and sentiment analysis. Foundations and Trends® in Information Retrieval 2(1–2), 1–135 (2008)

[14] Rettberg, J.W., Gajjala, R.: Terrorists or cowards: negative portrayals of male syrian refugees in social media. Feminist Media Studies 16(1), 178–181 (2016)

[15] Sang, E.T.K., Bos, J.: Predicting the 2011 dutch senate election results with twitter. In: Proceedings of the workshop on semantic analysis in social media. pp. 53–60. Association for Computational Linguistics (2012)

[16] Schreck, T., Keim, D.: Visual analysis of social media data. Computer 46(5), 68–75 (2013)

[17] Sharma, V., Kumar, A., Agrawal, N., Singh, P., Kulshreshtha, R.: Image summarization using topic modelling. In: Signal and Image Processing Applications (ICSIPA), 2015 IEEE International Conference on. pp. 226–231. IEEE (2015)

[18] Snavely, N., Seitz, S.M., Szeliski, R.: Photo tourism: exploring photo collections in 3d. In: ACM transactions on graphics (TOG). vol. 25, pp. 835–846. ACM (2006)

[19] Stepanova, E.: The role of information communication technologies in the arab spring. PONARS Eurasia Policy Memo 159, 12–16 (2011)

[20] Tumasjan, A., Sprenger, T.O., Sandner, P.G., Welpe, I.M.: Predicting elections with twitter: What 140 characters reveal about political sentiment. Icwsm 10(1), 178–185 (2010)

[21] UNHCR: United nations refugee agency. http://www.unhcr.org/figures-at-a-glance.html (2017), accessed: 2018-01-19

Cryptocurrency Word-of-Mouth Analysis via Twitter

Cagri Kaplan
Ankara Yildirim Beyazit University
Ankara - Turkey
ckaplan@ybu.edu.tr

Cagri Aslan
Ankara Yildirim Beyazit University
Ankara-Turkey
cbaslan@ybu.edu.tr

Abdullah Bulbul
Ankara Yildirim Beyazit University
Ankara-Turkey
abulbul@ybu.edu.tr

***Abstract*—In this work, we aim to understand whether the sharp variations on exchange rates of alternative coins, aka altcoins, can be foreseeable or not by analyzing the relevant data collected on Twitter. For this reason, first we specified various altcoins which match our requirements to be studied on such as exhibiting sudden bumps or pumps during the time interval we are interested in. Then we categorized the tweets of corresponding altcoins day by day in order to investigate their sentiment scores reflecting positive, negative and neutral speculations. On the other hand, prices of each altcoin provided by on-line cryptocurrency stock markets are obtained on the eve of sudden variations of exchange rates. We then try to reveal the effect of word-of-mouth through performing regression analysis on sentiment scores and market prices.**

I. Introduction

In the conventional finance system, exchange rates of currencies over the world are affected by several parameters such as inflation, interest rates, current-account deficits, public debts, etc. Moreover, only central banks are authorized to print money and release to market which is a centralized system in terms of the worth of a currency. On the other hand, bitcoin proposed as a digital money or payment system and alternative to centralized currencies is very popular in recent times. It is not subordinated to any central bank or stock market, on the contrary, any computer equipped with sufficient hardware to implement bitcoin mining algorithm can produce bitcoin or alternative coins which makes digital money market a decentralized system. Most of the researches ongoing for bitcoin are focused on the underlying reasons of its volatile nature and understanding the sustainability of this popularity. Table I is attached to emphasize the seriousness of the fluctiations on exchange rates of bitcoin from May 2013 to January 2018. In addition to bitcoin as a digital money, alternative coins have emerged with lower prices in market and they whet the appetite of investors especially those dreaming of being bazillionaire. To be so, perhaps one needs to answer the question naturally arises here which is *"What are the factors determining the prices or volatility of cryptomoneys?"* Unfortunately, any response to this question is nothing more than a prediction. This is because the supply and demand equilibrium of digital money differs from the standard economy since supplying Bitcoin is a publicly accessible algorithm and demand can not be related directly to an financial parameter [4]. However, there are studies claiming the technological and economical determinants of cryptocurrencies such as economic fundamentals, market conditions, impact of mining technology and difficulty [12]. In this paper, different than studies wherein stock market is predicted via sentiment analysis [2], [16], we present a work questioning the existence of speculation in social media that can affect the prices of cryptocurrencies. Speculation, as a word, is defined as trying to guess the answer of a question without having enough information [1]. Speculations can be considered as secret weapons in finance such that it can even cause a company to be bankrupted. Since there have been a huge demand on digital money as an investment tool, it is important to know the identity of the enemy to take precautions. For this reason, a social media platform, namely Twitter, is used to listen to rumors. Through Twitter, nowadays, we have the ability of monitoring others' lives, notions regarding daily events or opinions concerning political issues, products or even meals in the simplest term. Enormous quantity of data is released by the social sensors or namely users continually. Literature contains many studies related to retrieving data from Twitter and exploiting it to analyze various social disorders such as early detection and analysis of epidemics [17], efficiently responding to a disaster [11], detection of traffic events [6], revealing potential drug effects [7], detecting and predicting dynamic changes of social issues [1], understanding the reaction of companies when a specific event takes place and assessing leadership styles [10], analyzing the relationship between cybersecurity attitude and behavior and the way attitudes shape behavior [5]. The rest of this paper proceeds as follows. We provide some related works in Section 2. Then, in Section 3 we describe the method to select proper alternative coins to be investigated for this study and implementation of sentiment analysis on retrieved

TABLE I
Bitcoin exchange rates

Date	Price of a bitcoin
2013, May	117.0 USD
2013, Dec	1,077.12 USD
2014, Oct	321.40 USD
2015, Feb	218.89 USD
2015, Dec	462.06 USD
2016, Dec	949.30 USD
2017, Jun	2,910.44 USD
2017, Sep	4,527.40 USD
2017, Dec	19,537.70 USD
2018, Jan	10,513.30 USD

[1] https://dictionary.cambridge.org/tr/szlk/ingilizce/speculation

data from Twitter. Results obtained through correlation and regression analysis are given in Section 4 with a brief discussion explaining the effects of speculations on exchange rates. Finally, we conclude this study with Section 5 by providing directions to improve the results obtained and describing the road map of related future research.

II. Related Works

Bitcoin was first introduced by [15] as a peer-to-peer electronic cash system and proposed as an alternative to payment methods at the present time. However, nowadays it has been rarely preferred as a payment method due to wild fluctuations it exhibits on exchange rates but an investment tool. In this section, we present some of the studies in the literature analyzing the bouncy structure of cryptocurrencies and predicting the exchange rates according to public mood and on-line sources.

The study in [8] firstly categorizes tweets including the term "Bitcoin" according to positive, negative and neutral sentiments they contain in. Then, they correlate these classified information to Bitcoin market indicators to understand the causalities between these concepts. At the end, they explain Twitter as a virtual trading floor of Bitcoin wherein market is mirrored with emotional studies. Using time-series analysis to reveal the relationship between Bitcoin prices and measurements of collective mood derived from Twitter feeds is presented in [4]. This study constitutes a positive relationship between Bitcoin mining difficulty as a technological variable and Bitcoin price and furthermore it is stated that based on a sentiment classifier proposed as a state-of-the-art machine learning algorithm implemented on tweets, short-run movements of Bitcoin price can be predictable. Another study correlating the fluctuations of Bitcoin price to the volumes of related tweets is presented in [14]. In addition to the tweets with positive sentiments, this study takes into account Google Trends data cross correlated with the Bitcoin prices. As a conclusion, it is stated that while Twitter data is applicable on a short term work, Google Trends data has more impact on the prediction of digital money price. Additionally the study in [9] looking for a causality between market price of Bitcoin and search queries on Google Trends and Wikipedia. Interestingly, results show that this relationship is bidirectional which means public interest influences Bitcoin price and vice versa. This result may indicate that speculations are effective to change the price of digital currency. The market movement of cryptocurrencies is also analyzed in [3] via machine learning algorithms. It is claimed that hourly and daily prediction of Bitcoin is accomplished via related Twitter data and with prediction accuracy exceeding 90%.

III. Data Preprocessing

A. Dataset

The data we have collected for this study covers the timeframe between 26 December 2017 and 14 January 2018. During this time interval, 2,752,032 tweets containing any of the keywords[2] "*bitcoin*, *Bitcoin*, *altcoin*, *criptocurrency*, *criptomoney*" are retrieved via ELK stack with the connection to Twitter API[3]. Data collection structure with the utilized tools is depicted in Figure 1. Recall that one of the main goals of this study is to understand how frequently an altcoin is mentioned before it reaches its peaks. For this reason, we do not categorize whole tweets as retweet, tweet or reply to tweet since we are only interested in rumors regardless the way of its expression.

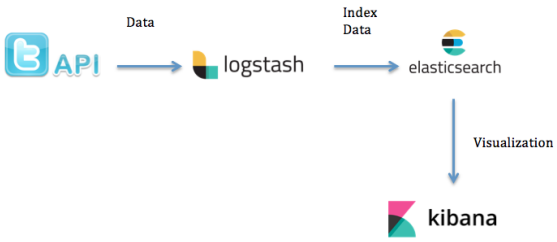

Fig. 1. Data Collection Schema

B. Specifying Altcoins

Recently, demand on the alternative coins with the growing popularity of bitcoin is increased drastically especially as an investment tool. We observe on our data that during the time period we collected data, various altcoins are mentioned in tweets more frequently compared to the others. To acquire trending alternative coins, a visualization tool of Elasticsearch named as Kibana is used by taking into account the hashtags attached to posted tweets. An example of such a visualization represented via vertical bars with ten most popular topics filtered out is shown in Figure 2. Notice that some of the hashtags referring to same concept are repeated such as *bitcoin*, *Bitcoin*, *btc*, *BTC* or *ethereum*, *Ethereum*. Later, we will treat such hashtags as an individual hashtag in order to prevent loss of information. To come to the point, altcoins to be analyzed are obtained by first filtering out 500 most frequent hashtags in all tweets. In the following step, we unified hashtags representing the same concept as mentioned before. The hashtag list so far we have obtained contains some irrelevant data. Hence, in order to get rid of any hashtag which is not an altcoin we extracted a list of altcoins currently operational from on-line criptocurrency market[4]. Afterwards, these lists are matched to eliminate all the hashtags do not represent an altcoin. This process gives 46 of popular criptocurrencies worth to talk among twitter subscribers in a time frame almost covers three weeks. List of extracted altcoins[5] is given in Table II. Notice from this table that some of the coins such as Altcoin, Crypto, Money are extremely noisy in terms of

[2]What is meant by keyword is any word in the text of the tweet and notice it differs from the hashtag notion beginning with the symbol #.

[3]https://developer.twitter.com/en/docs

[4]https://coinmarketcap.com/

[5]Coins are ordered according to their market capitalization.

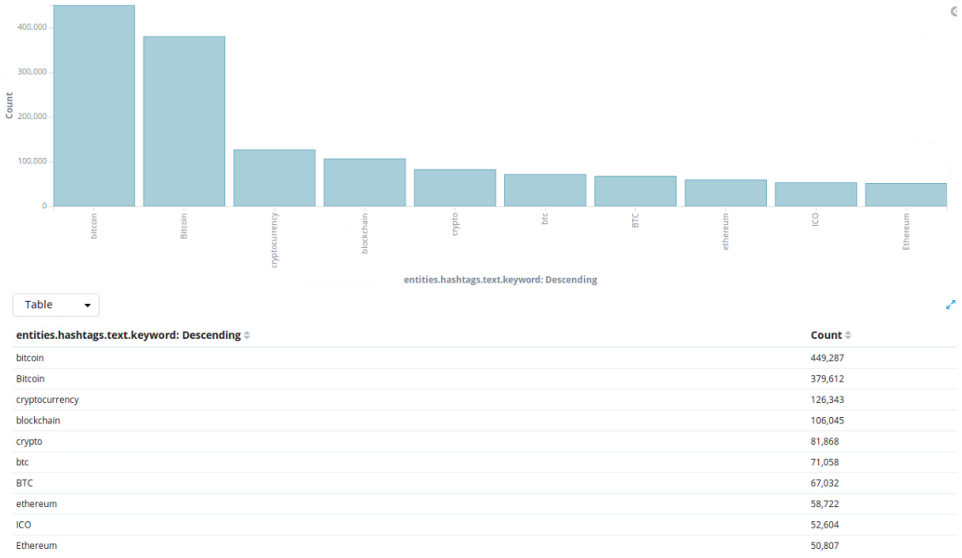

Fig. 2. Vertical bar visualization showing most popular 10 topics

TABLE II
FREQUENTLY RUMORED COINS

Rank on market	Coin	Symbol	Count	Rank on market	Coin	Symbol	Count
409	Aigang	AIX	2237	8	Litecoin	LTC	53741
250	Agrello	DLT	1072	322	Maecenas	ART	827
567	Altcoin	ALT	29996	13	Monero	XMR	9736
1	Bitcoin	BTC	978288	922	Money	$$$	14719
4	Bitcoin cash	BCH	9201	309	Mooncoin	MOON	1654
205	Bitconnect	BCC	2920	10	Nem	XEM	2061
31	Bitshares	BTS	3368	7	Neo	NEO	1745
190	Bread	BRD	5155	80	Nxt	NXT	928
30	Bytecoin	BCN	1001	120	Paccoin	PAC	5153
5	Cardano	ADA	10780	824	Postcoin	POST	1156
914	Compucoin	CPN	2187	18	Qtum	QTUM	842
225	Coss	COSS	1868	86	Reddcoin	RDD	4043
1078	Crypto	CTO	129366	3	Ripple	XRP	67723
12	Dash	DASH	12106	1244	Segwit2x	B2X	826
54	Digibyte	DGB	1805	435	Sphere	SPHR	6206
43	Doge coin	DOGE	5247	6	Stellar	XLM	4091
848	EOT Token	EOT	2758	106	Substratum	SUB	2205
2	Ethereum	ETH	147794	83	Syscoin	SYS	1530
100	Gamecredits	GAME	4174	22	Tether	USDT	1888
719	HOdlcoin	HODL	5961	14	Tron	TRX	25816
417	Icos	ICOS	3258	32	Verge	XVG	37048
1373	India coin	INDIA	823	38	Waves	WAVES	1390
11	Iota	MIOTA	6982	26	Zcash	ZEC	1754

the count numbers. This is due the conceptual conflicts of the semantics which the word itself evokes. To exemplify, when twitter users attach the hashtag altcoin (#altcoin) to their tweets, it is deceiving to think all of these hashtags are related to the alternative coin Altcoin since some of these hashtags are attached to emphasize the all alternative coins in the market. Moreover, the obtrusive inconsistencies in the popularity of a coin compared to its rank on the market are clues of the noise presented in the corresponding coin. Additionally, most popular cryptocurrencies such as Bitcoin, Ethereum, Ripple are excluded from the analysis. The reason is that we believe in a short term study, being able to discover if speculations affect the price of a coin which has already become popular is not realistic. More generally, We are mostly interested in cryptocurrencies that ruin their long-term stability with a sudden bump or pump in a given time interval. Bread and Dash altcoins fairly rehearse the behavior of an altcoin of interest and no interest, respectively as shown in Figure 3 and 4. Stability of Bread in a time frame between 26 December 2017 and 01 January 2018 may address ongoing speculations on the eve of its sudden bump in terms of its price. On the other hand, exchange rate of Dash is not changed reasonably compared to its past and future within the time frame we are able to observe its price. For this reason, we exclude such

Fig. 3. Bread market price

Fig. 4. Dash market price

cryptomoneys from further analysis. Moreover, we observed that some of the altcoins contain only spam or advertorial tweets totally irrelevant to the information we are interested in. Without loss of information, we exclude corresponding altcoins from our analysis as well. In the following step, peak of each selected coin where they reach maximum price on the market are obtained.

Taking into consideration the facts mentioned above, we select six of these cryptomoneys (highlighted in Table II) to understand whether speculations on Twitter caused to change their exchange rate reasonably or not.

IV. Analysis

Tweets concerning each selected altcoin are separated day by day to be compared to their daily market prices via statistical analysis. To do so, first of all, sentiment analysis via [13] is implemented for tweets of corresponding day and a quantitative score is obtained. The software produces a qualitative score for each tweet as very negative, negative, neutral, positive and very positive in terms of the sentiment it contains. We treated these results as -1, -0.5, 0, 0.5 and 1, respectively. Afterwards, by implementing sentiment analysis on the whole tweets of each altcoin for each day, we obtained daily scores reflecting the overall sentiment. Then data analysis plug-in of Microsoft Excel is exploited to perform regression analysis to see the effects of daily speculations on daily prices of alternative coins. Note that, market prices and sentiment scores are considered as dependent and independent variables in regression model, respectively. We focus on two parameters which are significance F and R-squared. Table III shows the outcomes of regression analysis for corresponding parameters.

TABLE III
Regression analysis results

Date	significance F	R-squared
Agrello	0,047	0,405
Bread	0,626	0,031
Bytecoin	0,410	0,076
Digibyte	0,033	0,449
Dogecoin	0,106	0,239
Icos	0,068	0,294

V. Results and Discussion

The maximum value of R-squared, which is 1, denotes that all of the sentiment scores perfectly fit the line based on prices. This value is far away from the perfect case for Bread and Bytecoin altcoins. On the other hand, R-squared parameter is not bad in the case of Agrello, Digibyte, Dogecoin and Icos. Another parameter significance F represent the consistency between the dependent and independent variables and usually assumed to be considerable when it is less than 0,05. Therefore, we observe that regression result for Agrello, Bytecoin and Icos can be significant by taking into account their significance F results. These results show that price of an alternative coin may cruise in real world in parallel to the rumors in social media. In other words, it may be possible to predict bumps or pumps on cryptocurrency prices by means of monitoring the sentiments of people through micro-blogging sites wherein users feel free to express their feelings or opinions. Moreover, based on these results, price manipulation may also be possible as well through intended groups organized for self benefits.

VI. Future Work

The first thing to emphasize is that, this study reflects the results of a short term data. For this reason we had to exclude many of the alternative coins in in Table II since they generally contain spam tweets instead of opinions or sentiments of users which can increase the performance of regression analysis. A future work with a long term data containing rumors of an altcoin which experiences several bumps or pumps during this period would be more beneficial to see exact relationship between two variables. Moreover, Bayesian regression model could also be implemented on such a big data confidently to obtain more accurate results.

References

[1] Bae, J.H., Son, J.E., Song, M.: Analysis of twitter for 2012 south korea presidential election by text mining techniques. Journal of Intelligence and Information Systems 19(3), 141–156 (2013)
[2] Bollen, J., Mao, H., Zeng, X.: Twitter mood predicts the stock market. Journal of computational science 2(1), 1–8 (2011)
[3] Colianni, S., Rosales, S., Signorotti, M.: Algorithmic trading of cryptocurrency based on twitter sentiment analysis
[4] Georgoula, I., Pournarakis, D., Bilanakos, C., Sotiropoulos, D.N., Giaglis, G.M.: Using time-series and sentiment analysis to detect the determinants of bitcoin prices (2015)

[5] Gupta, B., Sharma, S., Chennamaneni, A.: Twitter sentiment analysis: An examination of cybersecurity attitudes and behavior (2016)
[6] Gutierrez, C., Figuerias, P., Oliveira, P., Costa, R., Jardim-Goncalves, R.: Twitter mining for traffic events detection. In: Science and Information Conference (SAI), 2015. pp. 371–378. IEEE (2015)
[7] Jiang, K., Zheng, Y.: Mining twitter data for potential drug effects. In: International Conference on Advanced Data Mining and Applications. pp. 434–443. Springer (2013)
[8] Kaminski, J.: Nowcasting the bitcoin market with twitter signals. arXiv preprint arXiv:1406.7577 (2014)
[9] Kristoufek, L.: Bitcoin meets google trends and wikipedia: Quantifying the relationship between phenomena of the internet era. Scientific reports 3, 3415 (2013)
[10] La Bella, A., Fronzetti Colladon, A., Battistoni, E., Castellan, S., Francucci, M.: Assessing perceived organizational leadership styles through twitter text mining. Journal of the Association for Information Science and Technology
[11] Li, H., Guevara, N., Herndon, N., Caragea, D., Neppalli, K., Caragea, C., Squicciarini, A.C., Tapia, A.H.: Twitter mining for disaster response: A domain adaptation approach. In: ISCRAM (2015)
[12] Li, X., Wang, C.A.: The technology and economic determinants of cryptocurrency exchange rates: The case of bitcoin. Decision Support Systems 95, 49–60 (2017)
[13] Manning, C., Surdeanu, M., Bauer, J., Finkel, J., Bethard, S., McClosky, D.: The stanford corenlp natural language processing toolkit. In: Proceedings of 52nd annual meeting of the association for computational linguistics: system demonstrations. pp. 55–60 (2014)
[14] Matta, M., Lunesu, I., Marchesi, M.: Bitcoin spread prediction using social and web search media. In: UMAP Workshops (2015)
[15] Nakamoto, S.: Bitcoin: A peer-to-peer electronic cash system (2008)
[16] Nguyen, T.H., Shirai, K.: Topic modeling based sentiment analysis on social media for stock market prediction. In: Proceedings of the 53rd Annual Meeting of the Association for Computational Linguistics and the 7th International Joint Conference on Natural Language Processing (Volume 1: Long Papers). vol. 1, pp. 1354–1364 (2015)
[17] Velardi, P., Stilo, G., Tozzi, A.E., Gesualdo, F.: Twitter mining for fine-grained syndromic surveillance. Artificial intelligence in medicine 61(3), 153–163 (2014)

Real-time PID Control for Magnetic Levitation System with Special Hall Effect Sensor

Edison Wveimar Ayala Trejos
Automation Research Laboratory
Mechatronic Engineering, Kocaeli University
Kocaeli, Turkey
ayala.edison@gmail.com

Mohammad Javad Fotuhi
Automation Research Laboratory
Mechatronic Engineering, Kocaeli University
Kocaeli, Turkey
mohammad.fotuhi@kocaeli.edu.tr

Zafer Bingül
Automation Research Laboratory
Mechatronic Engineering, Kocaeli University
Kocaeli, Turkey
zaferb@kocaeli.edu.tr

***Abstract*—This paper describes the Magnetic Levitation System (MLS/maglev) focused on the design of a real time object-microcapsule-based in proportional-integral-differential (PID) control for levitated ferromagnetic objects. The maglev dynamic model including its equivalent circuit is first elaborated. The control objective is to design a real-time PID control methodology based on GoogolTech by feedback control method using a visual interface software to ensure stability. The effectiveness of the proposed PID control scheme for the magnetic levitation system is verified by numerical simulations and experimental results,**

Keywords: levitation, hall effect, electromagnet, Maglev, Magnetic levitation, PID Control.

I. INTRODUCTION

In recent years important advances have been made in different technologies using magnetic levitation systems (MLS) or Maglev, therefore, some of them are named and represent the main point of interest and departure with which the selection of levitation technology Magnetic

In the levitating system, a sphere of ferromagnetic material and mass is drawn upward by a magnetic force generated by an electromagnet; since the sphere has a weight, there is also a gravitational force that pulls it down. In this way, when a balance occurs between these two forces (magnetic force *Fm*, and gravitational force *Fg* are equal in magnitude) the levitated object in the air. Since the position of the sphere is never the same, as the system is easily destabilized, the magnetic force has to be controlled.

In Maglev technology, usually needs a mathematical model of the real system; once a good model is obtained and verified, thus a suitable control laws can be implemented to compensate the plant instability and improve performance.

Due to its nonlinear and unstable nature, the Maglev systems are very challenging projects. A PID feedback control is used to control magnetic field that levitates the objects to stabilize it in the platform. Linear system model only works well over a small region of operating point [1].

II. PLANT DESCRIPTION

The maglev device consists the electromagnet, the object position sensors, the levitating object, and the controller-computer interface board and drivers, real time control toolbox, see Fig. 1 and Fig. 2

Otherwise, Maglev is a nonlinear, open-loop unstable and time varying dynamic system. The basic principle of MLS operation is to apply the voltage to an electromagnet to keep a ferromagnetic object levitated. The object position is determined by two types of sensors (Hall Effect and distance), in other hand, the coil current is measured to identify and multi-loop or nonlinear strategies and to levitate the object a real-time controller it becomes necessary. The sensing stage is where a continuous monitoring of the position of the sphere is carried out and the information is transmitted to the control stage; in this system stage, the object position is adjusted through the control of algorithms, which tries to approximate to the set-point position with the real position, this determines the action that the electronic actuator must execute. The power stage receives the signal generated by the controller and interacts with the electromagnet. The PID controller proved to be effective for set point regulation and for tracking a changing input [2].

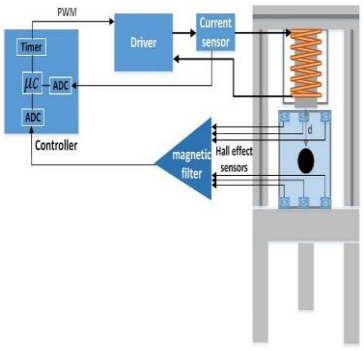

Fig. 1. A schematic representation of the plant model of the maglev system.

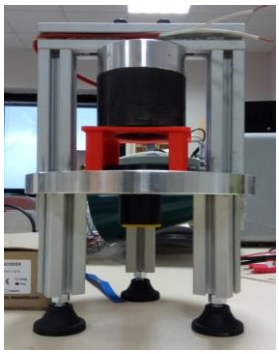

Fig. 2. Prototype Magnetic Levitation System

Furthermore, changes of the parameters of the plant, such as change of mass and suspension of the variations of resistance and inductance their magnetic susceptibility decreased with increasing temperature [3], must also be taken into account, thus the magnetic levitation system includes:

1) Measurement system, it is build by a double sensing mechanism the first one a hall effect sensor which all time is sensing the amount of magnetic flux, the other one a distance sensor wich detects the sphere movement in Z axis; according to this, the controller sends a control signal to the power stage to keep the feedback control to the error signal, it is the difference between the set-point position and the sensed position.

2) Control system, measuring the position of the object to levitate, the control signal reaches the power stage and the amplified control signal is produced, it regulates the quantity of current flowing through the electromagnet and with this the magnetic force necessary so that the object reaches the desired position.

3) Magnetic System, providing the necessary magnetic force induced over the object, in order to counteract the force of gravity and maintain a forces equilibrium. It is interesting that the force which is generated by this system varies depending on the position in which the sphere is suspended and motionless.

4) Power System, transforming the control signals of low voltage and low current signals useful for the actuator, in this particular case, are transformed into electric currents flowing through electromagnet.

5) Computer Control System, processing all the input-output information, which determines the state of the state in which the system is located. It is worth mentioning that this levitation system has a fast dynamic, then the response speed of this stage should be very high and a large bandwidth

III. MODELING

A. Nonlinear model

On the basis of electro-mechanical modeling nonlinear model of magnetic levitation system, it is described in terms of following set of differential equations [4] [5];

$$v = \frac{dx}{dt} \tag{1}$$

$$u = Ri\,\frac{dL(x)i}{dt} \tag{2}$$

$$m\ddot{x} = mg - C\left(\frac{i}{x}\right)^2 \tag{3}$$

B. State equations

The state variables are chosen according to criteria the energy storage. x_1 (Potential energy) is the position associated to the mass, x_2 (kinetic energy) associated to the velocity, associated to the inductance is x_3 (electromagnetic energy-current) defined as the third state variable, and u represent the control in 4-6 is shown the state equations.

$$x_1 = x \tag{4}$$

$$x_2 = \frac{dx}{dt} = \dot{x}_1 \tag{5}$$

$$x_3 = i \tag{6}$$

$$u = v(t) \tag{6.1}$$

Here equation (2) refers that L(x) is the constant inductance of the coil in the ball absence, L_0 is the additional inductance contributed by the presence of the ball, x_0 is the equilibrium position. The L(x) criteria is a nonlinear function of x (ball position) and it is given as:

$$L(x) = L + \frac{L_0 x_0}{x} \tag{7}$$

Where L is the constant inductance of the coil in the absence of ball, we get voltage substituting (7) into (2) yields in:

$$u(t) = iR + \frac{d}{dt}\left(L_c + \frac{L_0 x_0}{x}\right) i$$

$$u(t) = iR + L\frac{di}{dt} - \left(\frac{L_0 x_0 i}{x^2}\right)\frac{dx}{dt} \tag{8}$$

Substituting $L_0 x_0 = 2C$, results in:

$$u(t) = iR + L\frac{di}{dt} - C\left(\frac{i}{x^2}\right)\frac{dx}{dt} \tag{9}$$

C. Vector format

If $x_1 = x$, $x_2 = v$, $x_3 = i$ and $u = e$ they are given state variables the state variables are described as:

$$\frac{dx_1}{dt} = x^2 \tag{10}$$

$$\frac{dx_2}{dt} = g - \frac{C}{m}\left(\frac{x_2}{x_2}\right)^2 \tag{11}$$

$$\frac{dx_3}{dt} = \frac{Rx_3}{L} + \frac{2C\left(\frac{x_2 x_3}{x_1^2}\right)}{L} + \frac{u}{L} \tag{12}$$

Equations (1), (3) and (12) are expressed in vector format where position to ball is taken as output as below:

$$\begin{bmatrix}\dot{x_1}\\ \dot{x_2}\\ \dot{x_3}\end{bmatrix} = \begin{bmatrix} x^2 \\ g - \frac{C}{m}\left(\frac{x_2}{x_2}\right)^2 \\ \frac{Rx_3}{L} + \frac{2C\left(\frac{x_2 x_3}{x_1^2}\right)}{L}\end{bmatrix} + \begin{bmatrix}0\\0\\\frac{1}{L}\end{bmatrix} u$$

$$y = [x_1 \quad x_2 \quad x_3]^T = [1 \quad 0 \quad 0]$$

$$\dot{x} = f(x) + g(x)u$$

D. Linear Model

The maglev system is linearized around to the point $x_1 = x_0$, which results in a state vector as:

$$X_0 = [x0_1 \quad x0_2 \quad x0_3]^T$$

At equilibrium, time rate derivative of x must be equal to zero $x0_2 = 0$. Also, equilibrium current can be evaluated from equation (3) and it must satisfy the below condition:

$$x0_3 = x0_1\sqrt{\frac{mg}{C}} \tag{12.1}$$

Thus, we can write the linearized model in state space form as below using Taylor Series Expansions:

$$\frac{d^2x}{dt^2} = a_1(x - x_e) + a_2(\dot{x} - \dot{x}_e) + a_3(i - i_e) + b_1(v - v_e) \quad (13)$$

We can do

$$a_1 = \frac{\partial f_1}{\partial x}\Big|_{equil} = \frac{\partial}{\partial x}\left(g - \frac{K_c i^2}{mx^2}\right)\Big|_{equil} = \frac{2K_c i_e^2}{mx^3} \quad (14)$$

$$a_2 = \frac{\partial f_1}{\partial \dot{x}}\Big|_{equil} = \frac{\partial}{\partial x}\left(g - \frac{K_c i^2}{mx^2}\right)\Big|_{equil} = 0 \quad (15)$$

a_2 = equilibrium velocity at equilibrium point = 0

$$a_3 = \frac{\partial f_1}{\partial i}\Big|_{equil} = \frac{\partial}{\partial i}\left(g - \frac{K_c i^2}{mx^2}\right)\Big|_{equil} = \frac{2K_c i}{mx^2}\Big|_{equil} = \frac{2K_c i_e}{mx_e^2} \quad (16)$$

$$b_1 = \frac{\partial f_1}{\partial v}\Big|_{equil} = \frac{\partial}{\partial v}\left(g - \frac{K_c i}{mx^2}\right)\Big|_{equil} = 0 \quad (17)$$

At this point the system is almost already to be linear, since here the following variables are defined:

$$x_1 = x - x_e, x_2 = \dot{x} - \dot{x}_e, x_3 = i - i_e, u = v - v_e$$

Where:

$x_1 =$ object position
$x_2 =$ object velocity
$x_3 =$ drive current
$u =$ input voltage

Thus, we can write the linearized model in state space form as under [6];

$$A = \begin{bmatrix} 0 & 1 & 0 \\ \frac{Cx_{03}^2}{mx_{01}^3} & 0 & -2\frac{Cx_{03}}{mx_{01}^2} \\ 0 & 2\frac{Cx_{03}}{Lx_{01}^2} & -\frac{R}{L} \end{bmatrix} \quad B = \begin{bmatrix} 0 \\ 0 \\ \frac{1}{L} \end{bmatrix}$$

$$C = [1 \quad 0 \quad 0]$$

E. Magnetomotive force

The magnetic force is expressed according with:

$$f(x, i) = -K\frac{i^2}{(x+c)^2} \quad (18)$$

The differential equation that describes the interaction of the levitating object with the electromagnetic is given by the second Newton law as:

$$\ddot{x} = -\frac{k}{m}\frac{i^2}{(x+c)^2} + g \quad (19)$$

When the object is levitating, the equilibrium between the gravitational force and magnetic force is established, this situation is described in:

$$0 = g - \frac{K}{m}\frac{i^2}{(x+c)^2} \quad (19.1)$$

The objective is to establish a relation among the current flowing across the electromagnet and the object position. According the current i in the equation (3) the following is obtained:

$$i = \sqrt{\frac{mg}{K}}x + \sqrt{\frac{mg}{K}}c \quad (20)$$

Free body diagram of steel ball suspending by balancing the electromagnet force $F_{em}(x, i)$ and gravitational force F_g is show below.

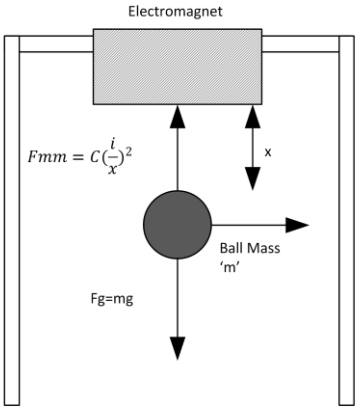

Fig. 3. Free body diagram of Magnetic Levitation System.

Net force F_{net} acting on the ball is given 3rd law of motion of Newton.

$$F_{net} = F_g - F_{em} \quad (21)$$

$$mx = mg - C\left(\frac{i}{x}\right)^2 \quad (22)$$

Where the following parameters are defined

Table 1. Parameters for Maglev System

Parameter	Description	Value
C	Magnetic constant	$1.477 * 10^{-4}\ Nm^2/A^2$
m	Object Mass	$0.01\ kg$
g	Gravitational acceleration	$9.82\ m/s^2$
F	Resultant force	N
x	Ball position	mm

Input voltage formula can be stated as:

$$e = R_i + \frac{d(L_i)}{dt} \quad (22)$$

IV. Control Block Diagram

To achieve control of the sphere in the stable levitation position, it is necessary to have a feedback system as shown in Fig. 4. The operation of the system can be explained as follows: In the controller, it has a reference position of the sphere, with which his objective will be to achieve that the real position is closest to the reference position. The controller will continuously receive information about the actual position in which the sphere is located, this information will be given by the sensors.

Depending on whether the position is greater or less than desired, the current applied to the electromagnet will be reduced or increased.

The electronic actuator (driver) is in charge of supplying the necessary electric energy to the electromagnet, so that it establishes the magnetic force on the metallic sphere. Therefore, certain important considerations for its design must be taken into account. The operation of this device is described by a block diagram.

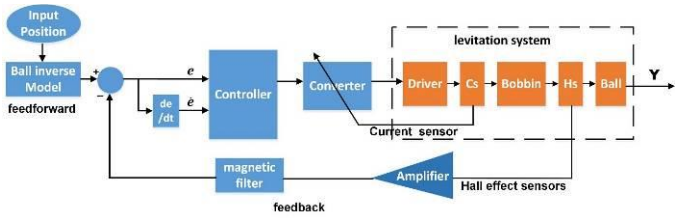

Fig. 4. A schematic representation of the Control Block Diagram.

A. *Maglev PID control*

The input voltage is applied to a coil that creates the electromagnetic field, to measure this field a Hall Effect sensor as main sensor is used, and a distance sensor as feedback sensor is used as well. The output voltage represents the position of the capsule in the magnetic field.

The physical system consists of a capsule (mass 0.00037 kg) which is under the influence of three forces:

- The magnetic field produced by an inductive coil. The force from the coil depends on the square of the current, the air-gap between the coil and the capsule, and the physical *properties of the capsule*. This produces an upward acting force on the capsule.
- The gravitational force acting downwards.
- A damping force which acts in a direction opposite to the velocity at any instant of time.

These three forces cause the resulting motion of the capsule and are modeled in Simulink as shown below.

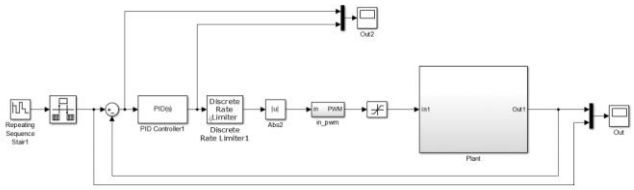

Fig. 5. Simulink block diagram for Maglev System

B. *Objective of PID Controller in Maglev System*

The controller's basic function is to respond to any variations in the capsule's vertical displacement from the electromagnet by taking necessary corrective actions.

The PID controller reads the error voltage generated by subtracting a predefined 'set point' from the 'measured' variable. Corrective effort is initiated using this error voltage in three ways. 1. Proportional control ensures that the corrective action is proportional to the amount of error. 2. Integral control takes into account the time duration of the error and completely eliminates steady state offset. 3. Derivative control ensures that the controller output is proportional to the rate of change of error. The mathematical equation describing a PID controller's behavior as follow:

$$y(t) = k_p(e(t) + \frac{\int_0^t e(\tau)d\tau}{T_i} + T_d\frac{de(t)}{dt} \quad (23)$$

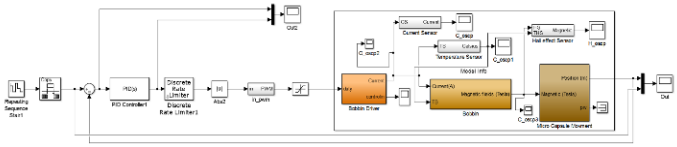

Fig. 6. PID control and Simulink block diagram

C. *Programmable Multifunction I/O Card General Description*

A multifunction I/O card is used for connecting the PC to real world signals (maglev system signals). The card contains channels, digital input/output ports, PWM A/B output, etc. The card is designed and allows standard data acquisition and control applications optimized for use with Real-Time Windows for Simulink Googooltech.

Fig. 7. Multifunction real time I/O Card

Using the data obtained by magnetic hall effect sensors when the microcapsule; the one consisting of ferromagnetic material, is moved on the vertical axis, the air gap at the starting point is 4mm and its displacement is formed by steps of 1 millimeter each one in downward direction, moreover figure 7 shows each sensor's trajectory, the amount of current is represented by relation distance (mm) vs magnetic field (T), some interesting that is made here, is related to the yellow line, which represents a signal filter of all sensors connected to the system, it is mean that we have the better data average which comes from all points of the system core.

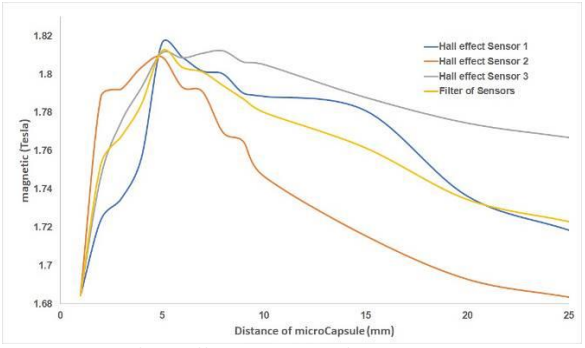

Figure 8. Chart of hall effect sensors and filter signal in maglev system

The system coefficients in (23) can be identified through an experimental approach. A series of experiments is arranged to

find the current required to levitate the object at set point-equilibrium position, the result is plotted in figure 9.

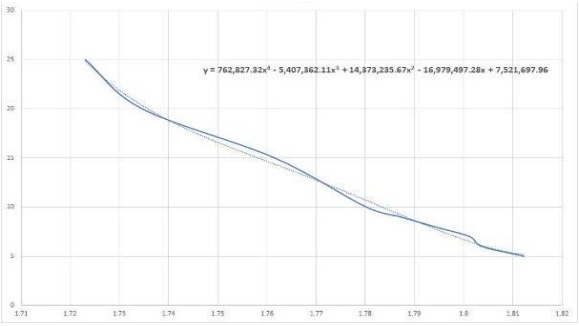

Figure 9. The equilibrium point respect to required current

As result of Simulink block diagram, the PID control simulation of the hardware platform is shown in Fig. 10. The PID gains are chosen as Kp = 15, Ki = 15; Kd = 0.5. The regulation results are shown in Fig. 10.

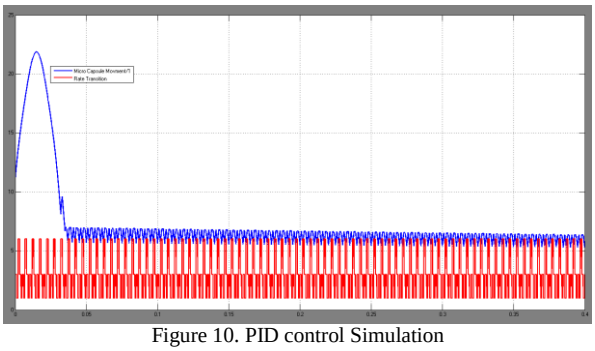

Figure 10. PID control Simulation

The PID controller has initial gains P = 1.45, I = 0.671; D = 2.71, the regulation is carry out by real time signal filtration and results are shown in Fig.11a, 11b, 11c

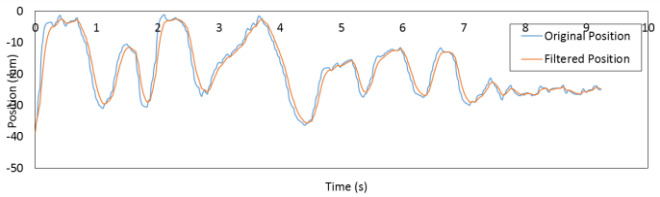

Fig. 11a Levitated object position

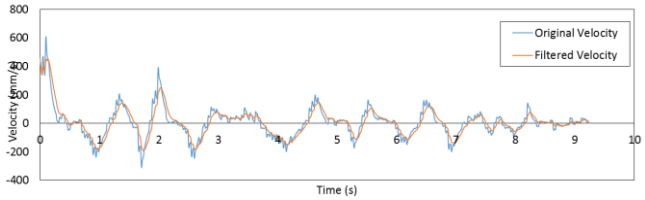

Fig. 11b Feedback velocity of levitated object

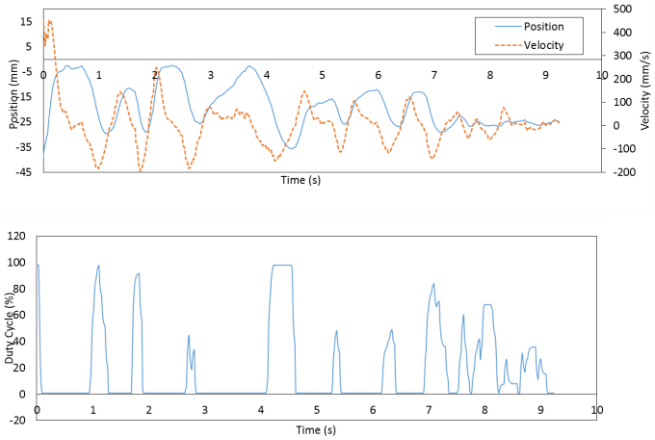

Fig. 11c PID Controller output (PWM) relative to Position and Velocity

V. Conclusion

In this paper, we use Maglev system to show how to realize the modeling and control. The modeling process includes mechanical model, electrical model and sensor model; the controller design includes: PID control, linear control, nonlinear feedback control. The modeling and design of a real-time magnetic-levitation system. The findings displayed are an agreement of the experimental data with simulation results obtained. The magnetic strength variation due the heat increasing is a factor to taken in account in maglev system,

References

[1] M. S. a. S. Akhtar, Artist, *Inverse Model Based Adaptive Control of Magnetic Levitation System*. 5th Asian Control Conference, 2004.

[2] T. M. G. a. D. G. Alciatore, Artist, *Model development and control Implementation for a magnetic levitation apparatus*. Proceedings of ASME Computers in Engineering Conference, Boston September 1995, U.S.A..

[3] G. Reis, Artist, *Thermal Influence on the Diamagnetic Properties of Pyrolytic Graphite: Applications in Space and High Speed Transportation*. Instituto Superior Técnico, Universidade de Lisboa, Lisboa, Portugal, April 2016.

[4] W. T., Artist, *Design of a magnetic levitation system - an undergraduate project.*. IEEE Transactions on Education , 1986.

[5] H. a. M. j. Wodson, Electromechanically Dynamics-Part 1: Discrete Systems, New York: Wiley, 1968.

[6] W. a. T.Chiasson, Artist, *Linear and nonlinear state-space controllers for magnetic levitation,*. International Journal of System Science, 1996.

Development of an Intelligent Energy Measurement Device for Buildings

Oğuzhan Timur
Department of Information Technologies
Çukurova University
Adana, Turkey
otimur@cu.edu.tr

Kasım Zor, Özgür Çelik
Department of Electrical and Electronic Engineering
Adana Science and Technology University
Adana, Turkey
kzor@adanabtu.edu.tr, ozgurcelik@adanabtu.edu.tr

Ahmet Teke
Department of Electrical and Electronics Engineering
Çukurova University
Adana, Turkey
ahmetteke@cu.edu.tr

***Abstract*— Depletion of nonrenewable energy resources and increasing energy demand have raised the importance of energy efficiency recently. In order to achieve an energy efficient future for the next generations of humanity, conventional devices having low efficiency should be replaced with intelligent devices possessing high efficiency. Owing to internet of things (IoT), classic devices have been converted to intelligent devices which can be remotely accessed, monitored and controlled by utilizing ubiquitous sensors. In this paper, a low-cost intelligent energy measurement device (iDev) is aimed to design in order to compute and store electrical energy consumption into a database by an embedded card, namely Arduino which measures voltage, current, frequency and power factor. When a traditional device is connected to the proposed iDev, the device turns into an intelligent device that is remotely controllable. As a result, if a whole building is equipped with the proposed iDev, it is considered that a large amount of electrical energy will be saved for a better and livable Earth.**

Keywords*— *Energy Measurement, Intelligent Device, Smart Building, Energy Saving, Energy Efficiency, Energy Management

I. INTRODUCTION

Energy is an indispensable necessity for human life. Technological developments, which push imagination limits of mankind, have caused an increase in energy demand. The rapid depletion of fossil fuels has enhanced the value of energy by making energy efficiency and energy saving compulsory. Dependency on fossil fuels has not died out completely because of the fact that the amount of energy production from renewable energy sources does not cover the whole demand. Utilization of advanced technology with an ascending trend indicates that increase in energy consumption will proceed in terms of future expectations.

Expanding awareness related to conscious consumption becomes more of an issue in order to avoid a future energy crisis. It is meaningless to estimate how much energy is saved without measuring how much energy is consumed. In such a case, it is impossible to mention about energy saving or energy efficiency. It is probable to determine the energy consumption amount of a device by carrying out measurement of the used device. Evaluating the measured values and creating scenarios with respect to the results of these evaluations are essential steps in energy management. By energy management, while energy saving is realized by preventing from unnecessary use of existing energy, energy efficiency is also provided by consuming less energy simultaneously

Energy consumption of devices should be kept under control 24/7 continuously. Auto-measurement of energy consumption amount via a computer is important from the point of view of data integrity. The requirement for controlling itself constantly has led to the emergence of "smart" and "intelligent". These concepts are used interchangeably in the literature. As a result of the measurements, saving scenarios should be identified by creating energy consumption profile of each device. Energy savings should be accomplished without lowering current living standards. Control and management by developing intelligent systems rather than direct human controlled inspections will increase the efficiency [1].

When energy consumption is investigated on a sectoral basis, it is seen that buildings have a significant place. In the investigated studies, buildings consume 40% of annual energy cost in U.S., and 30% of energy consumption is wasted [2], [3]. The energy consumption of buildings during the whole life cycle is responsible for 40% of total European Union energy consumption too. In addition, greenhouse gas emissions since buildings account for 36% of EU's total CO_2 emissions. Future projections indicate that in 2030 buildings will be responsible for 35.6% of primary energy use in the world, and continue to maintain its importance [1], [4].

Thanks to the construction of smart buildings and production of smart devices, more efficient utilization of energy sources has been provided. Furthermore, owing to embedded software programs, self-operating systems have been devised without the need of expensive computers. New intelligent systems have been developed by adding data storage units and the Internet, and this new system is named as the Internet of things (IoT) in the literature. Non-intelligent devices are turned into intelligent

The authors would like to thank the Scientific Research Project Unit of Çukurova University for financial support.

devices by creating intelligent networks which have provided communication particularly by preferring wireless connections among each device and between larger systems.

In this paper, a low-cost intelligent energy measurement device (iDev) is aimed to design in order to compute and store electrical energy consumption into a database by an embedded card, namely Arduino which measures voltage, current, frequency and power factor as shown in Fig.1. When a traditional device is connected to the proposed iDev, the device turns into an intelligent device that is remotely controllable.

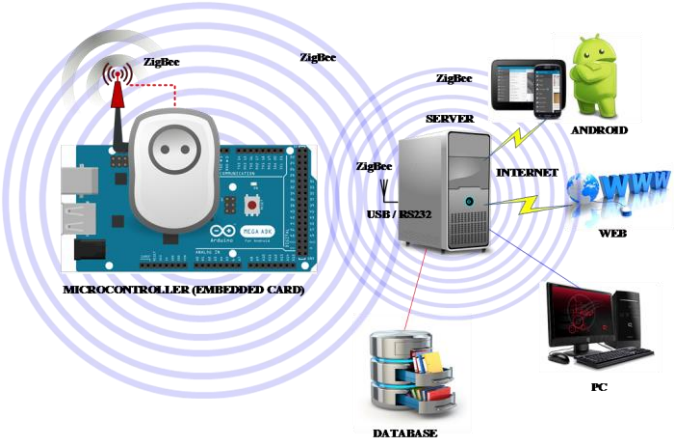

Fig.1. Schematic view of intelligent energy measurement device (iDev)

When previous studies are investigated, it is seen that wireless technologies are utilized in order to prevent new cable installation and labor costs. When compared to existing wireless technologies, because of security, low power consumption and, low cost, ZigBee / IEEE 802.15.4 wireless communication protocol has been preferred. ZigBee protocols can be used pair, star, mesh and other networking structures. Especially, mesh networking allows for reliable data transfer and it is flexibility in networking with multiple topologies. Data integrity verification and authentication are realized by using 128-bits AES (Advanced Encryption Standard) encryption algorithm at the MAC (Media Access Control) layer. ZigBee doesn't require any license for the wireless communication. Data which has 2.4 GHz ISM (Industrial Scientific Medical band) and 250 Kbps data transmission capacity can be moved between 10 meters and 70 meters. Devices which communicate with ZigBee protocol in latest emerging technologies can be communicated until approximately 42 km [5-8].

Today, the most widely used wireless communication protocol is Wi-Fi. When the ZigBee delay time compares with WI-FI delay time in lighting switch control, ZigBee has less delay time. ZigBee is about twice as fast [9].

Performances of sending and receiving data for selected embedded cards which communicate by 802.15.4 ZigBee protocol have been investigated [10]. Imote2, Mega, Telosb, Arduino, Waspmote, and Micaz boards have been examined in detail. The main goal of this study is to determine which board has the best performance. All boards have been tested with intensive data such as image and sound data. As a consequence of measurements, the communication delay time values shown in Fig.2 for a 100-byte packet. As illustrated in Fig.2, although arduino and waspmote boards are faster than the others at in sending data, they are slower than the others at in reading data. While sending throughput values are 10 ms and 11 ms for Arduino and Waspmote, reading throughput values are 35 ms and 50 ms respectively. According to measured delay times, the best performance belongs to MicaZ.

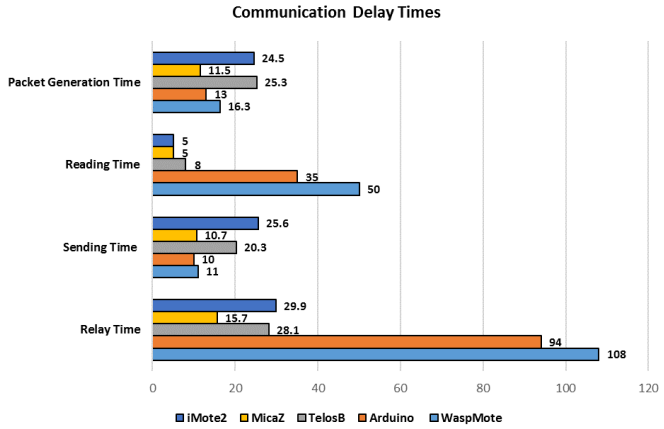

Fig.2. Communication delay times of some embedded cards [10]

When the previous studies are investigated, it is seen that the most used cards are Arduino and Raspberry Pi respectively in academic studies. In Turkey markets, almost all Arduino cards can be obtained easily. When Raspberry Pi compares with Arduino, it is second order. There are a lot of sample applications which are realized by using Arduino in literature. Because Arduino has many advantages, it has been chosen in this thesis.

II. Prepare Your Paper Before Styling

The main objective of iDev project is to develop a plug that can be controlled and monitored remotely. It is aimed to measure and record the consumed energy amount of single phase 220 V devices by developed iDev. In addition, it is aimed to control the plug by switching ON/OFF remotely. It is aimed to realize the remote monitoring and control of the plug by Windows, Web and Android based applications. Critical set values of measured values are determined and in case of exceeding these values, the energy connection of the devices are going to be automatically turned off. As a result of analyzing the recorded data, it is aimed the save energy by using energy more efficiently.

In this project, first of all, material selection is made in accordance to required properties for iDev. The implementation of material selection is done by following to perform accuracy tests of materials. It is targeted to measure voltage, current, frequency and cos φ values while the iDev is designed. By these measured values, it is going to be possible to calculate the power consumption of the device which is plugged into the iDev. Furthermore, relay with the microcontroller is used to switching the power supply of plugged in device. The microcontroller plays a key role in the implementation of both control and monitoring functions.

Arduino microcontroller with the ATMEL microprocessor is chosen because of the ease of use, cost, and the amount of similar applications, availability from the market, and the wide range of sensors and other equipment that can be used with it.

Essentially, an Arduino microcontroller comprises of Atmel microprocessor, USB serial programmer and power regulator units. Technical facilities for Arduino are given in Appendix A. The features of the Arduino Mega ADK include the Atmel 2650 processor, 54 digital I / O pins that can be used as 16-pulse PWM (Pulse Width Modulation) outputs, and 16 input pins that each of them are 10-bit analogue. It has a 256 KB flash memory totally. There are 4 UART communication pins that one of them is for programming.

The specificities of the microcontrollers are rather sufficient for iDev project. There is need for one digital input pin to turn on/off the iDev. Moreover, there is also need for two analogues and two digital input pins to measure voltage, current, frequency and cos φ values of energized plug.

Different types of sensors and devices can be supported at the same time with microcontrollers that the design of it brings multitenancy. Hence, a temperature and humidity sensor is assembled to iDev in order to measure the temperature and humidity of the environment.

Following the design of iDev is completed, it is tested with a calibrated HIOKI brand device which can make accurate measurements, in order to determine the accuracy of the measured values. The results of test measurements indicate that measurements can be made with maximum of % 2 accuracy.

It is seen in the literature that such embedded systems or microcontroller applications are specific according to project. In other words, the code that is used to control microcontroller is specific to application and it is difficult or impossible to make changes on the project or make an attachments to it. In order to overcome this problem a new system which is able to read the sensors and transmit data in spite of the type and intended use of sensors that can be mounted on them is designed. The main advantage of this system is opportunity of the standardized software usage by downloading it to another microcontroller in case of breaking down of the microcontroller. In addition, any microcontroller used elsewhere in the system can be removed and replaced directly, without any hardware or software modifications, in case of breaking down or alteration.

Development, maintenance, repair and training cost are minimized by this code standardization. Moreover, various applications that are required to be done can be realized in a simpler way.

Following the standardizing the codes, the electronic circuit is designed for microcontroller to switch the grid voltage and to read the voltage, current, frequency and cos φ. While the electronic circuit is being designed, the studies are performed by considering operating current and voltage of microcontrollers and other devices. The main objective of design is to make it practical, applicable, cost effective and coherent. Relay is preferred because of its ease applicability and cost advantage for switching operation.

In order to measure the grid voltage, step down transformer is used. Since the microcontroller only measures direct current, the output of the transformer is rectified and reduced with divider voltage resistors to keep it in the measurement limits of microcontroller.

The AC voltage from the step down transformer is rectified by low power single diode, filtered with fairly low power capacitance and connected to one of the analogue inputs of microcontroller in order to make measurement. In order to detect the minor variations in grid voltage, it is not rectified by full-wave and bridge diodes that can give better output and capacitor and filter circuits that can filter better. Half-wave rectification with a single diode reacts much faster than other rectification methods. The higher the quality of the rectifier and filter circuit, the more stable the voltage output will be, as the fluctuations from the network will compensate so well. This contradicts the aim of detecting the voltage sensitively, in other words detecting the small changes in grid voltage for his project. While calculating the voltage divider resistors, it has to be considered that analogue inputs of microcontrollers can stand to 5V DC voltage maximally. It is calculated by adding the safety margin that input voltage has to be 4V DC since maximum 5V DC voltage can be used. All calculations are made in according to 4V DC input value.

Since it is known that the main used voltage is 220 V AC, the voltage drop transformer ratio and the voltage divider resistors are selected as 100/1 in order to simplify the calculations. 2.2V DC voltage is provided to Arduino microcontroller as input voltage at the end of calculations. Microcontroller's input voltage drops to 2.1V DC following the grid voltage drops to 210V AC. Microcontroller's input voltage steps up 2.3V DC following the grid voltage steps up to 230V AC. If there is maximally 400V AC input, the input voltage of microcontroller can only be 4V maximally. Because of the input voltage can stands up to 5V, damage to the microcontroller is prevented consequently.

The rectifier which is at the output of step down transformer and voltage input at the output of filter elements are calculated as 6V DC when the grid voltage is 220V AC. The calculations are made in according to the resistance which feeds the analogue input of microcontroller is 2.20V voltage. The voltage of other resistor which is in voltage divider circuit is 3.80V. Total voltage is 2.20 + 3.80 = 6.00 V DC. According to this calculations, if the resistance which is connected to the analogue input of the microcontroller is 2.20 units, the other resistance value has to be 3.8 units. Resistance values have to be calculated correctly. It is aimed to consume minimum power due to minimum current is drawn from the rectifier and filter circuit. If the voltage divider resistance values are kept low, both the power consumption increases and the desired response speed cannot be obtained due to the excessive load on the rectifier and filter circuit. Conversely, when the voltage divider resistance values are too large, sufficient current pass is not provided for microcontroller to measure. Therefore, measurements result incorrectly.

The voltage from the microcontroller to analogue inputs is measured with 10 bit A / D converter (analogue digital converter) that is integrated into the microcontroller by converting it to digital. Since the microcontroller can accept input as a maximum of 5V DC, it corresponds to 10 bits i.e. 210 = 1024. It means that measurements can be made with 5/1024 = 0.00488 V, approximately 5mV, sensitivity. Since our measurement cycle ratio is 100/1, it means that the grid voltage measurement can be made with 0.005V x 100 = 0.5 V sensitivity. This obtained sensitivity is sufficient for the needs of

this project. Besides, the sensitivity level is reached to 0.1 V and 0.007 V respectively for more sensitive measurements by using 12 or 16 bit A / D converters externally and the average of all the measured values is found and this information is presented to the user as the mean value of the voltage.

ACS712 hall-effect current sensor is used for current measurement. The operation principle of hall-effect current sensor is finding a current that flows according to the amount of magnetic field generated by the current passing through a conductor. As the intensity of the current passing through the conductor increases, the effect of the magnetic field around the conductor also increases. The intensity of the current that is passing through the conductor can be calculated by measuring this generated magnetic field. The advantages of these sensors are that they can measure both AC and DC currents, they are sensitive and stable, and they provide good insulation even at high current ratings which are caused by the measurement of the magnetic field that is generated basically. Since it is calculated that the driven current in this project is 20A, it is decided to use the ACS712 current sensor of 30A by adding the safety margin. Since the alternating current measurement is performed, the current information from the sensor is continuously measured over a period of 1 second, and the current value is calculated by taking the average of all the measured values. Eventually, this average current value is sent to the user.

The voltage value which is obtained from the output of step down transformer for the measurement of frequency is applied directly to the inverting and non-inverting inputs of an Operational Amplifier (OPAMP), and an output voltage that is parallel to input voltage is obtained continuously except when the input voltage is 0. Because of corresponding of this obtained output voltage to each alternance of grid voltage that is given from input, frequency is double of input grid frequency. Researches on choosing proper OPAMP is completed and as a result, LM741 integrated circuit is preferred due to its wide operating voltage range, high input impedance and sensitivity, easy and cheap availability, rich documentation and application examples.

It is provided to generate an output signal for both positive and negative alternance which are supplied from input by supplying OPAMP +/- 5VDC with a symmetrical power supply. In addition, the values that are higher than 5 V are truncated and reduced to 5 V through this symmetrical feedback voltage. This produced output signal is given to one of the digital inputs of the microcontroller. The microcontroller has a function that can measure how long the signal applied to the digital inputs come both in negative and positive direction. It is reached to total number of positive and negative alternance by getting the duration of coming signal as microsecond and dividing it to 1 second time period. After that, this total number of alternans is divided by two to obtain the number of full alternans, that is, the network frequency. Since the measurement is made in microseconds, frequency measurement can be performed very sensitively. Firstly, a literature review is performed and a practically applicable circuit design was not encountered for power factor measurement. The phase angle between current and voltage must be known for the power factor measurement. It is decided to design a circuit that can follow both current and voltage based on this theoretical knowledge. Based on the idea that the OPAMP circuitry that is used in the frequency measurement circuit can generate signals for both voltage and current, one of these two OPAMP is connected to input voltage same as frequency measurement circuit and another one is connected to output of a current transformer which is used in order to detect the current drawn by the load

Output signals of both OPAMPs are 0 where the input voltage is 0. In other words, if the one of these two signals is 0, the counter begins to count until the other signal is being 0. If we find the duration time between first signal zero points and second signal zero points, we can find the duration between these two signals. That is phase difference. There are two different methods to do this calculation.

In the first method [1], the output signals of the OPAMPs are given to the digital inputs of the microcontroller. When one of these inputs is zero as a reference, a counter is operated and the other signal is expected to be zero and when the other signal is zero, the counter is stopped and the counter value is read. Thus, the phase difference can be measured as microseconds. It is necessary to work with a microcontroller which is fast and has a hardware interrupt support and sensitive counter for using of this method. This circuit is shown in Fig.3.

In Turkey, grid frequency value is 50 Hz and this means that one period is completed in 20 milliseconds. In the realized project, measurement period is one second. One second is a thousand milliseconds. If thousand milliseconds divides into twenty milliseconds, result obtains fifty. Because of measuring twice per period, a total of 100 measurements have been made. As a result of all measurement, the average value of total milliseconds are calculated. Obtained value is converted to radian value and radian value is also converted into degree value. In order to obtain power factor, the cosines of obtained degree value should be calculated.

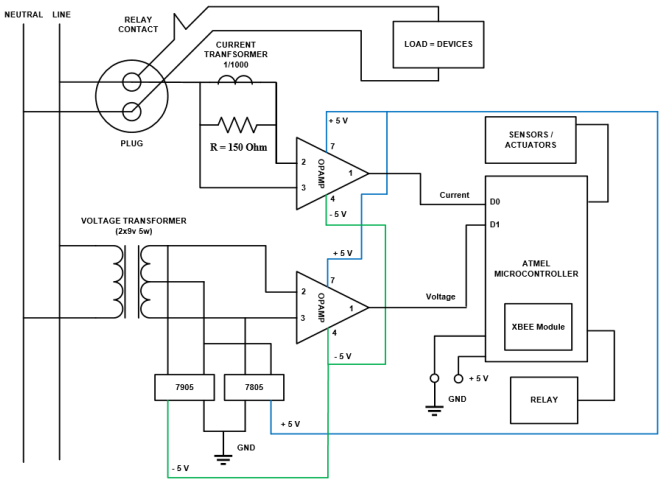

Fig.3. Circuit Design I of intelligent energy measurement device (iDev)

The other method used in the project is to connect an XOR gate to the output of the OPAMPs. It is seen that there is a logic structure that gives 0 when the inputs are the same, and 1 when the inputs are different according to the truth table of the XOR gate. Since the aim of the power factor measurement is to find the difference between voltage and current, it is correct to use the XOR gate.

As long as the outputs of the OPAMPs are different, in other words, as long as there is phase difference between the voltage and the current, the XOR gate outputs the logic 1 output signal. This output signal, obtained from the XOR gate, is given to a digital input of the microcontroller and how long the incoming signal remains at logic 1 level is measured in the level of microseconds at which the incoming signal remains at logic 1 level by the microcontroller. Since it is known that the grid frequency is 50 Hz, it is found that 1 full pulse is 1/50 equals 20 milliseconds. Because of 1 full pulse is 360 degrees, 20 milliseconds corresponds to 360 degrees. In this case, if found duration in microsecond level is 20 milliseconds and 360 degrees, the calculations are made by proportioning. The power factor between the voltage and the current is found by taking the cosine of this angle. This method is preferred due to ease of programming, the proper fastness that is targeted for this project of XOR gate operation and ability to detect even small time differences. The measurement is performed during 1 second and the average of the measured values is taken and sent to the user. Designed circuit by using XOR is shown in Fig. 4.

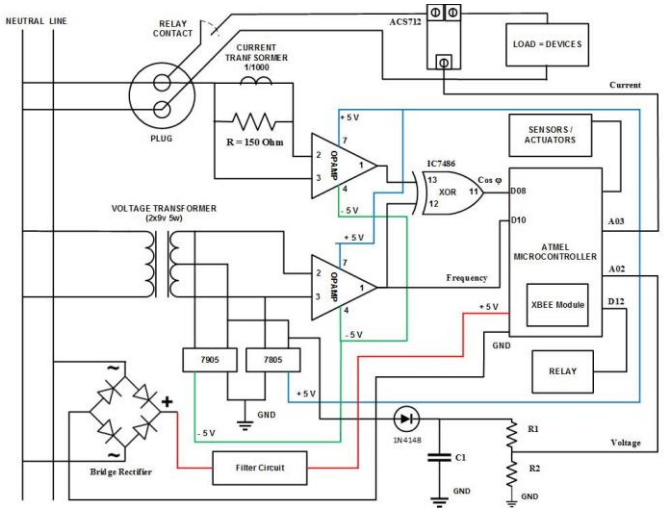

Fig.4. Circuit Design II of intelligent energy measurement device (iDev)

A power supply unit which supplies +/-5V DC to OPAMPs via the circuit that is designed for measurements, and supplies power to the microcontroller, other measurement devices and relays at the same time is designed. A transformer which gives 2 voltage outputs is chosen as step down voltage transformer. A 5W transformer is chosen considering the power requirements of symmetrical supply voltages, measurement sensors and other components. The bridge wave rectifier for rectifying and the pi type filter for filtering are used. 7805 and 7905 positive and negative voltage regulators which can regulate consistently are used for voltage regulation. It is prevented for obtained voltages to exceed +5 and -5V by these two voltage regulator. It is extremely important for fed power to be extremely linear and has the least noise because of demanding of power unit is a microcontroller, OPAMP and logic gates. In order to filter the noise that caused by regulators, the regulators are taken into pi type filters. Thus, it is possible to supply extremely linear and least noise power to demanding units.

The selected circuit elements are assembled in according to calculations as shown in Fig. 5. Application server software is developed following the connections that made between the designed circuit and the microcontroller card. It is provided to computer to read measurement results by the connection between embedded system software developed software and the embedded system to detect values entered to the computer. In addition, essential calibrations are made by test measurements of the designed circuit by means of this server software.

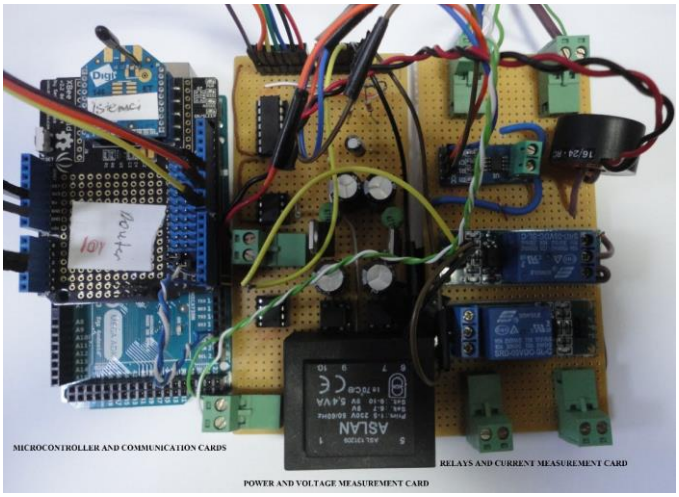

Fig.5. Implement of intelligent energy measurement device (iDev)

The implemented iDev design is tested on a 36-W fluorescent lamp circuit, fan and an electric stove that heats with resistance. Test results are shown in the Table I. As seen on the table, it is observed that measurement is made with accuracy of 2%-%3 maximally.

TABLE I. COMPARISON OF VALUES MEASURED WITH IDEV AND HIOKI

	Intelligent Energy Measurement Device (iDev)				Hioki 3334 AC/DC Power Tester			
	V	I	Hz	cos φ	V	I	Hz	cos φ
Fan	220.0	0.091	50.00	0.796	219.9	0.0930	49.97	0.784
	220.0	0.090	50.02	0.794	220.0	0.0920	50.00	0.784
	220.0	0.090	50.03	0.795	220.0	0.0920	50.01	0.785
	220.3	0.091	50.00	0.798	220.5	0.0918	49.97	0.785
	220.0	0.090	50.08	0.796	220.1	0.0917	50.02	0.785
Heater 1	216.1	3.35	50.01	0.997	216.0	3.318	49.96	0.997
	216.0	3.37	49.98	0.997	216.0	3.310	49.96	0.997
	216.1	3.35	49.98	0.998	216.0	3.312	49.97	0.997
	216.1	3.35	49.95	0.996	216.0	3.314	49.49	0.997
	216.0	3.35	50.12	0.997	216.0	3.312	49.99	0.997
Heater 2	213.2	6.55	50.03	0.996	213.2	6.54	50.09	0.997
	213.0	6.56	50.2	0.997	212.9	6.55	50.06	0.997
	213.1	6.57	50.15	0.997	213.3	6.56	49.98	0.997
	213.0	6.57	50.14	0.997	212.9	6.56	49.98	0.997
	213.1	6.57	50.12	0.997	213.3	6.56	49.99	0.997
Fluorescent Lamp	220.0	0.369	49.99	0.306	220.2	0.363	50.02	0.303
	219.7	0.363	49.99	0.325	219.8	0.359	49.99	0.32
	220.1	0.365	49.98	0.325	220.3	0.361	49.98	0.32
	220.5	0.350	49.99	0.333	220.7	0.346	49.97	0.329
	218.7	0.362	49.99	0.329	218.8	0.357	49.97	0.323

III. CONCLUSION

An intelligent energy measurement device (iDev) has been aimed to design in order to measure the electrical energy consumption of the devices real-timely. Energy saving has been provided by using embedded systems and wireless network protocol for measuring, monitoring, and controlling of electrical energy. Then, by comparing the current consumption with past consumptions, a consumption pattern has been determined for each measured device.

By the iDev design, electrical energy consumption of the devices has been measured by the electric plug and delivered to the server software program. In order to determine how much electrical energy is consumed by which device, it is adequate to connect power supply of the device to the designed iDev. Values such as current, voltage, temperature, humidity, cos φ, and frequency have been measured and saved by sensors on iDev with respect to the specified sampling period. The amount of consumed power and energy of the device has been calculated with respect to the values. A software program operating on the server and all data received from the iDev have been stored in database files. Peak times and maximum energy consumption values in a day can be determined by analysis of the data in the database. Measurement results of the developed iDev have been tested by a calibrated device which measures more precisely. After test results, the error of the developed iDev has been confirmed as maximum between 2% and 3%. In the software, maximum and minimum levels of measured values have been identified parametrically and in case of a violation of these threshold values, an interruption in energy has been provided. Owing to this feature, the risk of electric shock has been kept at a minimum.

ACKNOWLEDGMENT

The authors would like to thank the Scientific Research Project Unit of Çukurova University for project named as "Design and Implementation of a Wireless Sensor Network for Energy Monitoring, Analysis and Management in Smart Buildings" and numbered as "FDK-2016-5772".

REFERENCES

[1] O. Timur, K. Zor, O. Celik, H.B. Yıldırım, A. Teke, "Design and Implementation of Smart Energy Measurement Plug in Smart Buildings,".Digital Proceedings of the 12th Conference on Sustainable Development of Energy, Water and Environment Systems (SDEWES2017), (0732), pp.1-12, 4-8 October 2017. (Dubrovnik, Croatia)

[2] L. Jiechao, "A software approach for combining real time data measurement and building energy model to improve energy efficiency," Electrical Engineering and Computer Sciences University of California at Berkeley: Technical Report: UCB/EECS-2014-37. 14 p, 2014.

[3] A. Costa, M.M. Keane, J.I. Torrens, E. Corry, "Building operation and energy performance: Monitoring, analysis and optimization kit," Elsevier: Applied Energy, Vol.101, pp. 310-316, 2013.

[4] H.U. Gokce, K.U. Gokce, "Multidimensional energy monitoring, analysis and optimization system for energy efficient building operation," Elsevier: Sustainable Cities and Society, Vol.10, pp 161-173, 2014.

[5] O. Arslan, "ZigBee ile Bina İçi Güvenlik Otomasyon Sistemi," İTÜ. Elektrik Elektronik Mühendisliği - Bitirme Tezi. 50 p, 2009.

[6] N.C. Batista, R. Melicio, J.C.O. Matias, J.P.S. Catalao, "Photovoltaic and wind energy systems monitoring and building/home energy management using ZigBee devices within a smart grid," Elsevier: Energy, Vol.49, pp 306-315, 2013.

[7] C. Jin, "A Smart Home Networking Simulation for Energy Saving," Master of Applied Science in Electrical and Computer Engineering at Carleton University, 2011.

[8] R.V. Sakhare, B.T. Deshmukh, "Electric Power Management using ZigBee Wireless Sensor Network," IJAET: International Journal of Advances in Engineering & Technology, Vol.4, pp 492-500, 2012.

[9] K. Gill, S.H. Yang, F. Yao, X. Lu, "A ZigBee-Based Home Automation System," IEEE Transactions on Consumer Electronics, Vol.55, No:2, pp. 422-430, May 2009.

[10] C.Pham, "Communication performances of IEEE 802.15.4 wireless sensor motes for data-intensive applications: A comparison of WaspMote, Arduino, MEGA, TelosB, MicaZ and iMote2 for image surveillance," Elsevier: Journal of Network and Computer Applications Vol.46, pp. 48-59, 2014.

Very Short-Term Internet of Things Based Forecasting of Air Conditioning Loads: A Case Study for a Server Room in a Hospital

Oğuzhan Timur
Department of Information Technologies
Çukurova University
Adana, Turkey
otimur@cu.edu.tr

Kasım Zor, Özgür Çelik
Department of Electrical and Electronic Engineering
Adana Science and Technology University
Adana, Turkey
{kzor, ozgurcelik}@adanabtu.edu.tr

Ahmet Teke
Department of Electrical and Electronics Engineering
Çukurova University
Adana, Turkey
ahmetteke@cu.edu.tr

***Abstract*— Feeding air conditioning loads continuously secures the uninterruptible operation of server rooms which is critical for the communication in hospitals, and supplying the loads by photovoltaic (PV) modules creates an alternative in addition to the existing grid. In order to install a viable PV system, investigating load forecasting opportunities not only provides finding base and peak demands by monitoring, but also enhances energy management quality of the server rooms for smart grid integration. Furthermore, traditional devices have been recently converted into smarter devices owing to the revolution of ubiquitous Internet of Things (IoT) devices which may be used as data acquisition terminals for load forecasting process. In this paper, a designed smart plug by using Arduino is employed as a data logger for measuring, monitoring, and storing electric demand in the server room in a hospital, and input parameters such as air conditioning loads, outdoor ambient temperature, and outdoor relative humidity are utilized for 10-minute ahead IoT based air conditioning load forecasting by implementing artificial neural networks (ANN) and support vector machines (SVM) in the very short-term horizon. Consequently, mean absolute percentage error (MAPE) performance metric results show that SVM has better performance in comparison with ANN for very-short term IoT based forecasting of air conditioning loads.**

Keywords—very-short term; internet of things; load forecasting; air conditioning; server room

I. INTRODUCTION

In the near future, fossil fuels seem to be on the depletion which make renewable energy resources an environmentally friendly option to produce electrical energy for forthcoming years of humanity. Renewable energy technologies such as PV systems not only make the Earth a better place to live, but also present a reliable alternative in case of a sudden power outage in the existing grid.

For viable investments of the renewable energy technologies such as PV systems, IoT load forecasting is a suitable method by ubiquitous sensor mechanisms to determine the optimal plant capacity rating owing to finding base and peak demands by monitoring. IoT load forecasting is frequently divided into 4 categories according to time horizon, namely ultra- or very-short term, short-term, mid- or medium-term, and lastly long-term [1] as demonstrated in Fig. 1.

Long-term IoT load forecasting stands for the prediction among 3-year and 50-year electric load, medium-term IoT load forecasting contains predictions from 2 weeks to 3-year, short-term IoT load forecasting refers to hour, day or week ahead predictions, and finally very short-term IoT load forecasting includes few minutes to an hour ahead forecasting of electric loads [2].

In this paper, a designed smart plug by using Arduino is employed as a data acquisition terminal for very-short term IoT based load forecasting of an air conditioner in a server room of a hospital to monitor base and peak demands before installing a PV system to supply the air conditioner.

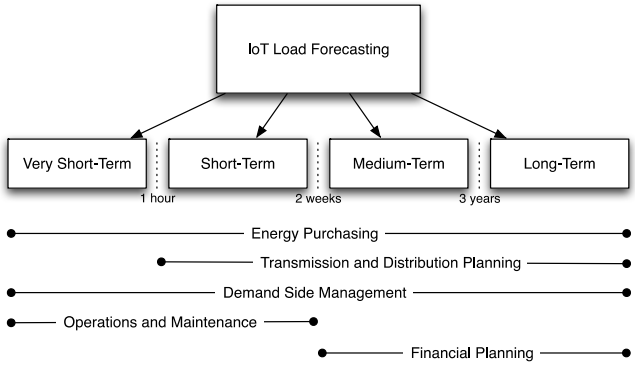

Fig. 1. IoT load forecasting applications and classification [2].

II. Literature Survey

Studies related to the forecasting of air conditioning loads in the literature go back to the mid-1980s. In 1986, Carl and Gray from Pacific Gas and Electric Company investigated residential air conditioning load prediction on hourly basis [3]. Hull and Reddy recommended a procedure to group residential air conditioning load profiles during the hottest days in summer [4]. In 1993, Gustafson et al. presented an engineering model for estimating air conditioning load control effectiveness on three utility systems in the western United States [5]. In the same year, Yu and Wong researched on estimating residential air conditioner loads by using consumer survey information [6]. At the mid-2000s, Chen et al. performed short-term electricity forecasting of air conditioners of hospital by using backpropagation ANN [7]. In 2006, Yao et al. developed an innovative air conditioning load forecasting model based on radial basis function neural network (RBFNN) and combined residual error correction [8]. Mise et al. examined curtailment of air conditioning systems during peak load caused by the congestion of the grid power in Keio University Shonan Fujisawa Campus [9]. Xuemei et al. proposed a novel air conditioning load prediction based on autoregressive integrated moving average (ARIMA) and backpropagation neural network (BPNN) in 2009 [10]. At the beginning of 2010s, Chen et al. presented an algorithm based on differential evolution (DE) and SVM for air conditioning load prediction [11]. In 2012, Liao suggested a novel method combines wavelet neural network (WNN) and improvement differential evolution algorithm (IDEA) for air conditioning load forecasting [12]. McLorn et al. evaluated peak shifting techniques for residential air conditioning demand in Saudi Arabia [13]. Horowitz et al. forecasted residential air conditioning loads by using a doubly censored Tobit model [14]. Liao presented a hybrid differential evolution and WNN with a fuzzy expert system for the problem of air conditioning load forecasting [15]. In 2016, Su et al. researched on non-intrusive load monitoring of air conditioning using low-resolution smart meter data [16]. Hong et al. investigated optimal scheduling of energy consumptions for air conditioners in a smart community with renewables [17]. Ninagawa et al. predicted aggregated power curtailment of smart grid demand response of a large number of building air conditioners [18]. Yang et al. proposed a forecasting method of air conditioning energy consumption based on extreme learning machine (ELM) algorithm in 2017 [19]. Lork et al. presented an adaptive data driven approach for single unit residential air conditioning load forecasting using regression trees [20] and suggested a data driven framework for 15-minute ahead air conditioning load forecasting based on modern machine learning techniques such as SVM, ensemble trees, and ANN [21]. Finally, Mahdavi et al. employed model predictive control of distributed air conditioning loads in order to compensate fluctuations in solar power [22].

III. Material and Methods

A smart plug [23], is capable of measuring electrical parameters such as voltage, current, frequency, cos φ to calculate the consumed power and weather parameters including ambient temperature and indoor relative humidity, is used as a data acquisition terminal for air conditioning load forecasting in the server room of the hospital. Technical specifications of the air conditioner located in the server room are given in Table 1.

TABLE I. Technical Specifications of Air Conditioner [24]

Technical Specifications	**Unit**	
Operating Voltage	V	230
Frequency	Hz	50
Cooling Capacity	kW	6.8
Heating Capacity	kW	7.4
Power Consumption for both Cooling and Heating	kW	2.4
Running Current for Cooling	A	10.6
Running Current for Heating	A	10.5
Operating Temperature for Cooling	ºC	between 0 and 43
Operating Temperature for Heating	ºC	between -6 to 24
Refrigerant	N/A	R410A

Data set is constituted of values belonging to a period between December 5 and 12, 2017. Sampling period of the data acquisition terminal is 10-minute which is in the scope of very-short term horizon.

Input parameters of the forecasting process not only includes historical electric load of air conditioner, but also contains weather parameters such as outdoor temperature and outdoor relative humidity obtained from an external temperature-humidity transmitter mechanism operating with 4-20 mA analog output.

In order to treat missing values in the transmitter data, the data set is firstly imported into MATLAB, missing and erroneous values are examined, the cells having missing and erroneous values are converted into 'NaN', and then linear interpolation method is applied in the MATLAB environment to fill the estimated values instead of 'NaN' by using built-in 'linear' function.

The graphs illustrating temperature and humidity data with missing values of the transmitter are given in Fig. 2 and Fig. 3 respectively.

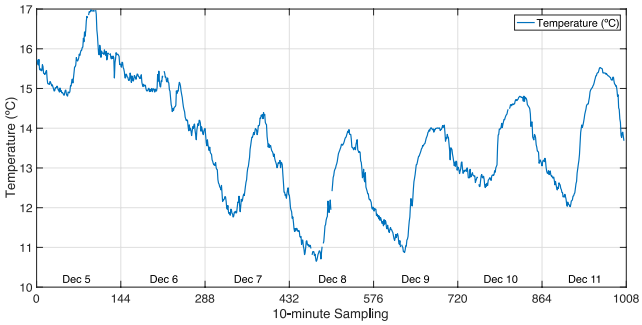

Fig. 2. Outdoor temperature between December 5 and 12, 2017.

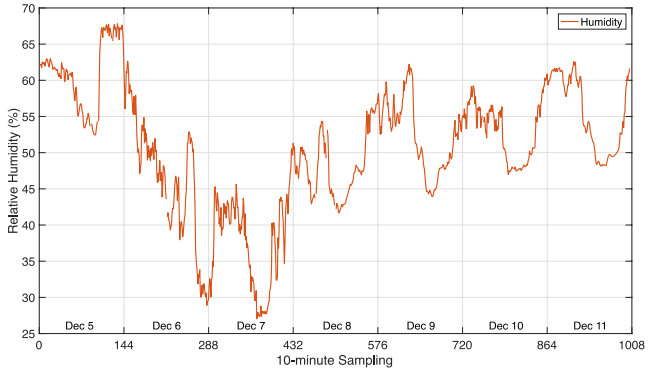

Fig. 3. Outdoor relative humidity between December 5 and 12, 2017.

In order to perform the forecast process, scaled conjugate gradient (SCG) algorithm is used with multilayer perceptron (MLP) ANN as shown in Fig. 4.

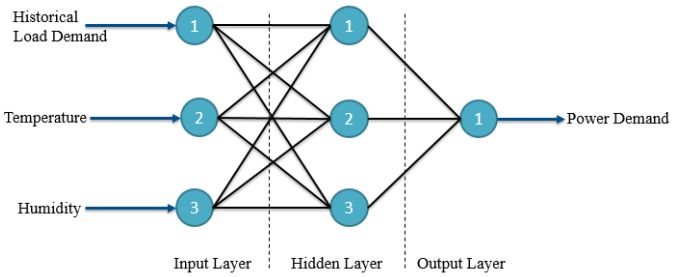

Fig. 4. MLP ANN topology.

For comparison, SVM model which performs epsilon type support vector regression (ε-SVR) with a Gaussian RBF kernel is utilized. 10-fold cross validation (CV) technique is employed for both MLP and SVM models.

IV. Discussion and Results

In order to determine an accurate ANN model that predicts 10-minute sampling air conditioning load, the number of hidden neurons is altered in every training process. The data are separated into two parts for training and testing. Thereby the trained model is validated by testing stage.

Evaluating the performances of different machine learning methods on data sets, the most commonly used performance metric for error calculation in the energy forecasting literature is MAPE which can be formulated as

$$\mathrm{MAPE}(\%) = 100 \times \frac{\sum_{t=1}^{n} |(X_t - X_t')/X_t|}{n} \qquad (1)$$

where X_t is actual or measured output, X_t' shows predicted output, and *n* indicates the number of observations [25].

From Table 2, the SCG learning algorithm based ANN model with 18 hidden neurons gives a better consequence when compared to other ANN models with different number of neurons in the hidden layer.

TABLE II. Result Table of Applied Models

Model	Neuron Number in Hidden Layer	MAPE (%)	
		Training	Testing
MLP ANN	11	8.04	8.35
	18	7.93	8.31
	25	7.92	8.33
	36	7.85	8.33
	42	7.80	8.37
SVM (ε-SVR) (RBF)	N/A	**7.78**	**8.17**

In SVM method it is important to specify cost parameter (C), regularization parameter gamma (γ), and ε parameter. These parameters directly affect the accuracy of the model and decreases the error rate. According to performance metric MAPE results, SVM model results in performing the best training and testing MAPE values. The best value of MAPE is calculated as 7.78% and 8.17% for training and testing stages sequentially.

V. Conclusions

For the continuous operation of server rooms in hospitals, supplying air conditioners without any interruption is vital. Installing PV systems to feed in the air conditioners not only make the Earth a better place, but also increases the reliability of the air conditioners while ensuring the nonstop execution of the server room.

Monitoring has come into prominence by the recent integration of smart grid, and load forecasting is an essential way to find base and peak demands of a facility. With the advancements in IoT, remote sensor mechanism has provided ubiquitous monitoring for achieving load forecasting in various horizons.

In this paper, a designed smart plug by using Arduino is utilized as a data logger for measuring, monitoring, and storing electric load demand in the server room in a hospital, and input parameters are employed for 10-minute ahead IoT based air conditioning load forecasting by applying ANN and SVM in the very short-term horizon.

As a result, MAPE performance metric results show that SVM has better performance with respect to ANN for very-short term IoT based forecasting of air conditioning loads.

Acknowledgment

The authors would like to acknowledge the Scientific Project Unit of Çukurova University for the financial support for project named as “Design and Implementation of a Wireless Sensor Network for Energy Monitoring, Analysis and Management in Smart Buildings” and numbered as “FDK-2016-5772”.

REFERENCES

[1] K. Zor, O. Timur, and A. Teke, "A State-of-the-Art Review of Artificial Intelligence Techniques for Short-Term Electric Load Forecasting," presented at the 6th International Youth Conf. on Energy, DOI:10.1109/IYCE.2017.8003734, Budapest, Jun. 21-24, 2017.

[2] O. Timur, "Design and Implementation of a Wireless Sensor Network for Energy Monitoring, Analysis and Management in Smart Buildings", Ph.D. dissertation, Dept. Elect. and Electronics Eng., Çukurova University Institute of Natural and Applied Sciences, Adana, 2018.

[3] M. E. Carl and B. M. Gray, "Predicting hourly residential air conditioning load," vol. 9, pp. 42, Proc. ACEEE Summer Study on Energy Efficiency in Buildings, Washington, DC, 1986.

[4] D. A. Hull and T. A. Reddy, "A procedure to group residential air conditioning load profiles during the hottest days in summer," Energy, vol. 15, no. 12, pp. 1085-1097, 1990.

[5] M. W. Gustafson, J. S. Baylor, and G. Epstein, "Estimating air conditioning load control effectiveness using an engineering model," IEEE Trans. Pow. Syst., vol. 8, no. 3, pp. 972-978, 1993.

[6] C. W. Yu and Y. K. Wong, "Estimating residential air conditioner loads using consumer survey information," Proc. IEE 2nd International Conference on Advances in Power System Control, Operation and Management, Hong Kong, December 1993.

[7] C. Chen, S. Shih, and S. Hu, "Short-term electricity forecasting of air conditioners of hospital using artificial neural networks," Proc. IEEE/PES Transmission and Distribution Conference & Exhibition: Asia and Pacific Dalian, China, 2005.

[8] Y. Yao, Z. Lian, Z. Hou, and W. Liu, "An innovative air conditioning load forecasting model based on RBF neural network and combined residual error correction," International Journal of Refrigeration, vol. 29, pp. 528-538, 2006.

[9] A. Mise, H. Nishi, and H. Sato, "Energy assessment of cogeneration and air conditioning system on Keio University Shonan Fujisawa Campus," Proc. 4th IEEE International Conference on Industrial Informatics, Singapore, Aug. 16-18, 2006.

[10] L. Xuemei, D. Lixing, S. Ming, X. Gang, and L. Jibin, "A novel air conditioning load prediction based on ARIMA and BPNN model," Proc. Asia-Pacific Conference on Information Processing, Shenzen, Jul. 18-19, 2009.

[11] Z. Chen, Y. Sun, G. Yang, T. Wu, G. Li, and L. Xin, "Air conditioning load precition based on DE-SVM," Proc. 3rd International Symposium on Intelligent Information Technology and Security Informatics, Jinggangshan, Apr. 2-4, 2010.

[12] G. C. Liao, "Application a novel evolutionary computation algorithm for load forecasting of air conditioning," Proc. Asia-Pacific Power and Energy Engineering Conference, Shanghai, Mar. 27-29, 2012.

[13] G. McLorn, A. Sheikh, and R. Rob, "Evaluation of peak-shifting techniques for residential air conditioning demand in Saudi Arabia," Proc. 5th IEEE PES Innovative Smart Grid Technologies Europe (ISGT Europe), İstanbul, Oct. 12-15, 2014.

[14] S. Horowitz, B. Mauch, and F. Sowell, "Forecasting residential air conditioning loads," Applied Energy, vol. 132, pp. 47-55, 2014.

[15] G. Liao, "Hybrid improved differential evolution and wavelet neural network with load forecasting problem of air conditioning," Electrical Power and Energy Systems, vol. 61, pp. 673-682, 2014.

[16] S. Su, Y. Yan, H. Lu, L. Kangping, S. Yujing, W. Fei, L. Liming, and R. Hui, "Non-intrusive load monitoring of air conditioning using low-resolution smart meter data," Proc. IEEE International Conference on Power System Technology (POWERCON), Wollongong, Sep. 28 – Oct. 1, 2016.

[17] Y. Hong, W. Chang, Y. Chang, Y. Lee, and P. Liu, "Optimal scheduling of energy consumptions for air conditioners in a smart community with renewables," Proc. IEEE PES Asia-Pacific Power and Energy Engineering Conference (APPEEC), Xi'an, Oct. 25-28, 2016.

[18] C. Ninagawa, S. Kondo, and J. Morikawa, "Prediction of aggregated power curtailment of smart grid demand response of a large number of building air conditioners," Proc. International Conference on Industrial Informatics and Computer Systems (CIICS), Sharjah, Mar. 13-15

[19] X. Yang, J. Gao, L. Zhang, X. Li, L. Gu, J. Ciu, and C. Tong, "A forecasting method of air conditioning energy consumption based on extreme learning machine algorithm," Proc. IEEE 6th Data Driven Control and Learning Systems Conference, Chongqing, May 26-27, 2017.

[20] C. Lork, Y. Zhou, R. Batchu, C. Yuen, and N. Pindoriya, "An adaptive data driven approach to single unit residential air conditioning prediction and forecasting using regression trees," Proc. 6th International Conference on Smart Cities and Green ICT Systems (SMARTGREENS 2017), pp. 67-76, 2017.

[21] C. Lork, B. Rajasekhar, C. Yuen, and N. M. Pindoriya, "How many watts: A data driven approach to aggregated residential air conditioning load forecasting," Proc. IEEE International Conference on Pervasive Computing and Communications Workshops, Kona, HI, Mar. 13-17, 2017.

[22] N. Mahdavi, J. H. Bravslavsky, M. M. Seron, and S. R. West, "Model predictive control of distributed air conditioning loads to compensate fluctuations in solar power," IEEE Trans. on Smart Grid, vol. 8, no. 6, pp. 3055-3065, November 2017.

[23] O. Timur, K. Zor, Ö. Çelik, H. B. Yıldırım, and A. Teke, "Design and Implementation of Smart Energy Measurement Plug in Smart Buildings," presented at the 12th Conference on Sustainable Development of Energy, Water and Environment Systems, Dubrovnik, Oct. 4-8, 2017.

[24] Fujitsu General Co., Ltd., 'General Air Conditioner Catalogue', April 2010, Split Type Air Conditioners, pp. 11, Indoor Unit Model: ASG24UBBN, Outdoor Unit Model: AOG24UNBNL. [Online]. Available: http://yenikazanciklima.com/images2/general_duvar.pdf. [Accessed: 13-Jun-2018]

[25] K. Zor, Ö. Çelik, O. Timur, H. B. Yıldırım, and A. Teke, "Simple approaches to missing data for energy forecasting applications," presented at the 16th International Conference on Clean Energy, Gazimağusa, May 9-11, 2018.

The Behaviour Of Piled Raft Foundations At Different Configurations Under Static And Repetitive Loads

Baki Bagriacik
Cukurova University
Civil Engineering Deparment
Adana, Turkey
bakibagriacik@gmail.com

Sefer Ercan Epsileli
6th Regional Research and Development
Headquarters Engineering of Highways
Civil Engineering Deparment
Kayseri, Turkey

Mustafa Belen
5th Regional Research and Development
Headquarters Engineering of Highways
Civil Engineering Deparment
Mersin, Turkey

Emre Pinarci
Cukurova University
Geology Engineering Deparment
Adana, Turkey

***Abstract*—In this study, the behaviors of piled raft foundation consisting of four piles in different configuration under static and repetitive conditions were investigated by large scale laboratory tests. Two different configurations were chosen in order to determine the effect of different configurations at same piles.**

Keywords—repetitive load; static load; piled raft foundation; different pile configuration

I. INTRODUCTION

Site feasibility studies for geotechnical engineering projects are most beneficial before a project can take off. Site feasibility studies usually takes place before the design process begins to understand the characteristics of foundation soil. The following geotechnical design criteria have been adopted during site feasibility studies. These criterias are: design load, the type of foundation and bearing capacity of soil. If the bearing capacity of the soil is poor, the following operations are usually performed before.

- The project site may abandon.
- The project site's soil with a low bearing capacity may replace with high bearing capacity.
- Deep foundation systems may applicate.
- Soil stabilization methods may applicate.

When engineers are abandon project sites due to undesirable soil bearing capacities, these project sites dramatically increase. But project site's soil with a high bearing capacity has become unable to meet the demand of the increasing population. In recent years there has been a need to use these project site's soil with a low bearing capacity due to the growing population.

So, these project site soil's are improved by soil replacement methods, deep foundation systems or soil stabilization methods. Nowadays, piled raft foundations from deep foundation systems are preferred as an alternative method.

There are a lot of studies in the literature [1, 2, 3, 4, 5, 6, 7, 8, 9, 10, 11, 12, 13] about the behavior of piled raft foundations under static loads. However, there is a very limited study of the behavior of piled raft foundations under both static and repeated loads.

II. MATERIAL AND METHODS

A. Test Equipment

Experimental studies were performed at 5th Regional Research and Development Headquarters Engineering of Highways by using a test box and a data acquisition system (Figure 1 and Figure 2). The tests box is designed as a rigid and length, width and height 2 m. The model raft and model piles were produced from steel which has stiffness 210000 Mpa, unit weight 77 kN/m^2. The model raft foundation's width, length and thickness are respectively 300 mm, 300 mm and 20 mm (Figure 3). The model pile's dimension and length are 0.05 m and 0.4 m respectively (Figure 3) and the placement of piles to soil is shown at Figure 4. The actuator produce monotonic or repeated loads to a maximum capacity of 245 kN. This actuator give different amplitudes and frequencies which produce static

and cycling load with electromechanical control system. In order to determine the values of the load and settlement which were applied on the foundation plate, an electronic load cell and a Linear Variable Displacement Transformer (LVDT) were used.

FIGURE 1. TEST BOX

FIGURE 2.DATA ACQUISITION SYSTEM

FIGURE 3. MODEL PILES AND RAFT FOUNDATION

FIGURE 4. THE PLACEMENT OF PILES

B. Soil Properties

In the examinations, sand samples which were taken from river bed in Çukurova District were used. Experiments were performed at soil mechanics laboratory on oven-dried sand samples. The sand was classified as uniform clean sand (SP) according to TS 1500. Test results of the sieve analysis are given in Table 1.

TABLE I. SOIL PROPERTIES

Granulometric Parameters	**Unit**	**Value**
Percentage of Medium Grained Sand	%	46.40
Percentage of Fine Grained Sand	%	53.60
Effective Grain Size, D_{10}	m	0.0018
D_{30}	m	0.0030
D_{60}	m	0.0050
Coefficient of Uniformity, C_u	-	2.78
Coefficient of Curvature, C_c	-	1.00
Soil Class	-	SP
Maximum Dry Specific Gravity	kN/m^3	17.06
Minimum Dry Specific Gravity	kN/m^3	15.03
Specific Gravity	kN/m^3	26.80

C. Research Parameters

In this study, the behavior of the same piles placed in different configurations under static and repetitive loads was investigated. The two selected configurations are shown at Figure 5 and Figure 6.

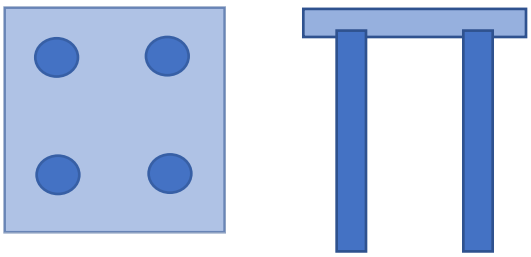

PLAN SECTION

FIGURE 5. THE FIRST CONFIGURATION OF PILES

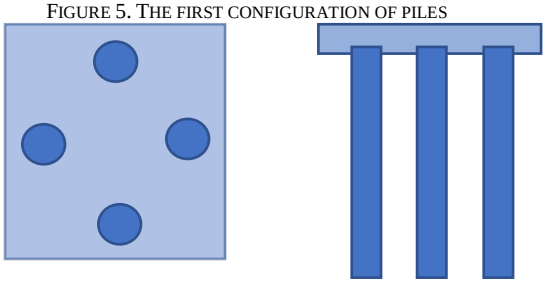

PLAN SECTION

FIGURE 6. THE SECOND CONFIGURATION OF PILES

The bearing capacity and displacement graphs were obtained by experiments under static and repetitive loading for two different configuration of piles. According to the results obtained, suggestions were made for engineering applications.

III. FINDINGS AND DISCUSSION

In this study, the behaviors of piled raft foundation consisting of four piles in two different configuration under static and repetitive loading conditions were investigated by large scale laboratory tests. The findings obtained from the experimental results were shown in Figure 7 and Table 2 under static load. The bearing capacity is defined as the vertical displacement value corresponding to 10 percent of the raft foundation. All the test results were interpreted using this approach.

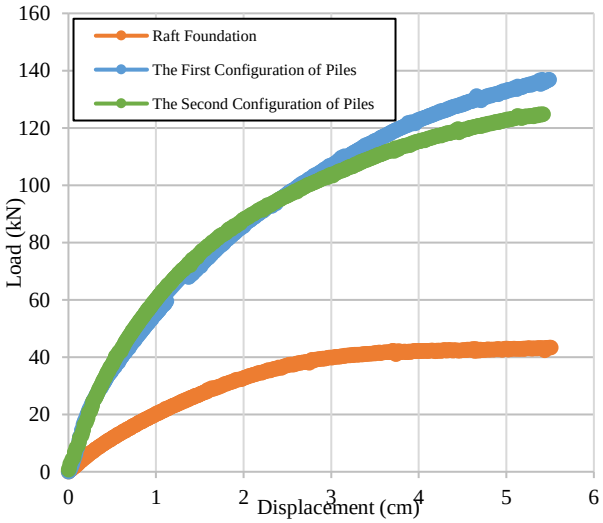

FIGURE 7. STATIC LOAD DISPLACEMENT GRAPHICS

TABLE II. THE BEARING CAPACITY OF EXPERIMENTS

Alternatives	**Bearing Capacity (kN)**
Raft Foundation	41.150
The First Configuration of Piles	106.942
The Second Configuration of Piles	103.715

From Fig. 7, it was determined that the bearing capacity graphs are not linear. The bearing capacity for raft foundation, piled raft foundation at first configuration and second configuration are 41.150 kN, 106.942 kN and 103.715 kN respectively. It has been determined that the lowest bearing capacity is the only raft foundation. It has seen that the use of piles has increased the bearing capacity at a considerable rate. It has also been determined that different pile configurations affect the bearing capacity of piled raft foundation.

The findings obtained from the experimental results were shown in Figure 8, Figure9 and Figure 10 under repetitive load after static conditions.

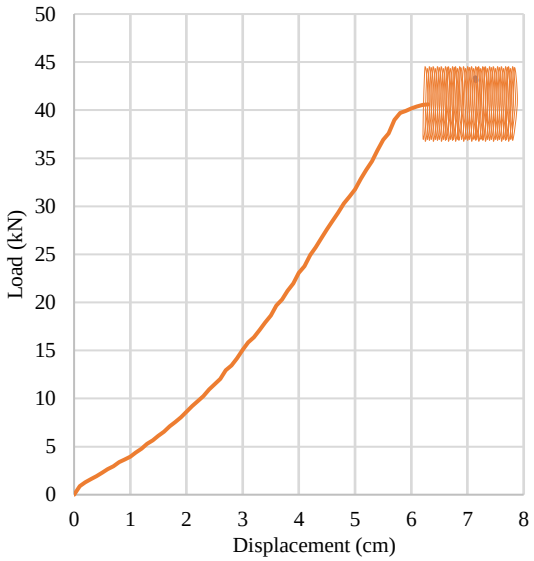

FIGURE 8. REPETITIVE LOAD DISPLACEMENT GRAPHICS FOR RAFT FOUNDATION

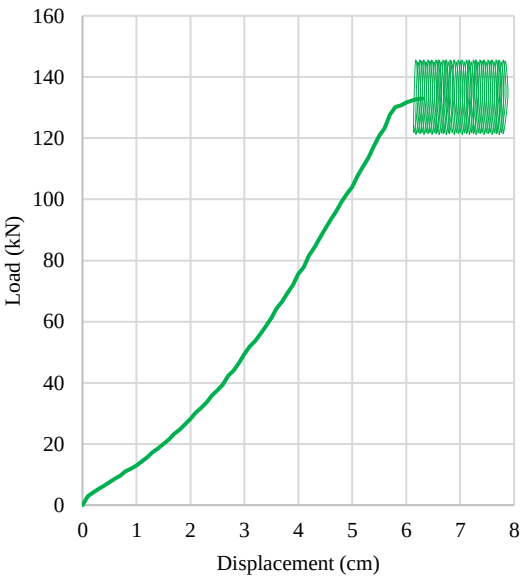

FIGURE 9. REPETITIVE LOAD DISPLACEMENT GRAPHICS FOR THE FIRST CONFIGURATION

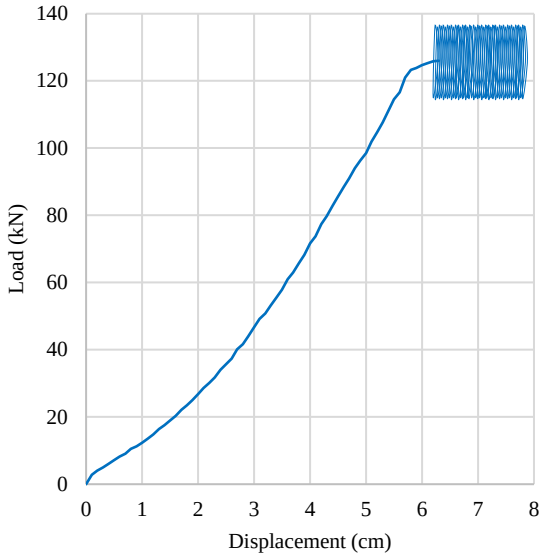

FIGURE 10. REPETITIVE LOAD DISPLACEMENT GRAPHICS FOR THE SECOND CONFIGURATION

From Figure 8, Figure 9 and Figure 10, the lowest strength is obtained at raft foundation at the same displacement value under repetitive load. The more strengths are obtained at the same displacement value at two different configurations of piles. It has been determined that the piles increases the strength of piled raft foundations under repetitive load. In addition, different strengths were obtained at the same displacement value by changing the pile configuration. For this reason, it has been seen that the change of pile configuration is important for piled raft foundation under repetitive load.

IV. RESULTS

In this study, the behaviors of piled raft foundation consisting of four piles in different configuration under static and repetitive conditions were investigated by large scale laboratory tests. Two different configurations were chosen in order to determine the effect of different configurations at same piles.

As a result of the large-scale experimental study, the following results were obtained.

It was determined that the bearing capacity graphs are not linear all of the results.

The bearing capacity for raft foundation, piled raft foundation at first configuration and second configuration are 41.150 kN, 106.942 kN and 103.715 kN respectively.

It has been determined that;

- the lowest bearing capacity is the only raft foundation under static load.
- the use of piles has increased the bearing capacity at a considerable rate.
- different pile configurations affect the bearing capacity of piled raft foundation.
- the piles increases the strength of piled raft foundations under repetitive load.
- the change of pile configuration is important for piled raft foundation under repetitive load.

REFERENCES

[1] T. Whitaker, “Some Experiments on Model Piled Foundations in Clay,” 6th International Congress of International Association of Bridge Structure Engineering, Stockholm, Sweden, pp. 124-139, 1961.

[2] H. Kishida, K. Matsushita and I. Sakamoto, “Soil-Structure Interaction of the Elevator Tower and Concrete Footings,” Proceedings of the 4th World Conference on Earthquake Engineering, Vol. 3, Santiago de Chile, pp 101–115, 1969.

[3] K. G. Garg, “Bored Pile Groups Under Vertical Load in Sand,” Journal of the Geotechnical Engineering Division, Asce, Vol. 105, No:Gt8, pp. 939-955, 1979.

[4] K. Horikoshi, “Optimum Design of Piled Raft Foundations,” PhD Thesis, University of Western Australia, Perth, 1995.

[5] G. T. Kempton, D. Russell, N. D. Pierpoint and C. J. P. F Jones, “Two and Three Dimensional Numerical Analysis of the Performance of Geosynthetics Carrying Embankment Loads Over Piles,” Proceedings of the 6th International Conference on Geosynthetics, Atlanta, Georgia: pp. 767-772. 1998.

[6] N. F. Ismael, “Axial Load Tests on Pile and Pile Group in Cemented Sands,” Journal of Geotechnical and Geoenvironmental Engineering. Vol. 42(3), pp 767-773, 2001.

[7] M. U. Ergun and H. K. Türkmen, “Kazıklı Radye Temellerin Etkin Tasarımı,” 103I007 nolu Tübitak Projesi, Ankara, 2007.

[8] S. Gök, “Kazıklı Radye Temellerin Analizi,” Doktora Tezi, İstanbul Teknik Üniversitesi, Fen Bilimleri Enstitüsü, İstanbul, 101s, 2007.

[9] H. Alsaleh, and I. Shahrour, “Influence of Plasticity on the Soil-Micropiles-Structure Interaction,” Soil Dynamics and Earthquake Engineering, Vol. 29 (3), pp. 574-578, 2009.

[10] A. Yalçin, “Kazıklı Radyejeneral Temellerin Düşey ve Yatay Yükler Altında Davranışının Sonlu Elemanlar Yöntemi ile İncelenmesi,” Yüksek Lisans Tezi, İstanbul Teknik Üniversitesi, Fen Bilimleri Enstitüsü, İstanbul, 209s, 2010.

[11] N. Erdemir and V. Okur, “Kazık Gruplarının Sismik Etki Altındaki Performansı,” Eskişehir Osmangazi Üniversitesi Mühendislik Mimarlık Fakültesi Dergisi. Sayı. 24, No.1, s. 91-107, 2011.

[12] J. D. Patil, S. A. Vasanwala and C. H. Solanki, “An Experimental Investigation on Behavior of Piled Raft Foundation,” International Journal of Geomatics and Geosciences, Vol. 5(2), pp. 300-311, 2014.

[13] B. El-Garhy, A. A. Galil, A. F. Youssef and M. A. Raia, “Behavior of Raft on Settlement Reducing Piles: Experimental Model Study,” Journal of Rock Mechanics and Geotechnical Engineering. Vol. 5(2), pp. 225-237, 2013.

Solving Large Scale Optimal Control Problems

Paweł Kowal
Scientific Foundation of Applied Computational Methods
Warsaw, Poland
pawel.kowal@imapp.pl

***Abstract*— We present a new method of solving large scale optimal control problems. The most important parts of the algorithm are a method of reducing size of the eigenvalue problem, and an algorithm of solving problems in block upper triangular form. Numerical experiments show, that proposed algorithm can solve optimal control problems with ~10^3 variables in few seconds.**

Keywords*— Optimal Control, Linear Rational Expectations Models, Schur Decomposition, Computational Methods

I. THE PROBLEM

Consider a system of a linear stochastic optimal control problems in the discrete time. The first order necessary conditions for a solution can be represented as the following linear system (see for example [8]):

$$0 = Ay_t + By_{t+1} + CE_t y_{t+1} + V\varepsilon_t \tag{1}$$

where y is a vector of control variables, ε_t is a vector of i.i.d. random variables with zero mean. Each variable with time subscript t belongs to information set in period t. We assume that matrices A, B, C are square and the matrix pair $(A, B + C)$ is regular. Let $D = B + C$.

Definition 1.1 A matrix pair (A, B) is regular if there exist scalars $\alpha, \beta \in \mathcal{C}$ such that $\det(\alpha A - \beta B) \neq 0$.

We are looking for a solution in the form

$$\begin{aligned} u_t &= Pu_{t-1} + Q\varepsilon_t \\ y_t &= Ru_{t-1} + S\varepsilon_t \end{aligned} \tag{2}$$

where $u \in \mathbb{R}^k$ is vector of state variables. Additionally we require the matrix R is stable. Substituting (2) to (1) yields

$$0 = \Phi_u u_{t-1} + \Phi_\varepsilon^1 \varepsilon_t + \Phi_\varepsilon^2 \varepsilon_{t+1} \tag{3}$$

where matrices Φ_u, Φ_ε^1, and Φ_ε^2 are defined by conditions:

$$\begin{aligned} \Phi_u &= AR + DRP \\ \Phi_\varepsilon^1 &= AS + DRQ + V^1 \\ \Phi_\varepsilon^2 &= BS \end{aligned} \tag{4}$$

equation (3) must be fulfilled for all u_{t-1}, ε_t, ε_{t+1}. Therefore $\Phi_u = 0$, $\Phi_\varepsilon^1 = 0$, and $\Phi_\varepsilon^2 = 0$, and matrices P, Q, R, S forming the solution (2) are determined by matrix equations:

$$0 = \Phi_u = AR + DRP \tag{5}$$

and

$$0 = \Phi_\varepsilon^1 = AS + DRQ + V^1 \quad 0 = \Phi_\varepsilon^2 = BS \tag{6}$$

We call the equation (5) the deterministic part and equations under (6) the stochastic part. In this paper we concentrate on solution to the deterministic part.

Definition 1.2 We call matrices M, N respectively a right range matrix and a right null matrix of a matrix A, if M, N have full column rank, and columns of M, N spans the right range space and the right kernel of the matrix A.

Definition 1.3 We call matrices M, N respectively a left range matrix and a left null matrix of a matrix A, if M, N have full row rank, and rows of M, N spans the left range space and the left kernel of the matrix A.

II. THE BASIC ALGORITHM

In this section we briefly present a method of solving the matrix equation $AR + DRP = 0$ for a regular matrix pair (A, D).

Theorem 2.1 The generalized Schur decomposition. For any square matrices $\mathcal{A}, \mathcal{B} \in R^{n \times n}$ there exist orthogonal matrices Q, Z, and real matrices R_A, R_B, such that R_B is upper-triangular, R_A is quasi-upper triangular and

$$\mathcal{A}Z = QR_A \qquad \mathcal{B}Z = QR_B$$

Additionally, eigenvalues of R_A, R_B can be sorted in any order.

Let us assume that a matrix pair (A, D) is regular[1]. Let us consider the generalized Schur decomposition of the matrix pair (A, D)

$$AZ = QT_A \qquad DZ = QT_D \tag{7}$$

where matrices Q and Z are orthogonal, the matrix T_A is quasi-upper triangular, and the matrix T_D is upper triangular. Such a decomposition always exists. Let λ_i^A, λ_i^D are i-th eigenvalues of T_A and T_D respectively.

Proposition 2.2 If the matrix pair (A, D) is regular and $\lambda_i^D = 0$, then $\lambda_i^A \neq 0$.

[1] This assumption guarantees that the Schur decomposition is numerically stable. In opposite case a matrix pair (A, D) has infinitely many eigenvalues. Small perturbations of (A, D) may drastically change matrices T_A and T_D.

Let $\lambda_i = \lambda_i^A / \lambda_i^D$. Let us sort eigenvalues of T_A and T_D is such a way that all eigenvalues λ_i, such that $|\lambda_i| < 1$ appears in left upper block of T_A and T_D. Then

$$\begin{aligned} [Q_s \quad Q_u]\begin{bmatrix} R_A & T_{12}^A \\ 0 & T_{22}^A \end{bmatrix} &= A[Z_s \quad Z_u] \\ [Q_s \quad Q_u]\begin{bmatrix} R_D & T_{12}^D \\ 0 & T_{22}^D \end{bmatrix} &= D[Z_s \quad Z_u] \end{aligned} \tag{8}$$

where R_A is quasi-upper triangular, R_D is upper-triangular, both matrices have the same size. This implies

$$AZ_s = Q_s R_A \qquad DZ_s = Q_s R_D \tag{9}$$

The matrix R_D is invertible by construction. Thus,

$$AZ_s = DZ_s (R_D)^{-1} R_A$$

Then we can take

$$P = -(R_D)^{-1} R_A \qquad R = Z_s \tag{10}$$

Proposition 2.3 The following conditions hold:

1. $\ker DR = 0$
2. T_{22}^A is an invertible matrix.
3. R is a stable matrix.

Proposition 2.4 If the matrix pair (A, D) is regular, then

1. the matrix $[A \quad DR]$ has full row rank
2. $null([A \quad DR]) = col(R, P)$

III. Reduction of size the eigenvalue problem

Usually the matrix D has large null space especially in case of large models. We can use this property to decrease computation cost of solving the problem (5).

Let $M = col(M_1, M_2)$ be an orthogonal matrix such that

$$MD = \begin{bmatrix} \widetilde{D}_1 \\ 0 \end{bmatrix} \equiv \widetilde{D} \tag{11}$$

where $\widetilde{D}_1$ has full row rank, and let $MA = col(\tilde{A}_1, \tilde{A}_2) \equiv \tilde{A}$ be the corresponding partition of the matrix MA. Then we have

$$\tilde{A}_1 R + \widetilde{D}_1 RP = 0$$
$$\tilde{A}_2 R = 0$$

Hence $R \in \ker \tilde{A}_2$, and there exists a T such that $R = NT$, where $N = null\tilde{A}_2$, and

$$(\tilde{A}_1 N)T + (\widetilde{D}_1 N)TP = 0 \tag{12}$$

Theorem 3.1 If the matrix pair (A, D) is regular, then matrices $\tilde{A}_1 N$ and $\widetilde{D}_1 N$ are square and the matrix pair $(\tilde{A}_1 N, \widetilde{D}_1 N)$ is regular. Additionally the matrix $\tilde{A}_2$ has full row rank.

By the theorem 3.1 instead of solving the problem (5) we can solve the problem (12) with respect to T and P as in section 2, and

$$R = NT \tag{13}$$

If $\ker \tilde{B}_1 N \neq 0$, then we can repeat this procedure.

IV. Block structure of the problem

Definition 4.1 A square matrix A of size $n \times n$, $n > 0$, is called indecomposable if there are no permutation matrices P, Q, such that

$$PAQ = \begin{bmatrix} A_{11} & A_{12} \\ 0 & A_{22} \end{bmatrix}$$

where A_{11}, A_{22} are square matrices of size $r \times r$ and $(n - r) \times (n - r)$ respectively, where $1 \leq r < n$.

Theorem 4.2 Block triangular form of a matrix. For any matrix A there exists permutation matrices P, Q, such that PAQ has the block upper triangular form

$$PAQ = \begin{bmatrix} A_u & X & X \\ 0 & A_s & X \\ 0 & 0 & A_o \end{bmatrix}$$

where A_u is an underdetermined matrix of size $m_u \times n_u$, A_s is a square matrix of size $m_s \times m_s$, A_o is an overdetermined matrix of size $m_o \times n_o$, X denote any matrix of appropriate dimension, and $n_u > m_u$ or $n_u = m_u = 0$, $n_o < m_o$ or $n_o = m_o = 0$, $m_s \geq 0$. Additionally if $m_s > 0$, then

$$A_s = \begin{bmatrix} A_{11} & \cdots & \cdots & A_{1k} \\ 0 & A_{22} & & \vdots \\ \vdots & \ddots & \ddots & \vdots \\ 0 & \cdots & 0 & A_{kk} \end{bmatrix} \tag{14}$$

where A_{ii}, $i = 1, \ldots, k$ is a square indecomposable matrix.

Theorem 4.3 Block triangular form of a square structurally nonsingular matrix. Block triangular form of a square structurally nonsingular matrix A as in (4.2) does not contain underdetermined part (A_u) and overdetermined part (A_o), i.e. there exists permutation matrices P, Q, such that PAQ has the form (14).

Proposition 4.4 If the matrix pair (A, D) is regular, then $|A| + |D|$ is a square, structurally nonsingular matrix.

By the proposition 4.4 and 4.3 we can find a permutation matrices P, Q, such that $P(|A| + |D|)Q$ has the block triangular form (14). Therefore matrices PAQ, PDQ also has the form (14). In rest of this section we assume, that matrices in (1) already have block triangular form (14) and for simplicity we assume, that $k = 2$, i.e.

$$A = \begin{bmatrix} A_{11} & A_{12} \\ 0 & A_{22} \end{bmatrix} D = \begin{bmatrix} D_{11} & D_{12} \\ 0 & D_{22} \end{bmatrix} \tag{15}$$

where each diagonal block A_{ii}, D_{ii} for $i = 1,2$ is square. Regularity of the matrix pair (A, D) implies regularity of each diagonal block (A_{ii}, D_{ii}) for $i = 1,2$.

Proposition 4.5 If matrices A, D have block triangular form (15), then there exist a solution to (1) in the form (2), where

$$R = \begin{bmatrix} R_{11} & R_{12} \\ 0 & R_{22}\Sigma \end{bmatrix}$$

where P_{ii}, R_{ii} solve the diagonal problem $A_{ii} R_{ii} + D_{ii} R_{ii} P_{ii} = 0$ for $i = 1,2$ and Σ is an invertible matrix.

Proposition 4.6 Let LN denote a block triangular matrix

$$LN = \begin{bmatrix} LN_{11} & LN_{12} \\ 0 & LN_{22} \end{bmatrix}$$

where LN_{11}, LN_{22} is a left null matrix of the matrix D_{11} and D_{22} respectively, and LN_{12} solves

$$LN_{11} D_{12} R_{22} + LN_{12} D_{22} R_{22} = 0 \tag{16}$$

Then $LNDR = 0$. Moreover, solution to (16) always exists.

Let LM denote

$$LM = \begin{bmatrix} LM_{11} & 0 \\ 0 & LM_{22} \end{bmatrix}$$

where LM_{ii} is a left range matrix of the matrix D_{ii} for $i = 1,2$. Observe, that LM is a left range matrix of the matrix D. Let $L = col(LM, LN)$.

Proposition 4.7 The matrix $L = col(LM, LN)$ is invertible.

Since the matrix L is invertible, matrix equation (5) is equivalent to $0 = LAR + LDRP$:

$$0 = LM \times AR + LM \times DRP \quad (17)$$

$$0 = LN \times AR + LN \times DRP \quad (18)$$

by proposition 4.6, $LN \times DRP = 0$, therefore

$$R = RN \times \tilde{R} \quad (19)$$

for some matrix $\tilde{R}$, where RN is a right null matrix of the matrix $LN \times A$.

Proposition 4.8

$$RN = \begin{bmatrix} RN_{11} & RN_{12} \\ 0 & RN_{22} \end{bmatrix}$$

where RN_{11}, RN_{22} is a right null matrix of the matrix $LN_{11}A_{11}$ and $LN_{22}A_{22}$ respectively, and RN_{12} solves

$$\begin{aligned} 0 \quad &= LN_{11}A_{11} \times RN_{12} + LN_{11}A_{12}RN_{22} \\ &+ LN_{12}A_{22}RN_{22} \end{aligned} \quad (20)$$

Equation (20) has at least one solution RN_{12}.

Let $\tilde{A} = LM \times A \times RN$, $\widetilde{D} = LM \times D \times RN$. We have

$$\tilde{A} \equiv \begin{bmatrix} \tilde{A}_{11} & \tilde{A}_{12} \\ 0 & \tilde{A}_{22} \end{bmatrix} \quad (21)$$

$$\widetilde{D} \equiv \begin{bmatrix} \widetilde{D}_{11} & \widetilde{D}_{12} \\ 0 & \widetilde{D}_{22} \end{bmatrix} \quad (22)$$

where

$$\begin{aligned} \tilde{A}_{11} &= LM_{11}A_{11}RN_{11} \\ \tilde{A}_{12} &= LM_{11}(A_{11}RN_{12} + A_{12}RN_{22}) \\ \tilde{A}_{22} &= LM_{22}A_{22}RN_{22} \end{aligned}$$

and

$$\begin{aligned} \widetilde{D}_{11} &= LM_{11}D_{11}RN_{11} \\ \widetilde{D}_{12} &= LM_{11}(D_{11}RN_{12} + D_{12}RN_{22}) \\ \widetilde{D}_{22} &= LM_{22}D_{22}RN_{22} \end{aligned}$$

Consider generalized Schur decomposition in the form (8) of regular matrix pairs $(\tilde{A}_{ii}, \widetilde{D}_{ii})$ for $i = 1,2$:

$$\begin{aligned} [Q_s^i \quad Q_u^i] \begin{bmatrix} R_A^i & T_{12}^{Ai} \\ 0 & T_{22}^{Ai} \end{bmatrix} &= \tilde{A}_{ii} [Z_s^i \quad Z_u^i] \\ [Q_s^i \quad Q_u^i] \begin{bmatrix} R_D^i & T_{12}^{Di} \\ 0 & T_{22}^{Di} \end{bmatrix} &= \widetilde{D}_{ii} [Z_s^i \quad Z_u^i] \end{aligned} \quad (23)$$

Let

$$Q = \begin{bmatrix} Q_s^1 & Q_u^1 & 0 & 0 \\ 0 & 0 & Q_s^2 & Q_u^2 \end{bmatrix}$$

$$Z = \begin{bmatrix} Z_s^1 & Z_u^1 & 0 & 0 \\ 0 & 0 & Z_s^2 & Z_u^2 \end{bmatrix}$$

Then

$$\begin{aligned} Q'\tilde{A}Z &= \begin{bmatrix} R_A^1 & T_{12}^{A1} & \tilde{A}_{12}^{ss} & \tilde{A}_{12}^{su} \\ 0 & T_{22}^{A1} & \tilde{A}_{12}^{us} & \tilde{A}_{12}^{uu} \\ 0 & 0 & R_A^2 & T_{12}^{A2} \\ 0 & 0 & 0 & T_{22}^{A2} \end{bmatrix} \\ Q'\widetilde{D}Z &= \begin{bmatrix} R_D^1 & T_{12}^{D1} & \widetilde{D}_{12}^{ss} & \widetilde{D}_{12}^{su} \\ 0 & T_{22}^{D1} & \widetilde{D}_{12}^{us} & \widetilde{D}_{12}^{uu} \\ 0 & 0 & R_D^2 & T_{12}^{D2} \\ 0 & 0 & 0 & T_{22}^{D2} \end{bmatrix} \end{aligned} \quad (24)$$

where $\tilde{A}_{12}^{pq} = (Q_p^1)'\tilde{A}_{12}Z_q^2$, $\widetilde{D}_{12}^{pq} = (Q_p^1)'\widetilde{D}_{12}Z_q^2$ for $p, q \in \{s, u\}$.

Observe, that (24) is the generalized Schur decomposition of the matrix pair $(\tilde{A}, \widetilde{D})$. However we need to swap second and third block in order to obtain the generalized Schur decomposition in the form (8). Since spectra of $(T_{22}^{A1}, T_{22}^{D1})$ and (R_A^2, R_D^2) are disjoint, we can always do that. Let U, V denote orthogonal matrices, such that

$$\begin{aligned} U' \begin{bmatrix} \bar{R}_A^2 & \bar{A}_{12}^{us} \\ 0 & \bar{T}_{22}^{A1} \end{bmatrix} V &= \begin{bmatrix} T_{22}^{A1} & \tilde{A}_{12}^{us} \\ 0 & R_A^2 \end{bmatrix} \\ U' \begin{bmatrix} \bar{R}_D^2 & \bar{D}_{12}^{us} \\ 0 & \bar{T}_{22}^{D1} \end{bmatrix} V &= \begin{bmatrix} T_{22}^{D1} & \widetilde{D}_{12}^{us} \\ 0 & R_D^2 \end{bmatrix} \end{aligned} \quad (25)$$

where $\lambda(\bar{R}_A^2, \bar{R}_D^2) = \lambda(\bar{R}_A^2, R_D^2)$ and $\lambda(\bar{T}_{22}^{A1}, \bar{T}_{22}^{D1}) = \lambda(T_{22}^{A1}, T_{22}^{D1})$. Here $\lambda(\cdot,\cdot)$ denotes the set of generalized eigenvalues of a matrix pair. Let $\bar{U} = diag(I, U, I)$, $\bar{V} = diag(I, V, I)$. Let $\bar{Q} = Q\bar{U}$, $\bar{Z} = Z\bar{V}$. Then

$$\begin{aligned} \bar{Q}'\tilde{A}\bar{Z} &= \begin{bmatrix} R_A & T_{12}^A \\ 0 & T_{22}^A \end{bmatrix} \\ \bar{Q}'\widetilde{D}\bar{Z} &= \begin{bmatrix} R_D & T_{12}^D \\ 0 & T_{22}^D \end{bmatrix} \end{aligned} \quad (26)$$

where R_A, T_{22}^A are quasi-upper triangular matrices, R_D, T_{22}^D are upper triangular matrices, $\lambda(R_A, R_D) = \lambda(R_A^1, R_D^1) \cup \lambda(R_A^2, R_D^2)$, $\lambda(T_{22}^{'} T_{22}^D) = \lambda(T_{22}^{A1}, T_{22}^{D1}) \cup \lambda(T_{22}^{A2}, T_{22}^{D2})$, and $\bar{Q}$, $\bar{Z}$ are orthogonal matrices. Hence, (26) is the generalized Schur decomposition of the matrix pair $(\tilde{A}, \widetilde{D})$ in the form (8). Let $\bar{Z} = [\bar{Z}_1, \bar{Z}_2]$ be a partition of the matrix $\bar{Z}$, where number of columns of $\bar{Z}_1$ is equal to the number of columns of R_D. Then solution matrices $\tilde{R}$, P are given by

$$\tilde{R} = \bar{Z}_1 \qquad P = -(R_D)^{-1}R_A \quad (27)$$

V. Implementation deails

The algorithms described in sections 4 and 3 are implemented in C++ using MATCL matrix library available at https://bitbucket.org/matcl/matcl and is a part of Morfa project.

A. Reordering to the block triangular form

The block triangular form of a matrix A in the form (4.2) can be found using the Dulmage-Mendelsohn decomposition of a bipartite graph associated with the matrix A. See [11] for details.

B. Finding null and range matrices

Consider the LU decomposition with rook pivoting of a (sparse) matrix A:

$$PAQ = L \times U \tag{28}$$

where P, Q are permutation matrices, L is unit lower triangular, and U is upper triangular in the form

$$U = \begin{bmatrix} U_{11} & U_{12} \\ 0 & 0 \end{bmatrix} \tag{29}$$

where U_{11} is an invertible matrix. Such decomposition is found using the LUSOL library [7].

As a right null matrix, RN, and a right range matrix, RM, we may take

$$RN = Q \begin{bmatrix} U_{11}^{-1} \times U_{12} \\ -I \end{bmatrix} \quad RM = Q \begin{bmatrix} I \\ 0 \end{bmatrix}$$

Let

$$L = \begin{bmatrix} L_{11} & 0 \\ L_{21} & L_{22} \end{bmatrix} \tag{30}$$

be the partition of the matrix L corresponding to the partition (29), where L_{11}, L_{22} are unit lower triangular matrices. As a left null matrix, LN, and a left range matrix, LM, we may take

$$\begin{aligned} LN &= [L_{21} \times L_{11}^{-1} \quad -I]P \\ LM &= [I \quad 0]P \end{aligned} \tag{31}$$

C. Solution to equation (16)

Consider the equation (16), i.e.

$$LN_{11}D_{12}R_{22} + LN_{12}D_{22}R_{22} = 0$$

Without loss of generality we can assume, that $LN_{12} = Y \times LM_{22}$, where LM_{22} is a left range matrix of D. Additionally, from (13), $R_{22} = RN_{22} \times T_{22}$ for some matrix T_{22}. Therefore the matrix Y solves

$$LN_{11}D_{12}R_{22} + Y \times (LM_{22}D_{22}RN_{22})T_{22} = 0$$

By (22), $LM_{22}D_{22}RN_{22} = \tilde{D}_{22}$. From the generalized Schur decomposition (23), and since $T_{22} = Z_s^2$ (see 10), we obtain

$$(LM_{22}D_{22}RN_{22})T_{22} = Q_s^2 R_D^2$$

Hence,

$$Y \times Q_s^2 = -LN_{11}D_{12}R_{22} \times (R_D^2)^{-1}$$

and as Y we may take $Y = -LN_{11}D_{12}R_{22} \times (R_D^2)^{-1} \times (Q_s^2)'$. Finally:

$$LN_{12} = -LN_{11}D_{12}R_{22} \times (R_D^2)^{-1}(Q_s^2)'LM_{22}$$

D. Computing the generalized Schur decomposition

The generalized Schur decomposition (7) of a regular matrix pair (A, D) can be computed using Lapack's DGGHRD and DGGES functions. Required eigenvalues reordering can be computed using the Lapack's DTGSEN function (see [2]). We use however more efficient algorithm presented in [1] and [10].

E. Matrix multiplication

Efficiency of a chained matrix multiplication

$$A_1 \times A_2 \times \ldots \times A_k \tag{32}$$

highly depends on order in which multiplication of two matrices is performed. Efficient sequence of matrix multiplications is determined by solving a dynamic programming problem.

VI. Related work

Since Blanchard and Kahn, 1980 [6] a number of alternative approaches for solving linear stochastic optimal control problems have emerged including the Anderson-Moor algorithm [4], the Sims' QZ method [12], the Klein's method [9], the Uhlig's method [13], and others. Numerical experiments conducted in [3] shows, that among methods [4], [12], [9], [13], the Anderson-Moor algorithm is usually the fastest and the most accurate.

All these methods, except the Anderson-Moor algorithm, solve the deterministic part using the generalized Schur decomposition (or the QZ decomposition), similarly as in the basic algorithm presented in section II.

To our knowledge, the algorithms of reduction of size of the eigenvalue problem, presented in section III and the algorithm for solving block triangular problems, presented in section IV are new.

VII. Numerical experiments

In this section we analyze efficiency and stability of presented algorithms applied to a large scale DSGE model. We consider the Memo III model [5] - a large scale multisector dynamic stochastic general equilibrium model that was constructed for the purpose of CO2 reduction policy assessment. This model, when represented in the form (1) has 7906 endogenous variables y and 130 shock variables ε.

In table I we compare the blocked (4) and unblocked (3) algorithm. The column time presents total time measured in seconds required to solve the model using given algorithm. The column r_d reports norms of residuals: $r_d = \| AR + DRP \|_1$, where R, P, form the solution obtained by given algorithm. Coefficient R_d is defined as $R_d = \| |A||R| + |D||R||P| \|_1$. Coefficient r_d/R_d gives insights about the backward stability of the blocked and unblocked algorithm. Performance and accuracy of the unblocked and blocked algorithm

TABLE I.

algorithm	time	r_d	R_d	r_d/R_d
unblocked	2.36	3.39e-13	2.25e2	1.50e-15
blocked	0.647	2.07e-10	2.21e5	9.36e-16

Computation is performed on Intel Core i5-7200U CPU @ 2.50GHz with two physical cores. Peak performance in double precision on a single core is 40 GFLOPS.

Table I shows, that both blocked and unblocked algorithm is able to solve a large optimal control problem in very short time. The blocked algorithm is substantially faster. The accuracy measure r_d/R_d suggests, that both algorithms are numerically stable. However in order to draw definite conclusion, much more detailed analysis is required. In the blocked algorithm, the consider three blocks as in (14), where the second block is the biggest irreducible block in decomposition the (14).

Table II presents a split of total computation cost of the blocked algorithm. Structure of computation cost of the blocked algorithm

TABLE II.

step	share
finding the block triangular form (14)	0.0285
reduction of diagonal subproblems	0.0548
forming the gen. Schur of diagonal blocks	0.6887
finding off-diagonal elements (20), (16)	0.1210
reordering the gen. Schur decomposition	0.0213
solving the stochastic problem	0.0813
other	0.0044
total	1.0000

Most of the computation cost is associated with finding the generalized Schur decomposition of diagonal blocks in the form (25). This shows, that the blocked algorithm can be highly efficient if the block triangular representation of the problem (14) consists of many small irreducible blocks. Cost of solving the stochastic problem (6) is low.

VIII. References

[1] Björn Adlerborn, Bo Kågström, and Daniel Kressner. A parallel qz algorithm for distributed memory hpc systems. SIAM Journal on Scientific Computing, 36(5):C480–C503, 2014.

[2] Edward Anderson, Zhaojun Bai, Christian Bischof, L Susan Blackford, James Demmel, Jack Dongarra, Jeremy Du Croz, Anne Greenbaum, Sven Hammarling, Alan McKenney, et al. LAPACK Users' guide. SIAM, 1999.

[3] Gary S Anderson. Solving linear rational expectations models: A horse race. Computational Economics, 31(2):95–113, 2008.

[4] Gary Anderson and George Moore. A linear algebraic procedure for solving linear perfect foresight models. Economics letters, 17(3):247–252, 1985.

[5] Marek Antosiewicz and Pawel Kowal. Memo III - a large scale multi-sector dsge model. IBS: Warsaw, Poland, 2016.

[6] Olivier Jean Blanchard and Charles M Kahn. The solution of linear difference models under rational expectations. Econometrica: Journal of the Econometric Society, pages 1305–1311, 1980.

[7] Philip E Gill, Walter Murray, Michael A Saunders, and Matgaret H Wright. Maintaining lu factors of a general sparse matrix. Linear Algebra and its Applications, 88:239–270, 1987.

[8] Judd, Kenneth L., and Kenneth L. Judd. Numerical methods in economics. MIT press, 1998.

[9] Paul Klein. Using the generalized schur form to solve a multivariate linear rational expectations model. Journal of Economic Dynamics and Control, 24(10):1405–1423, 2000.

[10] Daniel Kressner. Block algorithms for reordering standard and generalized schur forms. ACM Transactions on Mathematical Software (TOMS), 32(4):521–532, 2006.

[11] Alex Pothen and Chin-Ju Fan. Computing the block triangular form of a sparse matrix. ACM Transactions on Mathematical Software (TOMS), 16(4):303–324, 1990.

[12] Christopher A Sims. Solving linear rational expectations models. Computational economics, 20(1):1–20, 2002.

[13] Harald F Uhlig et al. A toolkit for analyzing nonlinear dynamic stochastic models easily. 1995.

[14] Sébastien Villemot et al. Solving rational expectations models at first order: what dynare does. Technical report, Citeseer, 20

ProLab: A New Process Mining Tool

İsmail Yürek
Graduate School of Natural and Applied Sciences
Dokuz Eylül University
İzmir, Turkey
ismail.yurek@gmail.com

Derya Birant
Department of Computer Engineering
Dokuz Eylül University
İzmir, Turkey
derya@cs.deu.edu.tr

***Abstract*—Process mining is a technique in the fields of both data mining and process management that provides the extraction of knowledge from event logs available in information systems. Every day information systems collect different kind of process instances of a business flow. As time goes on, size of collected data builds up speedily and constitutes a huge volume of data. It is a very challenging task to obtain valuable information and features of processes from such a large volume of data. In this paper, we propose a process mining tool, named ProLab, which constructs a process model from event logs and incorporate the execution records of ongoing processes into discovered process model instantly. Our goal is to develop a process mining tool which is able to work on large volume of event logs and handle the execution records of ongoing processes in a short time with low resource usage. This paper explains competitive advantages of ProLab over existing tools.**

Keywords—business process management; process mining; process model; pattern discovery

I. INTRODUCTION

Processes exist in many areas of the life such as health care, education, business operations, transportation, manufacturing, and others. In our daily lives and business lives, we are involved in various processes. These processes are recorded by information systems with information regarding the executed activities. These recorded execution traces are called as event logs. Event logs contain different types of important information about the processes. Event logs are analyzed under several aspects with the help of process mining algorithms. Process mining is a technical way to acquire information in order to analyze, discover, improve and manage the processes from event logs that contain elaborative materials about the history of business operations.

Every day an information system captures business operations; therefore the volume of data that event logs contain increases rapidly. This large data increase scales up the discovery time and causes performance problems. In general, current process mining tools analyze historical data. Incorporation of ongoing or newly completed process records has a major importance in terms of keeping the process model constantly up-to-date. Updating the process model instantly will provide the ability to see the problems in the progressive process records immediately.

Our goal is to develop a process mining tool which is able to work on large volume of event logs and incorporate the execution records of ongoing processes into discovered process model in a short time with low memory usage, and also support an interactive environment for process mining to give deep insights for event logs.

The main contributions of this paper can be summarized as three-fold: firstly, a novel tool, named ProLab, is proposed to analyze the large volume of event logs; secondly, it also proposes an interactive environment for process mining to give deep insights for event logs; lastly, it demonstrates the proposed tool on both real-life and experimental datasets to evaluate in terms of running time and memory usage.

The rest of the article is structured as follows: Section II summarizes the related literature and previous works on the subject. Section III explains the proposed process mining tool (ProLab) in detail. It describes the capabilities of the proposed tool and explains competitive advantages of ProLab over existing tools. It also gives a case study to demonstrate that ProLab has the option of advanced settings to perform detailed analysis from different point of views. In Section IV, experimental study is presented and the obtained experimental results are discussed. Finally, Section V presents some concluding remarks and future directions.

II. RELATED WORKS

At the end of the 90's, process mining concept began to become popular. A new approach was presented by Agrawal et al. [1] which copes with parallel structure and noise to expand the utility of actual workflow systems. With the help of this approach, the user is able to use existing event logs to model a given business process as a graph. Cook and Wolf [2] stated different techniques for process discovery and generated formal models based on the actual process executions.

The α-algorithm which is one of the most known process mining algorithms was introduced by Van der Aalst et al. [3] to discover a large and relevant class of workflow processes. This algorithm analyzes the event log, and then constructs various dependency relations between tasks. The goal of the α-algorithm is to analyze different kinds of workflow logs in the presence of noise and without any knowledge of the underlying process. Cook and Wolf [4] used probabilistic methods during the study about finding concurrent models of system behavior from event logs. Herbst and Karagiannis [5] was interested in duplicate tasks and they presented an algorithm based on an inductive manner in two steps: (i) induction and (ii) Stochastic Task Graph (SAG) generation. The SAG is converted to a blocked structured model using a definition language. Schimm [6] offered an approach to get an accurate model from event

logs. This approach deals with hierarchically structured workflow models that include the splits and joins.

Dongen and van der Aalst [7] specified a standard for storing event logs by introducing a data model and an XML format called MXML (Mining eXtensible Markup Language).

Weijters et al. [8] came up with an algorithm, called Heuristics Miner, which discovers main behavior registered in a noisy event log by including different threshold parameters in order to overcome two problems: noise and low frequency behavior.

Günther and van der Aalst [9] focused on existing problems in the traditional process mining methods when the processes are large and less-structured. In order to manage the problems, they built up a flexible approach based on their previous work [10]: Fuzzy Mining. Their approach analyzes, simplifies and visualizes mined process models based on the metrics significance and correlation of graph elements.

Fahland and van der Aalst [11] simplified discovered process models and demonstrated a post-processing approach to check the balance between overfitting and underfitting. They detailed the discovered process model in Petri net. Their approach can be combined with any process discovery method which generates Petri net.

Aleem et al. [12] proposed the comparison of different process mining methods in detail. The paper collects and shows all efficient and qualitative results of business process mining for researchers. Their article groups the process mining approaches to five sections: deterministic, heuristic, inductive, genetic and clustering-based mining approaches. Cheng and Kumar [13] suggested a method to eliminate noisy traces from event logs by way of building a classifier and applying classifier rules on event logs. They indicated that produced mined models from such preprocessed logs are superior on several evaluation metrics. Fahland and van der Aalst [14] investigated the problem of repairing discovered process model to align them to reality. They separated the event log into different sublogs of nonfitting traces to make conformance checking. Rovani et al. [17] demonstrated a methodology so as to analyze medical treatment processes through displaying how to apply process mining methods based on declarative models.

De Leoni at al. [16] suggested a framework to unify a number of approaches for correlation analysis. They tried to correlate different process characteristics related to different perspective. Mannhardt et al. [17] offered a process mining algorithm to control process conformance with respect to control flow, data dependencies, resource assignments and time constraints. Pika et al. [18] represented an approach which is based on the analysis of information about process executions recorded in event logs. They demonstrated a supporting tool to assess the overall risk of process and to forecast process outcomes.

Suriadi et al. [19] specified a set of data quality issues and suggested a patterns-based way to clean noisy event logs. Mitsyuk et al. [20] proposed a tool to produce event logs from Business Process Model and Notation (BPMN). They implemented script-based gateways and choice preferences to handle control flow. Bolt et al. [21] addressed the problem of comparing different variants of the same process and observed differences in behavior and business rules. They used transition systems which were annotated with measurements to model behavior and to underline differences.

Yürek et al. [22] proposed a novel algorithm, named Interactive Process Miner (IPM), that has the capabilities of working on huge volume of event logs and managing the execution records of running process instances to generate process model in a short time with high precision and fitness values and holds three different features, including activity deletion, aggregation and addition operations on the process model to support a simulation environment for users.

Process mining tools named as Little Thumb, EMiT and ProM are developed by Van der Aalst and his team. Little Thumb can get workflow nets from noisy and uncompleted logs [10]. EMiT can convey workflow models with Petri nets [23]. ProM is a generic open-source framework for implementing process mining projects that contains many packages with many plug-ins [24].

Differently from the previous studies, this paper proposes a novel tool to analyze large volume of event logs and to handle the execution records of running process instances in a short time with low memory usage, and also support an interactive environment for process mining to give deep insights for event logs.

III. ProLab: Process Mining Tool

There is a need for a software tool in order to analyze the process records and to extract the statistical information from event logs. This process mining tool should be able to work with low resource consumption on the large amount of event logs. An XML-based file called Mining eXtensible Markup Language (MXML) has been standardized to store event logs which is used in process mining. Thus, a general input format is provided for different process mining techniques and tools. In this study, our aim is to develop a process mining tool which is able to work with low resource consumption on huge amount of event logs and to provide an interactive environment for users.

A. Block Diagram of the Tool

The block diagram of the process mining tool we developed is shown in Figure 1. Event logs in MXML format are read using the file streaming method, so it is possible to read the event logs without loading the whole file into memory. The statistical information obtained from event logs during streaming is stored in a data structure. This data structure describes the summary information that will be used in process mining.

The process mining algorithm is executed on the data structure that holds the statistical information and a process model is created that represents the process flows. The generated process model is a summary information of the event logs. By visualizing the generated process model, this summary information is displayed to the user with a graphical interface. With the help of settings, users can filter both the event logs and change the visual appearance of the process model. These

features allow users to perform a detailed analysis on the event logs.

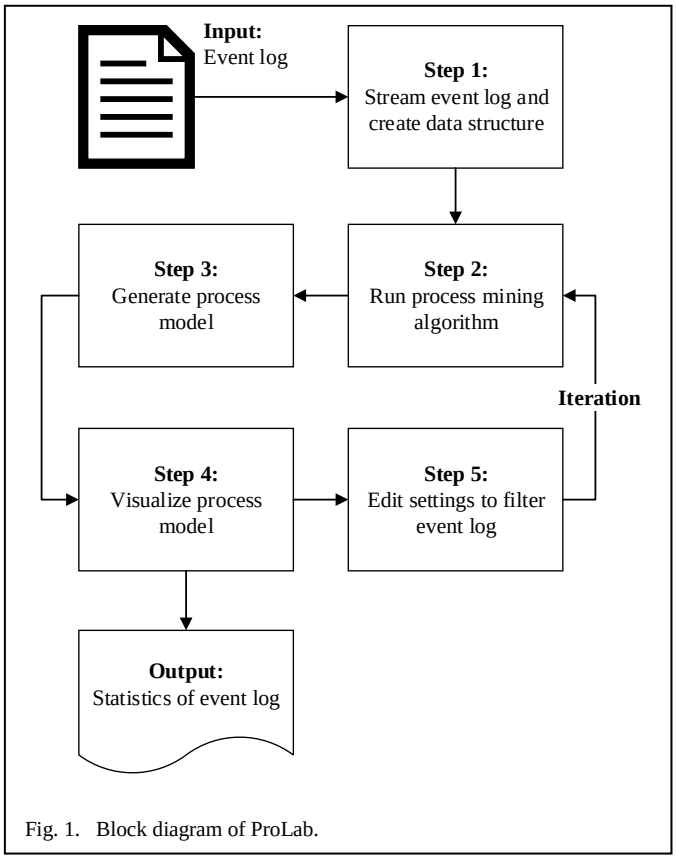

Fig. 1. Block diagram of ProLab.

In addition to visualization of the process model, statistical information about the event logs is presented to the user through a dashboard page with graphics and tables. With this dashboard page, users can get deep insights about the process flows.

B. Comparison of the Tool

Academic and commercial tools have been developed for process mining techniques. While ProM tool is used for academic purposes, Disco and Celonis tools are commercial software products developed by different companies. Table I presents the comparison of process mining tools.

The proposed tool, ProLab, uses streaming method to read event log files, while other tools work by loading the event logs into memory. Their methods lead to the problem of memory insufficiency in very large volume of event logs. All the tools visualize the representation of generated process model after analyzing the event logs. Disco, Celonis and ProLab tools play with the adjustment of visual settings, allowing quick access to desired information. All applications, except ProM, support to make visual adjustments and give detailed statistics of event logs on a dashboard page by using graphics and data tables so that the desired information can be accessed quickly.

In contrast to other tools, only the proposed tool provides an interactive environment for the users. This interactive environment allows the user to merge, delete, or add a new activity in the event logs. The user can immediately see the effects of this change on the process flows.

While *offline fashion* is a method to analyze the processes by using the historical event logs, *online fashion* is called instantaneous analysis of event records formed by ongoing process records. ProLab has the ability to analyze the processes with both offline and online fashion.

TABLE I. COMPARISON OF PROCESS MINING TOOLS

	ProM	**Disco**	**Celonis**	**ProLab**
Streaming	No	No	No	Yes
Model visualization	Yes	Yes	Yes	Yes
Visualization settings	No	Yes	Yes	Yes
Insights	No	Yes	Yes	Yes
Interactive environment	No	No	No	Yes
Offline fashion	Yes	Yes	Yes	Yes
Online fashion	No	No	No	Yes

C. Case Study

Table II shows an example event logs. Each row in the table represents a completed process flow. A, B, C, D, E, F in the process flow are the names of the activities that can take place in the process execution.

TABLE II. SAMPLE EVENT LOGS

Case ID	**Events**
Case 1	ABCDF
Case 2	ACDEF
Case 3	ACBDF
Case 4	ABEF
Case 5	ABCDF
Case 6	ABCDF
Case 7	ACBDF
Case 8	ACDEF
Case 9	ACBDF
Case 10	ACDEF
Case 11	ABCDF
Case 12	ABEF
Case 13	ACDEF
Case 14	ABCDF

The proposed tool, ProLab, has the option of advanced settings to perform detailed analysis from different point of views. *Case Frequency* and *Activity Frequency* options are available for filtering event logs.

The process instance, ABCDF, in the example event log repeated 5 times and the frequency is 35.71%. The second process instance, ACDEF, repeated 4 times and the frequency is %28.57. The third process instance, ACBDF, repeated 3

times and the frequency is %21.42. The last process instance, ABEF, repeated 2 times and the frequency is %14.28. When *Case Frequency* value is set to 15%, the process instance, ABEF, will be ignored in analysis. *Activity Frequency* filter allows filtering of activities A, B, C, D, E and F according to the ratio of the total number of activities in the event log.

The resulting process model that is created based on analysis can be drawn to show the frequency or time information. When it is desired to draw according to frequency value, there are two options. One of these options is *Absolute Frequency* that expresses total activity count and the other one is *Case Frequency* that expresses the activity count per case.

There are 4 different options when it is desired to draw the generated process model according to time value: (i) *total duration* refers to total time, (ii) *mean duration* refers to average time, (iii) *min duration* refers to minimum time and (iv) *max duration* refers to maximum duration in event logs. During visualization, different colors are used, which are divided into 5 categories for shapes. Thanks to this method, both the colored shapes and the numbers make the process model more understandable.

Figure 2 denotes the analysis that is performed on repair data set. The *Case Frequency* value for the analysis is defined as 10%, and the *Activity Frequency* value is defined as 20%. An analysis is performed for the frequency values of the activities and the *Absolute Frequency* option is marked. Frequency values are shown on the activities and on the edges that link the activities. The colors of the activities and edges vary depending on the value of frequency. Moreover, the edge thicknesses also vary depending on the value of dependency size of the activities.

IV. Experimental Results

To evaluate the developed tool, we performed experimental test by using 2.4 GHz quad core processor, 16GB RAM. The code was implemented in Java platform. Traffic [25], hospital [26] and repair datasets [27] are used to test the developed tool. Table III shows the detailed information about these datasets.

TABLE III. Data Characteristics

Dataset	Traces	Events	Event Classes	Events per case			Event classes per case		
				Min	Mean	Max	Min	Mean	Max
Repair	1,104	11,855	12	4	11	24	4	12	12
Hospital	1,143	150,291	624	1	131	1,814	1	33	113
Traffic	150,370	561,470	11	2	4	20	2	4	10

The hospital dataset includes real-life event logs of the clinical treatment process of an academic hospital in the Netherlands. It consists of 1143 traces and 150291 events. Hospital dataset is composed of long and complex event logs, which are defined as Spaghetti. Traffic dataset includes event logs generated by an information system that performs road traffic control. It consists of 150370 traces and 561470 events. The repair dataset consists of synthetically created event logs

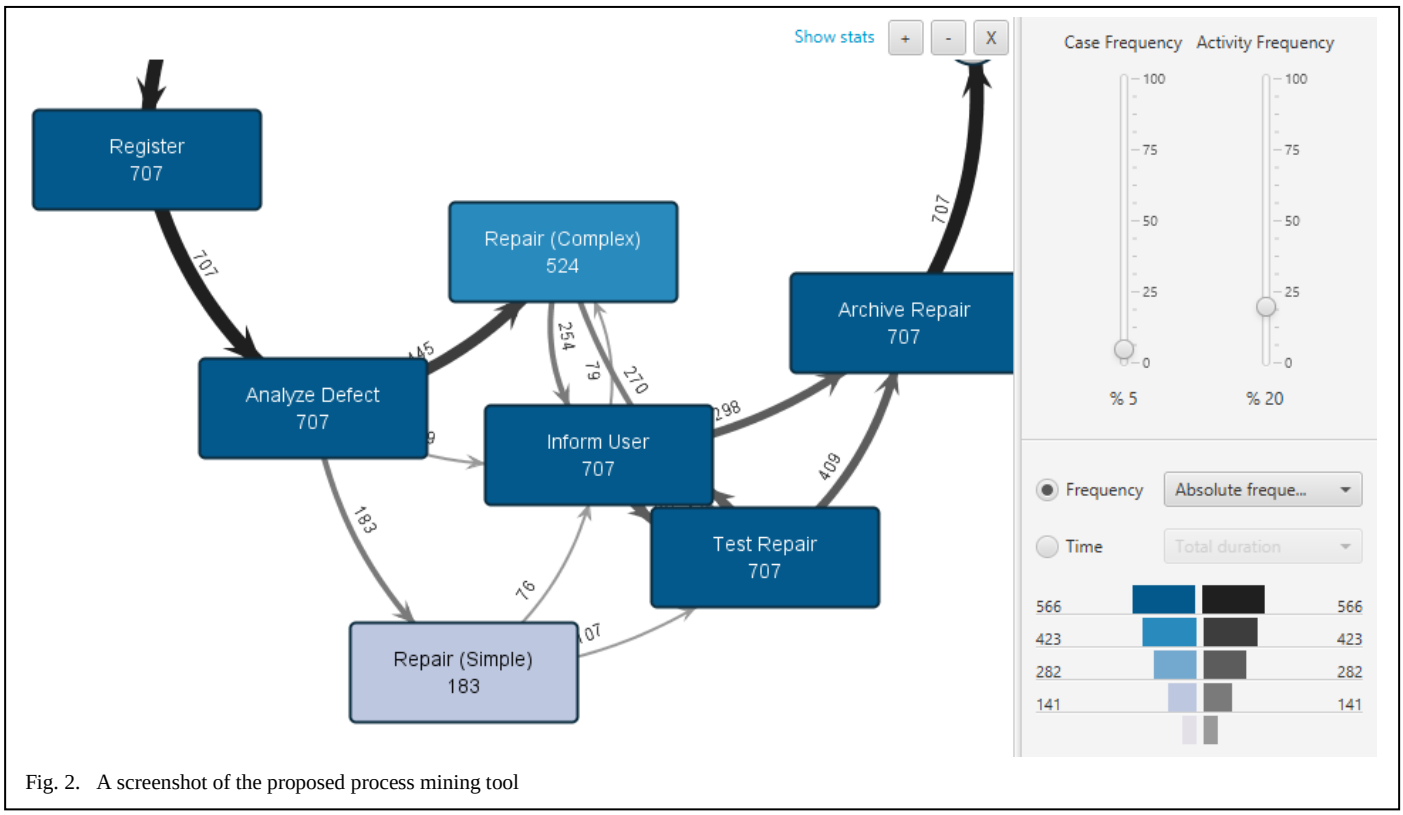

Fig. 2. A screenshot of the proposed process mining tool

for the telephone repair process. It consists of 1104 traces and 11855 events.

The experiment was executed on hospital, traffic and repair datasets to compare the running time and memory usage. The results of the experiment given in Table IV show the running time and memory usage of the developed tool for each datasets. The tool created the process model in 1 second by using 321 MB RAM on *repair* dataset and 5 seconds by using 745 MB RAM on *hospital* dataset and 17 seconds by using 826 MB RAM on *traffic* dataset. When we checked the running times and memory usage, we observed that the size of event logs increased the running time. The factor that affects the amount of memory usage is the complexity of the event logs and the length of each process instance. These two cases are the two most important factors affecting the size of the data structure in which summary information obtained from event logs. The results of the experiments point that it is possible to perform process analysis on a large volume of data by using limited resources with the developed process mining tool.

TABLE IV. PROLAB PERFORMANCE EVALUATION

Dataset	Log Size	Running Time	Memory Usage
Repair	3.31 MB	1 second	321 MB
Hospital	81.40 MB	5 seconds	745 MB
Traffic	176.00 MB	17 seconds	826 MB

V. CONCLUSION AND FUTURE WORKS

This paper proposes a novel process mining tool, named ProLab, that has the capabilities of working on a large volume of event logs and handling the execution records of running process instances to create process model in a short time and also supports an interactive environment for process mining to give deep insights for event logs.

The contribution of the proposed tool can be summarized as follows:

- Even though current tools analyze historical data, the purposed tool is able to analyze historical event logs as well as to incorporate the execution records of ongoing processes into the process model instantly.
- Experimental studies have proved that the proposed tool is able to analyze a large volume of event logs.
- The proposed tool enables for modification on the discovered process model. Thus, it provides to observe the effects of possible decisions to be taken in a simulation environment. It has an important feature in order to make the right decision and to observe possible problems in advance.

In the future, a new file format that takes less space for event logs can be created for ProLab. Thus, low-cost storage spaces for event logs will suffice. Furthermore, in order to make the process flow more understandable, a simulation framework can be developed which the event logs can be played as an animation within a predetermined time period.

REFERENCES

[1] R. Agrawal, D. Gunopulos, and F. Leymann, "Mining process models from workflow logs," Proceedings of the 6th International Conference on Extending Database Technology, Valencia, 1998, pp. 467-483.

[2] J. E. Cook, and A. L. Wolf, "Discovering models of software processes from event-based data," ACM Transactions on Software Engineering and Methodology, vol. 7, no. 3, pp. 215-249, 1998.

[3] W. M. P. van der Aalst, T. Weijters, and L. Maruster, "Workflow mining: discovering process models from event logs," IEEE Transactions on Knowledge and Data Engineering, vol. 16, no. 9, pp. 1128-1142, 2004.

[4] J. E. Cook, Z. Du, C. Liu, and A. L. Wolf, "Discovering models of behavior for concurrent workflows," Computers in Industry, vol. 53, no. 3, pp. 297-319, 2004.

[5] J. Herbst, D. Karagiannis. Workflow mining with InWoLvE. Computers in Industry, vol. 53, no. 3, pp. 245-264, 2004.

[6] G. Schimm. Mining exact models of concurrent workflows. Computers in Industry, vol. 53, no. 3 pp. 265-281, 2004.

[7] B. F. van Dongen, and W. M. P. van der Aalst. A Meta model for process mining data. In proceedings of the CAiSE WORKSHOPS, Porto, 2005, pp. 309-320.

[8] A. J. M. M. Weijters, W. M. P. van der Aalst, and A. K. A. de Medeiros. Process mining with the HeuristicsMiner algorithm. Technische Universiteit Eindhoven Technical Report, vol. 166, pp. 1-34, 2006.

[9] C. W. Günther, and W. M. P. van der Aalst. Fuzzy Mining: Adaptive process simplification based on multi-perspective metrics. In proceedings of the 5th International Conference on Business Process Management, Brisbane, 2007, pp. 328-343.

[10] A. J. M. M. Weijters, and W. M. P. van der Aalst. Rediscovering workflow models from event-based data using little thumb. Integrated Computer-Aided Engineering, vol. 20, no. 2, pp. 151-162, 2003.

[11] D. Fahland, W. M. P. van der Aalst. Simplifying discovered process models in a controlled manner. Inform Syst 2013; 38: 585-605.

[12] S. Aleem, L. F. Capretz, F. Ahmed. Business process mining approaches: a relative comparison. International Journal of Science, Technology and Management 2015; 4: 1557-1564.

[13] H. J. Cheng, A. Kumar. Process mining on noisy logs — Can log sanitization help to improve performance? Decis Support Syst 2015; 79: 138-149.

[14] D. Fahland, W. M. P. van der Aalst. Model repair — aligning process models to reality. Inform Syst 2015; 47: 220-243.

[15] M. Rovani, F. M. Maggi, M. de Leoni, W. M. P. van der Aalst. Declarative process mining in healthcare. Expert Syst Appl 2015; 42: 9236-9251.

[16] M. de Leoni, W. M. P. van der Aalst, M. A. Dees. A general process mining framework for correlating, predicting and clustering dynamic behavior based on event logs. Inform Syst 2016; 56: 235-257.

[17] F. Mannhardt, M. de Leoni, H. A. Reijers, W. M. P. van der Aalst. Balanced multi-perspective checking of process conformance. Computing 2016; 98: 407-437.

[18] A. Pika, W. M. P. van der Aalst, M. T. Wynn, C. J. Fidge, A. H. M. ter Hofstede. Evaluating and predicting overall process risk using event logs. Inform Sciences 2016; 352-353: 98-120.

[19] S. Suriadi, R. Andrewsa, A. H. M. ter Hofstedea, M. T. Wynna. Event log imperfection patterns for process mining: Towards a systematic approach to cleaning event logs. Inform Syst 2017; 64: 132-1564.

[20] A. A. Mitsyuk, I. S. Shugurov, A. A. Kalenkova, W. M. P. van der Aalst. Generating event logs for high-level process models. Simul Model Pract Th 2017; 74: 1-16.

[21] A. Bolt, M. de Leoni, A. H. M. ter Hofstedea, W. M. P. van der Aalst. Process variant comparison: Using event logs to detect differences in behavior and business rules. Inform Syst 2017; 0: 1-14.

[22] İ. Yürek, D. Birant, K. U. Birant. Interactive process miner: a new approach for process mining. Turk J Elec Eng & Comp Sci 2018, in press. doi: 10.3906/elk-1708-112

[23] B. F. van Dongen, W. M. P. van der Aalst. EMiT: A process mining tool. In Proceedings of the 25th International Conference on Application

and Theory of Petri Nets, Bologna, 2004, pp. 454-463. doi: 10.1007/978-3-540-27793-4_26

[24] B. F. van Dongen, A. K. A. de Medeiros, H. M. W. Verbeek, A. J. M. M. Weijters, W. M. P. van der Aalst. The ProM framework: a new era in process mining tool support. In Proceedings of the 26th International Conference on Application and Theory of Petri Nets, Miami, 2005, pp. 444-454. doi: 10.1007/11494744_25

[25] M. de Leoni, F. Mannhardt. Road traffic fine management process. Eindhoven University of Technology Dataset 2015. doi: 10.4121/uuid:270fd440-1057-4fb9-89a9-b699b47990f5

[26] B. F. van Dongen. Real-life event logs - Hospital log. Eindhoven University of Technology Dataset 2011. doi: 10.4121/uuid:270fd440-1057-4fb9-89a9-b699b47990f5

[27] R. P. J. C. Bose, W. M. P. van der Aalst. Trace alignment in process mining: Opportunities for process diagnostics. In: 8th International Conference on Business Process Management; 13-16 September 2010; Hoboken, NJ, USA. Heidelberg, Berlin, Germany: Springer. pp. 227-242.

Detection Mechanisms for Recent Mobile Malware

Mert Can ALICI
Zemana doo.
Sarajevo, Bosnia & Herzegovina
mertcan.alici@zemana.com

***Abstract*—Malware authors have been focused on the Android operating system since 2011. The operating system has dominated the mobile operating system market by 87 percent of market share. That causes malware authors to publish new 100.000 mobile malware each month just for the Android operating system. Those threats can harm mobile users in different aspects such as stealing their money, stealing their private information, disturbing them with advertising content and etc. On the other hand, antivirus vendors try to catch and fight against those threats. Malware evolve day by day and it makes antivirus products evolve to detect their complex obfuscated malicious activities and their antivirus bypass techniques as well. That is a war between antivirus vendors and malware authors. Antivirus vendors can detect a single mobile malware using static detection techniques, dynamic detection techniques, and anomaly detection techniques. While those techniques and correlation of those techniques can help to protect against advanced mobile malware, as a mobile operating system, Android has some limitations to not let antivirus vendors to develop those techniques such as limited battery power, the low processing unit, security concept of operating system and etc.**

Keywords—mobile threats; malware detection; pattern recognition;

I. INTRODUCTION

Increasing of the Android operating system usage in the world in 2008, it was pointed out for malware authors that it would be starting of the new era because mobile technologies have been developing and may be replaced with the personal computer systems. As the evolution of computer viruses, the viruses had the same evolutionary path for the Android operating system. First computer and mobile device viruses in the world have one simple aim to prove that is the authors' capabilities and experiences on computer systems. Later, malware authors had tried to convert those computer skills to make financial gain and they had created a market for vulnerabilities and data which is gathered from users all over the world.

II. HISTORY OF MOBILE MALWARE

A. Premium Short Message Services

As always, malware authors have been successfully proved that Android operating system vulnerable enough and has a big market share among mobile devices. Afterward, the malware authors tried to make financial gain just by converting their programming skills to money and the new market has been created by the malware authors. The malicious applications were started with the simple methods like sending messages to premium short message services(SMS) that was the same procedure as sending normal SMS, however, the money was shared between premium SMS provider and malware author [1]. Limitations and permission restrictions of the Android operating system on sending SMS feature of the Android application development process has blocked the malware authors to make the more financial gain on premium SMS services.

B. Banking Trojan

Two-factor authentication technologies and combined security of computer and mobile devices became popular in 2014 and that helps malware authors to create the new term, combined malware that was prepared malicious application sets which aim to exploit more than one devices. In the Android operating system, the security involving short messages and/or e-mail contents has been collected by the malware authors to access banking accounts of victims [2].

C. Ransomware

Ransomware is a special type of computer virus that blocks the system until some agreement are applied between victim and malware author [3]. That is mostly financial agreements. The increasing popularity of ransomware applications that perform on Windows-based operating systems in 2013 inspired the malware authors who develop malicious applications for Android operating systems [4]. However first ransomware application which encrypted all files of victims' mobile device has been spread in 2015 [5]. That mechanism was hard to make financial gain because the malware authors should have communicated with the victim to get money.

D. Adware

Recent malware application tries to be legalized and hard to detect by antivirus companies. Adware method has come up for that reason. The Advertisement is a legal operation for all over the world to announce or mention about a brand or a product. Therefore advertisers want to show their brand or product to as much as people using advertising services like television, radio, websites and the services which people can integrate into their solution to gain money. Although adware applications are not malicious applications, they are highly disturbing applications and they are mostly categorized as potentially unwanted applications(PUP).

III. DETECTION MECHANISM

It clearly needs to understand the Android application structure to detect them and block them because Android has its own unique application structure that only runs on the Android operating system. Android has permission system to restrict access to the critical components like the internet, SMS, browser utilities, camera etc [6]. However, detecting malicious applications using permissions or combination/sequence of permissions could not succeed in the wild. That is why recent malicious applications(adware applications) requires the permission that only normal applications use such as internet permission. Therefore, detection mechanism has been evolving to string and method features which are stored in the dex file format [7].

In the beginning, there were two sets of applications; malicious and benign. They are needed to extract string and method features to cluster them into multiple malware families. Because of application replication, which means appending malicious code to the legitimate application to replicate them with the malicious version, it is hard to cluster malicious application using generic features like strings and methods. Therefore, the strings and methods which belong to the malicious application need to be subtracted from all strings and methods which belong to clean applications. That will cause to have pure strings and methods which identify malicious behavior. That process will help further processes just by decreasing strings and method count and processing time as well.

Clustering mechanism relies on simple techniques like a threshold to achieve to join the cluster. A malware sample compared with all clusters and the sample will join the most similar cluster. However, in this research, there is another invention to make the clustering better and more accurate. The simple threshold mechanism does not fit into that research because as far as a cluster increases file number it should become more stable and more characteristic cluster that identify that malware family specifically. As you can see in "Fig. 1." the problem has been solved by logarithmic addiction technique.

Therefore, addiction method helps to solve the problem. In this research initial threshold set to 1 and as long as cluster become larger addictive value compound with the initial threshold to become harder to join a cluster. For that reason the first files in the clusters should be fit into the malware family characteristics otherwise some of the family may be divided into multiple clusters unnecessarily and that will cause the noisy data for further processes like signature creation.

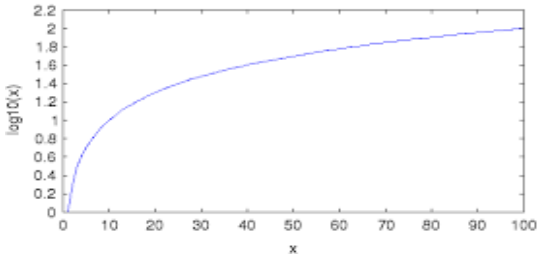

Fig. 1. Addictive function log10

The Similarity of a feature or feature sets was another challenge for this research topic. There are numerous algorithms to calculate the similarity of two files or even two text files. In this project, it has been solved by another simple solution like the function as shown in "Fig. 2.". It consists of two parts; string similarity function and method similarity function. Both functions have the same formula as the length of the intersection of the file which attempts to join the cluster and the cluster itself divided by the length of clusters. After calculating the values of those function, they are multiply by preset values respectively, 1.0 and 1.5 and at the end, the sum of those two values is the similarity of two files.

$$f_{string}() = \frac{|(cluster \cap strings)|}{|cluster|}$$

$$f_{method}() = \frac{|(cluster \cap methods)|}{|cluster|}$$

$$fsimilarity() = fstrings \times 1.0 + f_{method} \times 1.5$$

Fig. 2. Similarity formula

Those techniques which are mentioned in the above just for clustering malware samples into separate multiple groups to characterize them better. The next process to detect a malicious application is the generating a signature for a malware sample or for a malware family. Generating signature fully depends on the malware engine, which helps to scan the files and detect malicious files using the virus signature database because that engine will extract the features and try

to match the malicious applications with signatures which are stored in the virus signature database. Therefore, capabilities of detection mechanisms rely on signature database capabilities and it also relies on detection engine capabilities. The Assumption of having an engine that is capable of extracting and matching signatures will help to skip that section because detection engine and virus signature database are another research topic and both research topics have too many technical challenges inside.

Clustering and signature creation are two different bounded context and two separate research groups could work on each context. However, in this project limitation of time and people, the output of clustering process was used for the signature creation process. In short, the strings and methods processed in the previous clustering section were used to process signature creation.

There are multiple criteria to create a signature but the first concern in this research is the generality of signature to detect all samples of a malware family in the test set and the malware samples in the wild because too strict signatures most probably will cause true negative detection in the wild. This phase starts with scoring strings by different criteria such as string length, characters in the string, whether it is base64 string or not, if there is a space in the beginning or end of the string, strings that has more than 5 uppercase characters, string that starts with lowercase characters and ends with non-alphabetical characters. On the other hand, methods scoring are simply by method's opcode length.

After scoring operation for every single element which is gathered from malicious applications, those elements need to be selected by order to generate the most inclusive signature with the least number of elements. Therefore, in this research 6 elements have been chosen to generate the inclusive signature for a signature family just by starting to choose from string elements and if there are not enough string elements, method elements will be appended to the signature. At the end of the signature creating, there is a quality check operation to ensure that the signature will not cause the high number of false positive detections and will be successful in the wild. The quality of signature is decided by having more than 10 scores in the sum of all elements in the signature.

IV. RESULTS

The clustering mechanism and the signature creation process have successfully applied to a security product to test the results. Clustering success has been compared to Av-Test [8] malware family repository and the research has successfully achieved the %99.2 accuracy of clustering. However that could cause the too strict modelling to achieve this success. Signature creation and detection tests has been rewarded by %99.5 detection results by private test companies.

V. FUTURE WORKS

The processes mentioned above are not fully managed and be capable of processing thousands of files one by one in a day. Because the process needs to handle multiple files at one. Also, another problem of the research is that having more files may increase the process time even exponentially. Therefore the research project needs to be converted a flow process that can process each file separately and keep the processing time in reasonable time.

On the other hand, increasing speed of machine learning development, the research may focus on machine learning techniques to adopt new malicious applications and/or new malicious families easier. That may help to handle features easily instead of using preset multipliers and extraction routines.

The whole process may move to serverless architecture to gather malicious and benign samples and process them in the way that is provided features by the serverless provider. Development of tensorflow [9] and it's technologies have been spread into the serverless architecture to model machine learning procedures and run them in special computer parts named Tensorflow Processing Unit(TPU) [10].

Those technologies may speed up the research process and accuracy of clustering and accuracy of the generating signatures.

REFERENCES

[1] Hamandi, Khodor, et al. "Android SMS malware: Vulnerability and mitigation." Advanced Information Networking and Applications Workshops (WAINA), 2013 27th International Conference on. IEEE, 2013.

[2] Chebyshev, Victor, and Roman Unuchek. "Mobile malware evolution: 2013." Kaspersky Lab ZAO's SecureList 24 (2014).

[3] Wikipedia contributors. (2018, April 26). Ransomware. In Wikipedia, The Free Encyclopedia. Retrieved 21:46, April 29, 2018, from https://en.wikipedia.org/w/index.php?title=Ransomware&oldid=838351381

[4] O'Gorman, G., & McDonald, G. (2012). Ransomware: A growing menace. Symantec Corporation.

[5] Mercaldo, F., Nardone, V., Santone, A., & Visaggio, C. A. (2016, June). Ransomware steals your phone. formal methods rescue it. In International Conference on Formal Techniques for Distributed Objects, Components, and Systems (pp. 212-221). Springer, Cham.

[6] Wijesekera, P., Baokar, A., Hosseini, A., Egelman, S., Wagner, D., & Beznosov, K. (2015, August). Android Permissions Remystified: A Field Study on Contextual Integrity. In USENIX Security Symposium (pp. 499-514).

[7] Mercaldo, F., Nardone, V., Santone, A., & Visaggio, C. A. (2016, June). Ransomware steals your phone. formal methods rescue it. In International Conference on Formal Techniques for Distributed Objects, Components, and Systems (pp. 212-221). Springer, Cham.

[8] GmbH, A. (2018, April 24). AV-TEST – The Independent IT-Security Institute. Retrieved from https://www.av-test.org/en/

[9] Abadi, M., Barham, P., Chen, J., Chen, Z., Davis, A., Dean, J., ... & Kudlur, M. (2016, November). TensorFlow: A System for Large-Scale Machine Learning. In OSDI (Vol. 16, pp. 265-283).

[10] Jouppi, N. P., Young, C., Patil, N., Patterson, D., Agrawal, G., Bajwa, R., ... & Boyle, R. (2017, June). In-datacenter performance analysis of a tensor processing unit. In Proceedings of the 44th Annual International Symposium on Computer Architecture (pp. 1-12). ACM.

The Changing Relationship Between Linguistics, Natural Language Processing, And Applied Linguistics

[1]Abbas Hussein Tarish
Modern Languages and Literature (Philology)
Ph. D. Student; West University of Timisoara
Email: abbasamradu@yahoo.com

[2]Hasan K. Naji
MCSE Software Engineering
M.A; University of Technology in Bucharest
Email: pcenghasan@gmail.com

ABSTRACT---It is no exaggeration to say that linguistics has undergone a renaissance with the rapid development of computers and the internet. Every aspect of linguistics has been affected by the application of this technology. In particular, the development of our understanding of natural language processing has achieved hitherto unimagined levels of mastery regarding natural language processing. Far more than a theoretical exploration, a new level of applied linguistics now ushers every aspect of linguistic knowledge to the task of processing and learning languages.

Keywords: ***Software Linguistics, Applied Linguistics, E-Learning.***

I. COMPUTER-AIDED LANGUAGE LEARNING (CALL)

Computer-aided language learning (CALL) is a powerful example of the way linguistics has bridged the gap between the scholarly study of language in all its aspects, from vocabulary, to pronunciation, from syntax to semantics, from pragmatics to morphology, the use of CALL has revolutionized linguistics. The ultimate implementation of this new world of applied linguistics is represented by the sudden worldwide adoption of the World Wide Web. The internet allows CALL to enter scholarship, and pedagogy with an adroitness and joy that has not been previously experienced, for example, in foreign language classrooms.

Today, it is widely accepted that everyone must be technologically literate, and this has resulted in computers and the internet becoming an in expendable appendage to linguists, teachers, and students alike. The internet is routinely and commonly used for 'almost everything' including to perform searches for information, communicate with family and friends, conducting business negotiations, banking transactions, professional consultations, to buy all kinds of items and as a form of entertainment. Thus, the growing popularity of new technologies has led to its use in the field of linguistics and education for what has been referred to as e-learning or CALL. Every aspect of linguistics has been touched by this trend.

CALL originated in the last century, when the first mainframe computers were introduced in some universities. Michael Levy, a theorist, defined it as "the search and study of applications for teaching and learning of languages."[1] For example, through the project PLATO (Programmed Logic for Automated Teaching Operations), initiated at the University of Illinois.

In 1960, thousands of computers around the world were networked for education, and this was a milestone in the first stage of CALL. However, except for that project, implementation was minimal until the 1980s. Over the past two decades, however, the picture has changed dramatically. Since the 1990s, according to Hubbard "the question is no longer whether to use the computer, but how."[2] This usage extends from specific uses of computers in campus classes to completely virtual courses.

II. CREATING NEW SUBFIELDS OF LINGUISTICS WITH COMPUTERS

In fact, CALL has itself become a proper subfield of linguistics - much more than a passing trend. CALL is now a linguistic field that investigates any use of computers in teaching and learning of second languages and foreign languages. Simons (2012, p. 3) goes so far as to consider it the new technology-based linguistics as a branch of science. It is multidisciplinary; it is influenced by disciplines such as linguistics, computer science,

[1] M. Levy, *Computer-assisted Language Learning: Context and Conceptualization*. Oxford University Press, 1997. p. 1.
[2] P. Hubbard, ed. *Computer Assisted Language Learning: Critical Concepts in Linguistics. Present Trends and Future Directions in CALL*. Routledge, 2009. p. 1.

psychology, and pedagogy.[3] Within CALL is another subfield that is evolving significantly known as Computer Assisted Language Testing (CALT). There are already numerous specialized journals and conferences dedicated to CALL and CALT. In this way, the twenty-first century has blossomed into a veritable Golden Age of applied linguistics.

Another subfield currently under development, though still with very limited use, is intelligent systems for computer-aided language learning (CALL). This areas studies and implements technologies for performing the role or function of a teacher in that it entails the identification of errors in the output of the student, the offering of relevant feedback, the determination of the language level of fluency, the provision of appropriate materials and assignments for assisting students' progress, as well as interacting with students through conversation.

It other words, today the advent of CALL, CALT, and CALL are so pervasive and in expendable that suddenly it is nearly impossible to imagine teaching and learning language without computer assistance, either totally -in the case of virtual teaching or in part, as a support mechanism for traditional classroom teaching.

It may be argued that scholars of English, linguistics professors, and language teachers of all types are among the most committed to the implementation of computer technology to promote their work. In the fields of linguistics, education, and technology language teachers are typically on the forefront of relevant computer-assisted technologies.

III. THE LINGUISTICS REVOLUTION HAS BEGUN

Consider the word 'podcast'. Unknown in 2004 by 99% of the population, in 2005 it was selected as the 'word of the year' by the New Oxford American Dictionary.[4] These downloadable internet audio files with fixed periodicity have lent a new tactic to teachers of foreign languages. Indeed, the internet is already replete with web pages for dedicated language learning use by students and language teachers containing everything from actual recordings of language to prepared podcast lessons.

As for tools, the web offers a wide variety of functionalities that (a) create, manage and publish content, (b) enrich teaching and create teaching materials, (c) browse and search content for multimedia design and editing, (d) to enable office automation, and (e) to facilitate communication and collaboration on social networks. Two of the most popular tools are blogs and wikis.

A blog is a website that periodically updates articles collected chronologically from one or more authors, with the most recent appearing first. The author can allow other Internet users to make comments and always retains the right to post what is deemed appropriate. The possibilities are endless for implementing text and images, audio and video. Blog pedagogy is a growing subfield in academics.

A similar tool is the wiki. It is a collaborative web space, organized by a hypertext page structure in which users create, edit, delete, and modify the content asynchronously. The existence of numerous free of applications for creating wikis in different programming languages and various operating systems, has favored its development. Moreover, it is not necessary to master HTML5, the language in which web pages are coded, or to use a web page editor to collaborate on a wiki.

The language of the wikis eliminates non-essential elements of HTML and reduces participation to the essentials. Typical uses of wikis in linguistics and language education including appointment: (a) classroom communication and collaboration spaces, (b) the assignment of dedicated learning spaces and filing tasks, (c) text archiving, (d) collaborative authorship projects between students, teachers, and both, and (d) the ability to enhance motivation and inspiration for learning due to the pleasurable venue and prospects for attaining significant audiences, and the list goes on.

IV. COMPUTERIZED TOOLS FOR LANGUAGE LEARNING

The following software packages have each been researched and reviewed in scholarly publications.

1- JClic: a set of applications developed in Java 9 to make various types of activities: puzzles, associations, text exercises, and crossword activities are created and it also allows one to publish and display projects created to others.[5]

2- Hot Potatoes: a system created by the University of Victoria, Canada, which allows the creation of six types of interactive exercises to perform online: multiple choice, fill voids, order, crosswords, matching and short answer.[6]

3- Builder: another tool for creating digital educational content promoting multiliteracies and multimodalities with 47 models of activities.[7]

4- MALTED (Multimedia Authoring Tutors for Language and Educational Development): allows

[3] A. Cangelosi and Domenico Parisi, (eds). *Simulating the Evolution of Language*. Springer Science & Business Media, 2012. p. 3.

[4] R. Cain, 'Podcasting for Beginners'. *TESOL-Spain Newsletter,* vol. 31, no. 3, 2008. p. 10.

[5] E. Guerrero, A. Muñoz, and C. Sotelino. 'JClic: A New Software to Teach and Learn Easily. Implementation of Multimedia Activities in Our Classroom.' *ICT in Education: Reflections and Perspectives*, 2007, 172-176.

[6] H. Soleimani and Ali Raeesi. 'Hot Potatoes: The Merits and Demerits.' *Theory and Practice in Language Studies*, vol. 5, no. 6, 2015, 1291-1295.

[7] N. Eteokleous, Victoria Pavlou, and Simos Tsolakidis. "Integrating the Multimedia Builder Software as an Education Tool to Deliver Fairy Tales: Promoting Multiliteracies and Multimodality.' *Journal of Interactive Learning Research*, vol. 26, no. 1, 2015, 65-88.

creation of multimedia activities and courses for teaching languages by generating Java applets that may be executed later both on the computer's hard drive and through web sites in which they were published online.[8]

5- Squeak: one of many an open source applications to develop multimedia content without programming knowledge for making teaching units in text content, video, sound, music, 2D and 3D graphics, etc.; presentations include animations and all kinds of video and audio files. It is inspired by constructivist ideas in language learning and has been endorsed by numerous educational institutions.[9]

V. CONCLUSION

In short, the educational potential of CALL for teaching and learning languages is virtually endless. Such technologies allow for the practice of almost any all language skill, to one extent or another. According to Hubbard, the reason could be, on one hand, practical, since it is easy to gather data and one does not need to acquire or develop specific coding skills.[10] Furthermore, this type of CALL communication is of great interest for the high degree of similarity it shares with naturally occurring language as a face-to-face type of interaction.

"For these reasons, scholars are achieving a bridge between CALL technology and major learning theories, such as constructivism and cognitivism."[11,12] The key is that CALL seems to work because the realistic negotiation of meaning actually occurs. Therefore, it is safe to say that the linguistics revolution has begun, and the revolution is being computerized.

REFERENCES

1- Arslan, M. Oğuz. 'Free and Open Source Software as a Public Good: Implications for Education'. *European Journal of Research on Education*, no. 2(Special Issue), 2014, 158-165.

2- Bangs, P. 'Engaging the Learner - How to Author for Best Feedback'. In U. Felix (ed.), *Language Learning Online: Towards Best Practices*. Lisse: Swets & Zeitlinger Publishers, 2003.

3- Cain, R. 'Podcasting for Beginners'. *TESOL-Spain Newsletter*, vol. 31, no. 3, 2008, 10-12.

4- Cangelosi, Angelo, and Domenico Parisi, (eds.), *Simulating the Evolution of Language*. Springer Science & Business Media, 2012.

5- Ellis, Rod. *Task-based Language Learning and Teaching*. Oxford University Press, 2003.

6- Eteokleous, Nikleia, Pavlou, V., and Tsolakidis, S. 'Integrating the Multimedia Builder Software as an Education Tool to Deliver Fairy Tales: Promoting Multiliteracies and Multimodality.' *Journal of Interactive Learning Research*, vol. 26, no. 1, 2015, 65-88.

7- Guerrero, E., Muñoz, A., and Sotelino, C. 'JClic: A New Software to Teach and Learn Easily. Implementation of Multimedia Activities in Our Classroom.' *ICT in Education: Reflections and Perspectives*, June 2007, 172-176.

8- Hubbard, Philip, (ed.), *Computer Assisted Language Learning: Critical Concepts in Linguistics. Present Trends and Future Directions in CALL*. Routledge, 2009.

9- Levy, Michael. *Computer-assisted Language Learning: Context and Conceptualization*. Oxford University Press, 1997.

10- Robin, Richard. 'Commentary: Learner-based Listening and Technological Authenticity.' *Language Learning & Technology*, vol. 11, no.1, 2007, 109-115.

11- Soleimani, Hassan, and Raeesi, A. 'Hot Potatoes: The Merits and Demerits.' *Theory and Practice in Language Studies*, vol. 5,.no. 6, 2015, 1291-129.

12- Vygotsky, Lev. 'Interaction between Learning and Development.' *Readings on the Development of Children*, vol. 23, no. 3, 1978, pp. 34-41.

[8] P. Bangs, 'Engaging the Learner - How to Author for Best Feedback.' In U. Felix (ed.), L*anguage Learning Online: Towards Best Practices*. Lisse: Swets & Zeitlinger Publishers, 2003.

[9] M. Oğuz Arslan, 'Free and Open Source Software as a Public Good: Implications for Education'. *European Journal of Research on Education*, no. 2(Special Issue), 2014, 158-165.

[10] P. Hubbard, *Computer Assisted Language Learning: Critical Concepts in Linguistics. Present Trends and Future Directions in CALL*, p. 10.

[11] L. Vygotsky. 'Interaction between Learning and Development.' *Readings on the Development of Children* , vol. 23, no. 3, 1978, pp. 34-41.

[12] R. Ellis. *Task-based Language Learning and Teaching*. Oxford University Press, 2003.

CFD(computational fluid dynamics)-Based Optimal Design Aiming at Uniform Flow Distribution in Microchannels using a Simplified Conjugate-Gradient Method

Hsuan-Ju Chiang[1]
Department of Mechanical Engineering
National Cheng-Kung University
Tainan, Taiwan
E-mail address: xsmallwhite25@gmail.com

Jiin-Yuh Jang[2]
Department of Mechanical Engineering
National Cheng-Kung University
Tainan, Taiwan
E-mail address: jangjim@mail.ncku.edu.tw

***Abstract*—The study is focused on computational optimization of the geometry for the flow channels that are used to manufacture Hexanedinitrile ((CH2)4(CN)2).There is no denying that asking the average velocity in each microchannel to be nearly the same is extremely crucial during production;As a result,we are going to achieve this goal by adjusting the manifold shape of the inlet or outlet. Two-dimensional mass and momentum transport phenomena with a mixed fluid simulation in a microchannel are predicted using a commercial computational fluid dynamics code.At the same time,the whole optimization searching procedure will be conducted by fortran code,using simplified conjugate-gradient method.In the present study, the geometrical optimization tasks involve the designs of the inlet manifold or outlet manifold shapes under parallel flow or inverse flow, and the design purpose is to obtain a uniform flow distribution throughout every single microchannel so as to increase the production rate of Hexanedinitrile((CH2)4(CN)2). Cubic-spline interpolation is used in shape design to fit the points on the manifold shape more smoothly.**

The results show that the velocity standard deviation decreased from 0.25 to 0.0258 (parallel flow) and 0.178 to 0.00055 (inverse flow) after searching the optimal manifold shapes respectively. The manifold shapes of the inlet and outlet can efficiently lead to significant uniformity in the flow fields using a simplified conjugate-gradient method.

Keywords:Optimization;Shape design;Micro-channel

I. INTRODUCTION

Nylon,a Polyamide fiber, is first invented in 1935,created by a chemist who's name is Wallace Hume Carothers. He combined Hexamethylenediamine with hexanedioic acid, leading to the very first debut of nylon. With lots of advantages such as high strength, good flexibility and outstanding wear resistance, nylon has taken place other textiles since 1935.At the same time, the increasing need of nylon also increase the demands of other compounds, such as Hexanedinitrile, that is used to manufacture nylon. Hexamethylenediamine is made from Hexanedinitrile.It is estimate that there are currently 90 percent's Hexanedinitrile that is used to produce Hexamethylenediamine.It is also the most important industrial application of Hexanedinitrile .

When it comes to manufacturing Hexanedinitrile, there are three different methods. One is Electrolytic dimerization method, another is butadiene method and still another is Adipic acid method. In this study, we aim at improving the manufacturing process of Electrolytic dimerization method.

Electrolytic dimerization method was first adopted by Monsanto in 1921 to produce Hexanedinitrile. Its reaction equations are as follows:

cathode : $2CH_2=CHCN + 2H^+ + 2e^- \rightarrow NC(CH_2)_4CN$ (1)

anode : $H_2O \rightarrow 1/2\ O_2 + 2\ H^+ + 2e^-$ (2)

In order to raise the output, the electrobath will be arranged in a series connection or parallel connection. The reactant fluid flow injected from inlet will separate at inlet manifold, drifting into several microchannels. While electrolyzing the reactant fluid, it is required that the flow velocity of each microchannel should be confined to certain value. The flow velocity will impact the conversion rate of reactant, influencing the output greatly; Thus, the inlet manifold shape design is a huge issue in Electrolytic dimerization method.

Due to the improvement in computational fluid dynamics(CFD) and computer hardware,there is a growing trend of combining optimization method with CFD in industrial design. In this study, we are going to adopt simplified conjugate-gradient method(SCGM) to carry out our optimization design of manifold.

II. MATHEMATICAL ANALYSIS

A. Governing equation

Fig. 1. is the optimization model for parallel flow and inverse flow. Each microchannel has the length 900mm and width 2mm.In this study, we construct 7 moving point

controlled by optimization program that will change the shape of manifold. We also combine cubic spline method to smooth the generated shape of manifold. The shape optimization will involve both parallel flow and inverse flow.

The continuity equation, momentum equation are expressed as follows:

$$\frac{\partial \bar{u}}{\partial x}+\frac{\partial \bar{v}}{\partial y}=0 \tag{3}$$

$$\bar{u}\frac{\partial \bar{u}}{\partial x}+\bar{v}\frac{\partial \bar{u}}{\partial y}=-\frac{1}{\rho}\frac{\partial \bar{p}}{\partial x}+\frac{\mu}{\rho}\left(\frac{\partial^2 \bar{u}}{\partial x^2}+\frac{\partial^2 \bar{u}}{\partial y^2}\right)-\frac{\partial}{\partial x}\overline{(u'u')}-\frac{\partial}{\partial y}\overline{(u'v')} \tag{4}$$

$$\bar{u}\frac{\partial \bar{v}}{\partial x}+\bar{v}\frac{\partial \bar{v}}{\partial y}=-\frac{1}{\rho}\frac{\partial \bar{p}}{\partial y}+\frac{\mu}{\rho}\left(\frac{\partial^2 \bar{v}}{\partial x^2}+\frac{\partial^2 \bar{v}}{\partial y^2}\right)-\frac{\partial}{\partial x}\overline{(v'u')}-\frac{\partial}{\partial y}\overline{(v'v')}+g \tag{5}$$

In the above equation, u symbolizes velocity (m/s) in x direction, v symbolizes velocity (m/s) in y direction,x and y symbolize x and y axis, P symbolizes pressure (N/m^2), ρ symbolizes the density of fluid (kg/m^3) and g symbolizes gravitational acceleration (m/s^2).

The κ - ε turbulent transport equation are expressed as follows:

$$\rho\frac{\partial}{\partial x_j}\overline{u}_j\kappa=\frac{\partial}{\partial x_j}\left[\left(\mu_l+\frac{\mu_t}{\sigma_\kappa}\right)\frac{\partial \kappa}{\partial x_j}\right]+\rho\left(P_r-\varepsilon\right) \tag{6}$$

$$\rho\frac{\partial}{\partial x_j}\overline{u}_j\varepsilon=\frac{\partial}{\partial x_j}\left[\left(\mu_l+\frac{\mu_t}{\sigma_\varepsilon}\right)\frac{\partial \varepsilon}{\partial x_j}\right]+\rho\frac{\varepsilon}{\kappa}\left(c_1P_r-c_2\varepsilon\right) \tag{7}$$

In the above equation, μ_l symbolizes laminar viscosity coefficient, σ_κ symbolizes prandtl number for turbulent kinetic energy, u symbolizes velocity (m/s) in x direction, v symbolizes velocity (m/s) in y direction,x and y symbolize x and y axis, ρ symbolizes the density of fluid.

κ symbolizes turbulent kinetic energy, ε symbolizes turbulent energy dissipation ratio, μ_t symbolizes turbulent viscosity coefficient, P_r symbolizes turbulent kinetic energy production rate and they are calculated by the following equations.

$$\kappa=\frac{1}{2}\overline{u_i'u_i'} \tag{8}$$

$$\varepsilon=\frac{\mu}{\rho}\left(\overline{\frac{\partial u_i'}{\partial x_j}\frac{\partial u_i'}{\partial x_j}}\right) \tag{9}$$

$$\mu_t=\frac{\rho c_\mu \kappa^2}{\varepsilon} \tag{10}$$

$$P_r=\frac{\mu_t}{\rho}\left[2\left(\frac{\partial \bar{u}_i}{\partial x_i}\right)^2+\left(\frac{\partial \bar{u}_i}{\partial x_j}+\frac{\partial \bar{u}_j}{\partial x_i}\right)^2-\frac{2}{3}\left(\nabla \bar{u}_i\right)^2\right]-\frac{2}{3}\kappa\left(\frac{\partial \bar{u}_i}{\partial x_i}\right) \tag{11}$$

According to Launder and Spalding's suggestion, c_μ 、 c_1 、 c_2 、 σ_κ 、 σ_ε are equal to 0.09、1.44、1.92、1.0、1.3

B. Boundary Condition

Inlet volume flow rate is set at 30 liter/m-s.Outlet is deemed as pressure outlet. No-slip condition is applied to all walls and the turbulent intensity is 5 percent,turbulent viscosity ratio is 10.

III. Optimization

In this study,we have combined simplified conjugate-gradient method (SCGM) with a finite differential method (FDM) code as an optimizer to search the optimum manifold shapes. The objective functions are defined as follows:

$$J=1-\left\{\left[\sum_{n=1}^{n}\left(U_n-U_{ave}\right)^2\right]\frac{1}{n}\right\}^{0.5}\Big/U_{ave} \tag{12}$$

While performing the SCGM method, the initial guess for the value of each search variable is made, and in the successive steps, the conjugate-gradient coefficients and the search directions are evaluated to estimate the new search variables. The solutions solved by the finite difference method are used to calculate the value of the objective function, which is further transmitted back to the optimizer for the purpose of calculating the consecutive searching directions. The updated design variables will take place initial value and it will be solved for new objective function. These steps work in a roll to search for ultimate objective function.

In short, the main procedures of SCGM method are as follows:

(a) Generate an initial guess for original design variables (X1~X7) –manifold width.

(b) Utilize the commercial software to solve for the velocity field, calculating the objective function J_{obj}(X1~X7).

(c) When the value of J_{obj}(X1~X7) reaches a maximum, the optimization process is terminated. Otherwise, proceed to step (d).

(d) Determine the gradient functions, from ($\partial J_{obj}/\partial$X1)(k) to ($\partial J_{obj}/\partial$X7)(k), by applying a small perturbation (ΔX1~ΔX7) to X1~X7, and calculate the corresponding change in objective function (ΔJ_{obj}). Then, the gradient function with respect to each value of the design variables (X1~X7) can be calculated by the direct numerical differentiation.

$$\frac{\partial J_{obj}}{\partial X_i}=\frac{\Delta J_{obj}}{\Delta X_i},\ i=1\sim 7 \tag{13}$$

(e) Calculate the conjugate-gradient coefficients $\gamma^{(k)}$, and the search directions, $\xi_1^{(k+1)}$ to $\xi_7^{(k+1)}$, for each search variable. For the first step with k = 1, $\gamma^{(1)}$= 0.

$$\gamma^{(k)}=\left[\sum_{n=1}^{2}\frac{\partial J_{obj}^{(k)}}{\partial X_n}\Big/\sum_{n=1}^{2}\frac{\partial J_{obj}^{(k-1)}}{\partial X_n}\right]^2 \tag{14}$$

$$\xi_i^{(k+1)}=\frac{\partial J_{obj}^{(k)}}{\partial X_i}+\gamma^{(k)}\xi_i^{(k)},\ i=1\sim 7 \tag{15}$$

(f) Assign values to the coefficients of descent direction (β1~ β7) for all values of the design variables (X1~X7). Specifically, those values are chosen by a trial-and-error process.

(g) Update the design variables with

$$X_i^{(k+1)} = X_i^{(k)} + \beta_i \xi_i^{(k)}, i = 1 \sim 7 \quad (16)$$

IV. Result and Discussion

Fig. 2. is the optimized manifold shape. The standard deviation of velocity is 99.1%(100% is thoughly uniform) for optimization of parallel flow. Fig. 3. shows that flow velocity in all the microchannels is in the range of 1.47m/s~1.51m/s after conducting the optimization process. Manifold width decreases from 4.53mm to 0.4mm alongside the flow direction. The pressure drop of optimization manifold is 246pa.It takes 20 steps or so to find out optimization result.

Fig. 4. is the optimized manifold shape for inverse flow. The standard deviation of velocity is 99.9%. Fig. 5. Shows that flow velocity in all the microchannels is comparatively closed to 1.5m/s after conducting the optimization process. Manifold width increases from 3.2mm to 6.9mm alongside the flow direction. The pressure drop of optimization manifold is 123pa.It takes 15 steps or so to find out optimization result.

Conclusion

(a) Manifold optimization can greatly improve the non-uniformity in microchannels. With the aid of optimization, the standard deviation of velocity raises to 99.1% for parallel flow and 99.9% for inverse flow

(b) The pressure drop of manifold optimization of inverse flow is 123pa, which is about half the value of parallel flow.

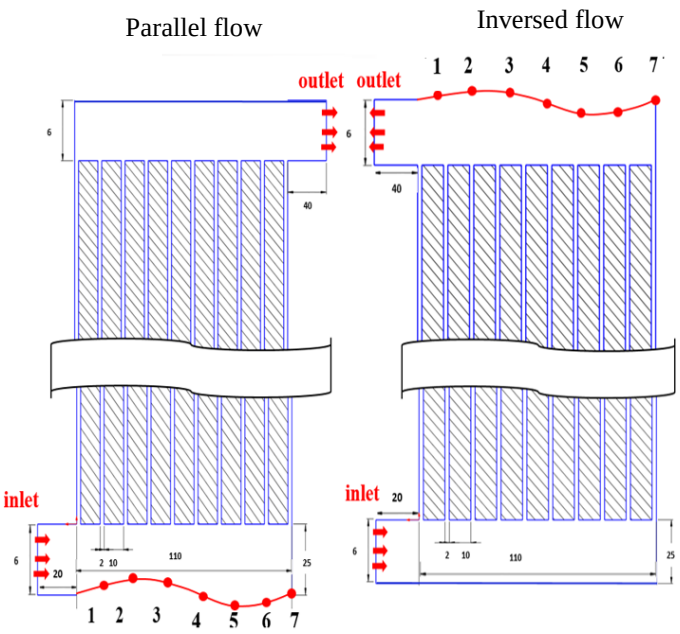

Fig. 1. optimization model

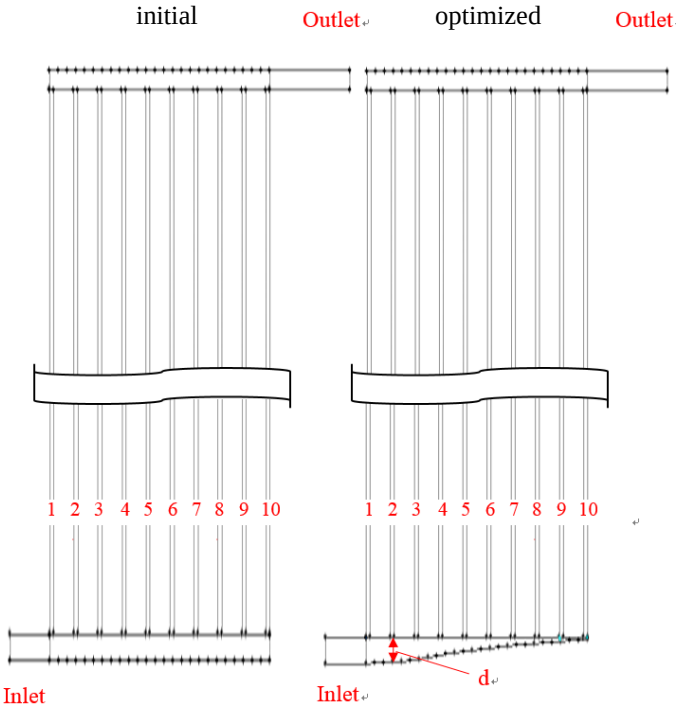

d(mm)	1	2	3	4	5	6	7	8	9	10
initial	3	3	3	3	3	3	3	3	3	3
optimized	4.53	4.29	3.73	2.9	2.4	1.82	1.37	1.1	0.74	0.4

Fig. 2. optimized manifold for parallel flow

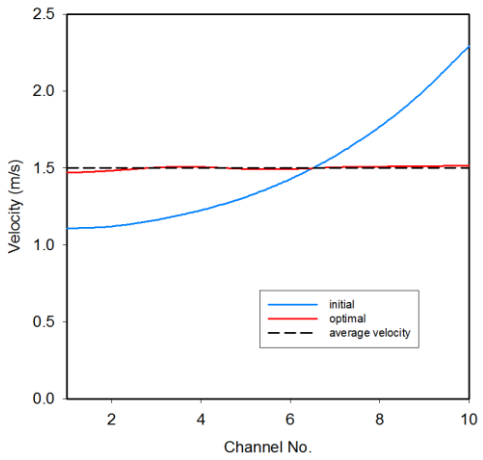

Fig. 3. Velocity distribution of microchannels(parallel flow)

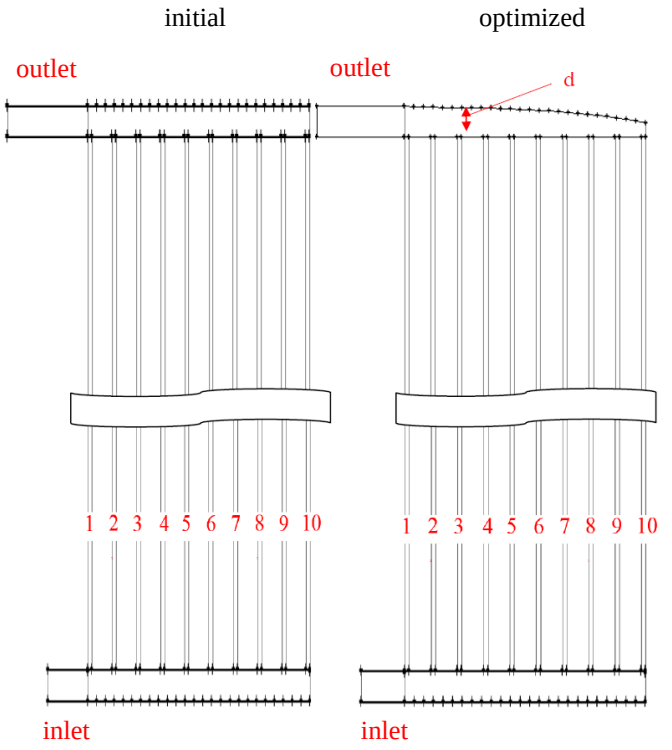

d(mm)	1	2	3	4	5	6	7	8	9	10
initial	3	3	3	3	3	3	3	3	3	3
optimized	6.9	6.6	6.5	6.4	6.3	5.9	5.5	5.1	4.3	3.2

Fig. 4. optimized manifold for inverse flow

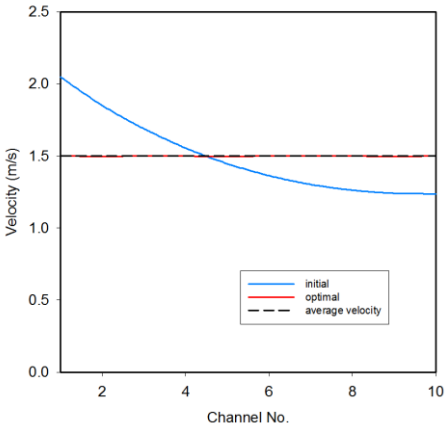

Fig. 5. Velocity distribution of microchannels(inverse flow)

The Thermal-Hydraulic Characteristics of a Double-Jet Flow over a Flat Plate

Cheng-Chan Chien
Department of Mechanical Engineering
National Cheng-Kung University
Tainan, Taiwan
d830214s@gmail.com

Jiin-Yuh Jang
Department of Mechanical Engineering
National Cheng-Kung University
Tainan, Taiwan
jangjim@mail.ncku.edu.tw

***Abstract*—This study investigates the heat transfer and hydraulic phenomena of the double-jet impingement on a hot steel plate with different flow rate and spray-angle of the flat fan nozzle. The heat transfer coefficients for 2 different kind of flat fan nozzles and 3 different flow rates(2.5L/min to 8 L/min) are calculated by the 3-D inverse heat transfer models solved by an algorithm developed with the conjugate-gradient method. The conjugate gradient method was an iterative method for solving an equation and used to optimize the heat transfer coefficient distribution.**

A test piece of steel plate was electrically heated from below heat pipe, its top surface was spray cooled and sides' heat transfer through natural convection. The spray was produced from a nozzle supplied with water from a pressurized pump and experimental temperature was measured by thermocouples connect to the data processor.

First, the flow field observation will show the hydraulic phenomena with a single nozzle jet impingement on a flat plate. Second, the cooling rate and heat transfer effects will be discussed in detailed.

Keywords—hydraulic phenomena, Double-Jet, Inverse Heat Transfer, conjugate-gradient method

I. INTRODUCTION

In recent years, countries around the world have paid more and more attention to the issues related to global warming and the environment. Energy conservation, carbon reduction, and green energy have gradually become an important indicator of engineering. China Steel Corporation also attaches more importance to the effective use of energy and environmental pollution. Today, the development of the steel industry in the global market is increasingly prosperous. More and more steelmaking plants have been set up around the world, with the pressure of global competition in the market. The quality requirements of steel products are also highly valued. In order to enhance the competitiveness of the steel industry in the global market while reducing the pollution to the environment, the improvement in the quality of steel products, as well as the control and evaluation of individual steelmaking process monitoring and production lines, which are the front line for improvement and breakthrough.

Most of steel products are produced by high-temperature steel embryos through rolling process. Because of the high temperature of high-temperature steel embryos, they are constantly reacting with the air to undergo high-temperature oxidation during the air-cooling process and the steel embryos are constantly being rusted. Therefore, during the rolling process, the steel blanks emerging from the continuous casting machine need to be cooled after entering the hot rolling process to reach a specific coil temperature and at the same time avoid the phenomenon of corrosion, so as to obtain the required mechanical properties. The mechanical properties of steel are mainly determined by the proportion of alloying elements contained in the crystal structure and the grain size. When the elements of the alloy are fixed, the growth and size of the crystal grains and the surface flatness of the steel material can be controlled by the temperature distribution of the steel when cooled and the jet impingement's cooling rate. Therefore, the control of the cooling rate in the rolling process of steel has become one of its key technologies.

The jet spray jet cooling with nozzles on the steel plate is a practical technique for rapid cooling in the industry. In the steelmaking plant, hot-rolled steel billets are now used as the main cooling method for jet cooling in the cooling process. The main principle is to use a fluid with high-speed and high-strength impact force to hit the high temperature object directly. The surface of the object, followed by the rapid flow of the fluid to the surface, takes a large amount of heat away from the surface of the object and produces an extremely high heat transfer rate to facilitate rapid cooling of the steel material. At present, the common cooling methods in the industry include laminar cooling, curtain cooling, spray cooling, and ultra-fast cooling. The cooling method in this paper belongs to nozzle fan spray. The high-speed cooling, however, different cooling methods have their advantages and disadvantages and their scope of application.

This study mainly focuses on the rapid cooling of high-temperature steel plates subjected to fan-shaped nozzles, and analyzes its cooling and heat transfer effect. The relationship between the distribution of heat convection coefficients and the corresponding flow rates in the cooling process is further explored. The equipment measures the physical quantities such as temperature in an experimental manner and combines the Fluent module in the commercial software ANSYS with the simple conjugate gradient method for Fortran calculation to calculate and analyze the optimization theory and then find out the distribution of the h value. In order to achieve the desired

mechanical properties and high quality goals for steel products, fast cooling is used to control the phase transition state of the steel in order to increase the mechanical properties and quality of the steel to increase the added value of the material to enhance its competitiveness in the global market.

II. Theoretical Analysis

In this study, the cooling of the fan-shaped atomization nozzles to the high-temperature plate was further investigated experimentally. As shown in the Fig.1, the flow fields at different nozzles were compared and the flow fields of two different types of nozzles were compared. Further experiments and the 3-D inverse heat transfer conjugate gradient method were used to calculate the heat transfer coefficient distribution of the stainless steel flat plate.

In terms of the type of nozzles, our experiments mainly used standard flat spray nozzles to perform experiments. Two types of nozzles were selected for nozzles with larger spray angles under standard pressure.

The part that is cooled by the nozzle is mainly a flat stainless steel with a size of 300mm×300mm×40mm to perform the experiment. The physical model is shown in Fig.2 and the 1/4 model is taken for the analysis in the calculation part of the inverse heat transfer process, and its governing equation is heat conduction equation as following:

$$\frac{\partial}{\partial x}\left(k\frac{\partial T}{\partial x}\right)+\frac{\partial}{\partial y}\left(k\frac{\partial T}{\partial y}\right)+\frac{\partial}{\partial z}\left(k\frac{\partial T}{\partial z}\right)=\rho C_p\frac{\partial T}{\partial t} \quad (1)$$

A. Assumption

(1) Steady-state turbulent flow field.
(2) Incompressible flow.
(3) The fluid properties are constant.
(4) Ignore thermal radiation effects.
(5) No heat generation
(6) Free liquid surface characteristics between air and liquid water
(7) Transient heat conduction process

B. Boundary & Initial Conditions

(1) Bottom surface boundary conditions: adiabatic boundary conditions: $\frac{\partial T}{\partial n}=0$
(2) Plate side boundary conditions: natural convection, let constant heat convection coefficient : h=50 W/m2-K
(3) Plate symmetry boundary conditions: adiabatic boundary conditions: $\frac{\partial T}{\partial n}=0$
(4) Top surface boundary conditions: Fourier Law &Newton cooling Law

$$q''=-k_n\left.\frac{\partial T}{\partial n}\right|_{n=surface}=h\,(T-T_\infty),\ T_\infty=27\,(^\circ C) \quad (2)$$

(5) Plate initial conditions: $T(t=0)=400\pm10\,(^\circ C)$
(6) Cooling time: 20(s)

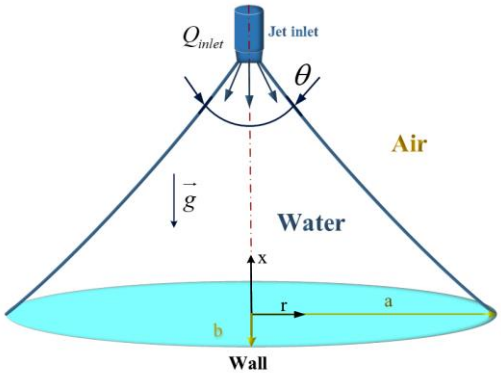

Fig. 1. Schematic diagram of nozzle flow filed

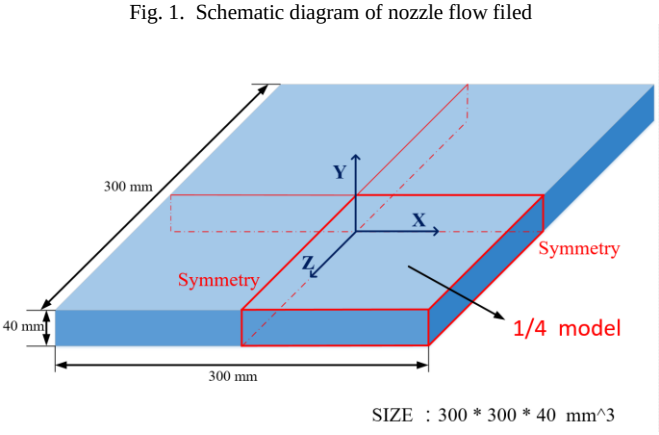

Fig. 2. Physical model of inverse heat conduction

III. Optimization Method

A. Simplified conjugate-gradient method

The Simplified conjugate gradient method was proposed by Prof. Zheng Jinxiang of Cheng-Gong University in 2003. The simple conjugate gradient method separates the step distances with the advantage of retaining the conjugate gradient method and gives it as manual input to avoid complicated calculation steps and geometric limitations. This method makes this method more widely used in the field of multi-variables. The simple conjugate gradient method directly uses the perturbation amount to calculate the gradient function by direct numerical differentiation without solving the gradient equation. Therefore, compared to the complex procedure of conjugate gradient method, we use the simple conjugate gradient method as the search tool to optimize the optimization of the heat transfer coefficient distribution on the plate surface.

The part of the experiment optimized for inverse heat transfer uses a simple conjugate gradient method to bring the objective function within the error of a relative temperature difference of less than 3%. Let $X_n^{(k)}$ be the nth design variable of the kth iteration. The gradient function is the partial differential derivative of the objective function $F(X_n^{(k)})$, ie $\partial F/\partial X_n$, can be obtained directly from the sensitivity analysis via the perturbation method. Sensitivity analysis can use the forward solution subroutine to find the objective function before

and after the fine tuning of the design variables, using the finite difference method, by its numerical solution $\partial F / \partial X_n$ usually to get an objective function $F^{(k)}$ without changing any design variables first, then only one trace of a design variable is changed at a time $X_n' = X_n + \Delta X_n$, and the function is brought into another new target function, which can be obtained by the following equation

$$(F_n^{(k)} - F^{(k)}) / \Delta X_n = \partial F_n^{(k)} / \partial X_n \tag{3}$$

The iterations are the following equation:

$$X_n^{(k+1)} = X_n^{(k)} + \beta_n^{(k)} \xi_n^{(k)} \tag{4}$$

The coefficient of the conjugate gradient method is determined by the ratio of the slope of the previous iteration to the slope of this iteration, as the following equation.

$$\gamma^{(k)} = \left[\sum_n \frac{\partial J_n^{(k)}}{\partial X_n} \Big/ \sum_n \frac{\partial J_n^{(k-1)}}{\partial X_n} \right]^2 \tag{5}$$

From this definition process, the program will reduce the rate of convergence when it reaches the optimum value quickly. Defining the conjugate gradient coefficient is also to let the program automatically determine the size of the correction to avoid exceeding the desired target value. According to the above method, it will automatically iterate until the convergence of the target function is satisfied. The optimization calculation process is summarized as follows:

(1) Define the starting design variable value $X_n^{(k)}$. In this study, the plate is cut into 1/4 models and the surface is cut into 26 regions, i.e. 26 variables $X_1, X_2, \ldots, X_{26}$, each representing the thermal convection coefficient h of each region.

(2) Set the step distance of each design variable $\beta_1, \beta_2, \ldots, \beta_{26}$.

(3) Use the forward solution subroutine (e.g. Fluent) to solve the desired equation after setting the relevant boundary conditions.

(4) Calculate its objective function $F(X_1, X_2, \ldots, X_{26})$. When the target function has satisfied that the relative temperature percentage is less than 3%, the program will stop; otherwise, step (5) will continue.

(5) Sensitivity analysis, calculating the gradient of each variable to the objective function $\partial F_1^{(k)} / \partial X_1, \partial F_2^{(k)} / \partial X_2, \ldots, \partial F_{26}^{(k)} / \partial X_{26}$.

(6) Calculate the conjugate gradient coefficients $\gamma^{(k)}$ and seek direction $\xi_1^{(k)}$ and $\xi_2^{(k)}$.

(7) After updating the design variable value, continue to the next iteration.

In this study, all internal point temperatures measured by the thermocouple during the experiment are defined on the basis of the objective function, and the temperature difference between the temperature and the temperature calculated by the inverse heat transfer calculated with the given initial value is divided by the measured temperature. When the maximum value of all points meets the relative temperature difference of less than 3%, that is:

$$F = \max\left\{ \left| \frac{T_{estimated,1} - T_{exact,1}}{T_{exact,1}} \right|, \left| \frac{T_{estimated,2} - T_{exact,2}}{T_{exact,2}} \right|, \ldots, \left| \frac{T_{estimated,25} - T_{exact,25}}{T_{exact,25}} \right| \right\} < 3\% \tag{6}$$

IV. Experimental Set Up & Method

The entire experimental system was set up to observe the actual flow of fluid from the nozzle to the high-temperature plate, and the cooling status of the high-temperature plate. The experiment of jet cooling was divided into two parts: flow field observation and thermal convection coefficient measurement of high-temperature plate cooling. The flow field observation part is an acrylic sheet whose surface is processed with a scale. The size of the acrylic sheet is 500mm×600mm×5mm, and the scale value can be conveniently used to record the radius of the water impingement zone. However, the test piece of the high-temperature flat plate cooling part is a 300mm×300mm×50mm integrally formed stainless steel plate. The experimental system diagram, as shown in Fig.3, contains four major parts: the test section, the water supply section, the heating section, and the control section. Its experimental entity figure shown in Fig.4.

The flow rate is read by a turbine electronic flowmeter with an accuracy of 2% and a measurement range of 1.8 to 32 L/min. The flow rate for this experiment ranges from 2 to 8.5 L/min. Because fan-shaped nozzles have greater friction at the nozzle opening, the pressure required is also relatively high. Therefore, a 0.5-hp pump is added to each pipe line to increase the pressure. The flow rate required for the experiment.

The main feature of the VVP series of standard fan-shaped nozzles formed by the fan-shaped nozzle used in this experiment is that the flow distribution at the center of the fan-shaped area gradually decreases with the two ends, and when the nozzles are arranged in plural, a nozzle spray shape overlaps at both ends to achieve uniform flow distribution. The angle of the nozzle opening is mainly between 15° and 115°, the standard pressure is 0.3 MPa, and the flow rate can range from 0.3 to 180 Liter/min.

The characteristics of the fan-shaped nozzle are mainly the angle of the nozzle and the amount of spray. The spray angle of the spray nozzle is mainly proportional to the pressure of the nozzle opening. The relationship between the spray amount and the pressure is as follows:

$$Q_{inlet} = Q \times \sqrt{P_{inlet} / P} \tag{7}$$

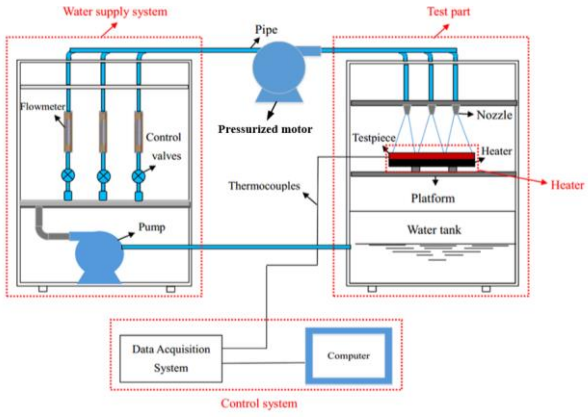

Fig. 3. Schematic diagram of experimental set up

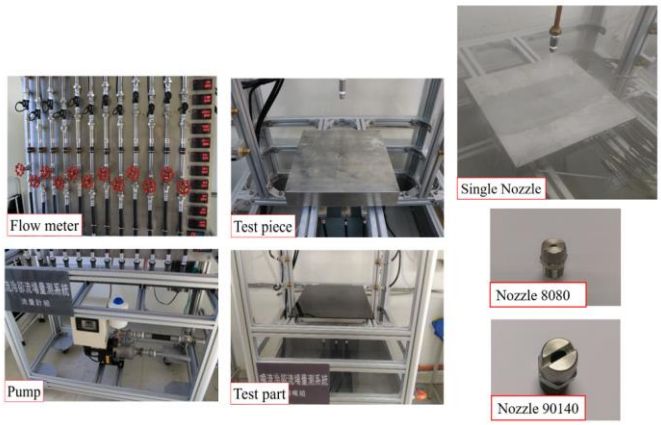

Fig. 4. Experimental apparatus

V. Results & Discussion

A. Different Type Nozzle Flow Field Observation

Fan-shaped nozzle cooling experimental flow field observations, from Fig.5 (a) and (b), see the overall impact area as the flow increases and then it becomes larger. As can be seen from the Fig.5 (c) and (d), which were taken with the camera's high-speed shutter, the shape of the atomization impact gradually increases from the centered phenomenon to the long axis as the flow increases. In the single-nozzle VVP8080 impact cooling high-speed shutter, it can be seen that as the flow rate increases from 2.5 L/min to 7.4 L/min, except that the impact shape of the atomized water gradually increases toward both sides, the water flow The impact speed can be clearly seen from the figure that the overall impact speed also increases significantly with the increase of flow rate.

Then from the point of view of spray angle, we discuss the flow field flow of two different types of nozzles VVP8080 and VVP90140 under the same flow conditions. From Figure 5(a), it can be clearly seen that the VVP8080 has a long axis length of 100 mm at the same flow rate of 2.5 L/min, and the VVP90140 has a length of 70 mm. In the clear observation of the impact area under the atomization impact, it can be seen that the long axis lengths of the atomization impacts of the two nozzles are 85 mm and 60 mm, respectively, and the distance between the fixed nozzle and the acrylic plate spacing is 200 mm. The relationship between the Pythagorean theorem and the trigonometric function can be further calculated as the spray angle angles of 46.05° and 33.40°, respectively. Therefore, the VVP8080 nozzle belongs to the long and short axis of the long flat short ellipse and the VVP90140 belongs to the same flow rate. The major axis is shorter than the minor axis.

Finally, the maximum pressure that can be driven by the pressure pump can be compared with the maximum flow that the two nozzles can impact. It can be found that the VVP8080 nozzle can reach the maximum flow rate of 7.4L/min under the pressure pump driving. From the Fig.6 (a), the long axis of the impact region of the elliptical shape was observed to increase to 260 mm and the length of the corresponding direct impact long axis was 160 mm. The spray angle calculated at this time was 77.32°. According to the relation between flow and pressure from equation (7), the maximum pressure of the pump driven by the nozzle VVP8080 is about 0.257 MPa. At the same time, the flow rate that the VVP90140 nozzle can reach is 8.4 L/min. From the Fig.6 (b), the long axis of the elliptical impact zone is increased to 240 mm and the length of the corresponding direct impact long axis is 170 mm. The angle is 80.72°. And from Equation(7) , the pressure it can reach is about 0.108 MPa, so comparing the pressures that the two can achieve under the same horsepower pump drive has more than one times of drop, mainly due to the two nozzle ports. Different friction causes the VVP90140's nozzle to have a greater pressure loss.

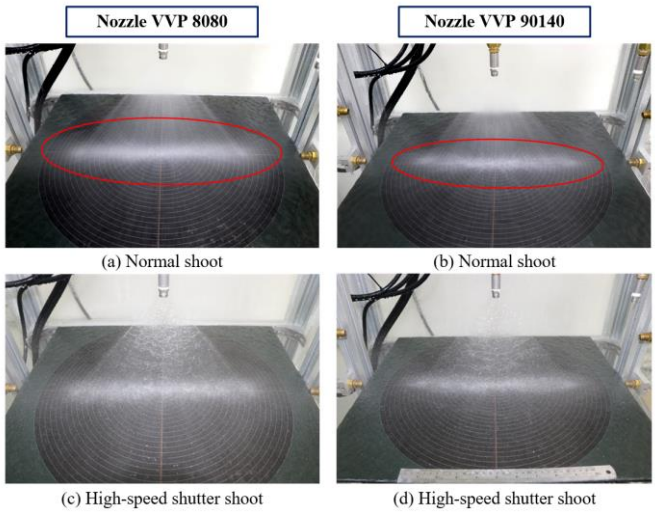

Fig. 5. Flow rate Q=2.5L/min flow field observation

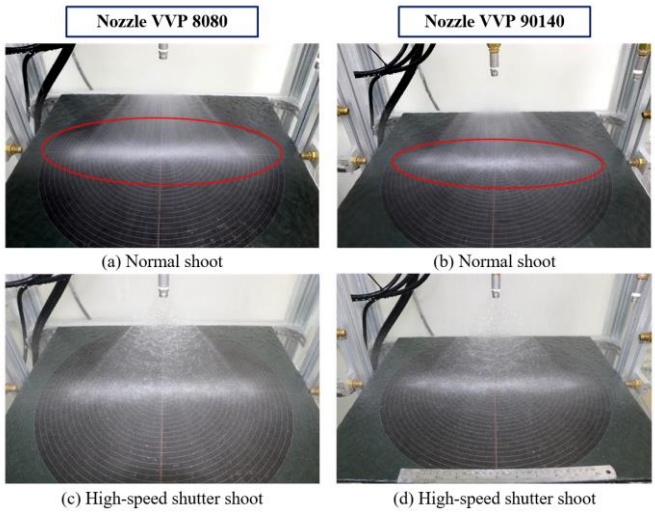

Fig. 6 Flow rate Q=7.4 & 8.5L/min flow field observation

B. Effect of Pitch of Double Nozzle

The phenomenon of interference is discussed by observing the change of the distance between the two nozzles. From Fig.7, the nozzle VVP8080 has three different flow rates: Q = 2.5 L/min, Q = 4 L/min, and At Q=5 L/min, the flow field at different nozzle spacing and the flow pattern of the interference phenomenon are observed from the Fig.7. The nozzle's spacing can be observed when the flow rate Q is 2.5 L/min. It can be clearly seen that the atomization and impact jets of the two nozzles converge at the center line, and this phenomenon still has obvious phenomena when P=150 but it reaches P=100. The

flow phenomenon disappears gradually. Then observe the double-nozzle flow field observation at flow rate Q=4L/min. It can be seen that the confluence can still be seen at the nozzle pitch P=200 and 150, but from the flow situation at P=100 in Fig.8 (b) have disappeared. When the flow rate Q = 5 L/min, the phenomenon of convergence can be clearly seen at P=200 and 150 as in Figs.7 (f) (i). This phenomenon disappears when the nozzle pitch is close.

The process in which we transform this phenomenon is called the distance at which the interference occurs. When the phenomenon of the current flow is not obvious, the two nozzles have the effect of interfering with each other. In this case, not only the interference effect is reduced at the interference point. Phenomenon in the impact cooling of the nozzle will also make the heat transfer effect significantly reduced. In order to avoid this phenomenon, in the experiment process, we changed the distance between two nozzles through the flow field to further find the distance between nozzles when two nozzles interfered at different flow rates and different heights. The nozzles VVP8080's interference distances shown in Table 1

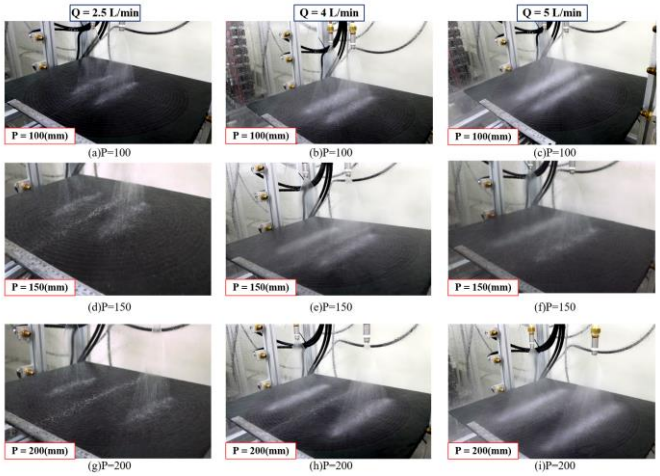

Fig. 7. NozzleVVP8080 different pitch

Nozzle VVP8080	H=200(mm)	H=250(mm)	H=300(mm)
Q = 2.5 L/min	84	110	156
Q = 4 L/min	110	148	200
Q = 5 L/min	120	160	230
Q = 6.4 L/min	180	210	240
Q = 7.4 L/min	250	280	300

C. Double Nozzle Temperature & Instaneous Cooling Rate

From the experimental test-piece temperature measurement position distribution Fig.8, it can be seen that there are ten temperature points located in the short axis area and the fourth quadrant area of the nozzle impact ellipse area in the first quadrant area. And the depth of each measurement temperature point is different. From the analysis of the flow field observation in the previous two nozzles, the whole block heating test-piece cannot be impinged at low flow rate. It can be seen from the Fig.9 that when the flow rate Q = 2.5L/min, two kinds of nozzle temperature diagram and its corresponding instantaneous cooling rate diagram. The distance r in the figure is the distance that extends outward from the center point of the impact area in the right half. From the Fig.9, it is found that when the VVP8080 nozzle is at this flow rate, the temperature at the center point 6 of the two nozzles of Fig.9 (a) is decreasing more slowly. From Fig.9 (b), it can be seen that it begins to cool after 15 seconds. This cooling effect is mainly It is the cooling effect produced by the water flow of the two nozzle jets. Compared to the VVP8080 nozzle VVP90140 (c) (d) the nozzle has a better cooling effect at the center point 6, and at the same time comparing the measurement point 1 because the nozzle VVP90140 has a wider spray angle at a flow rate, so the measuring point 1 of nozzle VVP90140 is faster than the VVP8080's nozzle cooling process, but compared to the nozzle in the long axis (indicated by the square shape of the measurement point)nozzle VVP8080 has a more uniform cooling trend can be seen from the comparison of Fig.9 (b) and (d). The measurement point 9 has a faster cooling phenomenon at VVP8080.

Then, when the maximum flow rate of the two nozzles is reached, it can be seen that both nozzles have reached the same trend in the cooling trend, but from the instantaneous cooling rate Fig.10 (b)(d), it can be seen that the measuring points 1 are respectively 6 seconds. The situation of cooling began only at 4 seconds, mainly because at the time of this flow that the two nozzles are unevenly distributed when the flow rate in the center is small, and the flow rate mainly increases toward both sides. From measurement point 6, it can also be seen that it shows an unstable cooling rate phenomenon at the beginning, which is mainly due to the phenomenon that the film boiling happen on the surface when the water hits the high temperature flat plate. Compared with the previous observation of the flow field, it is also the position where the interference occurs. Therefore, the film boiling effect will influence on the heat transfer phenomenon, then this phenomenon disappears after 9~10 seconds.

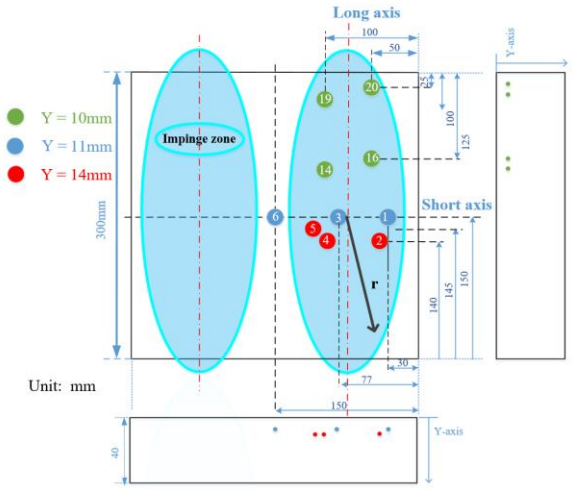

Fig. 8. Experiment measured temperature point

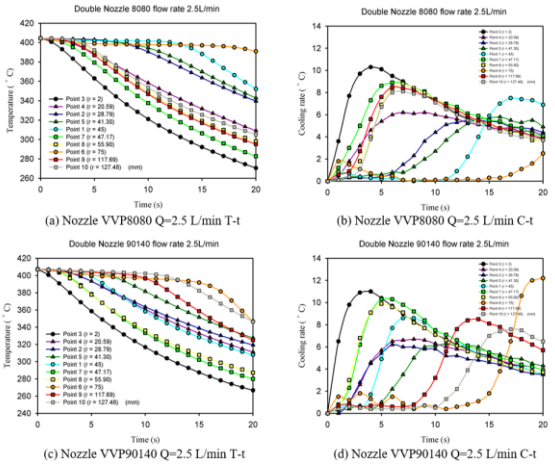

(a) Nozzle VVP8080 Q=2.5 L/min T-t (b) Nozzle VVP8080 Q=2.5 L/min C-t

(c) Nozzle VVP90140 Q=2.5 L/min T-t (d) Nozzle VVP90140 Q=2.5 L/min C-t

Fig. 9. Experiment temperature and cooling rate varied with time (Low Q)

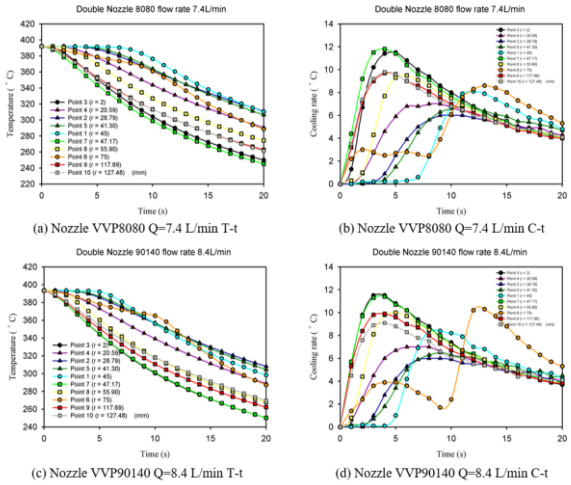

(a) Nozzle VVP8080 Q=7.4 L/min T-t (b) Nozzle VVP8080 Q=7.4 L/min C-t

(c) Nozzle VVP90140 Q=8.4 L/min T-t (d) Nozzle VVP90140 Q=8.4 L/min C-t

Fig. 10. Experiment temperature and cooling rate varied with time (High Q)

D. Double Nozzle Heat Transfer Coefficent

According to the simple conjugate gradient method of inverse heat transfer, the surface heat transfer coefficient distribution of the surface of the stainless steel plate at 20 seconds is solved and the trend of the 26 zones heat transfer coefficient values is used to perform the three-dimensional trend Contour diagram as shown in Fig.11 (a) (c). The heat transfer coefficient figure is projected to the x-y plane as shown in Fig.11 (b) (d). It can be found that when the two nozzles reach the maximum flow, their heat transfer coefficients are distributed at the center and have a limited number of peaks and begin to decline around the center zone, and can be seen from the Fig.11. Seeing that the VVP90140 has a uniform distribution at the centerline of the two nozzles is consistent with the flow field distribution discussed earlier.

The average heat transfer coefficient value is calculated by averaging the heat transfer coefficient distribution of each zone, and the average heat transfer coefficient value calculated at five different flow rates can be found in the value level. The nozzles have similar order, but it can be clearly seen that the VVP8080 has a better heat transfer effect at this distance and height than VVP90140. It can be seen from the Fig.12 that the heat transfer coefficient of both increases with the nozzle at a small flow rate. The area of the impact gradually increased. When the flow rate reached 5L/min and 6L/min respectively, the rising trend of the average heat transfer coefficient of the two nozzles gradually became smooth, mainly because the nozzle spray angle of the two nozzles just impacted the whole heating test-piece at both flow rates. After exceeding these flow rate, the heat transfer effect is enhanced by the effect of increasing the impact force as the flow rate increases.

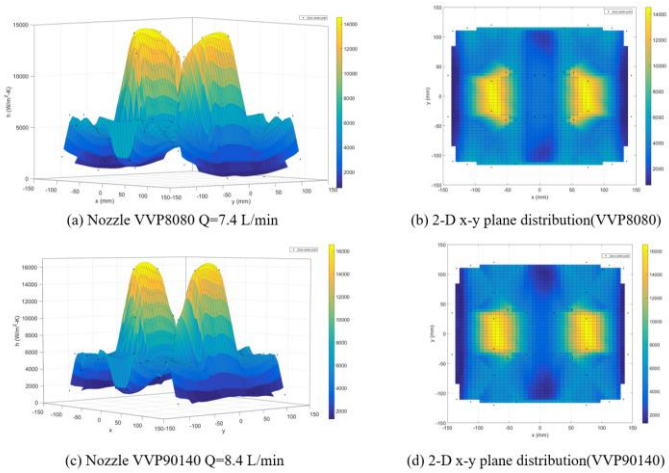

(a) Nozzle VVP8080 Q=7.4 L/min (b) 2-D x-y plane distribution(VVP8080)

(c) Nozzle VVP90140 Q=8.4 L/min (d) 2-D x-y plane distribution(VVP90140)

Fig. 11. 3-D & 2-D heat transfer coefficient distribution contour

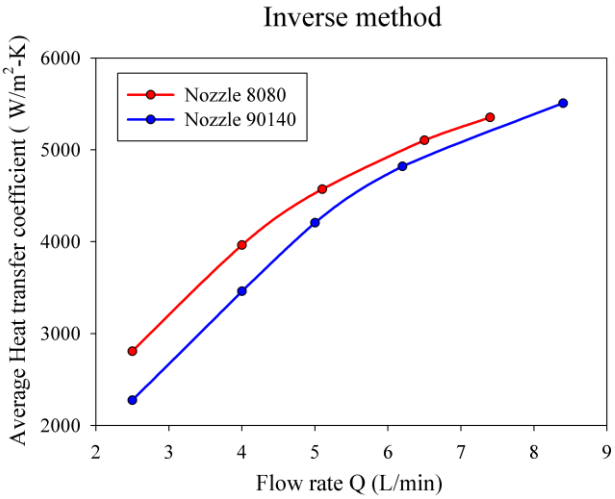

Figure 12 Average heat transfer coefficient v.s flow rate

VI. CONCLUSION

(a) From the observation of the flow field, it can be seen that as the flow rate increases, the fan-shaped nozzle also gradually expands in the impact area.

(b) The double nozzles have different interference distances under different flow rates. Through experimental observations, it was found that when the interference phenomenon occurs, the flow in the interference area will decrease, also the effect of heat transfer will be reduced greatly.

(c)According to the inverse heat transfer result, it can be found that fan nozzle's rapid cooling has a high order of the heat transfer coefficient up to about 5,000. It has excellent cooling effect on the rolling cooling in the steel industry, and it can also controls and improve the quality of steel.

2.International Conference on
Theoretical and Applied Computer Science and Engineering
(ICTACSE, 2018)
Istanbul, Turkey, June 29-30, 2018

Finite Element Analysis of Forced Vibration Problem in Bi-Layered Piezoelectric Plate-Strip Resting on A Rigid Foundation

Ahmet Daşdemir

Department of Mathematics, Faculty of Arts and Sciences, Kastamonu University, Kastamonu University, 37100, Turkey
ahmetdasdemir37@gmail.com

Abstract:

Within the scope of the piecewise homogeneous body model with utilizing of the three dimensional linearized theory of elastic waves in initially stressed bodies (TLTEWISB) the forced vibration of a bi-layered pre-stressed plate-strip under the action of a time-harmonic force resting on a rigid foundation is investigated. The considered plate-strip is constituted by compounding two discrete plate-strips side-by-side. It is assumed that there is complete contact interaction at the interface plane between the layers. To investigate the concrete examples, the materials such as Aluminum and Steel are selected. The mathematical modeling of the problem under consideration is introduced, and the governing system of the partial differential equations of motion is numerically solved by employing Finite Element Method (FEM). In particular, the numerical results exemplifying the influence of a change in the aspect length of each layer on the dynamic response of the plate-strip are investigated.

Keywords: Piezoelectric plate-strip, initial stress, time-harmonic force, forced vibration, rigid foundation.

2.International Conference on
Theoretical and Applied Computer Science and Engineering
(ICTACSE, 2018)
Istanbul, Turkey, June 29-30, 2018

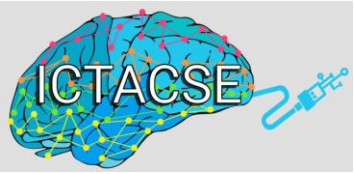

Special Properties of Horadam Quaternions

Ahmet Daşdemir

Department of Mathematics, Faculty of Arts and Sciences, Kastamonu University, Kastamonu University, 37100, Turkey
ahmetdasdemir37@gmail.com

Abstract:

It is the well-known fact that Horadam quaternions were introduced before. In this presentation, we define two new classes of quaternions and give their some properties. We show that there are certain important interrelationships between the Horadam quaternions and our quaternions. In particular, some special properties of Horadam quaternions, including Catalan's identity, d'Ocagne's identity and the Honsberger formula.

Keywords: Horadam quaternion, d'Ocagne's identity, matrix representation, forced vibration, generating function.

2.International Conference on
Theoretical and Applied Computer Science and Engineering
(ICTACSE, 2018)
Istanbul, Turkey, June 29-30, 2018

Mersenne, Jacobsthal and Jacobsthal-Lucas Numbers with Negative Subscripts

Ahmet Daşdemir

Department of Mathematics, Faculty of Arts and Sciences, Kastamonu University, Kastamonu University, 37100, Turkey
ahmetdasdemir37@gmail.com

Abstract:

In this presentation, we show how the Mersenne, Jacobsthal and Jacobsthal-Lucas numbers with negative subscripts can be defined. Furthermore, we present many identities of these sequences such as Catalan's identity and d'Ocagne's identity and certain formulas for computing the sums of their terms. In addition, we give the generating matrices of these sequences. We also that their sums can be obtained by employing matrix technique.

Keywords: Mersenne number, Jacobsthal number, negative subscript, Catalan's identity, matrix method, sum formula.

2.International Conference on
Theoretical and Applied Computer Science and Engineering
(ICTACSE, 2018)
Istanbul, Turkey, June 29-30, 2018

Modeling The Effect the Poling Direction Has on the Dynamic Response of a Pre-stressed Piezoelectric Plate-strip

Ahmet Daşdemir

Department of Mathematics, Faculty of Arts and Sciences, Kastamonu University, Kastamonu University, 37100, Turkey
ahmetdasdemir37@gmail.com

Abstract:

In this presentation, we report on our investigation of the forced vibrations caused by a time-harmonic force from a pre-stressed piezoelectric plate-strip resting on a rigid foundation. Our investigation was formulated within the framework of the piecewise homogeneous body model using exact equations of motion and the relations of the three-dimensional linearized theory of electro-elastic waves in initially stressed bodies (TLTEEWISB). We assumed throughout that there is complete contact between the plate and the rigid foundation. Our purpose in this paper is threefold: we will present the frequency response of pre-stressed piezoelectric plate-strip under consideration; we analyze the effect the poling direction has on that response; and finally, we show how there is a relationship between the initial stress and the poling direction. Given this, we developed a mathematical model, then solved it by employing a finite element method. We present our numerical results, which illustrate the influence of changes in the important problem factors such as initial stress parameter, on the dynamic behavior of the plate.

Keywords: Piezoelectric plate-strip, time-harmonic force, forced vibration, initial stress, rigid foundation.

2.International Conference on
Theoretical and Applied Computer Science and Engineering
(ICTACSE, 2018)
Istanbul, Turkey, June 29-30, 2018

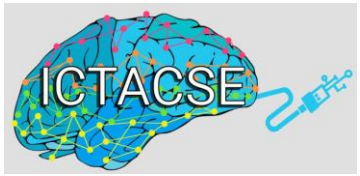

Mathematical Model Of Forced Vibration In A Pre-Stressed Compound Plate-Strip Made From Three Compressible Materials

Ahmet Daşdemir

Department of Mathematics, Faculty of Arts and Sciences, Kastamonu University, Kastamonu University, 37100, Turkey
ahmetdasdemir37@gmail.com

Abstract:

In this presentation, we consider the dynamic response of a pre-stressed plate-strip, which rests on rigid foundation, under the action of a time-harmonic force. The investigation is carried out within the scope of the piecewise homogeneous body model with utilizing the three-dimensional linearized theory of elastic waves in initially stressed bodies (TLTEWISB). The considered body is constituted by compounding three discrete plate-strips side-by-side. We assumed throughout that there is complete contact between the plate-strip and the rigid foundation; further, we assumed that there is complete contact interaction at the interface plane between the layers. A mathematical model of the problem is constructed, and the governing equations of motion are solved by employing the finite element method (FEM). To investigate the concrete examples, the materials such as Aluminum and Steel are selected. In particular, the numerical results exemplifying the influence of a change in the aspect length of each layer on the dynamic response of the plate-strip are investigated.

Keywords: Compressible material, finite element method, dynamic response, initial stress, complete contact condition.

2.International Conference on
Theoretical and Applied Computer Science and Engineering
(ICTACSE, 2018)
Istanbul, Turkey, June 29-30, 2018

Inverse Heat Transfer to Predict the Heat Transfer Coefficient for a Water Jet Impingement over a Flat Plate

Cheng-Chan Chien[1], and Jiin-Yuh Jang[2], and Yu-Feng Gan[3], and Chine-Nan Lin [4]

Department of Mechanical Engineering, National Cheng-Kung University, Tainan, Taiwan
1 E-mail address: d830214s@gmail.com , Tel:+886-62088573 2 E-mail address: jangjim@mail.ncku.edu.tw
3 E-mail address: N18043022@mail.ncku.edu.tw
4 E-mail address: lincn@mail.feu.edu.tw

Abstract

The purpose of the water jet impingement cooling is to improve the mechanical properties of the steel because the growth and the size of the grain and the flatness of the steel are controlled by the temperature distribution and the cooling rate of steel. Therefore, control cooling rate is the key technology in the rolling process to improve the mechanical properties.

This study investigates the heat transfer phenomena of the water jets impingement on a hot steel plate with different flow rate and spray-angle of the flat fan nozzle. The heat transfer coefficients for 2 different kind of flat fan nozzles and 3 different flow rates(2.5L/min to 8 L/min) are calculated by the 3-D inverse heat transfer models solved by an algorithm developed with the conjugate-gradient method. The conjugate gradient method was an iterative method for solving a equation and used to optimize the heat transfer coefficient distribution. A test piece of steel plate was electrically heated from below heat pipe, its top surface was spray cooled and sides' heat transfer through natural convection. The spray was produced from a nozzle supplied with water from a pump and experimental temperature was measured by thermocouples connect to the data processor. The cooling rate and heat transfer effects will be discussed in detailed.

Keywords: conjugate gradient, water jet, inverse heat transfer

2.International Conference on
Theoretical and Applied Computer Science and Engineering
(ICTACSE, 2018)
Istanbul, Turkey, June 29-30, 2018

Brain Tumor Extraction with Different Segmentation Methods

Merve Ozkan Okay[1], Pinar Kullu[2], Sevgi Yigit-Sert[3]
1 ComputerEngineering Department, Ankara University, Ankara, Turkey
merveozkan@ankara.edu.tr
2 ComputerEngineering Department, Ankara University, Ankara, Turkey
kocabasoglu@ankara.edu.tr
3 ComputerEngineering Department, Ankara University, Ankara, Turkey
syigit@ankara.edu.tr

Medical image processing is widely used in some important areas such as detection of cancerous cells in medicine, tissue analysis and pathological research [1]. Medical image processing applications allow numerical analysis and visualization of medical images of different methods such as PET, MRI, CT or microscopy.

The study that one of the most commonly developed in medical image processing is the segmentation of brain MRI images. In this study, the cancerous region, i.e. tumor, in brain was extracted from the original image and different segmentation algorithms were investigated similar to the work in [2]. The study consists of three phases. These are enhancement of the MRI image, segmentation of the enhanced image by different segmentation techniques and application of morphological operations to clearly visualized of extracted tumor from MRI image.

In this study, a methodology was applied to extract the tumorous region from the brain MRI image. In the first stage of the methodology, image enhancement operations are applied. Firstly, the MRI image is read. This image is converted into a grayscale image. The high-pass filter is applied to this converted image. After applying high-pass filter, the image is passed through the median filter to remove noise and increase the quality of the image. In the second step, Otsu thresholding, K-means, Watershed and Fuzzy c-means algorithms are applied on the enhanced image and the tumor region is extracted from the image like [1], [3]. In the final step, some morphological operations (erosion and dilation) are applied to eliminate meaningless points of the image and to highlight the extracted tumor region [4]. When looking at the results of applied different segmentation algorithms, fuzzy c-means can extract the tumorous region with a clearer and fewer meaningless points. However, this algorithm is an iterative process and the run time is more than the others. As a result, if a clearly visualization and accuracy are the main purpose, the methodology using fuzzy c-means algorithm should be selected. On the other hand, the Otsu method should be preferred if the execution time of extracting tumor is to be reduced by ignoring the accuracy of the system.

Keywords: MRI, brain tumor, segmentation, image enhancement, morphological operations

REFERENCES

[1] M.Y. Siyal, L. Yu, “An intelligent modified fuzzy c-means based algorithm for bias estimation and segmentation of brain MRI”, Pattern Recognition Letters 26, 2005, pp. 2052–2062.
[2] A. Kaur, “An Automatic Brain Tumor Extraction System using Different Segmentation Methods”. In: The 2nd International Conference on Computational Intelligence & Communication Technology, Ghaziabad, India, Feb 2016.
[3] E. Dam, M. Loog, M. Letteboer, “Integrating Automatic and Interactive Brain Tumor Segmentation”. In: The 17th International Conference on Pattern Recognition (ICPR’04), Cambridge, UK, Aug 2004.
[4] K. Thapaliya, G.R. Kwon, “Extraction of Brain Tumor Based on Morphological Operations”. In: The 8th International Conference on Computing Technology, Seoul, South Korea, April 2012.

2.International Conference on
Theoretical and Applied Computer Science and Engineering
(ICTACSE, 2018)
Istanbul, Turkey, June 29-30, 2018

Analog-Digital Converter Using Microcomputer

Erdem Özütürk[1]
1 Electrical and Electronics Engineering Department, Engineering Faculty, Uludag University, Bursa, Turkey
ozuturk@uludag.edu.tr

In many applications some analogue signals have been converted to digital signals. In such conditions analogue-digital converters (ADC) must be used. If the circuit is a microprocessor based system, the analogue-digital conversion process can be done by adding analogue-digital conversion subroutine to the programme and by using some additional environmental circuits.

In this study a microprocessor kit is used to perform ADC test circuit. A sample and hold circuit (S/H circuit), a 3-bit R-2R ladder DAC (Digital Analogue Converter), a comparator and a voltage follower circuit are used as environmental circuit. Some nodes of environmental circuits are connected to peripheral interface adapter (PIA) (parallel input-output unit, parallel I/O) pins of microprocessor kit. Four pins of PIA assigned as outputs pins and one pin is assigned as input pin by writing necessary binary word to the data direction register of PIA. 3 outputs of PIA are connected to 3-bit DAC's inputs, so 8 binary count from 000 to 111 can be applied to the inputs of DAC. 8 counts produce 8 voltage level at the output of DAC. Analogue voltage has been applied to the input of sample and hold circuit. Sampling pulse has been applied to the S/H circuit by fourth output pin of PIA. Sampled voltage has been hold at the output of S/H circuit during conversion process. S/H circuit output and DAC output have been connected to the inputs of comparator. Comparator output is connected to input pin of PIA. Comparator output voltage is logic compatible. Using a software, logic level of input pin of PIA can be read and which of the comparator input voltage is bigger can be determined. Logic level at the output of comparator (input pin of PIA) can be learnt by reading read/write (R/W) register of PIA.

Analogue voltage level can be determined as binary or hexadecimal count using the circuit descripted above and using an ADC software. In this study, such a hardware has been built and a machine code programme has been wrote.

Keywords: ADC, DAC, microcomputer, hardware, software.

REFERENCES

[1] E. Ozuturk, "Three bit ADC using microcomputer," final project, Uludag University, Bursa, 1984.
[2] H. Taub, D. Schilling, Digital Integrated Electronics, New York, McGraw-Hill, 1977.
[3] E. Adalı, Mikroişlemciler ve Mikrobilgisayarlar, Birsen Yayınevi, 2004.
[4] M. Rodoplu, "ADC using microcomputer," final project (supervisor E. Ozuturk), Uludag University, Bursa, 1993.

International Conference on
Theoretical and Applied Computer Science and Engineering
(ICTACSE, 2018)
Istanbul, Turkey, June 29-30, 2018

Credit Card Transaction Classification Using Deep Neural Network and Ensemble Methods

Kazım SOYLU[1], Şahin EMRAH AMRAHOV[2]

[1]Department of Computer Engineering, Ankara University, Gölbaşı, Ankara
ksoylu@ankara.edu.tr
[2]Department of Computer Engineering, Ankara University, Gölbaşı, Ankara
Sahin.Emrah@eng.ankara.edu.tr

Credit card frauds are one of the major problems in finance sector. Fraudsters steal card information on an unsecure network or they copy physical card while paying with POS device. After the fraudsters get the card information, they try to use card and cause a financial loss if they are successful. Financial companies intend to prevent fraudulent transactions in order to have customer satisfaction and make their financial loss as low as possible. Fraudulent transactions are impossible to detect by human eyes since many transactions occur every day. Therefore, credit card fraud detection system should be used to detect fraudulent transactions. Accuracy of detecting frauds should be as high as possible and the rate at which legitimate transactions are classified as frauds should be as low as possible. In order to classify credit card transactions into legitimate or fraud, machine learning methods were used. Deep neural network, random forest and stacked ensemble methods were used on a dataset which contains credit card transactions made by European cardholders in two day in September 2013. Stacked ensemble model performs best in terms of AUC and fraud detection rate, but as it requires training of both deep learning and random forest models, its training time is the longest. AUC value of the models were 0.95, 0.94 and 0.92 for the stacked ensemble model, random forest and deep neural network respectively.

Keywords: credit card, fraud, fraudulent transaction, machine learning, deep neural network, random forest, stacked ensemble

References

1. Bekkar M., Djemaa H.K, Alitouche T.A. 2013. Evaluation Measures for Models Assesment over Imbalanced Data Sets. Journal of Information Engineering and Applications, 3(10)
2. Pozzolo, A.D, Caelen, O, Borgne, Y.L, Waterschoot, S, Bontempi, G. 2014. Learned lessons in credit card fraud detection from a practitioner perspective. Expert Systems with Applications, 41(10), 4915-4928

3. Quah, J.T.S, Sriganesh, M. 2008. Real-time credit card fraud detection using computational intelligence. Expert Systems with Applications, 35, 1721-1732.
4. Albon C. 2018. Machine Learning for Python Cookbook. O'Reilly Media, 366, USA.
5. Pandey Y. 2017. Credit Card Fraud Detection Using Deep Learning, International Journal of Advanced Research in Computer Science, 8(5).

International Conference on
Theoretical and Applied Computer Science and Engineering
(ICTACSE, 2018)
Ankara, Turkey, June 29-30, 2018

TARLA LLRF System

Ayhan Aydın[1]

[1]*Department of Computer Engineering, Ankara University, Gölbaşı, Ankara*
ayaydin@ankara.edu.tr

TARLA (Turkish Accelerator and Radiation Laboratory in Ankara) is an accelerator based research facility, designed to generate free electron laser (FEL) and Breamstrahlung radiation using up to 40 MeV electron beam [1]. Electromagnetic fields are used to accelerate charged particle in RF cavities. TARLA have 6 cavities which are need to be controlled by low level radio system (LLRF). Each cavity will individually be driven by independent low-level RF controller. The main task of the LLRF system is to stabilize the amplitude and phase of RF fields. In order to control and monitor this system a MicroTCA.4 based LLRF system is foreseen [2]. MicroTCA is a modular, open standard for building high performance switched fabric computer systems in a small form factor [3].

Keywords: TARLA, LLRF, MicroTCA

Acknowledgments: The study is supported by Ministry of Development of Turkey under Grant No: DPTK2006K120470

References

1. Aksoy, A., Karsli, O., Aydin, A., Kaya, C., Ketenoglu, B., Ketenoglu, D., & Yavas, O. (2018). Current Status of Turkish Accelerator and Radiation Laboratory in Ankara: The TARLA Facility. *Canadian Journal of Physics*, (ja).
2. http://ipac2018.vrws.de/papers/wepmf054.pdf
3. www.picmg.org/openstandarts/microtca

International Conference on
Theoretical and Applied Computer Science and Engineering
(ICTACSE, 2018)
Ankara, Turkey, June 29-30, 2018

Design and Control Electronics Systems of The Beam Position Monitor For Tarla Facility

Ayhan Aydın[1]

[1]*Department of Computer Engineering, Ankara University, Gölbaşı, Ankara*
ayaydin@ankara.edu.tr

A beam diagnostics system is vitally important to operate all accelerator-based facilities Beam position monitors (BPMs) are an essential tool for diagnosing a system of accelerators. They are used to define the position of the beam traversing through the beam pipe at relativistic speed [1]. In this study, a simple, robust, and cost effective BPM front-end electronics and control system is designed and developed for the TARLA by using FPGA based controllers.

Keywords: TARLA, beam diagnostics, BPM

Acknowledgments: The study is supported by Ministry of Development of Turkey under Grant No: DPTK2006K120470

References

1. Aydin, A., & Kasap, E. (2017). Design studies for the beam position monitor (BPM) front-end electronics of the Turkish accelerator and radiation laboratory in Ankara (TARLA). *Turkish Journal of Physics*, *41*(3), 269-276.

2.International Conference on
Theoretical and Applied Computer Science and Engineering
(ICTACSE, 2018)
Istanbul, Turkey, June 29-30, 2018

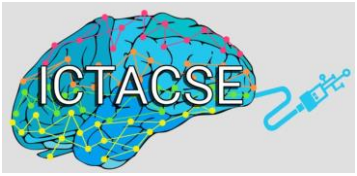

Improving the performance of Multi Layer Perceptron-Back-Propagation Neural Network to Diagnose Parkinson's Disease

Hira Majeed, Maryam Asad, Noman Tanveer, Muhammad Shahid Nazir, Muhammad Aqil
Department of Electrical Engineering
Pakistan Institute of Engineering and Applied Sciences
P.O. 45650, Islamabad, Pakistan
aqil@pieas.edu.pk

Abstract:

There has been active research going on in recent years to diagnose Parkinson's Disease (PD) employing features extracted from the subject's speech. Numerous machine learning approaches have been used for this purpose namely Support Vector Machines (SVM), k-nearest neighbors (k-nn) and Artificial Neural Networks (ANN) etc. Among these, ANNs are characterized by inherent parallelism, a property which enables their efficient implementation in parallel processing environments.

In this study, a type of ANN called Multi-Layer Perceptron-Backpropagation Neural Network (MLP-BPNN) is chosen for classification due to its relative ease of implementation. A previous study employed MLP-BPNN to classify PD patients but the error rates they obtained lied in the range of 40-55%. The target of this study is to improve the performance of MLP-BPNN for diagnosing Parkinson's Disease. The performance of MLP-BPNN is improved for PD detection by modifying the architecture, activation functions and training techniques. The MLP-BPNN with three layers being input, hidden and output layer. The network had twenty-six input neurons (unitary activation function) and two output neurons (softmax activation function). Whereas the number of hidden layer neurons (sigmoid activation function) was varied from 10 to 50 to find the optimized result.

A total of twelve extensively used backpropagation training algorithms were compared considering the accuracy of classification. The accuracy is highest for Bayesian Regularization (89.7%) and is followed by Levenberg-Marquardt (79.9%).

Keywords: parkinson's disease (pd), speech signals, artificial neural networks (ann), multi-layer perceptron-backpropagation neural network (mlp-bpnn)

2.International Conference on
Theoretical and Applied Computer Science and Engineering
(ICTACSE, 2018)
Istanbul, Turkey, June 29-30, 2018

The Role of Social Networks on the Diffusion of Innovation

Semra Gündüç

Department of Computer Engineering
Faculty of Engineering, Ankara University

Abstract

Introduction of a new product or ideal requires market research before the product is introduced in the markets. The success of a new product de-pends on the reactions of the potential customers. In a seminal work, Evert Rogers classified the responses of the prospective costumers, and the essential product features for a market success [2]. Bass introduced the first math-ematical model of diffusion of innovation [?]. The Bass model is based on Rogers' classification of potential adopters. Bass model considers innovation and imitation as the driving forces of diffusion of innovation. The original Bass model has three free parameters, p, q and M. Two of the parameters, (p rmand q) are individual-level characteristics while the third one, M is the size of the market. The firs one of the individual level parameters, p is named as innovation parameter while the second parameter, q is known as the immitation parameter. The initial driving force of a new product adoption process is the innovation parameter, p. Innovation parameter is the representative of the external/global influences such as mass media, online or off-line publicity. Immediately after the initial acceptance of the new prod-uct the imitation parameter, q come into play: The experienced individuals influence the other to adopt the product. In the original Bass model, ignores the social network structures and assumes a homogeneous society.

The relation between the adaptation process and the connectivity of the so-cial networks are subject to more recent investigations [3]. The models which take individual preferences and non-homogeneous connectivity structure are called agent-based models. The agent-based models can consider the differ-ences in the opinion of the individuals as well as the effects of the underlying social interaction networks. To investigate the results of the network and local interactions, recent investigations on the social network structures shed light on the choices. Three social network structures are shown to be the most representative of the social interactions [4]. These are a random net-work, small-world networks, and the scale-free networks.

In this work, the effects of two types of social interactions will be tested on random [5], scale-free [6], and small-world [7] networks. Interactions with the neighbors and influence of the majority are the two crucial concept in the decision-making process. The first effect is related to word-of-mouth. Individuals are affected by the first-hand experiences of their neighbors. The majority opinion also affects individuals. Majority opinion plays a role similar to that of the external influences. Hence the structure of the connectivity of the social network effect the decision mechanisms. At this point, an agent-based model is more appropriate since the heterogeneity of the interactions require a more complicated model that the analytical framework.

REFERENCES

[1] F. Bass, Management Sci. 15, 215 (1969).

[2] E. Rogers, Diffusion of Innovations, 5th ed. (Free Press, New York, 2003).

[3] A. Vespignani, Nature Physics 8 32 (2012).

[4] C. Castellano, S. Fortunato and V. Loreto,Reviews of Modern Physics 81, 592 (2009)

[5] P. Erd¨os, A. R´enyi, Publicationes Mathematicae. 6: 290297 (1959).

[6] A. Barab´asi and R. Albert, Science 286, 509 (1999).

[7] D. J. Watts, S. H. Strogatz, Nature. 393 (6684): 440 (1998).

[8] Z. Dezso and A.-L. Barab´asi, Phys. Rev. E 65, 055103 (2002).

2.International Conference on
Theoretical and Applied Computer Science and Engineering
(ICTACSE, 2018)
Istanbul, Turkey, June 29-30, 2018

Interview in Land Consolidation Using Genetic Algorithm

Şifa ÖZSARI[1], Harun UĞUZ[2], Tayfun ÇAY[3]
1 Computer Engineering, Ankara University, Ankara, Turkey
ozsaris@ankara.edu.tr
2 Computer Engineering, Selçuk University, Konya, Turkey
harun_uguz @selcuk.edu.tr
3 Geomatics Engineering, Selçuk University, Konya, Turkey
tcay@selcuk.edu.tr

Agriculture has ever been the main source of human life. However, as human population are growing day by day, earth's presence in the world remains same, even decreasing. Legal measures, which prevent further fragmentation of agricultural land, should be first taken and then the existing fragmented structure should be reassembled and regulated according to principles of modern agricultural management to increase agricultural productivity, i.e. land consolidation (LC) must be done. In this study, it was emphasized that the interview stage of the land consolidation process, which is currently being carried out manually, is carried out automatically.

In LC process, the stage, in which blocks which are landowners want to take part in are determined, is called interview. The information obtained at this stage is given as input to distribution phase. Therefore, the interview determines to which blocks landowner will take place after consolidation, so it determines success of consolidation. In this study, it is aimed to determine automatically the most appropriate blocks (interview lists) that can be chosen independently from interviewer and to save labour and time in the interview process.

In order to solve the interview problem, pre-processing was performed first. Fixed facilities (houses, wells, etc.) for enterprises are very important because they are not movable, so landowners do not want to change the location of the fixed facilities. In order to decrease the number of parcels used in genetic algorithm and to fulfil the requests of enterprises, pre-processing is carried out on fixed facilities. After the pre-processing was completed, the GA was applied to interview problem by using elitism, tournament selection, crossover and mutation process. According to the experimental results, the method yielded an average 74% accuracy rate.

Keywords: Land consolidation, interview, genetic algorithm

REFERENCES

[1] H. Hakli, H. Uguz, “A novel approach for automated land partitioning using genetic algorithm”, Expert Systems With Applications 82, 2017, pp. 10–18.

[2] J.H. Holland, “Adaption in Natural and Artificial Systems”, *The University of Michigan Press, 1975*.

2.International Conference on
Theoretical and Applied Computer Science and Engineering
(ICTACSE, 2018)
Istanbul, Turkey, June 29-30, 2018

A Link Prediction Approach to Recommender System with Using Cosine Similarity

Zühal Kurt[1], Kemal Özkan[2]
1 Mathematics and Computer Sciences, Eskişehir Osmangazi University, Eskişehir, Turkey
zkurt@ogu.edu.tr
2 Computer Engineering, Eskişehir Osmangazi University, Eskişehir, Turkey
kozkan@ ogu.edu.tr

Recommendation systems is constituted of a particular type of information filtering technique that provide recommendations about items according to the interest expressed by a user. Generally, recommender systems are employed for e-commerce sites utilizing such systems or customer adapted websites, hence their success is imperative for both users and the e-commerce sites. Selling more products and services depends on precise and dependable recommendations, and also increasing user satisfaction. Person–product recommender systems can be defined as adjacency matrix with persons and products nodes and represented as bipartite graphs, also paths of these graphs have odd lengths. Recommendation in bipartite graphs can be moderated as a sub-problem of link prediction, with particular nodes (persons and products) and links (similar relations among persons/ products, and interactions between persons and products). A good link prediction function should give a higher score when there are more paths connecting two nodes, give a higher score when paths are shorter. The purpose of the eigenvalue decomposition of the adjacency matrix is allows to compute a power of the adjacency matrix as $A^k = U\Lambda^k U^T$, which can be used to define link prediction methods such as the matrix exponential, triangle closing and the Neumann kernel [2,4]. Link prediction functions change the eigenvalues, but do not change the eigenvectors, since they are spectral transformations. In the power sum of biadjacency matrix, even powers contain only intra-group values and odd powers contain only inter-group values. Therefore the sum of odd powers of bipartite graphs is important in recommender systems, the resulting link prediction function is the odd polynomial function.

First, we randomly select 10% of the items rated by each user to form a test set. The test set contains only five-star ratings and the training set contains the remaining ratings. Ratings in the training set are converted to complex numbers, if the rating is greater than or equal to three, it is replaced by j, indicating that the user expresses like for the item, when the rating is less than three, -j is provided to represent dislike, if the (user; item) pair is not contained in the training set, it is replaced by 0. We find the user- user cosine similarity matrix for and we find the item- item cosine similarity matrix for

Movielens 100K dataset [1]. The adjacency matrix, A is a symmetric and a square matrix, hence we can use eigenvalue decomposition to A, and this matrix is formed as:

$$A = \begin{bmatrix} \left|\begin{matrix} user-user \\ similarity \end{matrix}\right| & \left|\begin{matrix} user-item \\ ratings \end{matrix}\right| \\ \left|\begin{matrix} item-user \\ ratings \end{matrix}\right| & \left|\begin{matrix} item-item \\ similarity \end{matrix}\right| \end{bmatrix}$$

Higher powers A^k generalize triangle closing to the closing of longer paths and this power sum of biadjacency matrix is yielding e^A. Only paths of odd length are suitable for recommendation in bipartite graphs, hence we use the hiyperbolic sine function to compute odd paths between two nodes into account. Breadth First Search (BFS) algorithm is used to find path of length 3.

The proposed algorithm differs slightly from the CORLP method [3], in adjacency matrix modeling, while calculating of powers of the adjacency matrix and yielding the final recommendation in the same procedure. The results show the proposed method gives much better results, and improves the result %10 percentage from CORLP method. As a future work, we will design a graph image-based recommender system based on semantic relationships among images.

Keywords: Adjacency, bipartite graphs, complex numbers, link prediction, recommender systems.

REFERENCES

[1] http://grouplens.org/datasets/movielens/100k/.

[2] J. Kunegis, G. Gröner, T. Gottron, "Online dating recommender systems: the split-complex number approach," In: Proc. Workshop on Recommender Systems and the Social Web, 2012.

[3] F. Xie, Z. Chen, J. Shang, X. Feng, J. Li, "A link prediction approach for item recommendation with complex number", Knowledge-Based Systems, 81, pp. 148–158, 2015.

[4] J. Kunegis, E. W. De Luca, S. Albayrak, "The Link Prediction Problem in Bipartite Networks," In: Proc. Int. Conf. On Information Processing and Management of Uncertainty in Knowledge-based Systems. pp 380-389, 2010.

2.International Conference on
Theoretical and Applied Computer Science and Engineering
(ICTACSE, 2018)
Istanbul, Turkey, June 29-30, 2018

A New Geometry Design to Adjust Sensor Sensitivity for Diaphragm-Based Optical Sensors

Timucin Emre Tabaru[1], Sekip Esat Hayber[2] and Omer Galip Saracoglu[1, 3]
1 Clinical Engineering Research and Application Center, Erciyes University, Kayseri, Turkey
etabaru@erciyes.edu.tr
2 Department of Electronic and Automation, Ahi Evran University, Kirsehir, Turkey
sehayber@ahievran.edu.tr
3 Department of Electrical and Electronic Engineering, Erciyes University, Kayseri, Turkey
saracog@erciyes.edu.tr

Diaphragm-based fiber optic sensors have been utilized in many application areas due to their high sensitivity, small size, immunity to electromagnetic interference, flexibility, easy adaptability to construction, low energy consumption and resistance to severe environmental conditions. Some of these are ultrasound applications [1], acoustic pressure [2], and partial discharge [3]. In these and similar studies, the sensitivity of the sensor depends on the geometric dimensions of the diaphragm. The sensitivity of a conventional circular diaphragm is determined by two parameters, only radius and thickness.

Increasing the number of parameters in the geometric dimension gives the idea that diaphragms with the desired sensitivity levels can be produced over a wider range. In this study, we have developed a Three Leaf Clover (TLC) -shaped structure that allows for easier adjustment of the desired sensitivity by increasing the number of geometric dimensions.

By showing that a conventional circular diaphragm can easily be converted to a TLC structure by means of MEMS, we have shown that the current sensitivity value can be adjusted to a desired value within a range of 5 times. We have developed an approximate expression for calculating the degree of sensitivity for the TLC structure. Moreover, this proposed structure does not require any external operations to compensate the internal and external pressures [3].

Keywords: diaphragm-based optic sensors, sensitivity, Finite Element Method (FEM), pressure

REFERENCES

[1] Rong, Q., Hao, Y., Zhou, R., Yin, X., Shao, Z., Liang, L., & Qiao, X. (2017). UW Imaging of seismic-physical-models in air using fiber-optic Fabry-Perot Interferometer. Sensors, 17(2), 397.

[2] Gong, Z.; Chen, K.; Zhou, X.; Yang, Y.; Zhao, Z.; Zou, H.; Yu, Q. X. High-sensitivity Fabry-Perot Interferometric Acoustic Sensor for Low-frequency Acoustic Pressure Detections. Journal of Lightwave Technology 2017, 35(24), 5276-5279, DOI: 10.1109/JLT.2017.2761778.

[3] Wang, X.; Li, B.; Xiao, Z.; Lee, S. H.; Roman, H.; Russo, O. L.; Farmer, K. R. An ultra-sensitive optical MEMS sensor for partial discharge detection. Journal of micromechanics and microengineering 2004, 15(3), 521, DOI: 10.1088/0960-1317/15/3/012.

2.International Conference on
Theoretical and Applied Computer Science and Engineering
(ICTACSE, 2018)
Istanbul, Turkey, June 29-30, 2018

Time Domain Analysis of Photoacoustic Wave Equation for Acoustic Pressure Sensor Designs

Timucin Emre Tabaru [1], Sekip Esat Hayber [2] and Omer Galip Saracoglu [1, 3]
1 Clinical Engineering Research and Application Center, Erciyes University, Kayseri, Turkey;
etabaru@erciyes.edu.tr
2 Department of Electronic and Automation, Ahi Evran University, Kirsehir, Turkey;
sehayber@ahievran.edu.tr
3 Department of Electrical and Electronic Engineering, Erciyes University, Kayseri, Turkey
saracog@erciyes.edu.tr

The main mechanism of the Photoacoustic (PA) effect is to apply low energy level laser pulses to an absorbing medium and to create an acoustic wave through it propagating. The light energy absorbed by the material is converted to heat energy. The heat change that occurs in the environment creates the photoacoustic pressure wave.

The pressure wave created by the photoacoustic effect is affected by the medium and laser parameters. The effect of these parameters on the generated pressure wave can be seen by solving the photoacoustic wave equation [1]. These solutions which are examined in the time domain should be considered for the researchers in acoustic sensor design. In particular, time domain analysis contains significant information for the sensor to be designed.

In this study, we make a rigorous analysis about the time domain approaches and the solutions in order to be used in the acoustic sensor designs. In particular, the results of these solutions have been obtained and the effects of the laser and the acoustic signal parameters at different values and boundary conditions on the PA wave are analyzed as well. The PA wave equation consists of a second-order partial differential equation and has temporal and spatial parts. Therefore, the solutions of this equation require quite challenging mathematical operations. For this reason different approaches are used for solutions in the literature. We focused on three of these approaches and analyzed them through solutions and simulations [1-3]. Thanks to these analyzes are showed the effects of laser parameters such as pulse duration, beam width, wavelength, fluence and the acoustic signal parameters such as amplitude, resonance frequency, and bandwidth on the acoustic sensor.

Keywords: pulsed laser photoacoustic method, acoustic pressure sensor, fourier transform, frequency domain solution, photoacoustic wave equation.

REFERENCES

[1] Erkol, Hakan, et al. "Analysis of laser parameters in the solution of photoacoustic wave equation." *Photons Plus Ultrasound: Imaging and Sensing 2013*. Vol. 8581. International Society for Optics and Photonics, 2013.

[2] Wang, Lihong V., and Hsin-I. Wu. *Biomedical optics: principles and imaging*. John Wiley & Sons, 2012..

[3] Kipergil, Esra Aytac, et al. "An analysis of beam parameters on proton-acoustic waves through an analytic approach." *Physics in Medicine & Biology* 62.12 (2017): 4694..

2.International Conference on
Theoretical and Applied Computer Science and Engineering
(ICTACSE, 2018)
Istanbul, Turkey, June 29-30, 2018

Fuzzy Logic and Computer Games

Tufan Kumbasar
Control and Automation Engineering Department,
Istanbul Technical University, Istanbul, Turkey
kumbasart@itu.edu.tr

Computer game industry is one of the biggest high-tech industry as well as its revenue. Depending on their virtual worlds which inspire from real-world dynamicity or facts, they are a perfect test-bed for computational intelligence methods or several types of research [1]-[3]. In the area of computational intelligence, Ordinary (Type-1) fuzzy logic has made a significant breakthrough, especially Type-2 (T2) Fuzzy Logic that is a generalization of Type-1 (T1) fuzzy logic. T2 Fuzzy Logic Controllers (FLCs) have been successfully employed in various engineering problems since IT2-FLCs have the capability of handling high-level uncertainties as well as nonlinear dynamics in comparison with its T1 and conventional counterparts [4], [5].

I will handle three popular computers, namely Flappy Bird Lunar Lander, The Open Racing Car Simulator (TORCS). The games inherent high level of uncertainties and randomness which are the main challenges of the games for a human player. Thus, they can be seen as challenging testbeds for benchmarking fuzzy logic control systems as they provide dynamic and competitive elements that are similar to real-world control engineering problems. As the game player can be considered as the main controller in a feedback loop, we will construct intelligent control systems that are capable to imitate the game player by using T1 and T2 FLCs.

The results of the paper will show that a fuzzy structure is capable to handle the uncertainties caused by the nature of the games by presenting both simulations and real-time game results.

Keywords: Fuzzy Logic, Type-2 Fuzzy Logic, Lunar Lander, Flappy Bird, TORCs

REFERENCES

[1] S. M. Lucas and G. Kendall, “Evolutionary computation and games,” IEEE Computational Intelligence Magazine, vol. 1, no. 1, pp. 10-18, 2006.

[2] A. Sahin, E. Atici and T. Kumbasar, “Type-2 fuzzified flappy bird control system,” in Proc. IEEE Int. Conf. on Fuzzy Syst., 2016, pp.1578-1583.

[3] A. Sahin and T. Kumbasar, “Landing on the Moon with Type-2 Fuzzy Logic,” in Proc. IEEE Int. Conf. on Fuzzy Syst., 2017

[4] J. M. Mendel, H. Hagras, W.W Tan, W.W. Melek, and H. Ying, “Introduction to type-2 fuzzy logic control”, John Wiley and IEEE Press, Hoboken, NJ, 2014.

[5] T. Kumbasar and H. Hagras, Interval type-2 fuzzy PID controllers, In Springer Handbook of Computational Intelligence, Springer Berlin Heidelberg, pp. 285-294, 2015.

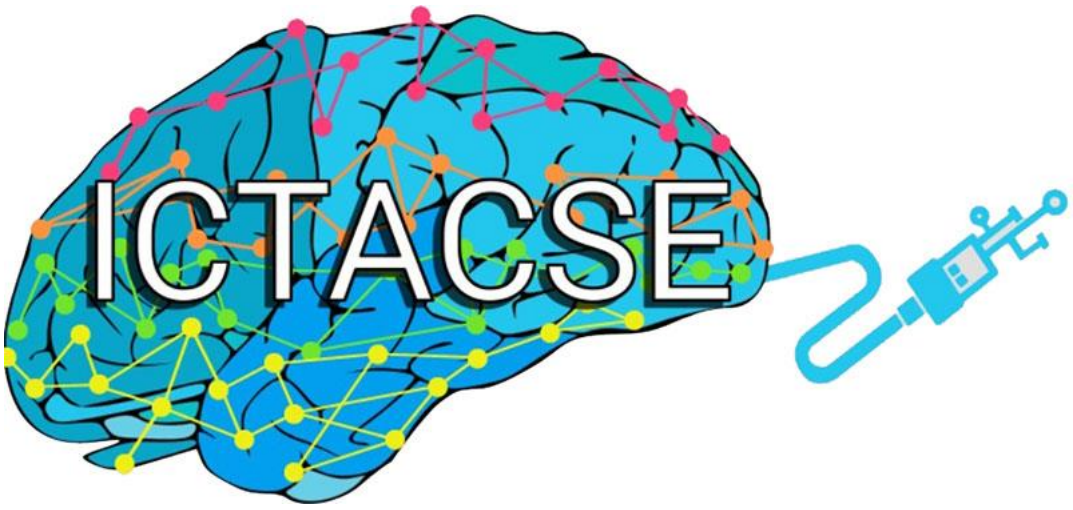

PROCEEDINGS OF BOOK

II. International Conference on Theoretical and Applied Computer Science and Engineering 2018-Summer

ICTACSE 2018

ISBN:978-605-9546-12-6

JUNE 29 – 30, 2018
ISTANBUL, TURKEY

FOREWORD

II. International Conference on Theoretical and Applied Computer Science and Engineering (ICTACSE) will take place on June 29, 2019 in İstanbul, the glamorous city at the heart of two large continents with significant historical heritage from both Byzantine ages and the Ottoman era.

Our conference aims at bringing together researchers and academics for the presentation and discussion of novel theories and applications of computer science and engineering. The conference covers a broad spectrum of topics in the field. Last conference was a great success and we hope that this second event will continue to constitute a base for a long lasting conference series to provide an environment that will strive for academic excellence in research.

ICTACSE provides an ideal academic platform for researchers and scientists to present the latest research findings in computer science and engineering. The conference aims to bring together leading academic scientists, researchers and research scholars to exchange and share their experiences and research results about computer science and engineering studies.

We would like to thank to Promech for their invaluable supports in organizing this event. We would also like to thank to all contributors to conference, especially to plenary speakers who share their significant scientific knowledge with us, to organizing and scientific committee for their great effort on evaluating the manuscripts and participants for sharing their research experience and findings with us. We do believe and hope that each contributor will benefit from the conference.

We hope to see you in our third conference ICTACSE 2018-Winter, which will be announced in our conference website shortly after the conference.

Yours Sincerely,

Asst. Prof. Dr. Gazi Erkan BOSTANCI
Chair of ICTACSE

SCIENTIFIC COMMITTEE

Dr. Ahmad Alzahrani, Umm Alqura University, SA

Dr. Ahmed Mohamed, British Telecom, UK

Dr. Anasol Pena-Rios, University of Essex, British Telecom, UK

Dr. Ayhan Aydın, Ankara University, TR

Dr. Aysenur Bilgin, University of Amsterdam, NL

Dr. Bülent Tuğrul, Ankara University, TR

Dr. Çiğdem Acı, Mersin University, TR

Dr. Erinç Karataş, Ankara University, TR

Dr. Fatih V. Çelebi, Yıldırım Beyazıt, University, TR

Dr. Felix Ngobigha, University of Essex, UK

Dr. Femi Adeyemi-Ejeye, University of Surrey, UK

Dr. Gazi Erkan Bostancı, Ankara University, TR

Dr. Hacer Yalım Keleş, Ankara University, TR

Dr. İman Askerbeyli, Ankara University, TR

Dr. Kurtuluş Küllü, Ankara University, TR

Dr. Mamoona Asghar, Islamia University, PK

Dr. Mehmet Acı, Mersin University, TR

Dr. Mehmet Dikmen, Başkent University, TR

Dr. Mehmet Serdar Güzel, Ankara University, TR

Dr. Murat Osmanoğlu, Ankara University, TR

Dr. Nadia Kanwal, Lahore College for Woman University, PK

Dr. Panitnat Yimyam, Burapha University, TH

Dr. Ramiz Aliguliyev, Azerbaijan National Academy of Sciences

POSTER PRESANTATIONS

Nonlinear Sliding Mode Control Based on Backstepping Approach Applied for 2DoF Planar Parallel Manipulator Biglide Type

El Mostafa LITIM
National Polytechnic School
Maurice Audin
Department of Electrical Engineering
ENPO-BP 1523 EL-M'naouer 3100
Oran Algeria
Email: lit_ldee@yahoo.fr

Abdelkader SAIDANE
National Polytechnic School
Maurice Audin
Department of Electrical Engineering
ENPO-BP 1523 EL-M'naouer 3100
Oran Algeria
Email: saidaneaek@yahoo.com

Abdelhafid OMARI
University of Sciences and Technology
Mohamed Boudiaf
Department of Electrical Engineering
USTO-MB BP1505
Oran, Algeria
Email: o_abdelhafid@hotmail.com

***Abstract*—This work presents the control of a two-degree of freedom parallel manipulator using nonlinear sliding mode based on Backstepping approach. The aim is to achieve a robust control for trajectory tracking, dynamic equations of motion for a two-degree of freedom parallel robot manipulator including structured and unstructured uncertainties are considered. The application of control technique for trajectory tracking in presence of parameter uncertainties in mass variation is studied. The advantage of control technique is that it imposes the desired properties of stability by fixing initially the candidate Lyapunov functions, then by calculating the other functions in a recursive way. Simulation results are presented in order to evaluate the tracking performance and the global stability of the closed loop system. Obtained results show the effectiveness of the proposed controller for a two-degree of freedom parallel robot Biglide type.**

***Keywords*—Parallel robot; Nonlinear control; stability; sliding mode control; Tracking.**

I. INTRODUCTION

Parallel robots are closed-loop mechanisms where all of the links are connected to the ground and the moving platform at the same time. They have high rigidity, load capacity, precision and especially structural stiffness, since the end effectors is linked to the movable platform at several points [1], [2], [3], [4], and [5]. Despite of their advantages, parallel manipulators have also some drawbacks, such as limited workspace and complex kinematic issues caused by the presence of multiple closed loop chains and singularities.

Two categories of parallel manipulators exist, spatial and planar robot. The first category composes of the spatial parallel robots that can translate and rotate in the three dimensional space. Gough-Stewart platform one of the most popular spatial manipulator, is extensively preferred in flight simulators [6], [7]. Therefore, they attracted a lots of researchers interests in recent decades [8] and [9].The planar parallel robot which comprises of second category, translates along the x and y axes, and rotates around the z axis, only. The planar parallel manipulators are increasingly being used in industry for many tasks such as a micro or nano positioning applications [10], and in industrial high speed applications [11]. In this paper, we will discuss the motion control of a planar parallel robot known as Biglide with two degrees of freedom (DoF) [12], [27], [13] and [14]. This type of parallel robot is used in the manufacturing industry of electronic products, as pick and place applications [12], [27]. A dynamical analysis of parallel robot is very complex because the existence of multiple close-loop chains. In addition, due to uncertainties such as not modeled errors of dynamic parameters, measurement noise and external disturbances. Many researchers worked on the dynamic modeling of parallel robots as in [15], [16] and [17]. The Conventional control methods of parallel manipulators have attracted many researchers in studying their performances. A proportional derivative (PD) controller [18], a nonlinear PD controller [19] and an adaptive switching learning PD control method [20], [21] were proposed for the motion control of parallel manipulators. It is also noted in [22] that all of these controllers are simple and easy to implement but they are not robust in presence of uncertainties or when the robot supports different payloads. Some other advanced controllers were proposed, such as the computed torque controller [12] [22], and the adaptive controller [24]. These approaches are based on a full knowledge dynamic model and require a computational power. However, it is complicated to obtain a precise dynamic model of the parallel manipulators, due to the aforementioned drawback [21]. In recent years many researchers are worked on the modern control methods for nonlinear mechanical systems [25],[28] such as adaptive control [26] and [25], TS disruptor [12], Sliding mode control [27] and computed torque control and neural network optimized [23]. These types of controller work very well when all dynamic and physical parameters are known, but when the manipulator has variation in dynamic parameters, the controller has no acceptable performance [12]. Sliding mode control, which is a method, can be a solution, but some bounds on system uncertainties must be pre estimated [27],[29].

In this paper, a new contribution of sliding mode control based on backstepping approach is proposed to control planar parallel robot in the cartesian space. This approach is based on the nonlinear direct dynamic model and sliding mode surfaces. The theories of sliding mode control and backstepping approach have been successfully applied to control planar

parallel robot as in [27] and [28]. The advantage of this type of controllers is low sensitivity versus parameter variations and disturbances. Sliding mode controller has been used for several applications such as Underwater vehicles [27], Active vehicle suspensions [30], Magnetic levitation [31], DC-DC converters [32] and photovoltaic solar in [33].
This paper is organized as follows. In Section2, the dynamic model of 2-DOF parallel manipulator is formulated in the Cartesian space. In Section3, sliding mode controller based on backstepping approach is developed and applied to the direct dynamic model of robot in Cartesian space the Section4, presents simulation results of the proposed controller. Finally, some conclusions are presented in the closing section.

II. Dynamics modeling of Biglide parallel robot

A. Kinematic and geometric analysis

For the geometric and kinematics modeling of a Biglide parallel manipulator, the following conventions are used according to [12], [27]. The manipulator provides 2DoF of translation on the XY plane, the positioning of end effector is represented by operational variables (x,y) driven by two prismatic active joints (q_1,q_2) in the same X axis.
The operational vector is then written as follow:

$$P = [x \quad y]^T \tag{1}$$

The generalized joint variable vector is:

$$q = [q_1 \quad q_2]^T \tag{2}$$

The mechanism has two constant length struts with moveable foot points Figure 1. Both struts have the same lengtha. The relationship between both coordinate vectors is written with kinematic loop-closure constraints Figure 1:

$$\Phi(P,q) = 0, \Phi(P,q) = \begin{pmatrix} (x-q_1)^2+y^2-a^2 \\ (q_2-x)^2+y^2-a^2 \end{pmatrix} \tag{3}$$

The Inverse geometric model (IGM) formula is given by:

$$q = g(P) \tag{4}$$

with

$$g(P) \equiv \begin{pmatrix} x-C(y) \\ x+C(y) \end{pmatrix}, C(y) \equiv \sqrt{a^2-y^2} \tag{5}$$

The direct geometric model (DGM) can be derived from (4):

$$P = g^{-1}(q) \tag{6}$$

with

$$g^{-1}(q) = \begin{pmatrix} \frac{q_1+q_2}{2} \\ \sqrt{a^2-\frac{(q_1+q_2)^2}{4}} \end{pmatrix} \tag{7}$$

The relation between the joint space and the operational space is conveniently described by two Jacobian matrices $J_p(P,q)$ and $J_q(P,q)$ is given as:

$$J_p(P,q)\dot{P} = J_q(P,q)\dot{q} \tag{8}$$

The parallel singularities occur when the Jacobian matrix J_p is rank deficient. The Biglide has two parallel singularities:[12]
• High singularity: $q_1 = q_2 = x$, the struts are superposed and

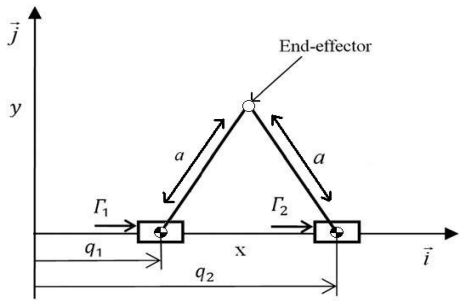

Fig. 1. kinematic schemes of Biglide robot.

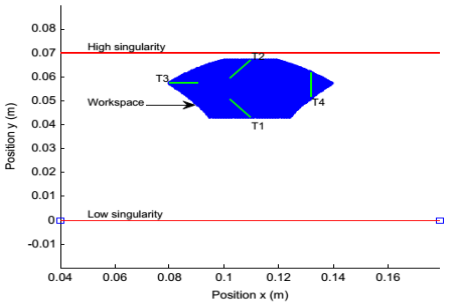

Fig. 2. Workspace and trajectories: $(T1)$ Low trajectory, $(T2)$ High trajectory, $(T3)$ Left trajectory, and $(T4)$ Right trajectory.

$y = 0.07$, Figure 2.
• Low singularity: $y = 0$, the struts are aligned, Figure 2
The kinematic relationship between end-effector velocities and joint velocities is computed by differentiating (3) with respect to time:

$$J_p(P,q)\dot{P} = J_q(P,q)\dot{q} with J_p(P,q) = \begin{bmatrix} x-q_1 & y \\ x-q_2 & y \end{bmatrix}$$

$$J_p(P,q) = \begin{bmatrix} x-q_1 & 0 \\ 0 & x-q_2 \end{bmatrix} \tag{9}$$

B. Dynamic Model

The dynamics equations of the Biglide in operational space are given as follows:

$$\Gamma = M(P)\ddot{P} + N(P,\dot{P}) \tag{10}$$

with

$P = [x,y]^T$, $M(P)$ is the inertial matrix given as follow:

$$M(P) = \begin{pmatrix} m_1 + \frac{1}{2}(m-\lambda_1+\lambda_2) & f_1(P) \\ m_2 + \frac{1}{2}(m-\lambda_2+\lambda_1) & f_2(P) \end{pmatrix} \tag{11}$$

with

$$\lambda_{1,2} = ms_{1,2}/a$$

$$\begin{cases} f_1(P) = [(2m_1-3\lambda_1-\lambda_2)y^2 + mC(y)^2 + J_1 \\ J_2]/(2C(y)\times y) \\ f_2(P) = -[(2m_2-3\lambda_2-\lambda_1)y^2 + mC(y)^2 + J_1 \\ +J_2]/(2C(y)\times y) \end{cases}$$

$$N(P,\dot{P}) = N(y,\dot{y}) + p(y)$$

$N(y,\dot{y})$ is a coriolis / centripetal matrix can be written as:

$$R(y,\dot{y}) = \begin{bmatrix} r_{11} & r_{12} \\ r_{21} & r_{22} \end{bmatrix} \tag{12}$$

$$\begin{cases} r_{11} = r_{12} = 0 \\ r_{12} = -[(2m_1 - 3\lambda_1 - \lambda_2)y^2 + (2m_1 - 3\lambda_1 - \lambda_2) \\ C(y)^2 + J_1 + J_2]\dot{y}/(2C(y)^3 \\ r_{22} = [(2m_2 - 3\lambda_2 - \lambda_1)y^2 + (2m_2 - 3\lambda_2 - \lambda_1) \\ C(y)^2 + J_1 + J_2]\dot{y}/(2C(y)^3 \end{cases}$$

$p(y)$ is a vector containing gravity torques can be written as:

$$p(y) = \begin{pmatrix} (gC(y)(m + \lambda_1 + \lambda_2))/2y \\ (-gC(y)(m + \lambda_1 + \lambda_2))/2y \end{pmatrix} \tag{13}$$

III. Controller design

Backstepping is a recursive procedure that guarantees asymptotic stability by interlacing the choice of a Lyapunov function with the design of feedback control [28].

In this section the control low based on sliding mode control based on Backstepping approach is applied on the direct dynamic model in operational space of 2DoF planar parallel manipulator Biglide type. The results obtained by Backstepping controller were compared to results of PID and Sliding mode control presented by [27].

Using the backstepping approach as recursive algorithm for the control-law synthesis, we simplify all the stages of calculation concerning the tracking error and Lyapunov function in the fallowing way.

$$e_i = \begin{cases} x_{ir} - x_i / i \in \{1,3,5,7,9,11\} \\ x_i - \dot{x}_{(i-1)r} - k_{(i-1)} e_{(i-1)} / i \in \{2,4,6,8,10,12\} \end{cases} \tag{14}$$

with $k_i > 0$

$$v_i = \begin{cases} \frac{1}{2} e_i^2 / i \in \{1,3,5,7,9,11\} \\ v_{(i-1)} + \frac{1}{2} s_i^2 / i \in \{2,4,6,8,10,12\} \end{cases} \tag{15}$$

We use the backstepping algorithm to develop the control allowing the system to follow the desired trajectories (x,y); in fact the algorithm backstepping is described step by step in following. For the first step we consider the tracking-error about x position

$$e_1 = x_r - x \tag{16}$$

Frome (10) the equation of direct dynamic model is given by

$$\ddot{P} = M(P)^{-1} \left[\Gamma - N(P,\dot{P})\right] \tag{17}$$

where $P = [x,y]^T$ is output trajectory position of the end-effector. The derivative equation of tracking-error (16) is computed as

$$\dot{e}_1 = \dot{x}_r - \dot{x} \tag{18}$$

We substituting the equation (16) and (18) in the Lyapunov function. Using the Lyapunov function as

$$V(e_1) = \frac{1}{2} e_1^2 \tag{19}$$

thus

$$\dot{V}(e_1) = e_1 \dot{e}_1 = e_1 (\dot{x}_r - \dot{x}_2) \tag{20}$$

The stabilization of e_1 can be obtained by introducing a virtual control input x_{2d} such that

$$x_{2d} = \dot{x}_r + k_1 e_1 \tag{21}$$

with $k_1 > 0$

$$\dot{x}_{2d} = \ddot{x}_r + k_1 \dot{e}_1 \tag{22}$$

Equation (21) is then

$$\dot{V}(e_1) = -k_1 e_1^2 \tag{23}$$

For the second step we consider variable change by making the dynamic of sliding surfaces, so from (14) we define

$$S_1 = \dot{x} - \dot{x}_r - k_1 e_1 \tag{24}$$

The derivative of S_1 is written as

$$\dot{S}_1 = \ddot{x} - \ddot{x}_r - k_1 \dot{e}_1 \tag{25}$$

We consider the augmented Lyapunov function

$$V(e_1, S_1) = \frac{1}{2}\left(e_1^2 + S_1^2\right) \tag{26}$$

The derivative of equation (26) is calculated as

$$\dot{V}(e_1, S_1) = \left(e_1 \dot{e}_1 + S_1 \dot{S}_1\right) \tag{27}$$

The chosen law for attractive surface is the time derivative of (21) satisfying($S\dot{S} < 0$).

$$\begin{aligned} \dot{S}_1 &= -q_1 sat(S_1) - a_1(S_1) \\ &= \ddot{x} - \ddot{x}_r - k_1 \dot{e}_1 \end{aligned} \tag{28}$$

$$\ddot{x} = \ddot{x}_r - k_1 \dot{e}_1 - q_1 sat(S_1) - a_1(S_1) \tag{29}$$

We consider the same steps for developing a law control to follow y desired trajectory.

$$\ddot{y} = \ddot{y}_r - k_2 \dot{e}_2 - q_2 sat(S_2) - a_2(S_2) \tag{30}$$

Substituting equation (29) and (30) in (10) we obtain the equations of control law as

$$\Gamma = M(P)\,\psi + N\left(P,\dot{P}\right) \tag{31}$$

where $\psi = \begin{bmatrix} \ddot{x}_r - k_1 \dot{e}_1 - q_1 sat(S_1) - a_1(S_1) \\ \ddot{y}_r - k_2 \dot{e}_2 - q_2 sat(S_2) - a_2(S_2) \end{bmatrix}$

$\Gamma = [\ \Gamma_1 \quad \Gamma_2\ ]$ is the vector of control signal.

Stability analysis is proved using Lyapunov theory as

$$V = \frac{1}{2}\left(e_1^2 + S_1^2\right) \tag{32}$$

where

$$S_1 = \dot{x} - \dot{x}_r - k_1 e_1 \tag{33}$$

Substituting equation (18) in (34) we obtain

$$\dot{e}_1 = -S_1 - k_1 e_1 \tag{34}$$

Using the time derivative of Lyapunov theory its trajectory yields

$$\dot{V} = \left(e_1 \dot{e}_1 + S_1 \dot{S}_1\right) \tag{35}$$

will cause

$$\dot{V} = -k_1 e_1^2 - a_1 S_1^2 - q_1 |S_1| \leq 0 \tag{36}$$

with

$$\dot{S}_1 = -q_1 sat(S_1) - a_1(S_1) \tag{37}$$

A. PID controller

The control law based on PID controller in the joint space is given by the following expression:

$$\Gamma = G(s)\varepsilon_q \tag{38}$$

Where Eq.(3) of invers geometric model is used to compute the desired joint positions.

$$q^d = g\left(P^d\right) \tag{39}$$

with $\varepsilon_q = q^d - q$ and the PID controller $G(s) = g_p + g_d s + g_i/s$ Gain g_p, g_d, g_i are $(n_{dof} \times n_{dof})$ positive definite diagonal matrices.
For PID control in the operational space, the control law is obtained by transforming the operational space error signal into the joint space as follows:

$$\Gamma = J^T G(s)\varepsilon_p \tag{40}$$

with $J = J_p^{-1} J_q$ and the PID controller $G(s) = g_p + g_d s + g_i/s$. The error vector is given by

$$\varepsilon_P = P^d - P \tag{41}$$

IV. Simulation result

This section presents the performance evaluation of the proposed Sliding mode based on backstepping approach. The reference trajectory tracking is a 5^{th}order polynomial interpolation. The 2DoF Biglide parallel robot parameters used in simulation are listed in Tab. 1 in appendix. Two cases are considered in the simulation test. In the first case, trajectory tracking with no parameter uncertainties is considered. When for the second case, the system is simulated with parameter uncertainties. The structured uncertainties are considered for a mass variation of the end-effector corresponding to $\Delta m = 0.816kg$; of course no uncertainty corresponds to $\Delta m = 0$. Simulation results of PID, Sliding mode (SMC) and Sliding mode based on backstepping approach (SMC-BS) controllers are presented in Figure 3 and Figure 5 for the trajectories T1 (near work space low boundary) and Figure 4 and Figure 6 for T2 (near work space high boundary), for each figure trajectories, parts (a) and (b) present the set Point and the response along x and y axes and parts (c) and (d) present the control input of both actuators. Note also that Figure 3 and Figure 4 are without mass variation $\Delta m = 0$ where as Figure 5 and Figure 6 uses a mass variation $\Delta m = 0.816kg$; . The mass variation is used to test the robustness and effectiveness of proposed controller, and compared to results of PID and Sliding mode controllers [27].

A. Discussion of simulation results

In the former case, $\Delta m = 0$ going from the best to the worst; The Sliding mode based on backstepping approach and Sliding mode Controller show a good capability of response. Whereas PID shows important overshoot. Based on Figure 5 and Figure 6 by comparing response trajectory with mass variation of platform $\Delta m = 0.816kg$ Sliding mode based on backstepping approach presents good results according to structured uncertainties (parametric variation), compared to Sliding mode which presents some oscillation in trajectory

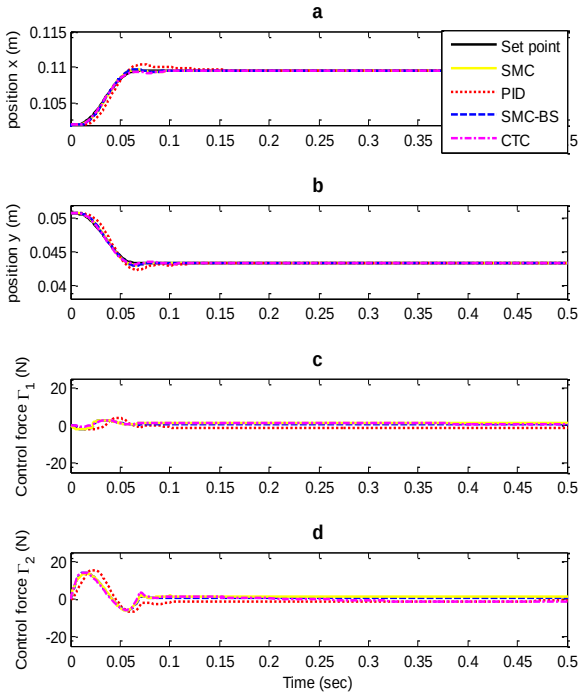

Fig. 3. Control schemes for low trajectory (T1) and $\Delta m = 0$

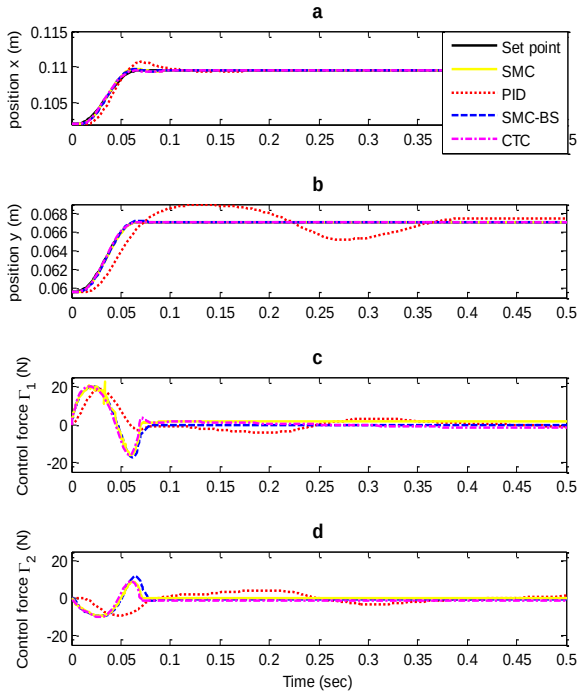

Fig. 4. Control schemes for high trajectory (T2) and $\Delta m = 0$

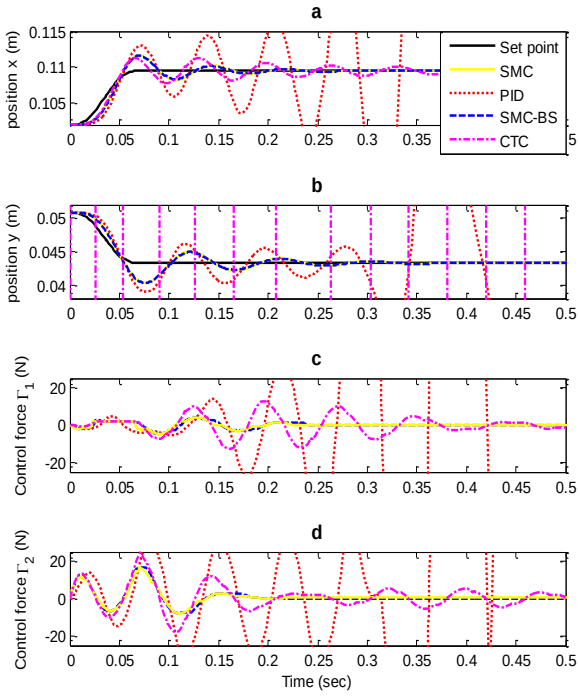

Fig. 5. Control schemes for low trajectory (T1) and $\Delta m = 0.816$

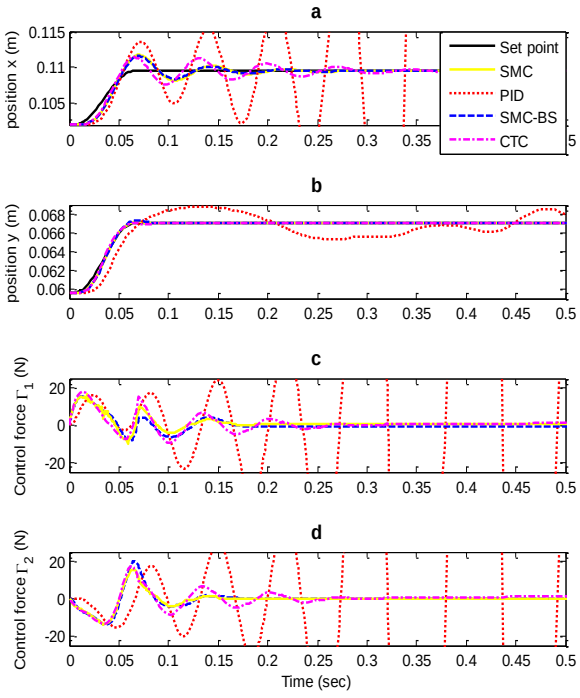

Fig. 6. Control schemes for high trajectory (T2) and $\Delta m = 0.816$

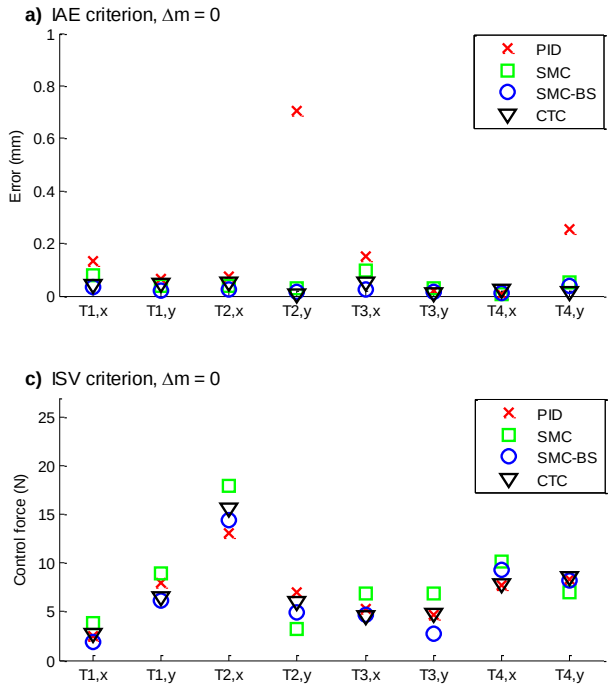

Fig. 7. (a)-(c) Performance criteria (position error and control force) computed for all displacements $(T1\&T4)$ trajectories along x and y axes),$\Delta m = 0$

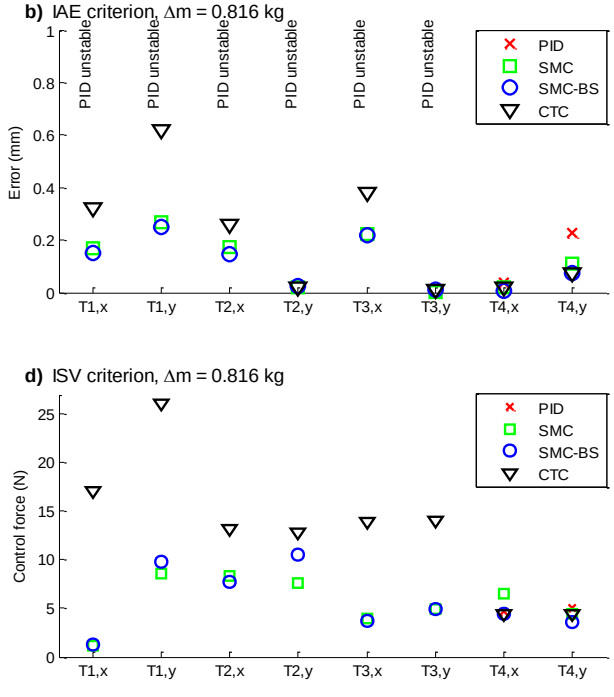

Fig. 8. (b)-(d) Performance criteria (position error and control force) computed for all displacements $(T1\&T4)$ trajectories along x and y axes),$\Delta m = 0.816$

response. PID is even worst with unstable closed-loop. In order to quantify the behaviour of the controllers, some well-known criteria are computed for 4 trajectories T1, T2, T3 and T4 in the work space [12],[27],[28]. The criteria are computed over a time simulation of $T = 2s$ using the error vector, and the control force input vector.
Based on Figure 7(a) and Figure 8(b), comparison is making for obtained results of error positions. In the different cases ($\Delta m = 0$, $\Delta m = 0.816kg$) the Sliding mode based on backstepping approach controller shows a good trajectories tracking with small error. However, Sliding mode controller presents important position error in trajectories tracking. Meanwhile, PID has unstable behaviour with mass variations. Figure 7(c) and Figure 8(d) present the different results of control force. In the different cases $(\Delta m = 0, \Delta m = 0.816kg)$, Sliding mode is much more sensitive to the variation than the Sliding mode based on backstepping approach.

V. Conclusion

This paper, present different results of a nonlinear control approach applied to a planar 2DoF parallel manipulator Biglide type. Using Sliding mode based on backstepping approach to achieve a best performance and robust control for trajectory tracking, the control is based on the direct dynamic model in the Cartesian space of the parallel manipulator. The Sliding mode based on backstepping approach is employed successfully for the regulation and tracking of a multi input multi output planar parallel robot in presence of nonlinearities. Asymptotic stability of the closed loop system is established in the Lyapunov sense.
The obtained results for position control problem are accepted and the control effort is reasonable.

References

[1] KANG, Bongsoo, CHU, Jiaxin, et MILLS, James K. Design of high speed planar parallel manipulator and multiple simultaneous specification control. In : Robotics and Automation, 2001. Proceedings 2001 ICRA. IEEE International Conference on. IEEE, 2001. p. 2723-2728.

[2] KANG, Bongsoo et MILLS, James K. Dynamic modeling and vibration control of high speed planar parallel manipulator. In : Intelligent Robots and Systems, 2001. Proceedings. 2001 IEEE/RSJ International Conference on. IEEE, 2001. p. 1287-1292.

[3] MERLET, Jean-Pierre. Parallel robots. Springer Science Business Media, 2012.

[4] TSAI, Lung-Wen. Robot analysis: the mechanics of serial and parallel manipulators. John Wiley Sons, 1999.

[5] UCHIYAMA, Masaru. Structures and characteristics of parallel manipulators. Advanced robotics, 1993, vol. 8, no 6, p. 545-557.

[6] Gough, V. E. Contribution to discussion of papers on research in automobile stability, control and tyre performance. Proc. Auto Div. Inst. Mech. Eng. Vol. 171. 1956.

[7] Stewart, Doug. A platform with six degrees of freedom. Proceedings of the institution of mechanical engineers 180.1 (1965): 371-386.

[8] Omran, A., and M. Elshabasy. A note on the inverse dynamic control of parallel manipulators. Proceedings of the Institution of Mechanical Engineers, Part C: Journal of Mechanical Engineering Science 224.1 (2010): 25-32.

[9] Cheng, Hui, Yiu-Kuen Yiu, and Zexiang Li. Dynamics and control of redundantly actuated parallel manipulators. Mechatronics, IEEE/ASME Transactions on 8.4 (2003): 483-491.

[10] HUBBARD, Ted, KUJATH, Marek R., et FETTING, H. Microjoints, actuators, grippers, and mechanisms. In : CCToMM Symposium on Mechanisms, Machines and Mechatronics. 2001.

[11] Weck, Manfred, and Dirk Staimer. Parallel kinematic machine tools-current state and future potentials. CIRP Annals-Manufacturing Technology 51.2 (2002): 671-683.

[12] Vermeiren, Laurent, et al. Motion control of planar parallel robot using the fuzzy descriptor system approach. ISA transactions 51.5 (2012): 596-608.

[13] Cheung, Jacob WF, and Y. S. Hung. Modelling and control of a 2-DOF planar parallel manipulator for semiconductor packaging systems. Advanced Intelligent Mechatronics. Proceedings, 2005 IEEE/ASME International Conference on. IEEE, 2005.

[14] Pierrot, FranÃ§ois, et al. Par2: a spatial mechanism for fast planar two-degree-of-freedom pick-and-place applications. Meccanica 46.1 (2011): 239-248.

[15] Khalil, Wisama, and Ouarda Ibrahim. General solution for the dynamic modeling of parallel robots. Journal of Intelligent and robotic systems 49.1 (2007): 19-37.

[16] Staicu, Stefan, Xin-Jun Liu, and Jinsong Wang. Inverse dynamics of the HALF parallel manipulator with revolute actuators. Nonlinear Dynamics 50.1-2 (2007): 1-12.

[17] Staicu, Stefan. Recursive modelling in dynamics of Agile Wrist spherical parallel robot. Robotics and Computer-Integrated Manufacturing 25.2 (2009): 409-416.

[18] Ghorbel, Fathi H., et al. Modeling and set point control of closed-chain mechanisms: theory and experiment. Control Systems Technology, IEEE Transactions on 8.5 (2000): 801-815.

[19] Ouyang, P. R., Wen-Jun Zhang, and Fang-Xiang Wu. "Nonlinear PD control for trajectory tracking with consideration of the design for control methodology." Robotics and Automation, 2002. Proceedings. ICRA'02. IEEE International Conference on. Vol. 4. IEEE, 2002.

[20] Ouyang, P. R., W. J. Zhang, and Madan M. Gupta. An adaptive switching learning control method for trajectory tracking of robot manipulators. Mechatronics 16.1 (2006): 51-61.

[21] Le, Tien Dung, Hee-Jun Kang, and Young-Soo Suh. Chattering-Free Neuro-Sliding Mode Control of 2-DOF Planar Parallel Manipulators. International Journal of Advanced Robotic Systems 10 (2013).

[22] Piltan, Farzin, et al. Sliding mode methodology vs. Computed torque methodology using matlab/simulink and their integration into graduate nonlinear control courses. International Journal of Engineering 6.3 (2012): 142-177.

[23] Yang, Zhiyong, Jiang Wu, and Jiangping Mei. Motor-mechanism dynamic model based neural network optimized computed torque control of a high speed parallel manipulator. Mechatronics 17.7 (2007): 381-390.

[24] Zhu, Xiaocong, et al. Integrated direct/indirect adaptive robust posture trajectory tracking control of a parallel manipulator driven by pneumatic muscles. Control Systems Technology, IEEE Transactions on 17.3 (2009): 576-588.

[25] Slotine, Jean-Jacques E., and Weiping Li. Applied nonlinear control. Vol. 199. No. 1. Englewood Cliffs, NJ: Prentice-Hall, 1991.

[26] Sadati, Nasser, and Rasoul Ghadami. Adaptive multi-model sliding mode control of robotic manipulators using soft computing. Neurocomputing 71.13 (2008): 2702-2710.

[27] LITIM, Mustapha, ALLOUCHE, Benyamine, OMARI, Abdelhafid, et al. Sliding mode control of Biglide planar parallel manipulator. In : Informatics in Control, Automation and Robotics (ICINCO), 2014 11th International Conference on. IEEE, 2014. p. 303-310.

[28] LITIM, Mustapha, OMARI, Abdelhafid, et LARBI, Mohamed El Amine. Control of 2dof Planar Parallel Manipulator Using Backstepping Approach. CONTROL ENGINEERING AND APPLIED INFORMATICS, 2015, vol. 17, no 2, p. 90-98.

[29] Sankaranarayanan, Velupillai, and Arun D. Mahindrakar. Control of a class of underactuated mechanical systems using sliding modes. Robotics, IEEE Transactions on 25.2 (2009): 459-467.

[30] Geravand, Milad, and Nastaran Aghakhani. Fuzzy Sliding Mode Control for applying to active vehicle suspentions. WSEAS Transactions on System and Control 5.1 (2010): 48-57.

[31] Lin, Faa-Jeng, Syuan-Yi Chen, and Kuo-Kai Shyu. Robust dynamic sliding-mode control using adaptive RENN for magnetic levitation system. Neural Networks, IEEE Transactions on 20.6 (2009): 938-951.

[32] Tan, Siew-Chong, Yuk-Ming Lai, and Chi Kong Tse. General design issues of sliding-mode controllers in DC-DC converters." Industrial Electronics, IEEE Transactions on 55.3 (2008): 1160-1174.

[33] Khiari, Br, et al. A Novel Strategy Control of Photovoltaic Solar Pumping System Based on Sliding Mode Control. International Review of Automatic Control 5.2 (2012).

VI. APPENDIX

TABLE I. PARAMETERS MODEL OF BIGLIDE PARALLEL ROBOT

Parameters	Values
Strut length (m) a	0.07
Mass (kg)	
m	0.034
$m1$	0.8040
$m2$	0.7940
First moment of links (kgm)	
ms_1	0.0045
ms_2	0.0043
Second moment of links (kgm^2)	
J_1	222.643×10^{-4}
J_2	2.539×10^{-4}
Gravity acceleration (ms^2)	
g	9.81
Additional parameter for the simulation model Mass (kg)	
λm	0.816

Design and Optimisation of MEMS Capacitive Accelerometer

BENMESSAOUD MOURAD,
Department of Electrical Engineering, National Polytechnic School of Oran Mauris Audin, BP-1523 El Mnaouer, 31000 Oran- Algeria
Mail: benmessaoud_mourad@yahoo.fr,

N.MEKKAKIA MAAZA,
Department of Electronic Engineering, Faculty of Electrical Engineering
University of Science and Technology of Oran, BP 1505, EL M'Naouer. Oran (31000). Algeria

Abstract
A micromachined accelerometer based on an area variation capacitive sensing for more applications was developed, in this case, we will describe and improve in this work the efficacy as well as the sensitivity of a capacitive accelerometer based on an area of variation capacitive sensing considered as a micro system electro mechanical (MEMS) available and realizable. However, the simulation was performed using *MATLAB* as software used in complicated situation with an optimization of the several parameters of accelerometer and a single direction, which is consisted with mobile fingers and fixed fingers, as two springs which ensures the damping of the system. The general concept, main design considerations and performance of the resulted accelerometer was optimized and elaborated in order to obtain a good improvement.

1. Introduction

The Micro Electro Mechanical System (MEMS) technology device design optimization is becoming an interesting and important research issue. However, various efforts on MEMS device design optimization and automation have been made as modeling and simulation of a capacitive micromachined accelerometer.

Compatibility with conventional CMOS provides advantages high yield and fast prototyping that should be adjustable and transferable to any CMOS foundry.
In this work, we present the difference and the relationship between the design optimization of a capacitance folded beam MEMS comb accelerometer device and the device sensitivity such as beam width, beam length, mass width. Based on the analysis, an optimized design of the MEMS comb capacitive accelerometer device is suggested.

2. CMOS micromachining process

The CMOS (complementary metal oxide semiconductor) micromachining accelerometer uses high technology, are made from custom processes combining polysilicon surface micromachining and electronic circuits processes [1]. It is fabricated using three-metal 0.5 µm n-well CMOS process through MOSIS [2]. After the fabrication, two dry etch steps, shown in figure1, are used to define and release the structure. Figure.1.a shows the cross section of the chip after regular CMOS fabrication. In the first step of post processing as shown in Figure.1.b, dielectric layers are removed by an anisotropic CHF_3/O_2 reactive-ion etch (RIE) with the top metal layer acting as an etch resistant mask [3].

After the sidewall of the microstructure is precisely defined, an isotropic SF_6/O_2 (RIE) is performed to etch away the bulk silicon and release the composite structure as shown in Figure.1.c [4]. Layout in the metal layers is designed to form beams, plates, and electrostatic comb fingers. Material property values for the composite structures include a density of 2300 kg/m^3 and a Young's modulus of 62 GPa.

Electrically isolated multi-layer conductors can be routed in the composite structures, enabling more design options (compared to homogeneous conductor structures). For example, electrically decoupled sensing and actuating comb fingers may be built on the same structure and full-bridge capacitive differential and common centroid comb-finger designs can be readily implemented [2].

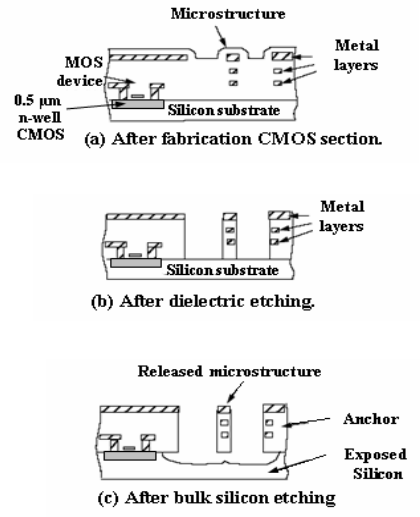

Figure 1.

A full-bridge capacitive sensor has double transducer sensitivity of a half-bridge. Higher transducer sensitivity improves the signal-to-electrical noise ratio. At the same time, since the full-bridge capacitive sensor has differential output, it has better ability to reject common mode noise. The undercut of silicon in the release step (Figure.2) constrains the placement of sensing circuits to at least 15 μm away from the microstructures. Compared to most commercialized polysilicon micromachining technology, the MEMS to electronics interconnect in CMOS-MEMS is shorter, and suffers less parasitic capacitance. Such parasitic on high impedance wiring can be made small relative to input capacitance of interface circuits, so the transducer sensitivity is larger when capacitive sensing is employed.

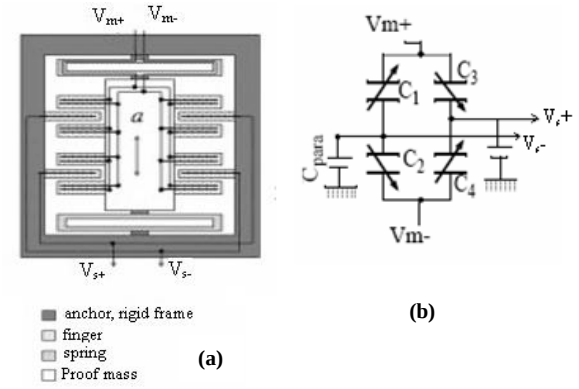

Figure.2.

C_{para}: is the parasitic capacitance and C_1,C_2,C_3,C_4 represent the differential capacities between the movable fingers and the sensing fingers.

Figure.2.a and Figure.2.b represent the schematic of accelerometer and the equivalent model. The topology used here is that of a single axis, common centroid, fully differential, capacitive sensing lateral accelerometer [3]. The proof mass is suspended using four serpentine springs attached to its corners. Interdigitated comb drives are used for differential capacitive sensing as shown in Figure.2.a. Each finger consists of two electrical nodes, one each for the two capacitors on the half capacitive bridge; and the sense nodes are located on the stator fingers. This is used to create a common centroid configuration, which is not possible in polysilicon MEMS. In order to counter out of plane curl mismatch between the comb fingers, the fingers are attached to a peripheral frame rather than being anchored to the substrate.

3. Principle of operation

A schematic of a capacitive micro accelerometer simplified is shown in Figure.4. The central part of the accelerometer is a suspended micromechanical proof mass. When an external acceleration is applied, the proof mass will move with respect to the moving frame of reference which acts as the sensing element [3].

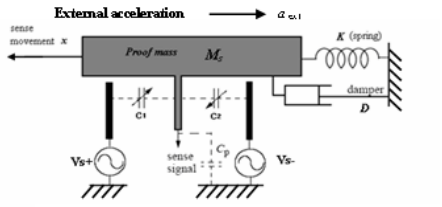

Figure.4.

The displacements of the proof mass imply an acceleration which can be measured by several methods. For the capacitive sensing approach, the displacement is detected by measuring the capacitance change between the proof mass and adjacent fixed electrodes. Low parasitic capacitance achieved from monolithic integration is the key to maximizing the performance with this technique.

On the basis of the mechanical parameters schematic for the sensing element shown in Figure.4, the differential equation for the displacement x as a function of external acceleration is that of a second-order mass-spring-damper system [2], [3]:

$$M_s \cdot \frac{d^2x}{dt^2} + D \cdot \frac{dx}{dt} + K_s \cdot x = M_s \cdot a_{ext} \qquad (1)$$

Where K_s is the spring constant, D is the damping coefficient, M_s is the proof mass and a_{ext} is the external acceleration.

With Laplace transform notation, the above equation converts to a second-order transfer function:

$$\frac{X(s)}{A(s)} = \frac{1}{s^2 + s \cdot \frac{D}{M_s} + \frac{K_s}{M_s}} = \frac{1}{s^2 + s \cdot \frac{\omega_r}{Q} + \omega_r^2} \qquad (2)$$

ω_r: is the resonant frequency,

Q: is the quality factor.

At low frequency (ω<< ωr):

$$\frac{X}{A} \approx \frac{1}{\omega_r^2} \qquad (3)$$

The sensitivity is inversely proportional to the square of the resonant frequency which means the lower the resonant frequency the higher the sensitivity. But actually, the lower limit of resonant frequency is bounded by many factors such as the mechanical shock resistance, the achievable lowest spring constant, the highest possible effective mass, and manufacturability.

4. Device Design

The structure design of a poly-silicon surface-micromachined MEMS comb accelerometer is shown in Figure.5.

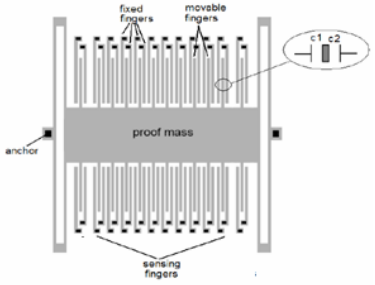

Figure.5.

The movable parts of this MEMS comb accelerometer consist of four folded-beams, a proof mass and some movable fingers. The fixed parts include two anchors and some left / right fixed fingers. The central movable mass is connected to both anchors through four folded beams.
In the right and left side of the each movable finger, there are left and right fixed fingers. The movable fingers constitute the differential capacitance pair C_1 and C_2 with left and right comb fingers [6].
If is no acceleration ($a = 0$) , the movable fingers are resting in the middle of the left and right fixed fingers, the left and right capacitance pairs C_1 and C_2 are equal. When is any acceleration a along horizontal direction parallel to the device plan, the proof mass M_s experiences an inertial force become $-M_s \cdot a$ along the opposite direction. However, the beams deflect and the movable mass and movable fingers move for a certain displacement x along the direction of the inertial force. That automatically changes the left and right capacitance gaps; hence the differential capacitances C_1 and C_2 will also be changed. One can know the value and direction of acceleration one measuring the difference of the capacities change.
When there is no acceleration, a driving voltage V_d is applied to the left or right fixed driving fingers.
The electrostatic force will attract the movable fingers toward the left or right direction. By measuring this displacement and comparing with good device response, one knows whether the device is good or faulty.

5. Mechanical Suspension

The topology of folded beam with turns can provide a lower spring constant, and thus higher sensitivity.

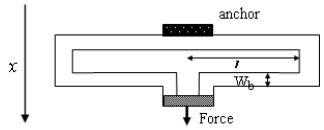

Figure.6.

The spring constant of this structure is:

$$K_s = \frac{1}{2} \cdot E \cdot h \cdot \left(\frac{w_b}{l_b} \right)^3 \qquad (4)$$

The four folded beam can be treated as four springs connected in parallel. Therefore, the spring constant along the Δx direction for a suspension structure as shown in Figure.6, can be determined as:

$$K_{total} = 2 \cdot E \cdot h \cdot \left(\frac{w_b}{l_b} \right)^3 \qquad (5)$$

Where:
Ks: is the constant of spring for one folded beam.
l_b: is the beam length,
w_b: is the beam width,
h: is the beam thickness,
E: is the Young's modulus of the structural material.

6. Damping and Quality Factor

There are two categories of damping mechanisms. First, structural damping is caused by friction within composite structural layers [3]. The second is viscous air damping at atmospheric pressure. For the lateral accelerometer, squeeze film damping which occurs when the air gap between two closely placed parallel surfaces changes, is not critical either.

The damping coefficient between a single comb finger gaps is giving by [8]:

$$D = N_f \cdot \eta_{eff} \cdot l_b \cdot \left(\frac{h}{d_0} \right)^3 \qquad (6)$$

N_f : total sensing finger number.
η_{eff} : is the effective viscosity of air.
d_o: capacitance gap.

However the quality factor is given by:

$$Q = M_s \cdot \omega_r / D \qquad (7)$$

Where:

$$\omega_r = \sqrt{K_s / M_s}$$

Reducing the damping increases the possibility of resonant behavior (high Q).

7. Basic Knowledge for Capacitive MEMS Devices

A typical MEMS differential capacitance structure is shown in Figure.7 where M_s represent the movable plate mass; F_1 and F_2 denote fixed or fingers plates, while B_1 and B_2 are both beams of the MEMS device [9].

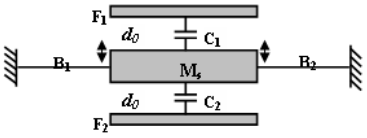

Figure.7.

The movable plate M_s is anchored to the substrate through two flexible beams B_1 and B_2. It constitutes differential capacitances C_1, C_2 with the top and bottom fixed plates. In the static mode, the movable plate M_s is located in the center between F_1 and F_2, therefore:

$$C_1 = C_2 = \frac{\varepsilon_0 \cdot S}{d_0} \qquad (8)$$

Where

ε_0 : is the dielectric constant of air.

S: is the overlap area between M_s and F_1, F_2.

d_0: is the static capacitance gap between M_s and F_1, F_2.

When there is acceleration will result in the deflection of beams and a certain displacement of movable plate M_s along the vertical direction. Assume the central movable mass moves upward

with a displacement of x. Given ($x << d_0$), C_1 and C_2 under the test stimuli can be derived by:

$$C_1 = \frac{\varepsilon_0 \cdot S}{(d_0 - x)} \approx \frac{\varepsilon_0 \cdot S}{d_0}\left(1 + \frac{x}{d_0}\right) \quad (9)$$

$$C_2 = \frac{\varepsilon_0 \cdot S}{(d_0 + x)} \approx \frac{\varepsilon_0 \cdot S}{d_0}\left(1 - \frac{x}{d_0}\right) \quad (10)$$

As there will be a displacement x of the movable plate M_s, modulation voltage V_{mp} and V_{mn} are applied to F_1 and F_2 separately:

$$V_{F1} = V_{mp} = V_0 sqr(\omega \cdot t) \quad (11)$$

$$V_{F2} = V_{mn} = -V_0 sqr(\omega \cdot t) \quad (12)$$

Where:

V_0: the modulation voltage amplitude.

ω: the frequency of the modulation voltage.

t: the time for operation.

According to the charge conservation law, the charge in capacitances C_1 and C_2 must be equal, so we have:

$$C_1(V_{F1} - V_M) = C_2(V_M - V_{F2}) \quad (13)$$

Where V_M is the voltage level sensed by the movable plate M_s. Solving the above equations, we have:

$$V_M = \left(\frac{x}{d_0}\right) \cdot V_0 \cdot sqr(\omega \cdot t) \quad (14)$$

The central movable plate M_s acts as a voltage divider between the top and bottom fixed plates F_1 and F_2 respectively. By measuring the voltage level on central movable electrode V_M, we can find the displacement x of the central movable plate M_s, which in turn is directly proportional to the physical stimuli. Thus, we can derive the value of the applied physical stimuli. This is the working principle for most differential capacitive *MEMS* devices. If voltage V_d is applied to the fixed plate F_1 and nominal voltage $V_{nominal}$ is applied to M_s, an electrostatic attractive force F_d will be experienced by the central movable mass:

$$F_d = \frac{\varepsilon_0 \cdot S \cdot V_d^2}{2 \cdot d_0^2} \quad (15)$$

For vertical electrostatic driving, the driving voltage cannot exceed a threshold value by which the deflection exceeds *1/3* of the capacitance gap d_0. Otherwise, the movable plate will be stuck to the fixed plate through a positive feedback, and a short circuit will occur.

8 Analysis of the Device

When an acceleration a along the horizontal direction parallel to the device plan is applied to the accelerometer, the beam deflects under the effect of inertial force. The deflection of beam is in opposite direction of the applied acceleration. The displacement sensitivity of the device is defined as the displacement of the movable mass and movable fingers per unit gravity acceleration g along devices sensitive direction. The beam-mass structure of the accelerometer can be treated as a simplified spring-mass model. The four folded beam can be treated as four springs connected in parallel.

In order to find out the sensitivity of a comb accelerometer, dynamic analysis must be performed. A MEMS comb accelerometer actually can be simplified by a spring-mass model. For each folded-beam, both sections of the beam can be treated as two springs connected in series. Each beam section can be treated as double-clamped beam model.

Assume for each section of the folded-beam, the beam width and length is W_b and L_b separately. The width and length of central proof mass are W_m and L_m separately. The device thickness (*thickness of the poly-silicon layer*) is h. There is N_f totally sensing finger groups. For each movable finger, the finger width and length are W_f and L_f separately. When there is no acceleration, the capacitance gap between each movable finger and its left / right fixed fingers is d_0. The density ρ, Young's modulus E of poly-silicon material and unit gravity are given as below [9].

Considering that the length not covered with mobile finger is null ($\Delta l_f = 0$) as shown in Figure.8. The static sensing capacitance of the *MEMS* comb accelerometer when there is no acceleration ($a = 0$), is:

From equation (8) we have [6]:

$$C_{10} = C_{20} = C_0 = \frac{\varepsilon_0 \cdot N_f \cdot L_f \cdot h}{d_0} \quad (16)$$

- When there is acceleration ($a \neq 0$) along left direction horizontally; the movable mass experiences an inertial force toward right by x (Figure.4.). Assume small deflection approximation ($x << d_0$), the left (right) capacitances C_1, C_2 are changed to:

$$C_1 = \frac{\varepsilon_0 \cdot N_f \cdot L_f \cdot h}{(d_0 + x)} = \frac{\varepsilon_0 \cdot N_f \cdot L_f \cdot h}{d_0 \cdot (1 + x/d_0)} \quad (17)$$

$$C_2 = \frac{\varepsilon_0 \cdot N_f \cdot L_f \cdot h}{(d_0 - x)} = \frac{\varepsilon_0 \cdot N_f \cdot L_f \cdot h}{d_0 \cdot (1 - x/d_0)} \quad (18)$$

The differential capacitance change ΔC is:

$$\Delta C = C_1 - C_2 = \frac{2 \cdot \varepsilon_0 \cdot N_f \cdot L_f \cdot h}{d_0} \cdot \left(\frac{x}{d_0}\right) \quad (19)$$

From equations (17) and (18), we obtain for small deflection approximation, differential capacitance change ΔC is directly proportional to the displacement x of the movable fingers.

For small beam deflection *(angle<5°),* we can consider the accelerometer as simplified spring-mass model. Assume the total sensing mass of the accelerometer as M_s, the inertial force $F_{inertial}$ experience by the sensing mass for acceleration a along sensitive direction is:

$$F_{inertial} = -M_s \cdot a \quad (20)$$

Take for the total spring constant of the beams as K_{total}, the displacement $\boldsymbol{x}$ of the movable mass can be calculated as:

$$x = \frac{F_{inertial}}{K_{total}} = -\frac{M_s \cdot a}{K_{total}} \qquad (21)$$

The resonant frequency f_0 of the spring-mass system is given by [9]:

$$f_0 = \frac{1}{2 \cdot \pi} \sqrt{K_{total} / M_s} \qquad (22)$$

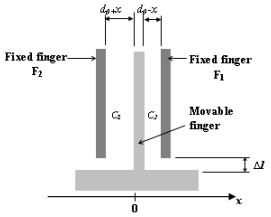

Figure.8.

The sensing mass M_s of the accelerometer includes the seismic mass and all the movable fingers attached to it, can be expressed as [6] :

$$M_s = \rho \cdot h \cdot \left(W_m \cdot L_m + N_f \cdot W_f \cdot L_f\right) \qquad (23)$$

ρ : The density of poly-Si.

h: Device thickness.

Spring constant K_s of one section of beam can be designed by:

$$K_s = \frac{12 \cdot E \cdot I_b}{L_b^3} \qquad (24)$$

Where I_b is the inertial momentum of the beam.

The spring constant K_{fold} of one folded beam [5] is:

$$K_{fold} = K_s = \frac{E \cdot h \cdot W_b^3}{2 \cdot L_b^3} \qquad (25)$$

Four folded beams are connected in parallel and have the same size. Thus, the total spring constant K_{total} of the device is given by:

$$K_{total} = 4 \cdot K_{fold} = \frac{2 \cdot E \cdot h \cdot W_b^3}{L_b^3} \qquad (26)$$

9. Sensitivity Analysis

From equation (21), the displacement of the device along the sensitive direction can be expressed as:

$$x = \frac{M_s \cdot g}{K_{total}} = \frac{\rho \cdot g \cdot \left(W_m \cdot L_m + N_f \cdot W_f \cdot L_f\right) \cdot L_b^3}{2 \cdot E \cdot W_b^3} \qquad (27)$$

And the displacement sensitivity S_d become**:**

$$S_d = \frac{\rho \cdot \left(W_m \cdot L_m + N_f \cdot W_f \cdot L_f\right) \cdot L_b^3}{2 \cdot E \cdot W_b^3} \qquad (28)$$

Given a displacement of the movable mass and fingers where x is much smaller than the static capacitance gap d_0 the capacitance sensitivity S_c can be expressed [8, 9] as:

$$S_C = \frac{2 \cdot N_f \cdot \varepsilon_0 \cdot h \cdot \left(L_{f\cdot} - \Delta L_f\right)}{d_0^2} \cdot S_d \qquad (29)$$

Where Δl_f is the length not covered of mobile finger, and if it is considered that Δl_f much lower ($\Delta l_f \approx 0$) however: The capacitance sensitivity *Sc* is given by [11]:

$$= \frac{2 \cdot \varepsilon_0 \cdot N_f \cdot L_f \cdot h}{d_0^2} \cdot \frac{M_s \cdot g}{K_{total}} \qquad (30)$$

10. Presentation and analyzes studied model

We use MATLAB software to calculate the displacement, capacitance and sensitivity.

For following data (see Table.1):

The structural thickness layer in this device is limited to be 6 μm.

Table.1: Physical and geometrical parameters of the model

Parameters	**Design**
Capacitance gap d_0	3 μm
Device thickness h	6 μm
Mass Width W_m	80 μm
Mass length L_m	200 μm
Beam Width W_b	3 μm
Beam length L_b	270 μm
Finger width W_f	3 μm
Finger length L_f	160 μm
Number of sensing fingers N_f	32
Young's modulus of poly-Si E	1.72 x10^{11} Pa
The dielectric constant of air ε_0	8.854 x 10^{-12} F/m
The density of poly-Si ρ	2.33 x 10^3 Kg/m^3
Gravity acceleration **g**	9.81 m/s^2
Movable sensing mass M_s	0.43841 μg
Spring constant K_{total}	2.8313 N/m

10.1 Movable mass displacement as a function of acceleration $x = f(g)$

The displacement behaviour of movable mass as a function of acceleration with the basis of 0 up to 10g by pad of 2g is shown in Figure.9.

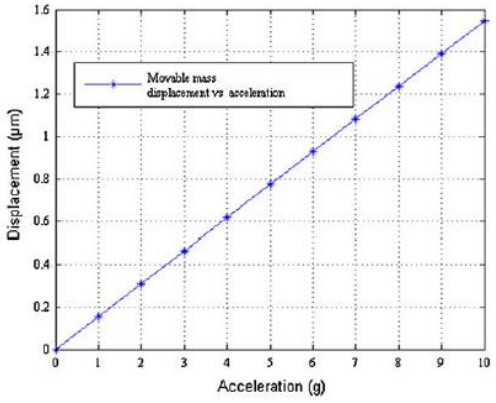

Figure.9.

However, we can conclude that the increase in acceleration implies an increase in the displacement sensibility.

10.2 Capacitance sensitivity S_c = f(x)

Knowing that x depends on g and $x<<d_0$ then, the simulation of sensitivity as a function of movable mass displacement is given in Figure.10:

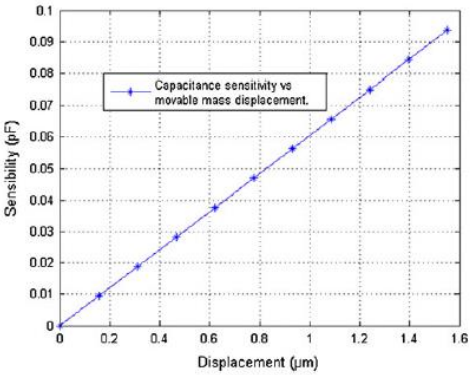

Figure.10.

We note that the difference in capacity is extremely sensitive at the minimum displacement of the mobile fingers that explains the effectiveness of the model.

10.3 Capacitance sensitivity S_c = f(g)

A graphics presentation of capacitance sensitivity as a function of acceleration with the 0g basis up to 5g, is shown in Figure.11.

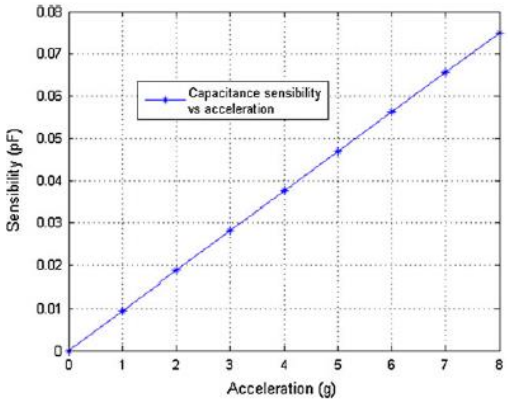

Figure.11.

It is clear that the accelerations increase implies an increase in the capacitance sensitivity S_c; this proves that one can count on this model to obtain a high precision sensitivity.

11. Conclusion

After the results obtained by simulation of some parameters accelerometer capacitive, we note that the geometry of the component such as the width and the length of the mobile fingers as those of spring take a very important role on the acceleration sensitivity.

Theoretically, we can narrow down the beam width W_b to achieve very high device sensitivity. However, there is always a bottom limit for the beam width set by the minimum line width in a fabrication process. If the beam width is too narrow less than 2µm, it will become very challenging to fabricate the beam because the beam is extremely fragile and can be easily broken.

Therefore, to obtaining a good performance and a good sensitivity of a capacitive accelerometer, it is necessary to choose better parameters such as the beam width and the beam length (W_b and L_b) which represents the suspension of the acceleration system.

Other share, the mobile fingers width and length (W_F and L_f) which constitute the capacities between the mobile fingers and the fixed fingers influence directly the value of these capacities then acceleration, which requires a choice very precise of these parameters.

References

[1] Huikai Xie and Gary K.Fedder; A CMOS Z-axis capacitive accelerometer with comb finger sensing, , Department of Electrical and computer Engineering and the Robotic Institute , Carnegie Mellon University, Pittsburgh, PA 15213-3890, USA.

[2] Hao Luo, Gang Zhang, L.Richard Carley, Fellow, IEEE, and Gray K.Fedder (2002). A post-CMOS micromachined lateral accelerometer. Journal of micro-electro-mechanical systems, vol.11. no. 3.

[3] Gang Zhang,B.S., Tsinghua (1994) Design and simulation of a CMOS-MEMS accelerometer, University, Carnegie Mellon University.

[4] Gang Zhang, Huikai Xie, Lauren E.de Rosset and Gary K.Fedder (1999), A lateral capacitive CMOS Accelerometer with structural curl compensation, Department of electrical and computer engineering and the robotics istitute, carnegie mellon university, Pittsburgh. PA15213-3890.IEEE 1999.

[5] Vishal Gupta and Tamal Mukherjeem. Layout synthesis of CMOS MEMS accelerometers. Department of ECE, Carnegie Mellon University, Pittsburgh, PA-15213.

[6] Kanchan Sharma, Isaac G. Macwan, Linfeng Zhang. Lawrence Hmurcik, Xingguo Xiong, Design optimization of MEMS comb accelerometer. Department of electrical and computer engineering, university of Bridgeport, Bridgeport, CT 06604.

[7] Cheng-Kuan Lu (2008). Wireless MEMS accelerometer for real-time. Department of electrical engineering and computer science, Case western reserve university.

[8] Babak Vakili Amini (2006). A mixed-signal low-noise sigma-delta interface IC for integrated sub-micro-gravity capacitive SOI accelerometers. School of Electrical and Computer Engineering ,Georgia Institute of Technology ,

[9] Xingguo Xiong (2005). Built-in self-test and self-repair for capacitive MEMS devices, Department of Electrical and Computer Engineering and Computer Science of the College of Engineering .

A Power System Connected Fuel Cell Based On Instantaneous P-Q Theory

Rachid. Dehini
University of Bechar , Algeria,
Department of Electrical Engineering, Faculty of Technology,Postal address1, B.P 417 Bechar, Algeria, E-Mail1: dehini_ra@yahoo.fr
Berbaoui Brahim
Centre de Developpement des Energies Renouvelables, Unité de Recherche en Energies Renouvelables en Milieu Saharien, Adrar, Algiers, b_berbaoui@yahoo.fr, ORCID: https://orcid.org/0000-0003-1655-9768

***Abstract* – A leading factor in the evolutionary change of fuel cells is the need to reduce green house gas emissions (especially CO2), less polluting means of energy production are searched, such as fuel cells that are highly energy efficient. The Proton-exchange membrane Fuel cells (PEM) are more and more involved in various applications, the primary objective of this work is to present the uses of (PEM) in supplying the active compensator. The use of instantaneous p-q theory as a control system of the inverter results the multi-operation inverter, such as harmonic elimination, reactive power control and uninterruptible power supply will be achieved. The system consisting of Fuel cells, connected to a diode rectifier feeding a parallel active power filter. The simulation results prove the efficiency of using the proposed method for power quality improvement and Feed-in of Fuel cells -generated electricity into the public grid.**

Keywords – PEMFC cells energy, voltage source inverter, , PAPF, current harmonics, p-q theory.

I. INTRODUCTION

Energy and fuel exigency is rapidly increasing with time, and the fossil fuel time is getting missing. At the same time energy cost is also continuously rising. So as to overcome these anxieties we can use renewable resources at our disposal from which energy can be tapped; a fuel cell converts chemical energy to direct electric energy [1]. This alternative source is the clean energy, without any harmful emissions to the environment, and has high power density [2]. One of the most popular fuel cell is the Proton Exchange Membrane (PEM).it has been researched and developed, that they have gradually been recognized to work in a comparatively high efficiency and low temperature condition [3-4-5].

The harmonics injected by the non-linear loads have several impacts on the utilities grid and loads connected to system [6]. To solve these power quality problems, Parallel active power filter (PAPF) is extensively used in the system. This device is a power converter utilized to compensate current disturbances (harmonics, reactive power and unbalance) [7].Several topologies have been introduced in the literature and in commercial implementations for this filter that highlight different aspects of its compensation tasks. The most common topology of the shunt active power filter is shown in fig. 1. Its main components are voltage source inverter, DC bus (in our situation is a capacitor or fuel cell), output passive filter and a control system. The most important objective of the PAPF is to compensate the current harmonics generated by non linear loads. The reference currents consist of the harmonic components of the load currents which the active filter must supply [8-9]. These reference currents are fed through a controller to generate switching signals for the power switching devices of the voltage source inverter (VSI). Finally, the AC supply will only need to provide the fundamental component for the non linear load.

In this paper, the analysis are focused on the system configuration with a direct coupling between the (PEM) fuel cells and the shunt active power filter employed to inject the fuel cell power into the utility grid under fixed fuel cells power conditions. The proposed design is not only able of delivering the chemical power to the grid, but will also act as a parallel active power filter (PAPF) to mitigate the current harmonics and regulate reactive power injected by the non-linear loads. In order to reduce the impact of harmonic currents and strengthen the overall capacity of the proposed system ; a 100KW fuel cells power with shunt active power filter connected to a three-phase power grid feeding non-linear load was simulated in MATLAB / SIMULINK environment.

II. PEM FUEL CELL GENERATOR MODELING

Electrical energy needs are still increasing over these last years but production constraints like pollution and global warming lead to development of renewable energy sources, particularly chemical energy. Fuel cells (FCs) are static energy conversion devices that convert the chemical energy of fuel

directly into DC electrical energy [10]. The fuel cell consists of two porous electrodes (anode and cathode) and an electrolyte layer in the middle. Figure (2) illustrate Fuel cell (PEMFC) [11].

The chemical energy of a fuel is converted, the fuel H2 is supplied under certain pressure. The hydrogen concentration should be determined in the mixture. The fuel spreads through the electrode until it reaches the catalytic layer of the anode where it reacts to form protons and electrons, as given in the following reaction:

$H_2+1/2O_2 \rightarrow H_2O+heat+electrical$ energy (1)

Hydrogen oxidation and oxygen reduction are separated by a membrane, which is conducting protons from the anode to the cathode side [10].

$H_2 \rightarrow 2\ H^+ + 2\ e^-$ anode (2)

$O_2 + 4\ e^- \rightarrow 2\ O^{-2}$ cathode (3)

The protons are diffused through the membrane, and the electrons are carried across an electric circuit, the electrical energy is produced. The cell voltage was defined as:

$$V_{FC} = E_{nernst} - V_{act} - V_{ohm} - V_{conc} \quad (4)$$

E_{nernst} is the thermodynamic potential of the cell and its represents reversible voltage;

V_{act} is the voltage drop due to the activation of the anode and of the cathode.

V_{ohm} is the ohmic voltage drop, a measure of the ohmic voltage drop associated with the conduction of the protons through the solid electrolyte and electrons through the internal electronic resistances.

V_{conc} represents the voltage drop resulting from the concentration or mass transportation of the reacting gases .

V_{FC} represents the open circuit voltage.

Each term in (4) can be calculated by the following equations [4].

$$E_{nerst} = 1{,}229 + 0{,}85.10^{-3}(T - 298{,}15) + 4{,}31.10^{-5}.T.\ln(P_{H2}.P_{O2}^{0.5}) \quad (5)$$

P_{H2} and P_{O2} are the partial pressures of hydrogen and oxygen (atm) respectively, T the cell operation temperature (K).

$$V_{act} = -\left[\xi_1 + \xi_2 T + \xi_3.T.\ln(Co_2) + \xi_4.\ln(I_{stack})\right] \quad (6)$$

Where I_{stack} is the cell operating current (A), and the ξ_i 's represent parametric coefficients for each cell model, whose values are defined based on theoretical equations with kinetic, thermodynamic, and electrochemical foundations [11]. Co_2 is the concentration of oxygen in the catalytic interface of the cathode mol/cm, determined by:

$$Co_2 = \frac{Po_2}{5{,}08.10^6.e^{(-498/T)}} \quad (7)$$

$$V_{ohmic} = I_{stack}.(R_m + R_c) \quad (8)$$

Where Rc represents the resistance to the transfer of protons through the membrane, usually considered constant and: $R_m = \frac{\rho.l}{A}$ with:

ρ : is the specific resistivity of the membrane for the electron flow (cm), A is the cell active area (cm) and l is the thickness of the membrane (cm), which serves as the electrolytic of the cell.

$$V_{conc} = B.\ln\left(1 - \frac{J_n}{J_{\max}}\right) \quad (9)$$

Where B (V) is a parametric coefficient, which depends on the cell and its operation state, and J_n represents the actual current density of the cell (A/cm).

Due to very limited conversion efficiency, it is necessary to optimize all the conversion chain and specifically DC-DC converters [12].There are many types of DC/DC converters. In this paper, only typical boost converter is discussed. Figure (3) shows the circuit diagram of a boost DC/DC converter (inside the rectangle). The output voltage regulation feedback is also given in the figure (4).

The average value of the output voltage is given as:

$$V_{FCout} = \frac{V_{FCin}}{(1-d)} \quad (10)$$

Where d is the duty ratio of the switching pulse.

Since $0 \le d \prec 1$, the output voltage is always higher than the input voltage. That is why the circuit (in Figure (3) is called a boost DC/DC converter. PWM used to generate a pulse with the right duty ratio so that the output voltage follows the reference value.

Our PEMFC generators consist of two modules interconnected in parallel for a given operating voltage an output power.

The VSI is controlled in such a way that it can be used to inject sinusoidal current into the grid for energy extraction from the PEMFC cells during linear or non-linear load conditions. During non-linear load conditions, VSI can be used also as PAPF for

harmonic and reactive compensation. To control the performance and the effectiveness of the PEMFC cells, the VSI is operated based on the concept of p-q theory Figure (4). The control input is a current error signal which in this application, is the difference between the actual current injected by VSI and the desired or reference current waveform[13].

III. REFERENCE CURRENTS GENERATION

So as to estimate the harmonic component of load current, the reference injected current generation is needed. Thus, reference filter current can be obtained when it is subtracted from total load current. For this purpose the active and reactive power analysis in a stationary αβ frame (p-q theory) have been used [14]. Load currents and source voltages of expressed in αβ frame are given by:

$$\begin{bmatrix} i_\alpha \\ i_\beta \end{bmatrix} = \begin{bmatrix} 1 & -1/2 & -1/2 \\ 0 & \sqrt{3}/2 & -\sqrt{3}/2 \end{bmatrix} \begin{bmatrix} i_a \\ i_b \\ i_c \end{bmatrix} \tag{11}$$

$$\begin{bmatrix} e_\alpha \\ e_\beta \end{bmatrix} = \begin{bmatrix} 1 & -1/2 & -1/2 \\ 0 & \sqrt{3}/2 & -\sqrt{3}/2 \end{bmatrix} \begin{bmatrix} e_a \\ e_b \\ e_c \end{bmatrix} \tag{12}$$

Where i_a, i_b, i_c are the load currents and e_a, e_b, e_c are the three-phase grid voltages.

The instantaneous active and reactive powers in the $\alpha - \beta$ coordinates are calculated with the following expressions:

$$p_l(t) = e_\alpha(t) i_\alpha(t) + e_\beta(t) i_\beta(t) \tag{13}$$

$$q_l(t) = e_\beta(t) i_\alpha(t) - e_\alpha(t) i_\beta(t) \tag{14}$$

The instantaneous active and reactive powers can be expressed From above Esq. in terms of the dc components plus the ac components, that is:

$$p_l = \overline{p_l} + \tilde{p}_l \tag{15}$$

$$q_l = \overline{q}_l + \tilde{q}_l \tag{16}$$

Where $\overline{p}_1$ and $\overline{q}_1$ are DC components due to fundamental currents while $\tilde{p}_1$ and $\tilde{q}_1$ are AC components due to harmonic currents.

For estimating the reference currents, the instantaneous powers provided by the source and the PAPF to load is to be computed. If p_g and q_g are the real and imaginary instantaneous powers supplied by the utility, on the other hand to compensate reactive power and harmonic current, the PAPF supplies the real and imaginary instantaneous powers p_f and q_f , the main should supply $p_g = \overline{p}_1$ and q_g=0, while the harmonic component is provided by PAPF, as well as q_l. The oscillatory part of p_l is fed to the nonlinear load by the PAPF, so the source current keep its sinusoidal waveform, while the load receive the same amount of harmonic and fundamental current[13]. So in the normal operation of the capacitor on the DC side of the inverter we have:

$$\begin{aligned} p_g &= \overline{p_l} \\ q_g &= 0 \\ p_f &= p_l - p_g = p_l - \overline{p_l} = \tilde{p}_l \\ q_f &= q_l - q_g = q_l \end{aligned} \tag{17}$$

In these conditions the PAPF supply only the reactive power .As a result, capacitor voltage level is constant during the steady state.

When the load absorbs an exact amount of power $\overline{p_l}$ and if $p_g \prec \overline{p_l}$, the PAPF supplies the rest part to regulate DC voltage level, so it is necessary to control active power balance among the grid, load and PAPF and we have:

$$\overline{p_g} + \overline{p_f} = \overline{p_l}$$

Therefore the Previous equations (17) need to be modified in order to control the proper amount of active power fed by the PAPF, it is necessary to introduce a gain factor k [3].

$$k = \frac{\overline{p_g}}{\overline{p_l}} \tag{18}$$

To recharge the capacitor value requested VDC voltage, grid must supply an additional amount of active power to the PAPF case of the gain factor is above unity.

When the capacitor voltage is too high, so a grid power is less than $\overline{p_l}$, so the rest part of $\overline{p_l}$ is supplied by the PAPF to the load, case of the gain factor is lower than unity,

Hence the instantaneous reference powers for the PAPF are:

$$\begin{aligned} p_f^* &= \tilde{p}_l + (1-k)\overline{p_l} \\ q_f^* &= q_l \end{aligned} \tag{19}$$

In this case the reference currents required by the PAPF are calculated with the following expression:

$$\begin{bmatrix} i_{f\alpha} \\ i_{f\beta} \end{bmatrix} = \begin{bmatrix} e_\alpha & e_\beta \\ -e_\beta & e_\alpha \end{bmatrix}^{-1} \begin{bmatrix} p_f \\ q_f \end{bmatrix} \quad (20)$$

IV. SIMULATION RESULTS AND DISCUSSION

In order to demonstrate the validity of the concepts discussed previously a simulation using MATLAB/SIMULINK environment is done as it is shown in Figure 1.

Our circuit uses tow Fuel Cell Stack. Each Stack is modelled at 625Vdc, 50kW PEM Fuel Cell Stack, connected to a 1515Vdc DC/DC converter. The converters are connected to PAPF in parallel. The utilization of the hydrogen is constant to the nominal value (Uf-H_2 = 99.25%) and oxygen (Uf-O_2=56.67%) ,each Stack has 900 cells, nerst voltage of one cell is about 1.138v.The parameters of the system are shown in table I.A three-phase diode rectifier with an RL load was used as a harmonic producing load.

GRID	
Source Voltage V_s	220 V
Load Power P_L	82 kVA
Frequency f_s	50 Hz
PAPF	
Switching Frequency	12 kHz
Output Filter	1 mH
DC Link Capacitor	8.8 mF
Capacitor DC Voltage	1215 V
VSI control	PWM + PI

Table I : System parameters

Initially, the fixed 4.4 mF capacitor on the dc side provides the PAPF energy storage capabilities. A breaker on the PEMFC side is closed at t=1sec, which allows the PEMFC to supply energy at dc side of PAPF.

Phase-a load current is presented in Fig. 5 , then the total harmonic distortion has been taken up to 2.5 kHz Fig. 6.According to Fig. 9, it is observed that the PAPF decrease the THD of supply current, The deformations have now been reduced and the harmonic has been weakened.

PEMFC cells produces 30kW at 220 Volts, so cells are connected in parallel to produce enough power. At 1 second the PEMFC power is increasing what makes the absorbed current from the source by the non linear load decreases to 76.01 A (RMS), as the PAPF injects the active power to release the excess power in the DC bus condenser (fig.8). At approximately 1.025 second the PEMFC cells produces about 38% of the power needed by the non linear load (fig.10), so as to stabilize its voltage (fig.12).We can say that the PEMFC cells starts delivering power to the grid after it has finished feeding the PAPF by all the power it needs.

V. CONCLUSION

PEMFC system shows great potential for energy production on the future, thanks to their many benefits that it provides, such as rapid technology development and low emission (of pollutant gases). This paper proposes a direct coupling of PEMFC cells with parallel active power filter (PAPF). The simulation results indicate that by using the proposed system, the chemical power can be easily extracted from PEMF cells and injected into the electricity grid and other public utilities by PAPF which has many functions; the protection of supply systems and sensitive loads against harmonics currents, correction of power factor, as well as release the excess active power into electricity grid. According to the obtained results, It could be considered that the proposed system to be efficient solution to the growing demand of electrical power.

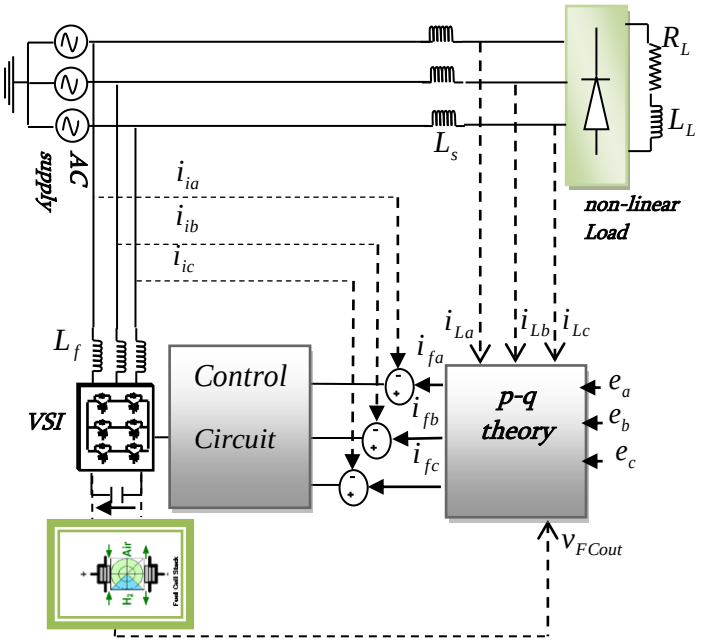

Fig. 1: General structure of parallel active power filter with PEMFC

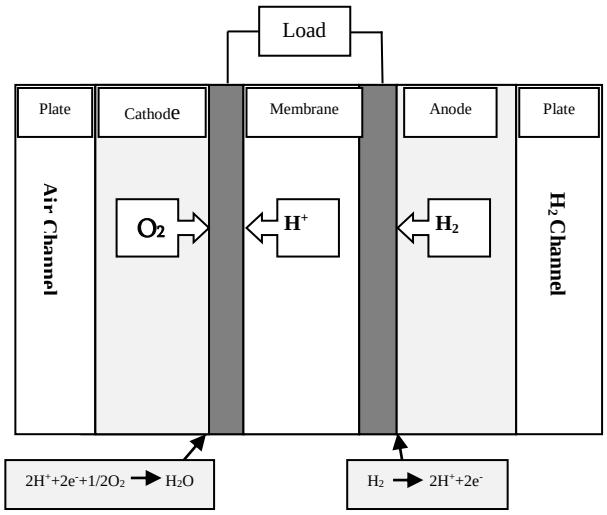

Fig.2. Basic PEMFC operation

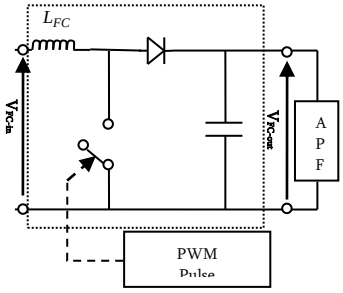

Fig.3. Boost DC/DC converter

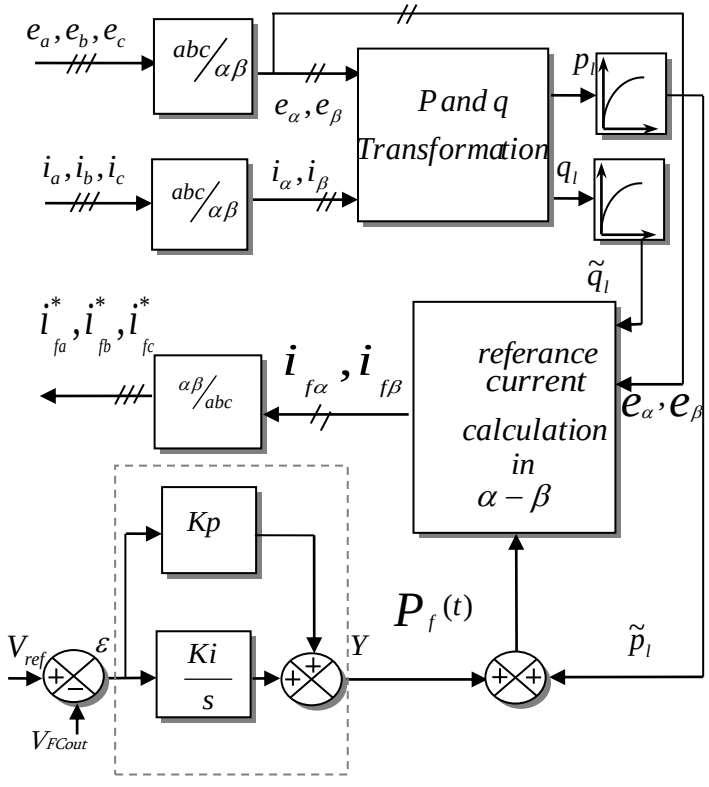

Fig. 4.Block diagram for the instantaneous active and

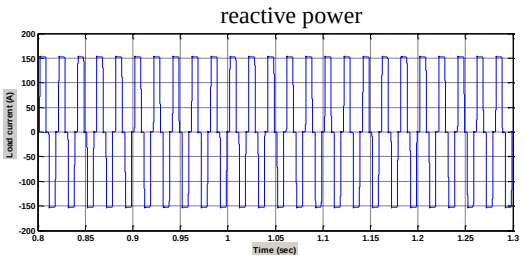

Fig. 5 load current Phase ‘a’

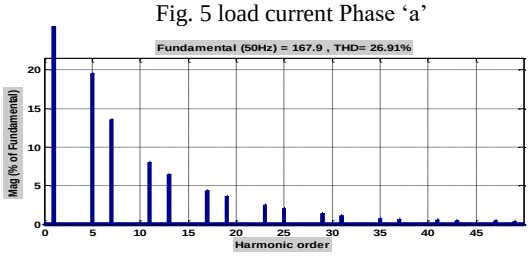

Fig. 6 Harmonic spectrum of load current Phase ‘a’

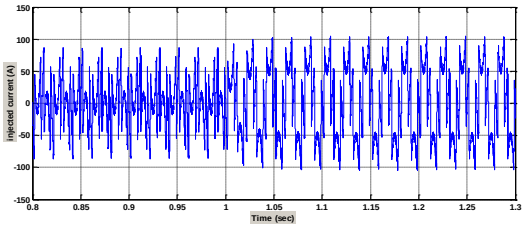

Fig. 7 injected current by PAPF Phase ‘a’

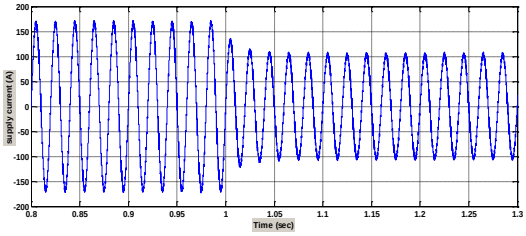

Fig. 8 supply current Phase ‘a’

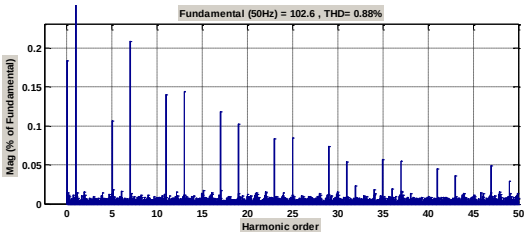

Fig. 9 Harmonic spectrum of supply current Phase ‘a’

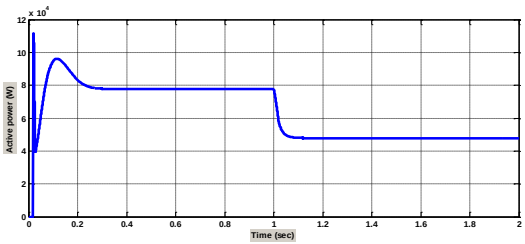

Fig. 10 active power produced by the source

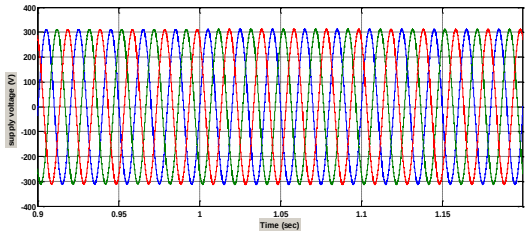

Fig. 11 Supply voltage

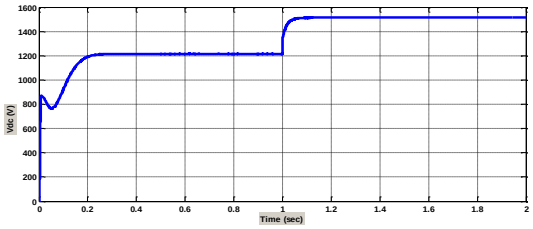

Fig. 12 DC-link voltage

TABLE I : SYSTEM PARAMETERS

VI. REFERENCES

[1]Yun.SY, John.R and Bing.JH(2012) "Water Soluble Polymers as Proton Exchange Membranes for Fuel Cells"Polymers review, Volume 4,pp. 913-963.

[2] Sid A.A. ; Kamal M ; Abderrezzak C ; Bruno F"Multilevel Inverter Topology for Renewable Energy Grid Integration" IEEE Transactions on Industrial Electronics ,28 December 2016. doi: 10.1109/TIE.2016.2645887.

[3]Dallia A ; Daniel D. Aklil-D "Modeling a Proton Exchange Membrane (PEM) Fuel Cell System as a Hybrid Power Supply for Standalone Applications"Power and Energy Engineering Conference (APPEEC), 2011 Asia-Pacific, 25-28 March 2011, doi: 10.1109/APPEEC.2011.5749114.

[4]Khaled.M and Chaker.A (2009)"FUZZY LOGIC CONTROL OF FUEL CELL SYSTEM FOR RESIDENTIAL POWER GENERATION "Journal of ELECTRICAL ENGINEERING, VOL. 60, NO. 6,pp. 328–334.

[5]Younane N ; Hani H,"Modelling and Parameter Observation for Proton Exchange Membrane Fuel Cell" International Conference on Developments of E-Systems Engineering (DeSE), 13-14 Dec. 2015, **doi:** 10.1109/DeSE.2015.46.

[6]Yuri R. R ; Maíra R. M ; Juliana R. M ; Paulo F. R ; Fernando N. B ; A. C. Zambroni "Impact of non-linear loads and renewable generation on a university research building" 17th International Conference on Harmonics and Quality of Power (ICHQP), 16-19 Oct. 2016, doi: 10.1109/ICHQP.2016.7783438.

[7]Izhar. M, Hadzer. CM, Syafrudin .M, Taib. S, and Idris. S,(2004)"Performance for passive and active power filter in reducing harmonics in the distribution system,". Power and Energy Conference, PECon. Proceedings. National, pp104-108.

[8]Jeong.GY, Park. TJ and Kwon. BH, (2000)"Line-voltage sensorless active power filter for reactive power compensation," Electric Power Applications, IEE Proceedings-, vol. 147,pp. 385-390.

[9]Lucian A, Frede B, Steffan H, Paul T(2008) Adaptive Compensation of Reactive Power with Shunt Active Power Filters" Published in: IEEE Transactions on Industry Applications (Volume: 44, Issue: 3, 16 May 2008) ,pp. 867 – 877. doi: 10.1109/TIA.2008.921366.

[10]Suresh.D, Jaiganesh.K, Duraiswamy.K (2013) " AC-AC MULTILEVEL CONVERTER BASED WIND ENERGY SYSTEM"International Journal of Advanced Research in Electrical, Electronics and Instrumentation Engineering, Vol. 2, Issue 5, pp. 1686-1673.

[11]Khaled.M and Chaker.A (2013) "A Central Composite Face-Centered Design for Parameters Estimation of PEM Fuel Cell Electrochemical Model" Leonardo Journal of Sciences, Issue 23, pp. 84-96.

[12]Samosir.AS, Sutikno.T, Yatim.AHM (2011) "Dynamic Evolution Control for Fuel Cell DC-DC Converter '' TELKOMNIKA, Vol.9, No.1, pp.183-190.

[13]Berbaoui.B, Dib.S, Dehini.R (2014)"Grid-connected Photovoltaic Power Systems and Power Quality Improvement Based on Active Power Filter "TELKOMNIKA Indonesian Journal of Electrical Engineering Vol. 12, No. 8, pp.5861 – 5868.

[14]João L. Afonso, , M. J. Sepúlveda Freitas, and Júlio S. Martins" p-q Theory Power Components Calculations",ISIE'2003 - IEEE International Symposium on Industrial Electronics,Rio de Janeiro, Brasil, 9-11 Junho de 2003, ISBN: 0-7803-7912-8.

2.International Conference on
Theoretical and Applied Computer Science and Engineering
(ICTACSE, 2018)
Istanbul, Turkey, June29-30,2018

Comparative Study Of Photovoltaic Models By Bond Graph For The Electrification Of Rural Areas

Abd Essalam Badoud[1], Samia Latreche[2]and Mabrouk Khemliche[3]
1 Automatic laboratory of Setif, Electrical engineering department, University of Setif1, Algeria
badoudabde@univ-setif.dz
2 Automatic laboratory of Setif, Electrical engineering department, University of Setif1, Algeria
Samia.khamliche@univ-setif.dz
3XYZ Automatic laboratory of Setif, Electrical engineering department, University of Setif1, Algeria
mebroukkhemliche@univ-setif.dz

To enable a balanced development of the country and improve the living conditions of the urban and rural populations, the new orientations of the energy policy consist in developing the existing potentialities, in particular the renewable energies which mainly include, the solar, the wind, the biogas and micro-hydroelectric plants. Each of these energies represents a more or less important energy potential but little exploited.

This work deals with the modelling, simulation, and analysis of a graphical method (Bond Graph) allowing the extraction of model parameters from the current-voltage characteristic of a solar cell. The electrical model of a PV module is presented on the basis of Shockley diodes. The simple model is a photocurrent (current source), a single diode junction and a series resistor, and especially the temperature dependence. The second model is a two-diode model. The method of parameter extraction and model evaluation in Symbols is demonstrated for a typical solar panel, in our case it is the SM110-24 module. These models are used to study the variation of the maximum power and the current-voltage characteristic with temperature and illumination. A comparison between the two models is made.

Keywords: Photovoltaic System, Single Diode Model, Two Diode Model, Bond Graph, Photovoltaic Generator.

REFERENCES

[1] Alonso-Garcia M. C, Ruiz J. M, Chenlo F, "Experimental study of mismatch and shading effects in the I-V characteristic of a photovoltaic module", Solar Energy Materials & Solar Cells Volume 90, Issue 3, 15 February 2006, Pages 329-340.

[2] Saida Madji, Aissa Kheldoun, Bond graph based modeling for parameter identification of photovoltaic module, Energy, vol. 141, pp. 1456-1465, 2017.

[3] Gow, J. A, Manning, C.D. "Development of a photovoltaic array model for use in power-electronics simulation studies", IEE Proceeding Electronics Power Applications, Vol. 146, No.2, March 1999, pp.193-200.

[4] IbrahimAbdallah, Anne-Lise Gehin, Belkacem Ould Bouamama, Event driven Hybrid Bond Graph for Hybrid Renewable Energy Systems part I: Modelling and operating mode management, international journal of hydrogen energy (2017), https://doi.org/10.1016/j.ijhydene.2017.10.144

2.International Conference on
Theoretical and Applied Computer Science and Engineering
(ICTACSE, 2018)
Istanbul, Turkey, June29-30,2018

Bond Graph Modelling And Control Of Smart Home Energy Management Considering Electric Vehicle Battery Energy Storage And Photovoltaic

Abd Essalam Badoud[1], Samia Latreche[2]and Mabrouk Khemliche[3]
1 Automatic laboratory of Setif, Electrical engineering department, University of Setif1, Algeria
badoudabde@univ-setif.dz
2 Automatic laboratory of Setif, Electrical engineering department, University of Setif1, Algeria
Samia.khamliche@univ-setif.dz
3XYZ Automatic laboratory of Setif, Electrical engineering department, University of Setif1, Algeria
mebroukkhemliche@univ-setif.dz

As a next-generation power system, smart grid is typified by an increased use of information and communications technology in the generation, transmission, distribution, and consumption of electrical energy.

Smart homes hold the potential for increasing energy efficiency, decreasing costs of energy use, decreasing the carbon footprint by including renewable resources, and transforming the role of the occupant. At the crux of the smart home is an efficient electric energy management system that is enabled by emerging technologies in the electricity grid and consumer electronics.

With the emergence of smart grid, which presents the next generation of electrical power systems, residents have the opportunities to manage their home energy usage to reduce energy expenditure. This paper presents a bond graph model to optimize the energy production and consumption systems in a smart home with the integration of renewable energy resources, battery storage systems, and gridable vehicles. Numerous case studies are presented by varying significant factors through the design of experiments. After that, a bond graph technique is proposed to solve the problem of residential energy management and to minimize the electricity cost of the consumer. Results find the global optimum solution for many consecutive days with important reduction of execution time and by achieving significant energy cost savings of the considered scenarios.

Keywords: Smart home, energy cost, electric vehicle, energy storage, Photovoltaic

REFERENCES

[1] Byun J.; Park S.; Kang B.; Hong I. Design and implementation of an intelligent energy saving system based on stand by power reduction for a future zero-energy home environment. IEEE Trans. Consum. Electron. 2013, 59, 507–514.

[2] A. Kavousi-Fard, A. Abunasri, A. Zare, R. Hoseinzadeh, Impact of plug-in hybrid electric vehicle scharging demand on the optimal energy management of renewable micro-grids, Energy78 (0) (2014) 904-915.

[3] L. Yu, T. Jiang, and Y. Zou, Distributed real-time energy management in data center microgrids, IEEE Trans. Smart Grid, DOI10.1109/TSG.2016.2640453,2016.

[4] W. Shi, N. Li, C. Chu and R. Gadh, Real-time energy management inmicrogrids, IEEE Trans. Smart Grid, vol.8, no.1, pp. 228-238, Aug. 2017.

[5] S. S. Intille, The goal: smart people, not smart homes, in Proceedings of the International Conference on Smart Homes and Health Telematics, 2006, pp. 3–6.

[6] L. Yu, T. Jiang, and Y. Zou, Distributed online energy management for data centers and electric vehicles in smart grid, IEEE Internet of Things Journal, vol. 3, no. 6, pp. 1373-1384, 2016.

[7] S. Shao, M. Pipattanasomporn, and S. Rahman, Grid Integration of Electric Vehicles and Demand Response With Customer Choice, IEEE Transactions on Smart Grid, vol. 3, no. 1, pp. 543 –550, Mar. 2012.

[8] W. Mert, M. Watts, and W. Tritthart, Smart Domestic Appliances in Sustainable Energy Systems - Consumer Acceptance and Restrictions, in Proceedings of the ECEEE 2009 Summer Study, 1751, vol. 1761.

2.International Conference on
Theoretical and Applied Computer Science and Engineering
(ICTACSE, 2018)
Istanbul, Turkey, June 29-30, 2018

Bond Graph Modeling Procedures For Fault Detection And Isolation Of Mechatronic Process

Samia Latreche[1], Abd Essalam Badoud[2] and Mabrouk Khemliche[3]

1 Automatic laboratory of Setif, electrical engineering department, university of Setif 1, Algeria
ksamia2002@univ-setif.dz
2 Automatic laboratory of Setif, electrical engineering department, university of Setif 1, Algeria
badoudabde@univ-setif.dz
3Automatic laboratory of Setif, electrical engineering department, university of Setif 1, Algeria
mabroukkhemliche@@univ-setif.dz

A Mechatronic system is composed by multi energy domains (mechanical, electrical, pneumatic....) which exchange powers. Fault detection methods are becoming year by year of great importance in industry application, especially in robotic and Mechatronic applications that concerns as well economical and human. The improvement of their safety essentially rests on fault detection and isolation (FDI) procedures, which mainly consist in the comparison of the actual behavior of the system with reference behaviors describing detection and isolation. The aim objective of this work is to detect quickly the various faults existing on the Mechatronic process to avoid the degradation of its performances and to increase the safety of the operators and the environment. The diagnostic strategy and the form in which knowledge is available condition the method used to design the monitoring algorithm. Our contribution relates to the methods containing model.

In fact, model used in the analytical redundancy method has often low or none relation with the physical structure of the monitored system and, therefore, it is quite to understand that physical system component has been damaged.

Bond graph modeling is based on observation of energetic exchanges among system components, thus it can be applied to either linear or non-linear systems and to any physical domain (electrical, hydraulic, mechanical, etc.). The basic idea is to monitor any energetic variation in the system, searching for any energy modification which can be linked to a parameter variation. Once the fault is detected and isolated, bond graph network topology is then exploited in order to identify the actual fault source.

This paper describes the application of our FDI approach to a mechatronic system. We develop a pseudo Bond Graph model of the system and demonstrate the FDI effectiveness with real data collected from our automotive test bed. We introduce the analysis of the problem involved in the faults localization and identification in the complex industrial processes. We propose a method of fault

detection applied to the diagnosis and to determine the gravity of a detected fault. We show the possibilities of application of the new diagnosis approaches to the complex system control.

Keywords: Modeling, Monitoring, Mechatronic, Detection, Isolation

2.International Conference on
Theoretical and Applied Computer Science and Engineering
(ICTACSE, 2018)
Istanbul, Turkey, June 29-30, 2018

Analysis And Real-Time Monitoring On A PEM Fuel Cell System With Bond Graphs

Abd Essalam Badoud[1], Samia Latreche[2] and Mabrouk Khemliche[3]

1 Automatic laboratory of Setif, electrical engineering department, university of Setif 1, Algeria
badoudabde@univ-setif.dz
2 Automatic laboratory of Setif, electrical engineering department, university of Setif 1, Algeria
ksamia2002@univ-setif.dz
3Automatic laboratory of Setif, electrical engineering department, university of Setif 1, Algeria
mabroukkhemliche@@univ-setif.dz

In recent years, according to the upcoming challenge of pollution, fuel saving, to use on FCEV is increasing. It can be that fuel cell power train divided in the PEMFC, Batteries, DC/DC converters, DC/AC inverters and electrical motors. The Proton Exchange Membrane Fuel cells (PEMFC) have consistently been considered for transportation application. Characteristic features of PEMFC include lower temperature (50 to 100 °C) and solid polymer electrolyte membrane.

The performance of a PEMFC unit is governed by three interdependent physical phenomena: heat, mass, and charge transfer. When modeling such a multi-physical system it is advantageous to use an approach capable of representing all the processes in a unified fashion.

In this work a new model was proposed to improve the lifetime and reliability of the power train and to detect online faults. The model-based fault diagnosis is based on comparing on-line the real behaviour of the monitored system obtained by means of sensors with a predicted behaviour obtained using a bond graph model with an observer scheme. In case of a significant discrepancy (residual) is detected between the model and the measurements obtained by the sensors, the existence of a fault is assumed. If a set of measurements is available, it is possible to generate a set of residuals (indicators) that present a different sensitivity to the set of possible faults.

Keywords: PEM fuel cells, Bond graph, Multi-physics, Faults detection and location

2.International Conference on
Theoretical and Applied Computer Science and Engineering
(ICTACSE, 2018)
Istanbul, Turkey, June 29-30, 2018

A Power System Connected Fuel Cell Based On Neural Network Theory

Rachid. Dehini[1]✉, Glaoui Hachemi[1], Berbaoui Brahim[2]

[1] University of Tahri Mohamed , Department of Electrical Engineering, Faculty of Technology, Bechar, Algeria
[2]Centre de Developpement des Energies Renouvelables, Unité de Recherche en Energies Renouvelables en Milieu Saharien, Adrar, Algiers,

The growing demand for electric power and the increasing decline in global fossil fuel reserves have stimulated researchers and institutions to improve renewable energies, such as fuel cells that are highly energy efficient and environmentally friendly. The primary objective of this work presents a Parallel Active Power Filter (PAPF) powered by Fuel cells in order to mitigate harmonics current caused by nonlinear loads, and to supply these loads by the Fuel cells energy excess. The use of artificial neural network (ANN) as a control system of the inverter results the multi-operation inverter, such as harmonic elimination, reactive power control and uninterruptible power supply will be achieved. The system consisting of Fuel cells, connected to a diode rectifier feeding a parallel active power filter. The simulation results prove the efficiency of using the proposed method for power quality improvement and Feed-in of Fuel cells -generated electricity into the public grid.

Keywords: PEMFC cells energy, voltage source inverter, , PAPF, current harmonics, ANN

Acknowledgements

The authors express thanks to all Laboratory staff of Smart Grids & Renewable Energies Lab, Tahri Mohamed University, for their kind technical assistance.

References

[1] Yun.SY, John.R and Bing.JH(2012) "Water Soluble Polymers as Proton Exchange Membranes for Fuel Cells"Polymers review, Volume 4,pp. 913-963.

[2] Sid A.A. ; Kamal M ; Abderrezzak C ; Bruno F"Multilevel Inverter Topology for Renewable Energy Grid Integration" IEEE Transactions on Industrial Electronics ,28 December 2016. doi: 10.1109/TIE.2016.2645887.

[3] Dallia A ; Daniel D. Aklil-D "Modeling a Proton Exchange Membrane (PEM) Fuel Cell System as a Hybrid Power Supply for Standalone Applications"Power and Energy Engineering Conference (APPEEC), 2011 Asia-Pacific, 25-28 March 2011, doi: 10.1109/APPEEC.2011.5749114.

[4] Khaled.M and Chaker.A (2009)"FUZZY LOGIC CONTROL OF FUEL CELL SYSTEM FOR RESIDENTIAL POWER GENERATION "Journal of ELECTRICAL ENGINEERING, VOL. 60, NO. 6,pp. 328–334.

[5] Younane N ; Hani H,“Modelling and Parameter Observation for Proton Exchange Membrane Fuel Cell” International Conference on Developments of E-Systems Engineering (DeSE), 13-14 Dec. 2015, doi: 10.1109/DeSE.2015.46.

[6] Yuri R. R ; Maíra R. M ; Juliana R. M ; Paulo F. R ; Fernando N. B ; A. C. Zambroni “Impact of non-linear loads and renewable generation on a university research building” 17th International Conference on Harmonics and Quality of Power (ICHQP), 16-19 Oct. 2016, doi: 10.1109/ICHQP.2016.7783438.

[7] Izhar. M, Hadzer. CM, Syafrudin .M, Taib. S, and Idris. S,(2004)"Performance for passive and active power filter in reducing harmonics in the distribution system,". Power and Energy Conference, PECon. Proceedings. National, pp104-108.

[8] Jeong.GY, Park. TJ and Kwon. BH, (2000)"Line-voltage sensorless active power filter for reactive power compensation," Electric Power Applications, IEE Proceedings-, vol. 147,pp. 385-390.

[9] Lucian A, Frede B, Steffan H, Paul T(2008) Adaptive Compensation of Reactive Power with Shunt Active Power Filters” Published in: IEEE Transactions on Industry Applications (Volume: 44, Issue: 3, 16 May 2008) ,pp. 867 – 877. doi: 10.1109/TIA.2008.921366.

[10] [10]Suresh.D, Jaiganesh.K, Duraiswamy.K (2013) " AC-AC MULTILEVEL CONVERTER BASED WIND ENERGY SYSTEM”International Journal of Advanced Research in Electrical, Electronics and Instrumentation Engineering, Vol. 2, Issue 5, pp. 1686-1673.

[11] Khaled.M and Chaker.A (2013) “A Central Composite Face-Centered Design for Parameters Estimation of PEM Fuel Cell Electrochemical Model” Leonardo Journal of Sciences, Issue 23, pp. 84-96.

[12] Samosir.AS, Sutikno.T, Yatim.AHM (2011) “Dynamic Evolution Control for Fuel Cell DC-DC Converter ‘’ TELKOMNIKA, Vol.9, No.1, pp.183-190.

[13] Berbaoui.B, Dib.S, Dehini.R (2014)“Grid-connected Photovoltaic Power Systems and Power Quality Improvement Based on Active Power Filter “TELKOMNIKA Indonesian Journal of Electrical Engineering Vol. 12, No. 8, pp.5861 – 5868.

[14] João L. Afonso, , M. J. Sepúlveda Freitas, and Júlio S. Martins“ p-q Theory Power Components Calculations“,ISIE’2003 - IEEE International Symposium on Industrial Electronics,Rio de Janeiro, Brasil, 9-11 Junho de 2003, ISBN: 0-7803-7912-8.

2.International Conference on
Theoretical and Applied Computer Science and Engineering
(ICTACSE, 2018)
Istanbul, Turkey, June 29-30, 2018

Diagnosis Of Lung Diseases Using Adaptive Neuro-Fuzzy Inference System Based On Clustering Methods

Hilal KAYA[1], I.N.ASKERZADE[1]

[1]Ankara University, Department of Computer Engineering, Turkey

Malignant mesotheliomas (MM) are very aggressive tumors of the pleura, that develops in the lining of the lungs (pleura), abdomen or heart. These tumors associate expecially with exposure to asbestos. It may also be related to previous simian virus 40 (SV40) infection and considerable possible for genetic inclination. Caused by asbestos, mesothelioma has no known treatment and has a very weak prognosis [1][2]. Therefore for recognition of sickness most correctly, modelling experts systems step in at this stage. At this point in recent researches, Adaptive Neuro-Fuzzy Inference System based applications have shown positive results and solutions in forecasting of disease [3][4].

Adaptive Neuro-Fuzzy Inference System (ANFIS) is one of the useful and powerful neural network approaches for the solution of function approximation and pattern recognition problems in the last decades. ANFIS has become an attractive, powerful modelling technique, combining well established learning laws of ANNs and the linguistic transparency of fuzzy logic theory within the framework of adaptive networks. Fuzzy inference systems (FIS) are one of the most well-known applications of fuzzy logic theory. Because of this qualities ANFIS usage have seen in a great deal of article for creating estimation model approach about medical field. In case of using ANFIS some studies also based on clustering methods and comparing results [5][6][7].

The aim of this study, diagnosis of lung diseases (mesothelioma) with implementing Adaptive Neuro-Fuzzy Inference System based on clustering methods and examining results and performance of these methods. Three ANFIS models were implemented including Grid Partitioning (GP), Subtractive Clustering method (SCM), Fuzzy C-Means clustering method (FCM) and evaluated results of these studies. This study shows that the ANFIS approach can be applied as a effective tool for modeling some problems involved diagnosis with multiple inputs.

REFERENCES

[1]https://archive.ics.uci.edu/ml/datasets/Mesothelioma%C3%A2%E2%82%AC%E2%84%A2s+disease+data+set+#

[2]https://www.mesothelioma.com/mesothelioma/

[3]M. Wei , Baojun Bai, A.H. Sung , Q. Liu, J.Wang , M.E. Cather, , Information Sciences 177, 4445–4461 (2007)

[4]N. Ziasabounchi , I. Askerzade, International Journal of Electrical & Computer Sciences IJECS-IJENS, 14(02)7-12(2014)

[5]A. Akgundogdu, S. Kurt, N. Kılıç, O.N. Ucan, Journal of Medical Systems 34(6), 1003–1009 (2010)

[6]A.M. Abdulshahed, Andrew P. Longstaff, Simon Fletcher, Applied Soft Computing 27, 158–168 (2015)

[7]N. Ziasabounchi , I.Askerzade, , Turkish Journal of Mathematics and Computer Science.,2(1) 1-11(2014)

2.International Conference on
Theoretical and Applied Computer Science and Engineering
(ICTACSE, 2018)
Istanbul, Turkey, June 29-30, 2018

Tension Control Of Paper Webs

Hachemi Glaoui

Faculty of Sciences and technology, Béchar University B.P. 417 Béchar, 08000, Algeria
E-mail: glaouih@yahoo.fr

The objective is to control a web transport system with winder and unwinder for elastic material. A physical mod-eling of this plant is made based on the general laws of physics. For this type of control problem, it is extremely important to prevent the occurrence of web break or fold by decoupling the web tension and the web velocity. Due to the wide-range variation of the radius and inertia of the rollers the system dynamics change considerably during the winding/unwinding process. Different strategies for web tension control and linear transport velocity control are presented in this paper. First, a sliding mode control strategy which reduces the coupling between tension and velocity is compared to the de-centralized control strategy with proportional integral (PI) controllers commonly used in the industry. Second, a sliding mode control strategy.

Keywords: Web transport, winding process. Multi-Induction Motors system, Sliding mode control, proportional integral (PI) controllers.

2.International Conference on
Theoretical and Applied Computer Science and Engineering
(ICTACSE, 2018)
Istanbul, Turkey, June 29-30, 2018

A Electrical Network Connected Fuel Cell Based On (MLFFN) Multilayer Feed Forward Neural Network

Rachid Dehini [1], Berbaoui Brahim [2]

[1]Electrical engineering Department, University of Tahri Mohamed, Bechar , Algeria. [2]Centre de Developpement des Energies Renouvelables, Unité de Recherche en Energies Renouvelables en Milieu Saharien, Algiers.
dehini_ra@yahoo.fr

Electrical Power utility should continually provide the flow of energy at their customers, with maintaining sinusoidal and symmetrical voltage at the constant frequency and rms value of supply voltage. But due to power system variations under normal operation and to unwanted events like short-circuit faults, the Power utility never assure these requirements. The aim of this paper is to present a shunt active compensator supplied by the Fuel cells, in shunt active compensator feeds the linear and nonlinear loads by harmonics and reactive currents and the overload energy is released to the power system.

In order to reach multifunctions as harmonic mitigation, reactive and active power control, this paper uses the (MLFFN) Multilayer Feed Forward Neural Network as a control system; the plan is made up of fuel cells, linked to a shunt active compensator. The simulation results prove the efficiency of this plan with the mentioned method for release the fuel cell energy to the power system and power quality improvement.

Keywords: PEMFC, MLFFN, Power-Factor, active compensator, harmonics current

2.International Conference on
Theoretical and Applied Computer Science and Engineering
(ICTACSE, 2018)
Istanbul, Turkey, June 29-30, 2018

Synchronous Inductor Machines

Glaoui Hachemi

University of Tahri Mohamed , Department of Electrical Engineering, Faculty of Technology, Bechar, Algeria

This work for the study of the comportment of the synchronous inductor machine with variable speed, fed by a three-phase inverter. Several transients were treated by simulation (start unloading, introducing a torque load, reversing and speed change). Then engine cushion at both loss and when starting without the damper. In addition, robustness tests on the parametric variation of (MSRB) were also performed. The control technique studied makes it possible to obtain good dynamic and static performances and has a robustness with respect to the external perturbation and the parametric variation.

Keyword: Modeling, Command, Synchronous machine, Inductor, Inverter.

2.International Conference on
Theoretical and Applied Computer Science and Engineering
(ICTACSE, 2018)
Istanbul, Turkey, June 29-30, 2018

Fuzzy Logıc Based Control Of Hvac Systems For Office Areas

Ecehan KANSU ATEŞ[1], I.N.ASKERZADE[1]

[1]Ankara University, Department of Computer Engineering, Turkey

HVAC (Heating, Ventilation and Air Conditioning) applications is to provide the appropriate comfort conditions in a healthy way. The targeted air quality in applications, affects human health and comfort at the top level. For this reason, HVAC systems have a very important role in implementing health and comfort conditions [1].

In recent years, HVAC systems operating according to constant air quantity (CAV) and variable air quantity (VAV) methods, the VAV methods have been more flexible in multi-zone air conditioning systems such as multi-energy structures and high-rise building applications, although VAV techniques have higher installation costs than CAV techniques. In the recent researches, Fuzzy Logic applications have shown positive results in the management of HVAC systems [2,3].

In HVAC systems; the use of Fuzzy Logic applications [4-7] is more favorable in cases where it is very difficult to use the mathematical texts containing nonlinear equations and classical computing methods, such as areas with multiple management variables. Fuzzy logic approach contains the analysis of system variables, the association and transformation of fuzzy logic elements and variable units The fuzzy logic solution, unlike the classical algorithm, contains a heuristic approach similar to that of human perception. Rather than making sharp results with sharp ideas, fuzzy sets can provide smoother results with more precise results.

The aim of this study, which is done with Matlab software program, is to enable people working in a office to work healthily and efficiently in accordance with the thermal comfort conditions with the fuzzy logic based air conditioning system. The system has been designed to change the temperature, humidity, air flow parameters in the environment to create thermal comfort conditions in accordance with ASHRAE data standards. ASHRAE (American Society of Heating, Refrigerating and Air Conditioning Engineers) was established in 1894; building installation systems, energy efficiency, indoor air quality, sustainability.

REFERENCES

[1] M. Arima., et al Proceedings of the IEEE WESCANEX'95-1, New York, (133-138)(1995)

[2] E.H. Mathews, ,et al., Energy and Buildings,(853-863)(2001).

[3] D.R. Clark, et al. ASHRAE Transactions. (737-750)(1985)

[4] I.N.Askerzade, M.Mahmood, Int. J. of Electrical & Comp.Sci. IJECS–IJENS,10(2)48(2010)

[5] N. Ziasabounchi, I. Askerzade, Int. J. of Electrical & Comp.Sci. IJECS–IJENS, 14(2) 7(2014)

[6] I.N.Askerzade, M. Mahmud, International Journal of Research and Reviews in Applied Sciences 6 (2), 196-202(2011)

[7] S.E. Amrahov,I.N.Askerzade CMES-Computer Modeling in Engineering and Sciences 70, 1-9(2010)

2.International Conference on
Theoretical and Applied Computer Science and Engineering
(ICTACSE, 2018)
Istanbul, Turkey, June29-30,2018

Simulation and Analysis of Hybrid Piezoelectric PZT-PVDF Pump using Bond Graph Approach

Samia Latreche [1], Abd Essalam Badoud[2]and Mabrouk Khemliche[3]
1 Automatic laboratory of Setif, Electrical engineering department, University of Setif1, Algeria
Samia.khamliche@univ-setif.dz
2 Automatic laboratory of Setif, Electrical engineering department, University of Setif1, Algeria
badoudabde@univ-setif.dz
3Automatic laboratory of Setif, Electrical engineering department, University of Setif1, Algeria
mabroukkhemliche@univ-setif.dz

The piezoelectric effect, or the separation of charge within a material as a result of an applied strain, was first discovered by Jacques and Pierre Curie in 1880 [1]. They discovered that if certain crystals such as quartz were subjected to mechanical strain, they became electrically polarized and the degree of polarization was proportional to the applied strain.

The piezoelectric materials found so a field of application particularly interesting in the electric energy transformation: the piezoelectric transformers make it possible to replace advantageously the electromagnetic transformers in particular for applications prone to the miniaturization [2]. Micro-pumps have special characteristics able to transport minute and accurate amount of liquid or gas. Hence, micro-pumps are fit to serve chemical, biological substances analyzing system as micro-fluid flow control appliance [3].

The benefits of such a model are its simplicity and lending of closed form solutions to power and efficiency. The drawbacks are that the solutions exist only in the frequency domain (i.e. steady state) and the inability to capture transients and nonlinearities that are critical to the design of a real world pump system.

Aiming at providing an integral model, this paper shall introduce the use of bond graph for the modeling of hybrid piezoelectric PZT-PVDF Pump. Bond graph modeling is the most suited method for dealing with complex systems of different physical domains. First because the object oriented modeling proportioned by bond graph allows an interchange ability of the subparts of the pump [4]. Then, the fact that different energetic domains are represented with the same basic elements allows the implementation of complete models. Examples include an electroacoustic transducer [5], multi-phase systems [6], fluid flow [7], [8] traffic flow [9] and an electrically controlled actuator [10].

The whole article is organized as follows: second section an overview of modeling, simulation and control using bond graph approach is presented; the third section presents the working principle of piezoelectric pump. The fourth section presents the details of proposed bond graph model for each subsystem. The fifth section briefs the simulation results and discussions. Finally we present a brief summary for this work.

Keywords: Simulation and Analysis, hybrid PZT-PVDF pump, Flow Rate, Piezoelectric, Bond Graph

REFERENCES

[1] J. Curie, and P. Curie, Développement par pression, de l'électricité polaire dans les cristaux hémièdres a faces inclinées," Comptes rendus de l'académie des sciences. série II. Fascicule a, Sciences de la terre et des planètes, 91pp. 294, 1880.

[2] J.L. Balino. Galerkin finite element method for incompressible thermo-fluid flows framed within the bond graph theory. Simulation Modelling Practice and Theory, 17(1):35-49, 2009.

[3] J. L. Balino, A. E. Larreteguy, and E. F. Gandolfo Raso. A general bond graph approach for computational fluid dynamics. Simulation Modelling Practice and Theory, 14(7):884-908, 2006.

[4] C. M. Chera, J. L. Balino, and Genevieve Dauphin-Tanguy. Two-equation traffic flow models framed within the bond graph theory. In Spring Sim, page 219, 2010.

[5] A. Alabakhshizadeh, Y. Iskandarani, G. Hovland, and O.M. Midtgard. Analysis, modeling and simulation of mechatronic systems using the bond graph method. Modeling, Identification and Control, 32(1): 35-45, 2011.

[6] François Cellier. Mathematical modeling of physical systems. http://www.inf.ethz.ch/personal/fcellier/, 2011.

[7] W. Borutzky. Bond graph modeling and simulation of multidisciplinary systems an introduction. Simulation Modelling Practice and Theory, 17(1): 3, 2009.

[8] P.J. Gawthrop and G.P. Bevan. Bond-graph modeling. Control Systems, IEEE, 27(2):24 {45, april 2007.

2.International Conference on
Theoretical and Applied Computer Science and Engineering
(ICTACSE, 2018)
Istanbul, Turkey, June29-30,2018

Control of Piezoelectric Actuator Hysteresis by Bond Graph Tool

Samia Latreche [1], Abd Essalam Badoud [2]and Mabrouk Khemliche[3]
1 Automatic laboratory of Setif, Electrical engineering department, University of Setif1, Algeria
Samia.khamliche@univ-setif.dz
2 Automatic laboratory of Setif, Electrical engineering department, University of Setif1, Algeria
badoudabde@univ-setif.dz
3Automatic laboratory of Setif, Electrical engineering department, University of Setif1, Algeria
mabroukkhemliche@univ-setif.dz

During the past few decades, piezoelectric devices have become very important part of today's modern engineering [1]. Their importance is growing with increasing demands for miniaturization and higher precision positioning. It is one of the goals of the project to get familiar with this broad subject connected to many other scientific and engineering disciplines. Since system modelling and control engineering are the main subjects of our study, exploring piezoelectric devices with tools provided by these disciplines was a great idea that led to selection of the topic for our project.

Nano-positioning systems play a leading role in this modern positioning control world that usually employ a piezoelectric actuator as a key component, which makes motion control at the sub-nanometer level possible. However, the inherent hysteresis nonlinearity dramatically degrades the tracking performance of piezoelectric actuators under conventional control methods. Furthermore, the hysteresis nonlinearity of piezoelectric actuators is also affected by the changing rate of the input voltage of piezoelectric actuators called rate-dependent property, which increases the difficulty of designing a desired controller [2]. Therefore, how to overcome these difficulties has become a challenging and attractive topic in the literature.

Several mathematical models have been proposed to describe hysteresis nonlinearities. Prandlt-Ishlinskii model is a superposition of elementary stop or play operators that are parameterized by a threshold variable [3]. Presach model and Krasnosel'skii- Pokrovskii model are parameterizing by a pair of threshold variable [4]. Bouc-Wen model consists of a first-order nonlinear differential equation [5], [6]. Among these models, Bouc-Wen model has received an increasing interest due to the capability to describe a wide class of hysteresis system such as piezoelectric actuators [7], magneto rheological dampers [5] and forced vibration of mechanical systems [4].

Among these hysteresis models, the PI model is very suitable for real time application because it has simpler implementation procedures and has analytical inverse [8]. Using PI approach can reduce maximum hysteretic error to about 1-3% in open-loop control with quasi-static tracking [9] and to

about 1% in tracking of a non-stationary constant-rate saw-tooth profile with closed-loop adaptive control [10].

Recently, the inversion-based method is widely adopted in the field of tracking control of piezoelectric actuators. This kind of method is based on a common model structure which is composed of a linear dynamics sub-model and the hysteresis sub-model [11].

This paper presents a modified hysteresis model which is established by a bond graph approach for their advantages of self-learning, self-tuning, fault tolerance, and parallel processing. The mechanism of piezoelectric actuator is presented in first time. In the second time and the nonlinear hysteresis is expressed by the bond graph model. In order to validate the effectiveness of the proposed method, a low frequency triangle actuating voltage with variable amplitude is given to the actuator.

Keywords: Piezoelectric actuator, Bond Graph Modelling, Hysteresis nonlinear control, Micro displacement.

REFERENCES

[1] N. Chuang, A Robust Extended Kalman Filter for Modeling Piezoelectric Actuators, 2016 American Control Conference (ACC), Boston Marriott Copley Place, July 6-8, 2016. Boston, MA, USA.

[2] W. Liu, L. Cheng, Z. G. Hou, M. Tan, An Inversion-free Model Predictive Control with Error Compensation for Piezoelectric Actuators, American Control Conference, Palmer House Hilton, July 1-3, 2015. Chicago, IL, USA.

[3] A. Visintin, Differential Models of Hysteresis, Berlin, Germany: Springer-Verlag, 1994.

[4] I. Mayergoyz, Mathematical Models of Hysteresis and their applications, Netherlands, Elsevier. 2003.

[5] Y. K. Wen, Method for random vibration of hysteresis system, Journal of Engineering Mechanics. ASCE, vol 102, 1976, pp. 249-263.

[6] M. Ismail, F. Ikhouane, J. Rodellar, “The Hysteresis Bouc-Wen Model, a survey”, Arch Comput Methods Eng 16, Barcelona, Spain, 2009, p161-188.

[7] C. Lin and S. Yang, Precise positioning of piezo-actuated stages using hysteresis-observer based control, Mechatronics, vol 16, 2006, p 417-426.

[8] K. Kuhnen, H. Janocha. Inverse feed forward controller for complex hysteretic nonlinearities in smart-material systems. Control and Intelligent Systems, 2001, 29(3):74-83.

[9] P. Krejci, K. Kuhnen, Inverse control of systems with hysteresis and creep. IEE Proceedings Control Theory and Applications, 2001, 148(3):185-192

[10] K. Kuhnen, H. Janocha, Adaptive inverse control of piezoelectric actuators with hysteresis operators. Proceedings of the 1999 European Control Conference. Karlsruhe, pp. 791-796, 1999.

[11] W. T. Ang, F. A. Garmón, P. K. Khosla, C. N. Riviere, Modeling rate-dependent hysteresis in piezoelectric actuators, Proceedings of the 2003 IEEE/RSJ international conference on intelligent robots and systems, Las Vegas, Nevada, October 2003.